Delineating the causal role of the gut microbiota in experimental colitis

Rebecca Jeffery



University of Oxford
Jesus College

Thesis submitted for the degree of
Doctor of Philosophy

Michaelmas 2022

Abstract

The gut microbiota is altered (dysbiosis) in patients with inflammatory bowel disease (IBD), although it is not currently understood whether this is causal of, or consequential to, disease development. Delineating the nature of these associations is imperative to inform microbiota-based IBD therapeutics. One such avenue is targeting of Enterobacteriaceae expansion, a dysbiotic signature common to murine and human colitis, through tungstate-mediated inhibition of Enterobacteriaceae growth. Although Enterobacteriaceae expansion is common to multiple animal models, tungstate inhibition of Enterobacteriaceae and amelioration of pathology has been predominantly shown in dextran sodium sulfate (DSS) colitis. Thus, in this thesis we aimed to replicate and expand on the therapeutic potential of tungstate in animal models, namely DSS, *Helicobacter hepaticus* + anti-interleukin-10 receptor (aIL-10R) and *Citrobacter rodentium* colitis. We found limited effects of tungstate on DSS-induced Enterobacteriaceae expansion and no effects on pathology development across all models. Thus, the ability of tungstate to ameliorate disease appears context-dependent. Although tungstate targets a feature of dysbiosis, it does not inform on the bacteria-bacteria and host-bacteria interactions which underpin disease pathogenesis. The *H. hepaticus* + aIL-10R model is poised to explore such interactions, as disease is dependent on the presence of other commensals, including the gnotobiotic 12-member Oligo-Mouse-Microbiota (OMM^{12}). In this thesis, we characterise dysbiosis and intestinal metabolite alterations in the *H. hepaticus* + aIL-10R OMM^{12} model and show that *E. clostridioformis* YL32 is a key colitogenic member in this context. This is likely due to interactions between *E. clostridioformis* YL32 and *H. hepaticus*, as *H. hepaticus* upregulates putative virulence gene expression in *E. clostridioformis* YL32 mice, in-turn associated with changes in host inflammatory gene expression. Importantly, these interactions are therapeutically targetable as selective depletion of *E. clostridioformis* YL32 reverts established colitis. This work serves as proof of concept that microbiota inter-bacterial and host-bacterial interactions serve as novel therapeutic strategies for IBD.

Acknowledgements

Firstly, I would like to thank my primary supervisor Prof. Fiona Powrie for the continuous support throughout my DPhil, for providing excellent scientific guidance to shape my research ideas and freedom to pursue novel experiments. Thank you to my co-supervisor Dr. Nick Ilott for being an outstanding mentor and friend, for discussing with me at length with matched enthusiasm about experimental results and avenues. For the extensive informatic support and reading and providing of feedback to help me write and refine this thesis. For worrying about the other things that come with doing a DPhil and checking up in various ways, e.g., of most recent note herbal teas. Thank you to my co-supervisor Prof. Colin Kleanthous for providing support and excellent suggestions throughout my DPhil at thesis committee meetings. In addition, thank you to Dr. Jethro Johnson for being an invaluable thesis committee member and supporting me throughout my DPhil.

Thank you to every member of the Powrie lab for providing scientific and technical support and for creating a fun and collaborative work environment. In particular, thank you to Lilian whose infectious enthusiasm for science and the microbiota started me on this journey. Thank you to the germ-free girls, Claire, Eli and India. Claire for your help with anything and everything extending from germ-free and for your unwavering support of, and exclusive subscription to, my bug art works. Eli for showing me how things work in germ-free, the countless hours spent doing gnotobiotic work and emotional support over bottomless cocktails. India, for being my DPhil sister, for a friendship that will last a lifetime and is borderline weird. For being there for every experiment and putting me on the car insurance. For supporting me through the toughest times inside and outside the lab. Thank you to Alina, Cornelia and Dorothee for letting me look over their theses, for the support and encouragement to get me over the final hurdle and for making my DPhil such a positive experience through Hh co-parenting, prepping me for snowboarding and/or accompanying

me to bingo. Thank you to Alice and Xinyue, for the friendship and sustenance support in addition to the extensive scientific discussions.

To the Wellcome trust for their generous DPhil funding and the BSU, histology and core facility teams.

To Vivian, my dearest friend and adopted family member, for sharing Oxford and home life with me. For being my cell and crew mate, for introducing me to Popeyes, for being with me on this journey from the beginning until the end. To Libby, for being a snatched baddie and injecting fun into everything we do. To Anna, for the friendship that originated from discussing Michael Madsen over wine and cheese in Oxford and continues to withstand a 5-hour time zone difference.

Finally, I would like to thank my family, my mum, dad, grandma, brother, sister-in-law and Gavin for their unwavering love and support. I could not have done this without you.

Declaration of authorship

Data presented in this thesis are all from the authors' own experiments. However, Dr. Nick Ilott conducted processing of RNA-sequencing data to generate a counts dataset analysed by the author in figures 5.9 and 5.10.

Parts of the introduction of this thesis were submitted for authors' own publication and remain largely unaltered from the published material [1]. Published contents are clearly highlighted in the relevant sections. Co-authors (Dr. Nick Ilott and Prof. Fiona Powrie) were notified and provided written agreement for the reproduction of the mentioned published material in this thesis.

Table of Contents

List of figures ..... *x*

List of tables ..... *xiv*

List of abbreviations ..... *xv*

Chapter 1 Introduction *1*

1.1 Host-microbial interactions underpin colonic homeostasis **1**

1.1.1 Host control of the colonic microbiota 1

1.1.2 Microbial control of host immunity 5

1.2 Inflammatory bowel disease **7**

1.2.1 Genetic and immunological drivers 7

1.2.2 Disease-associated dysbiosis 8

1.3 Attributing causality to host-microbiota interactions in intestinal inflammation: Animal models of IBD **9**

1.3.1 Modelling barrier breakdown with dextran sodium sulfate 10

1.3.2 Infectious colitis driven by the murine pathogen *C. rodentium* 10

1.3.3 Modelling host-microbe maladaptation with *Helicobacter hepaticus* 12

1.4 Attributing causality to host-microbiota interactions in intestinal inflammation: Gnotobiotics **15**

1.4.1 Insights gained from GF mice 16

1.4.2 The Oligo-Mouse-Microbiota: A standardised and tractable model mouse microbiota 17

1.5 Informing microbiota-based therapeutic strategies by attributing causality to microbiota members in animal colitis models **19**

1.5.1 Enterobacteriaceae expansion 20

1.5.2 Complex microbial involvement underpins IBD pathogenesis 21

1.6 Thesis aims **21**

Chapter 2 Materials and methods ***23***

2.1 Mice **23**

2.1.1 Generation and maintenance of gnotobiotic colonies 23

2.2 Bacterial culture **24**

2.2.1 *Citrobacter rodentium* 24

2.2.2 Endogenous Enterobacteriaceae 24

2.2.3 *Helicobacter hepaticus* 24

2.2.4 Oligo-Mouse-Microbiota members 25

2.3 *In vitro* bacterial growth assays **25**

2.3.1 Tungstate susceptibility assay 25

2.3.2 Antibiotic susceptibility assay 26

2.4 Colitis induction and animal models **26**

2.4.1 *C. rodentium* 26

2.4.2 DSS 26

2.4.3 *H. hepaticus* + aIL-10R 27

2.4.4 *H. hepaticus*-specific T cell transfer 27

2.5 Histopathological scoring **28**

2.6 Assessment of immune cell populations by flow cytometry **30**

2.6.1 Processing of secondary lymphoid organs 30

2.6.2 Isolation of colonic lamina propria leukocytes 30

2.6.3 Staining and fixation 30

2.6.4 Data acquisition 31

2.7 Lipocallin-2 (LCN2) ELISA **31**

2.8 Host RNA analysis **32**

2.8.1 RNA extraction 32
2.8.2 qRT-PCR 32
2.8.3 RNA Sequencing (RNA-seq) 33
2.8.4 RNA-seq data processing 33
2.8.5 RNA-seq downstream analysis 34
2.9 Bacterial DNA analysis 34
2.9.1 DNA extraction 34
2.9.2 Quantification of Oligo-Mouse-Microbiota members 35
2.9.3 Quantification of *H. hepaticus* 37
2.9.4 16S sequencing 38
2.10 Bacterial RNA analysis 38
2.10.1 RNA extraction 38
2.10.2 Assessment of *C. rodentium* molybdenum-related gene expression 39
2.10.3 Assessment of *H. hepaticus* putative virulence gene expression 40
2.11 Untargeted metabolomics 41
2.11.1 Sample preparation 41
2.11.2 IC-MS and metabolite identification 41
2.11.3 Untargeted metabolomics downstream analysis 42
2.12 ICP-MS 42
2.13 General data analysis 43
Chapter 3 Targeting molybdenum-dependent respiratory processes in colitis 44
3.1 Introduction 44
3.2 Results 48
3.2.1 Tungstate inhibits Enterobacteriaceae anaerobic, nitrate-dependent growth *in vitro* 48

3.2.2 Tungstate has limited effects on Enterobacteriaceae growth across multiple colitis models 48

3.2.3 Tungstate fails to control pathology development in murine colitis models 51

3.2.4 *Citrobacter rodentium* expansion is independent of tungstate-mediated suppression of molybdenum-related gene expression 56

3.3 Discussion 58

Chapter 4 Characterising Oligo-Mouse-Microbiota community dynamics over the course of Helicobacter hepaticus-induced colitis 62

4.1 Introduction 62

4.2 Results 64

4.2.1 *H. hepaticus* + aIL-10R-induced inflammation coincides with dysbiosis in OMM^{12} gnotobiotic mice 64

4.2.2 *H. hepaticus* + aIL-10R-induced OMM^{12} dysbiosis coinciding with inflammation development is characterised by changes in 5 OMM^{12} members 67

4.2.3 Reductions of *E. clostridioformis* YL32 and *M. intestinale* YL27 and an expansion of *E. faecalis* KB1 are robust signatures of OMM^{12} dysbiosis coinciding with *H. hepaticus* + aIL-10R colitis 71

4.2.4 Discrepancies in dysbiotic signatures inferred by 16S sequencing and qPCR analysis are largely due to relative versus absolute quantification 75

4.2.5 *H. hepaticus* + aIL-10R colitis is associated with alterations in intestinal metabolite composition 79

4.2.6 Metabolite disturbances in OMM^{12} mice recapture signatures seen in IBD 84

4.2.7 Benzenoids are a unique chemical class downregulated across all intestinal sampling sites in *H. hepaticus* + aIL-10R colitis 88

4.3 Discussion 90

Chapter 5 Enterocloster clostridioformis YL32 is a key facilitator of H. hepaticus-induced colitis ***97***

5.1 Introduction **97**

5.2 Results **100**

5.2.1 *E. clostridioformis* is a key colitogenic member of the OMM[12] 100

5.2.2 *H. hepaticus* colonization alone does not determine disease outcome 106

5.2.3 The ability of commensals to promote homeostatic *H. hepaticus*-specific T cell responses is not indicative of disease development in IL-10 deficiency 109

5.2.4 *E. clostridioformis* YL32 promotes *H. hepaticus* expression of a putative T6SS component 111

5.2.5 *H. hepaticus* colonisation in *E. clostridioformis* YL32 mice leads to increased expression of molecular inflammatory signatures in the absence of disease 114

5.2.6 Selective targeting of *E. clostridioformis* YL32 reverts established colitis 118

5.3 Discussion **122**

Chapter 6 General discussion ***128***

6.1 Unravelling human dysbiotic signatures in animal models **128**

6.2 IBD as the perfect host-microbial storm **133**

6.3 Targeting of the microbiota to ameliorate established disease **137**

6.4 Conclusion **137**

References ***139***

A. Appendix ..... ***I***

List of figures

Figure 1.1. Host-microbiota interactions underpin intestinal homeostasis 4

Figure 1.2. Pathophysiology of H. hepaticus-induced colitis 14

Figure 1.3. Gnotobiotic approaches to attributing causality to host-microbiota interactions 18

Figure 3.1 Enterobacteriaceae expansion in chemically-induced colitis is fuelled by molybdenum-dependent respiratory processes which are inhibited by sodium tungstate 46

Figure 3.2. Tungstate transporter upregulation by Desulfovibrio species precedes Enterobacteriaceae expansion and colitis in the H. hepaticus + aIL-10R model 47

Figure 3.3. Tungstate inhibits Enterobacteriaceae nitrate-dependent anaerobic growth in vitro 49

Figure 3.4. Tungstate administration in the drinking water leads to tungsten accumulation in the large intestine 50

Figure 3.5. Tungstate has limited effects on Enterobacteriaceae growth across colitis models 52

Figure 3.6. Tungstate does not influence animal weight loss or recovery in DSS colitis 53

Figure 3.7. Tungstate does not alter pathology development in murine colitis models 55

Figure 3.8. Tungstate fails to control inflammation in murine colitis models 57

Figure 3.9. C. rodentium growth in vivo is independent of tungstate mediated suppression of molybdenum cofactor related gene expression 59

Figure 4.1. H. hepaticus requires other commensals to induce colitis in IL-10 deficiency 65

Figure 4.2. OMM^{12} mice develop typhlitis following H. hepaticus + aIL-10R treatment 66

Figure 4.3. H. hepaticus-induced inflammation is associated with dysbiosis in OMM^{12} mice 68

Figure 4.4. H. hepaticus-induced colitis is associated with alterations in the relative abundance profiles of 8 OMM^{12} members 70

Figure 4.5. OMM^{12} longitudinal dysbiotic signatures are shared in end-point caecum and colon contents 72

Figure 4.6. OMM^{12} mice reproducibly develop inflammation in the colon and caecum following H. hepaticus + aIL-10R treatment 73

Figure 4.7. Inflammation develops robustly around day 5 after H. hepaticus + aIL-10R treatment in OMM^{12} mice and is not associated with a drop in H. hepaticus levels 74

Figure 4.8. An expansion of E. faecalis KB1 and reductions in E. clostridioformis YL32, M. intestinale YL27 and A. muciniphila YL44 are robust signatures of H. hepaticus-induced OMM^{12} dysbiosis 76

Figure 4.9. Longitudinal signatures of H. hepaticus-induced OMM^{12} dysbiosis are present in end-point intestinal contents 77

Figure 4.10. Contradictory signatures obtained by 16S versus qPCR analysis are due to discrepancies between relative versus absolute quantification 78

Figure 4.11. Metabolites with a putative identification are at low count but high abundance in untargeted IC-MS data 80

Figure 4.12. Abundance versus prevalence profiles of faecal and intestinal content metabolite data 81

Figure 4.13. Metabolite data from OMM^{12} mice displays distinct clustering according to colitic status 82

Figure 4.14. Annotated metabolite fractions show clear separation according to colitic status following outlier removal 83

Figure 4.15. H. hepaticus-induced colitis in OMM^{12} mice is associated with shifts in faecal and intestinal metabolite composition 85

Figure 4.16. Inflammatory-associated shifts in faecal metabolite profiles recapitulates signatures seen in human IBD 86

Figure 4.17. Inflammatory-associated shifts in intestinal content metabolite profiles recapitulate signatures seen in human IBD 87

Figure 4.18. Benzenoids represents a chemical class uniquely downregulated in H. hepaticus + aIL-10R colitis in OMM^{12} mice 90

Figure 5.1. Susceptibility to H. hepaticus + aIL-10R colitis is not ubiquitous to OMM^{12} members and instead requires C. innocuum I46 and E. clostridioformis YL32 100

Figure 5.2. Generation of stably colonised E. clostridioformis YL32 and C. innocuum I46 mice 101

Figure 5.3. E. clostridioformis YL32 mice are susceptible to H. hepaticus + aIL-10R-induced colon pathology 103

Figure 5.4. E. clostridioformis YL32 mice are susceptible to H. hepaticus + aIL-10R-induced caecum pathology 104

Figure 5.5. H. hepaticus-induced colitis in E. clostridioformis YL32 mice is characterised by Th17 cell expansion 107

Figure 5.6. H. hepaticus colonisation is microbiota-dependent but does not determine disease outcome in IL-10 deficiency 110

Figure 5.7. OMM^{12} members promote the generation of H. hepaticus-specific responses regardless of pathology development in IL-10 deficiency 112

Figure 5.8. H. hepaticus upregulates putative gene expression in the presence of E. clostridioformis YL32 114

Figure 5.9. H. hepaticus colonisation in E. clostridioformis YL32 mice alters host gene expression 115

Figure 5.10. H. hepaticus colonisation in E. clostridioformis YL32 mice leads to the induction of a molecular inflammatory signature in the absence of disease 117

Figure 5.11. Preventative treatment with vancomycin leads to select targeting of E. clostridioformis YL32 and impaired H. hepaticus colonisation 119

Figure 5.12. Preventative treatment with vancomycin ameliorates H. hepaticus-induced colitis in E. clostridioformis YL32 mice 120
Figure 5.13. Intervention treatment with vancomycin leads to select targeting of E. clostridioformis YL32 without altering H. hepaticus colonisation 121
Figure 5.14. Selective depletion of E. clostridioformis YL32 reverts established H. hepaticus-induced colitis 123
Figure 6.1. Microbiota-based therapeutic strategies 129
Figure 6.2. Proposed mechanism for the role of E. clostridioformis YL32-H. hepaticus interactions leading to disease in IL-10 deficiency 136
Figure A.1 Tungstate does not influence animal weights in murine colitis models I
Figure A.2 Gating strategy for flow cytometry II
Figure A.3 Tungstate does not influence mucosal inflammation in murine colitis models III
Figure A.4 Tungstate does not influence systemic immune responses across murine colitis models IV
Figure A.5 Outliers in annotated metabolite PCA are driven by elevated zero status ... V
Figure A.6. Inter-bacterial interactions drive subtle changes in homeostatic host gene expression VI

List of tables

Table 2.1. Antibodies used for H. hepaticus-specific T cell transfer 28

Table 2.2. Scoring system used for histopathological scoring of colitis models 29

Table 2.3. Antibodies used for flow cytometric analysis of immune cell populations. 31

Table 2.4. Taqman probes used for host qPCR 33

Table 2.5. Primer and probe sequences used to quantify OMM^{12} members 37

Table 2.6. Primer and probe sequences used to quantify H. hepaticus 37

Table 2.7. Primer sequences to assess C. rodentium molybdenum-related gene expression 40

Table 2.8. Primer sequences used to assess H. hepaticus putative virulence gene expression 41

Table 4.1. H. hepaticus + aIL-10R colitis in OMM^{12} mice is associated with shifts of distinct metabolites across intestinal sites..... 89

List of abbreviations

A. muciniphila	*Akkermansia muciniphila*
A. muris	*Acutalibacter muris*
ACK	Ammonium-Chloride-Potassium
AE	Attaching and effacing
AHR	Aryl hydrocarbon receptor
AIEC	Adherent invasive *Escherichia coli*
aIL-10R	Anti-interleukin-10 receptor
AMP	Antimicrobial peptide
APC	Antigen presenting cell
ASA	Aminosalicylic acid
ASF	Altered Schaedler flora
ASV	Amplicon sequence variant
ATG16L1	Autophagy-related 16-like 1
B. animalis	*Bifidobacterium animalis*
B. caecimuris	*Bacteroides caecimuris*
B. coccoides	*Blautia coccoides*
B. fragilis	*Bacteroides fragilis*
BMCA	β-muricholic acid
BMDM	Bone marrow-derived macrophage
BSA	Bovine serum albumin
C. innocuum	*Clostridium innocuum*
C. rodentium	*Citrobacter rodentium*
CA	Cholic acid
CARD	Caspase recruitment domain-containing
CD	Crohn's disease

CDT	Cytolethal distending toxin
CFU	Colony forming units
CO_2	Carbon dioxide
Ct	Cycle threshold
CXCR	Chemokine receptor
DAMP	Damage-associated molecular pattern
DC	Dendritic cell
DCA	Deoxycholic acid
DNA	Deoxyribonucleic acid
E. clostridioformis	*Enterocloster clostridioformis*
E. coli	*Escherichia coli*
E. faecalis	*Enterococcus faecalis*
EDTA	Ethylenediaminetetraacetic acid
EHEC	Enterohaemorrhagic *Escherichia coli*
ELISA	Enzyme-linked immunosorbent assay
EPEC	Enteropathogenic *Escherichia coli*
F. plautii	*Flavonifractor plautii*
F. prausnitzii	*Faecalibacterium prausnitzii*
FBS	Fetal bovine serum
Fdh	Formate dehydrogenase
FFAR	Free fatty acid receptor
FMT	Faecal microbiome transplantation
FOXP3	Forkhead box P3
FSC	Forward scatter
GATA3	GATA binding protein 3
GF	Germ-free
GI	Gastrointestinal

GM-CSF	Granulocyte-macrophage colony-stimulating factor
GOI	Gene of interest
H. hepaticus	*Helicobacter hepaticus*
H_2	Hydrogen
H_2S	Hydrogen sulfide
HMP	The Human Microbiome Project
IBD	Inflammatory bowel disease
IC-MS	Ion chromatography mass spectrometry
ICP-MS	Inductively coupled plasma mass spectrometry
IEC	Intestinal epithelial cell
IEL	Intraepithelial lymphocyte
IFN	Interferon
Ig	Immunoglobulin
IL	Interleukin
IL-10R	Interleukin-10 receptor
IL10RA	Interleukin-10 receptor alpha chain
IL10RB	Interleukin-10 receptor beta chain
IL23R	Interleukin-23 receptor
IL2RA	Interleukin-2 receptor alpha chain
ILA	Indolelactic acid
ILC3	Innate lymphoid cell
iNKT	Invariant natural killer T
iNOS	Inducible nitric oxide synthase
IPEX	Immunodysregulation polyendocrinopathy enteropathy X-linked
IRF5	Interferon regulatory factor 5
IRGM	Immunity Related GTPase M
iTreg	Induced T regulatory

JAK	Janus kinase
L. reuteri	*Limosilactobacillus reuteri*
LB	Lysogeny Broth
LBP	Live biotherapeutic products
LCA	Lithocholic acid
LCN2	Lipocalin-2
LPS	Lipopolysaccharide
LYPD8	Ly6/PLAUR domain containing protein 8
M. intestinale	*Muribaculum intestinale*
MAF	Musculoaponeurotic fibrosarcoma
MCFA	Medium chain fatty acid
MD	Mendelian disorder
MHC-II	Major histocompatibility complex-II
mLN	Mesenteric lymph node
MoCo	Molybdenum cofactor
Muc2	Mucin-2
N_2	Nitrogen
NF	Nuclear factor
NLRP	NOD-like receptor family pyrin domain-containing
NOD	Nucleotide-binding oligomerization domain-containing
NOS	Nitric oxide synthase
O_2	Oxygen
OD	Optical density
OMM	Oligo-Mouse-Microbiota
OMV	Outer membrane vesicle
OXPHOS	Oxidative phosphorylation
PAMP	Pathogen-associated molecular pattern

PBA	Primary bile acid
PBS	Phosphate buffered saline
PCA	Principal component analysis
PCR	Polymerase chain reaction
PPAR	Peroxisome proliferator-activated receptor
PRR	Pattern recognition receptor
PSA	Polysaccharide A
qPCR	Quantitative polymerase chain reaction
RNA	Ribonucleic acid
RNS	Reactive nitrogen species
ROR	RAR-related orphan receptor
ROS	Reactive oxygen species
rRNA	Ribosomal ribonucleic acid
RT	Reverse transcription
SAA	Serum amyloid A
SBA	Secondary bile acid
SCFA	Short chain fatty acid
SCID	Severe combined immunodeficiency
SFB	Segmented filamentous bacteria
SIgA	Secreted immunoglobulin A
SPF	Specific-pathogen-free
SSC	Side scatter
T. muris	*Turicimonas muris*
T3SS	Type 3 secretion system
T4SS	Type 4 secretion system
T6SS	Type 6 secretion system
TCA	Tricarboxylic acid

TCR	T cell receptor
TF	Transcription factor
Tfh	T follicular helper
Tg	Transgenic
Th	T helper
TLR	Toll-like receptor
TNF	Tumor necrosis factor
T_{reg}	T regulatory
TSB	Trypticase soy broth
TVP	Trimethoprim, vancomycin and polymyxin B
UC	Ulcerative colitis
WT	Wild-type

Chapter 1 Introduction

The gut microbiota is the term for the highly diverse collection of bacteria, viruses, fungi and archaea that reside in the mammalian intestine. Gut homeostasis is governed by symbiosis between commensal microbes and the host, which is maintained through bidirectional host-microbe interactions leading to reinforcement of the mucosal barrier, innate defence and the generation of commensal-specific adaptive immune responses (figure 1.1) [2]. Dysregulation of the host-microbiota interface is implicated in the pathogenesis of inflammatory bowel disease (IBD) [3] yet we are only beginning to delineate the mechanistic basis of how commensal microbes contribute to disease. Thus, the microbiome serves as an exciting space in which to delineate mechanisms of IBD pathogenesis with the potential to inform the development of novel therapeutics.

1.1 Host-microbial interactions underpin colonic homeostasis

The following contains sections of my own work which has been published [1].

1.1.1 Host control of the colonic microbiota

While the gut microbiota and host colonic tissue are in relatively close proximity, the presence of a single cell layer of intestinal epithelial cells (IECs) forms a physical barrier that separates immune cells present in the underlying connective tissue (lamina propria) from the microbiota. In addition, production of a ~150μm-thick gel mucus layer by specialist secretory IECs called goblet cells allows for further microbiota compartmentalisation, demonstrated by increased susceptibility to spontaneous and infectious colitis in mucus-deficient mice either through lack of the major constituent of mucus, Mucin-2 (*Muc2)*, or following mucus degradation by *Akkermansia muciniphila* in fibre-limiting conditions [4–8]. Host-microbe stratification is reinforced by several factors which operate in colonic mucus to limit host-microbial contact. Indeed, ly6/PLAUR domain containing 8 (LYPD8) protein is constitutively

shed by IECs to inhibit motility and mucosal encroachment of flagellated bacteria [9]. Moreover, secreted immunoglobulin A (SIgA), produced by plasma cells in the lamina propria, is actively translocated across the epithelium to bind to commensal microbes in the gut lumen (figure 1.1). SIgA is abundant in the intestine and can be both cross-reactive and highly specific to microbiota members, facilitating pan control over microbiota composition and direct targeting of flagellated bacteria which reside within the colonic mucosa [10–12]. Indeed, flagellin-specific IgA responses protect against mucosal encroachment by the microbiota and spontaneous colitis development [12].

In addition to acting as a physical barrier, IECs express pattern recognition receptors (PRRs), such as toll-like receptors (TLRs), which bind to pathogen-associated molecular patterns (PAMPs) or host-derived damage-associated molecular patterns (DAMPs). This in-turn leads to the production of various mediators which can modulate both the host and microbiota. For example, PRR engagement results in the production of anti-microbial peptides (AMPs) which regulate microbiota composition, and cytokines and chemokines which influence innate and adaptive cells in the underlying lamina propria (figure 1.1) [13–16].

Indeed, both innate and adaptive immunity contribute to control of homeostatic microbiota interactions. In addition to the expression of PRRs and phagocytosis of bacteria that have breached the epithelium, CX3CR1^{+} macrophages capture microbiota-derived antigen through trans-epithelial dendrites (figure 1.1) [17–19]. In homeostasis, such microbe-macrophage interactions lead to the generation of a tolerogenic microenvironment. For example, resident intestinal macrophages retain a state of inertia, in-part through autocrine anti-inflammatory interleukin-10 (IL-10) signalling, which limits pro-inflammatory cytokine production even following phagocytic activity and PRR engagement [17,20]. Antigen captured by macrophages is transferred to dendritic cells (DCs) which traffic to the mesenteric lymph nodes (mLNs) to prime adaptive CD4 T cell responses (figure 1.1) [21]. As

with resident macrophages, intestinal DCs maintain a tolerogenic phenotype through autocrine IL-10 signalling which limits pro-inflammatory cytokine production following activation [22]. This hyporesponsive phenotype translates to the preferential induction of tolerogenic T regulatory (T_{reg}) cells in the mLNs [21,23].

Macrophage and DC responses can be shaped by RORγt^+ type 3 innate lymphoid cells (ILC3s), which respond to stress signals, microbial compounds and cytokines produced in the tissue [24]. For example, macrophage production of IL-1β in response to the microbiota induces the production of granulocyte-macrophage colony-stimulating factor (GM-CSF) by ILC3s, which in turn acts on macrophages and DCs to promote the production of T_{reg} cell differentiation factors, including IL-10 (figure 1.1) [25]. In addition to regulating innate responses, ILC3s can influence the generation of adaptive microbiota-specific responses. Indeed, ILC3s, through the expression of major histocompatibility complex II (MHC-II), induce commensal-specific T_{reg} cell, whilst restraining that of pathogenic T cell, responses and induce commensal-specific IgA production through interactions with CD4 T follicular helper (Tfh) cells in mLNs [11,26,27].

Whilst CD4 T cell specificity is determined by the T cell receptor (TCR) generated during thymic development, CD4 T cell phenotype is determined by cytokine cues encountered during T cell activation by an MHC-II expressing antigen presenting cell (APC) (figure 1.1). It is of note that microbiota-specific CD4 T cells are present in healthy individuals [28], due to priming of cross-reactive self-recognising T cells in the mLN with antigen sampled from the microbiota [29]. In addition, for some bacterial species, trafficking of microbiota-derived antigen from the intestine to the thymus by DCs in early life may further facilitate microbiota-reactive T cell generation [30]. A number of mucosal microbe-reactive T cells isolated from and studied in animal models differentiate into IL-10 producing RORγt^+ induced T_{reg} (iT_{reg}) cells during homeostasis and adopt pathogenic interferon-γ (IFN-γ)/IL-17 producing

Th1/Th17 cell phenotypes in the context of immune deficiency, such as lymphopenia or loss of IL-10 [31–33]. In contrast, T cells specific to CBir1 flagellin derived from *Clostridium* XIVa cluster bacteria adopt Th1 or Th17 cell phenotypes exclusively in the context of barrier breakdown and fail to become activated when the epithelium is intact despite antigen availability in the intestinal lumen [34–36]. This emphasises the importance microbial ecology exerts over gut mucosal immune responses, as spatial organization clearly influences the modulatory potential of a given bacterium in homeostatic and disease contexts.

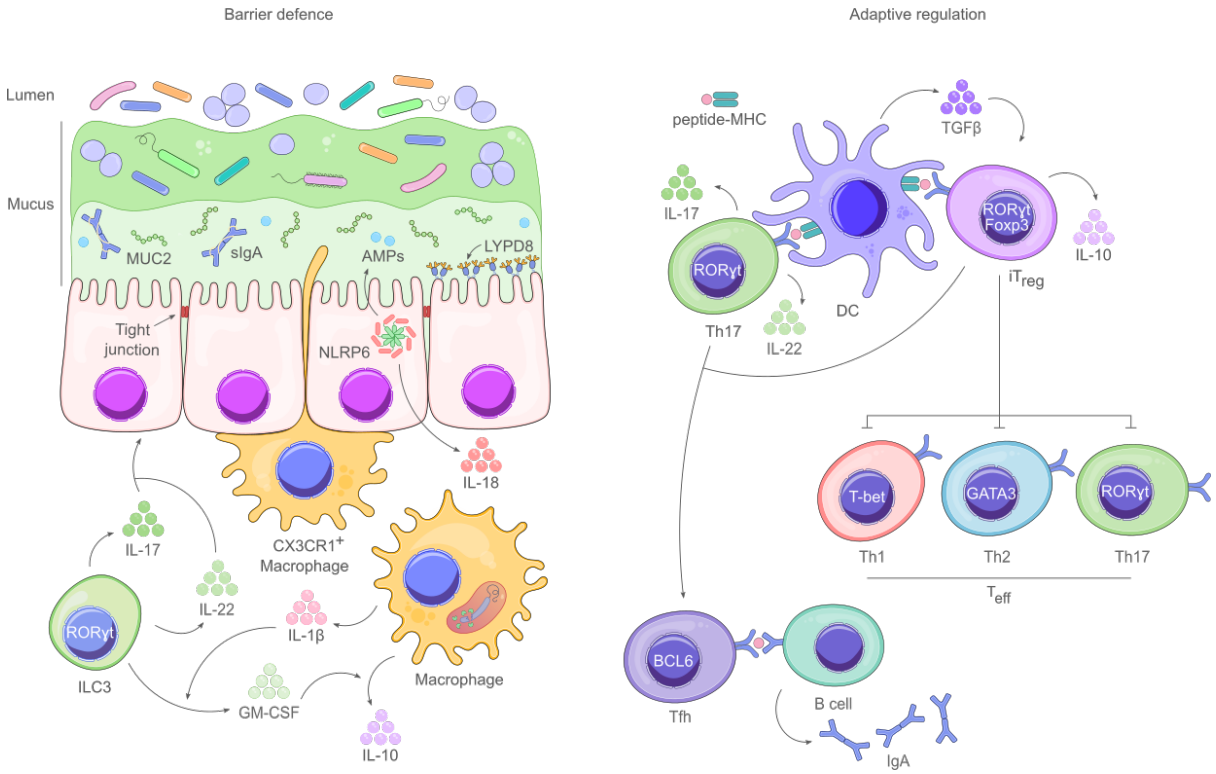


Figure 1.1. Host-microbiota interactions underpin intestinal homeostasis. (Left) Host pathways that maintain barrier function and microbial compartmentalization. This includes a stratified mucus layer, the inner layer of which is dense and prevents bacterial adherence to the epithelium. Secreted immunoglobulin A (sIgA) and Ly6/PLAUR domain containing 8 (LYPD8) interact with bacteria to prevent mucosal encroachment. The epithelium comprises a single layer of cells that are closely connected through the formation of tight junctions. Intestinal epithelial cells (IECs) can respond to microbial derived signals through pattern recognition receptors (PRRs) including NOD-like receptor family pyrin domain-containing 6 (NLRP6), which leads to inflammasome formation, antimicrobial peptide (AMP) and interleukin-18 (IL-18) production. Dendritic cells (DCs) and macrophages interact with bacteria to create a tolerogenic microenvironment. Innate lymphoid type 3 cells (ILC3s) can interpret signals from macrophages to further promote tolerance and maintain barrier function. (Right) Polarization of the T cell axis by commensal antigen-loaded DCs leads to the generation of T regulatory (T_{reg}) cells, which can broadly suppress T effector (T_{eff}) cell responses, and T helper 17 (Th17) cells which produce barrier-protective cytokines. T follicular helper (Tfh) cells influence the generation of commensal specific IgA by mucosal B cells. Figure and legend prepared by Rebecca Jeffery and used for publication in Current Opinion in Microbiology [1].

1.1.2 Microbial control of host immunity

The human body is colonised by trillions of microbes (microbiota), which exist in a harmonious, symbiotic relationship with the host. Indeed, the number of bacteria in the body is estimated to equate that of human cells, with the vast majority of them housed within the colon [37,38]. Staggeringly, the gut metagenome (the genes encoded by gut microorganisms) contains on average 0.8 million genes, which outnumbers the ~40,000 genes comprising the human genome [39,40]. Our understanding of the gut microbiota and the functional niche to which they contribute (microbiome) has been facilitated by advancements in non-culture-based methods of analysing microbial species. Indeed, the Human Microbiome Project (HMP) spearheaded the rapid expansion of our knowledge on the microbiome and undertook the mammoth task of characterising the taxonomic structure and functional capacity of the microbiome in health and various disease states including IBD [41–43]. Such extensive efforts have led to the identification of over 1000 bacterial gut microbiota constituents. However, an individual on average only harbours ~160 species. Thus, the gut microbiota is extremely personalised and highly variable between individuals. Although this makes species-level definition of a healthy gut microbiota impossible, characterisation at higher levels of taxonomic classification show that it is dominated by obligate anaerobic members of the Firmicutes and Bacteroidetes phyla [44]. Of the Firmicutes, the majority of species belong to the Clostridia class, namely Clostridial IV and XIVa clusters [45]. Although present, facultative anaerobic bacteria of the phyla Pseudomonadota (previously Proteobacteria), Actinobacteria, Fusobacteria and Verrucomicrobia are at low relative abundance, reflective of the hypoxic nature of the intestinal lumen [45,46].

Far from being an innocuous antigenic load in the intestinal lumen, the gut microbiota exerts profound effects over the mucosal immune system [4]. Perhaps the most well characterised bacterially-derived metabolite with homeostatic properties is the short chain fatty acid

(SCFA) butyrate, produced from dietary fibre predominantly by *Faecalibacterium prausnitzii*, *Eubacterium rectale*, *Eubacterium hallii* and *Ruminococcus bromii* (phylum Firmicutes) [45,47]. Butyrate serves as the primary energy source for colonic IECs (colonocytes) [48] and activates peroxisome proliferator-activated receptor-γ (PPAR-γ) signalling to promote oxygen consumption through mitochondrial β-oxidation of fatty acids, in turn limiting oxygen diffusion into the intestinal lumen [49]. In addition to regulating colonocyte metabolism, butyrate reinforces the epithelial barrier [50], promotes antimicrobial macrophage function whilst maintaining hyporesponsiveness [51,52] and induces the differentiation of colonic T_{reg} cells [53]. Other examples of physiologically relevant bacterial-derived metabolites originating from dietary components include derivatives of the essential amino acid tryptophan, which serve as ligands for the aryl hydrocarbon receptor (AHR) [54]. AHR signalling plays an important role in colonic homeostasis through the maintenance of barrier-protective ILC3 and Th17 cell populations which confer resistance to infectious colitis [55].

In addition to metabolism of dietary components, bacterial conversion of primary bile acids (PBAs) synthesised in the liver to secondary bile acids (SBAs), namely deoxycholic acid (DCA) and lithocholic acid (LCA), in the colon has important influence over host physiology [56]. For example, SBAs have been shown to induce colonic iT_{reg} cells, which confers protection in experimental colitis [57–59]. In addition to influencing the host, microbiota-derived SBAs can inhibit the growth of intestinal pathogens [60–62]. Finally, examples of microbial influence over gut physiology extends from that of metabolites. Perhaps most prominently, polysaccharide A (PSA) a secreted component derived from *Bacteroides fragilis* has been shown to correct splenic defects seen in germ-free (GF) mice and induce the differentiation of colonic T_{reg} cells [63,64]. Notably, this T_{reg} cell induction can be achieved through direct stimulation of T cells with PSA or through DC-mediated uptake of PSA-loaded OMVs [65,66]. Similar to PSA, *Helicobacter hepaticus* produces a secreted polysaccharide that induces IL-10 production in caecal macrophages [67].

1.2 Inflammatory bowel disease

1.2.1 Genetic and immunological drivers

The following contains sections of my own work which has been published [1].

IBD is a group of chronic relapsing-remitting inflammatory disorders of the gastrointestinal (GI) tract, the major clinical manifestations of which are Crohn's disease (CD) and ulcerative colitis (UC). CD and UC are classified according to whether disease manifests anywhere along the GI tract or exclusively in the colon, respectively [68]. Histopathological features include crypt abscesses, extensive mucosal immune cell infiltrate and goblet cell depletion. Clinical manifestations include abdominal cramps, diarrhoea and weight loss and it is estimated that ~75% of CD patients will ultimately require surgical intervention [69,70]. In 2017, IBD prevalence in the UK population was ~0.97%, although this is predicted to rise to 1.1% by 2025 [71].

The precise aetiology of IBD is unknown but thought to be driven by aberrant mucosal immune responses to the microbiota. Indeed, despite extensive disease heterogeneity, unique and shared risk loci place maladapted host-microbial interactions at the centre of IBD pathologies [72–74]. For example, variants within genes involved in innate recognition of microbial products, microbial clearance and T cell differentiation confer polygenic risk in both CD (*NOD2*, *CARD9*, *ATG16L1*, *IRGM*, *IL23R*, *IL2RA* and *JAK2*) and UC (*IRF5*, *CARD9*, *IRGM*, *IL23R*, *IL2RA* and *JAK2*) [74]. Moreover, loss of anti-inflammatory interleukin-10 (IL-10) signalling (*IL10*, *IL10RA*, *IL10RB*) and tolerogenic T regulatory (T_{reg}) cell activity (*FOXP3*) underlie two major forms of Mendelian disorders with IBD-like intestinal inflammation (MD-IBD), infantile-onset IBD and IPEX syndrome, respectively [3].

Current IBD therapeutics include immunosuppressive and anti-inflammatory drugs, including glucocorticoids and biologics [75], with monoclonal antibodies targeting tumour necrosis

factor α (TNF-α) being gold standard treatments for IBD. However, ~1/3 patients are primary non-responders to anti-TNFα and a further 50% of initial responders lose responsiveness within a few years of initiating treatment [76], supporting a requirement for the development of new therapeutic targets. Of note, the IL-23/IL-17 pathway has been implicated in IBD pathogenesis [77], and while IL-17 production is implicated in pathogenic responses to the microbiota in animal models [78], homeostatic roles of Th17-produced IL-17 likely contributes to observed adverse events in clinical trials of IL-17 blockade in IBD [79]. In contrast, Ustekinumab, which targets the p40 subunit shared between IL-12 and IL-23, is an approved therapy that induces clinical response in moderate to severe UC and CD patients [80,81]. The implication of IL-23 in preclinical studies has led to the pursuit of IL-23-specific monoclonal antibody therapies, although these are still in clinical trials [82]. Given the complexity of IBD and the presence of distinct histological pathotypes [72], it is likely that personalised characterisation of immunopathology is needed to deliver targeted therapeutics with high efficacy in patients.

1.2.2 Disease-associated dysbiosis

Although multiple genetic risk loci have been identified in IBD and increasing polygenic risk is associated with higher disease prevalence, genetic risk factors only account for a minority of disease variance [74,83]. Thus, environmental factors clearly play a role in IBD pathogenesis. Whilst current IBD therapies are focused on immunological drivers of disease, it is becoming increasingly clear that the microbiota plays an important role in IBD pathogenesis. Indeed, the composition of the microbiota is altered in UC and CD patients relative to healthy controls, a state often referred to as dysbiosis [42].

Although dysbiotic signatures can be highly variable between studies, the microbiome in IBD is characterised by an overall loss of community diversity [42], reduced relative abundance of Firmicutes and increased relative abundance of Pseudomonadota bacteria [84]. These

broad taxonomic changes can, in part, be attributed to reductions in protective, anti-inflammatory species such as *F. prausnitzii* [85,86] and increases in pro-inflammatory pathobionts such as strains of adherent-invasive *E. coli* (AIEC). [87,88].

The extent of functional and immune modulating activity that alters in IBD as a consequence of taxonomic changes is not fully understood. However, numerous bacteria-derived metabolites are altered in IBD and include, for example, butyrate, which is consistently reduced in IBD patients. The ability of butyrate to enhance regulatory immune function [53] and protect mice from colitis in pre-clinical models [89–91], supports it as a potential therapeutic target in IBD. Of note, dietary intervention to increase fibre intake and subsequently faecal butyrate levels, is an avenue with therapeutic potential in IBD patients [92,93]. Moreover, SBAs are reduced in surgically-created ileal pouches in colectomy-treated UC patients, administration of which ameliorates pathology in pre-clinical models [94]. In addition to alterations in the microbiota itself, host microbiota-specific responses are altered in IBD. For example, IBD patients display elevated intestinal IgA and IgG responses, which identify bacterial populations with elevated colitogenicity [95–97]. Moreover, microbiota-reactive CD4 T cell responses in the circulation and intestine of IBD patients differ from those seen in health and more frequently produce IL-17A [28]. Thus, the microbiota appears to play a role in IBD pathologies, although it is not currently understood whether such changes are causal of, or consequential to, disease development.

1.3 Attributing causality to host-microbiota interactions in intestinal inflammation: Animal models of IBD

Probing causal roles for the microbiota in IBD requires a mouse model that encompasses genetic predisposition with an easily manipulated and tractable microbiota. Due to its complexity, no animal model can recapitulate the full breadth of IBD pathologies. Instead, individual models, all of which develop IBD-like inflammation in the large intestine,

recapitulate aspects of the pathological spectrum that constitutes IBD [98]. Prominent models in the field include dextran sodium sulfate (DSS), *Citrobacter rodentium* and *H. hepaticus* + anti-IL-10 receptor (aIL-10R) colitis.

1.3.1 Modelling barrier breakdown with dextran sodium sulfate

DSS is administered at various concentrations (2-5%) in the drinking water for short periods (4-9 days) to induce acute weight loss and colitis characterised by mucin degradation, death of IECs, neutrophil infiltration into the colonic mucosa and the development of crypt abscess [99,100]. Of note, DSS can induce colitis in mice lacking T and B cells and thus innate immune responses are sufficient to drive pathology [101]. Mechanistically, DSS is thought to exert toxic effects on colonocytes [102], impairing intestinal barrier integrity leading to luminal antigen entry into the lamina propria [103]. Thus, DSS-induced colitis serves as model of intestinal barrier breakdown, a feature of human IBD that manifests as alterations to mucus structure, impaired AMP production, and disturbances to the epithelium [104] that includes IL13-dependent epithelial apoptosis and inter-epithelial pore formation [105,106]. In addition to recapturing host aspects of IBD, DSS-induced colitis is associated with dysbiosis, characterised by loss of diversity and an increase in facultative anaerobic bacteria such as Verrucomicrobia and *Escherichia* species [107,108]. As DSS pathology is thought to be driven by the loss of host-microbiota stratification, it is unsurprising that the microbiota plays a critical role in determining disease severity. Indeed, DSS outcomes are highly variable across institutions, which is linked to the presence or absence of species such as *Duncaniella muricolitica* and *Alistipes okayasuensis* [109,110].

1.3.2 Infectious colitis driven by the murine pathogen *C. rodentium*

C. rodentium (family Enterobacteriaceae) is a gram-negative murine pathogen, which induces attaching and effacing (AE) lesions in the colon. AE pathogens, namely

enteropathogenic and enterohaemorrhagic *E. coli* (EPEC and EHEC) are clinically relevant diarrheagenic human pathogens [111,112]. Of note, *C. rodentium* shares several virulence factors with EPEC and EHEC, including a type 3 secretion system (T3SS), and as such serves as model for host-pathogen interactions in this context [112,113]. However, *C. rodentium* also serves as a model for IBD pathogenesis due to its influence on barrier integrity, intestinal inflammation and the gut microbiota [114]. Innate responses to *C. rodentium* infection comprise the production of IL-23 by DCs, which in turn stimulates ILC3s to produce IL-17 and IL-22. IL-22 acts on IECs to reinforce barrier function through the production of AMPs. In addition, IL-22-mediated protective responses are reinforced by IL-22-producing neutrophils which accumulate in the lamina propria. Infection in wild-type (WT) mice is self-resolving and clearance is mediated by intestinal T-dependent IgG responses which target virulence factors expressed by mucosal-associated *C. rodentium* [115]. Notably, avirulent *C. rodentium* relocate to the intestinal lumen, where despite avoiding IgG-directed responses, are outcompeted by the microbiota due to nutrient competition [115,116]. The CD4 T cell response to *C. rodentium* is characterised by the induction of IL-17 producing RORγt$^+$ Th17 cells, which transition into IFN-γ/IL-17 producing RORγt$^+$T-bet$^+$ Th1/Th17 cells before becoming IFN-γ^+T-bet$^+$ “ex-Th17” cells [117]. This plasticity is also seen in *H. hepaticus* + aIL-10R colitis [117] and the IL-23/IL-17 pathway is a feature of IBD, as discussed previously.

The microbiota influences and is influenced by *C. rodentium* infection. For example, differences in microbiota composition drive differential susceptibilities to *C. rodentium* infection. This in turn has been attributed to microbiota production of butyrate, which directly inhibits *C. rodentium* growth *in vitro* and confers protection to susceptible mice *in vivo* [118]. Moreover, colonisation with segmented filamentous bacterium (SFB), which is a potent inducer of Th17 cells predominantly in the small intestine, confers colonisation resistance and protects against *C. rodentium*-colitis [119]. Conversely, in addition to conferring

resistance, commensals influence the ability of *C. rodentium* to colonise the colonic mucosa [120]. Finally, *C. rodentium* infection itself drives changes in microbiota composition [121]. Of note, *C. rodentium* has been shown to induce proliferation and metabolic reprogramming of IECs upon its immediate arrival in the colon, reducing oxidative phosphorylation (OXPHOS) prior to the onset of intestinal inflammation, which is met with a commensal enterobacterial bloom at the mucosal surface [122].

1.3.3 Modelling host-microbe maladaptation with *Helicobacter hepaticus*

The following is my own work that has been published [1].

Helicobacter hepaticus is a gram-negative Epsilonproteobacteria that colonises the murine large intestine. Since its discovery in immunodeficient mice with chronic hepatitis and colitis [123,124], numerous experiments have formally established *H. hepaticus* as colitogenic predominantly in the context of defective IL-10 and T_{reg} cell function [32,78,125–132]. Notably, IL-10 deficiency can be induced through genetic ablation of the *Il10* gene ($Il10^{-/-}$) or pharmacological blockade of IL-10 signalling with aIL-10R [78,126]. *H. hepaticus* is a pathobiont, a bacterium with pathogenic potential in the face of impaired intestinal homeostasis. Notably, whilst *H. hepaticus* serves as the prototypical mouse pathobiont, there are now multiple examples within and extending beyond the *Helicobacter* genus relevant to both mouse models and IBD patients [31,133–140].

In *H. hepaticus* + aIL-10R colitis, $Ly6C^{hi}$ monocytes recruited into the lamina propria differentiate into IL-23 and IL-1β producing macrophages. This differentiation process is orchestrated by interferon regulatory factor 5 (IRF5), which operates downstream of PRR engagement [141]. IL-23 is critical to *H. hepaticus* + aIL-10R colitis, as pharmacological blockade ameliorates disease development [78]. IL-23 acts on ILC3s to produce inflammatory cytokines including IL-22 and GM-CSF, which promote neutrophilia and

eosinophilia, respectively. Notably IL-22 mediated neutrophil infiltrate is indirect and mediated by chemokine production by the epithelium. In addition, IL-23 promotes the differentiation of IL-17 producing Th17 cells, which acquire the ability to produce IFN-γ as described for *C. rodentium* (figure 1.2) [128,142–147].

The majority of the clonotypes comprising pathogenic Th17 cell expansion are specific to *H. hepaticus*, which has led to the generation of *H. hepaticus*-specific transgenic T cells [32]. These in turn have been used to show that commensal-specific T cell phenotype is context dependent. Indeed, when transferred into a colonised immunocompetent host, *H. hepaticus*-specific T cells differentiate into RORγt$^+$ iT$_{reg}$ and, to a lesser extent, Tfh cells [32]. iT$_{reg}$ cell generation is intrinsically controlled by the transcription factor c-MAF and plays a non-redundant role in mediating homeostasis [32]. Whilst CD103$^+$ DC, in-turn linked to iT$_{reg}$ cell, deficiency leads to colitis development in *H. hepaticus* colonised mice [132], MHC-II$^+$ ILC3s have been specifically implicated in the generation of *H. hepaticus*-specific iT$_{reg}$ cells [148].

By contrast, in colonised IL-10 deficient mice, *H. hepaticus*-specific T cells deviate to a pathogenic Th1/Th17 phenotype, directed by non-ILC3 APCs, the aforementioned IL-23 along with serum amyloid A proteins (SAAs) (figure 1.2) [32,148,149]. Thus, the T cell response to *H. hepaticus* can be pathogenic or homeostatic depending on environmental cues controlled by host genetics. It is noteworthy that treatment of colitis in the *H. hepaticus* + aIL-10R model is refractory to anti-TNF-α and therefore may be used to understand the efficacy of alternative immunologically-based treatment strategies [150].

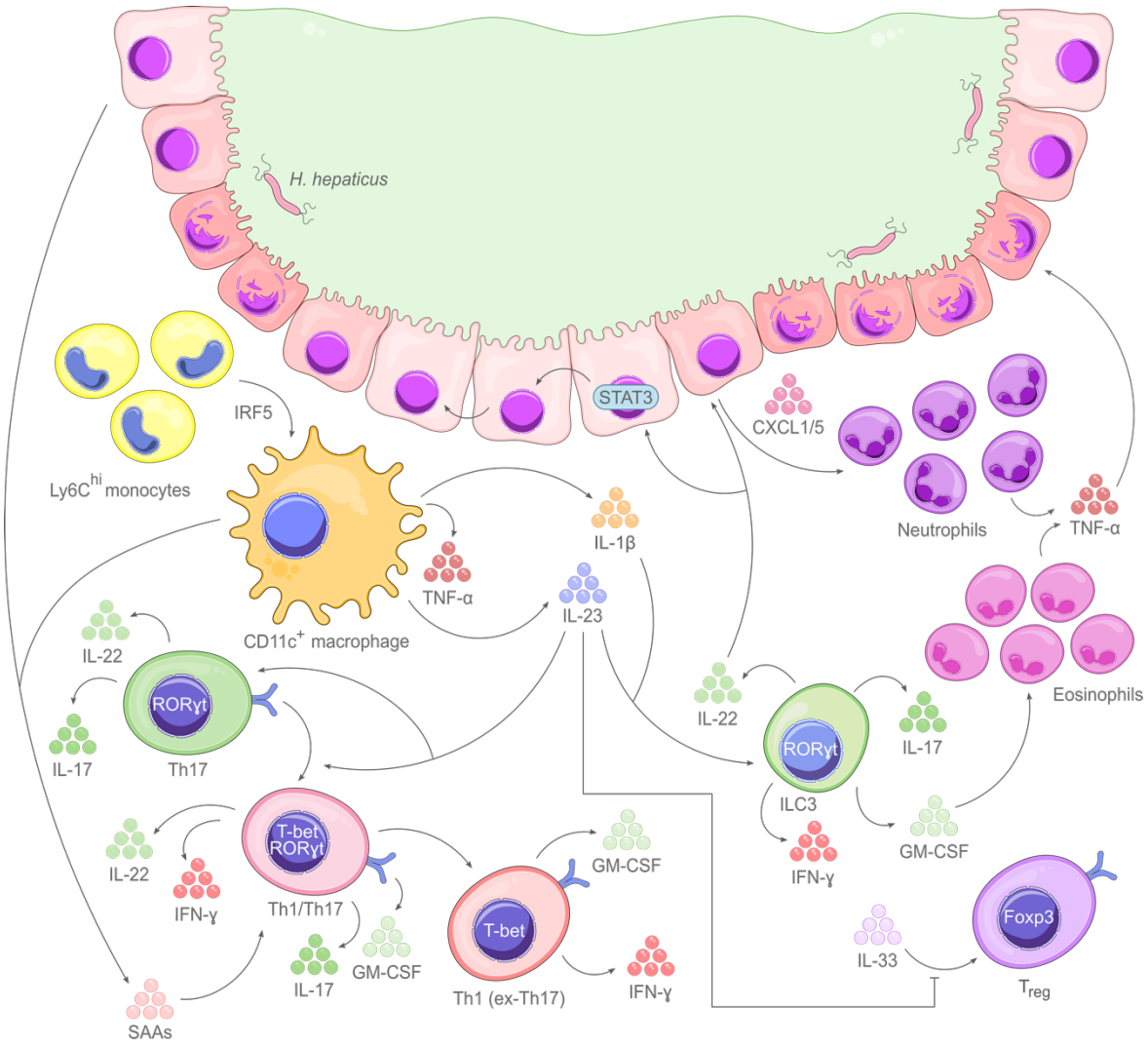


Figure 1.2. Pathophysiology of *H. hepaticus*-induced colitis. *H. hepaticus* infection in susceptible aIL-10R treated mice leads to inflammation in the colon and caecum. Recruited Ly6C^{hi} monocytes differentiate into CD11c^{+} macrophages under the guidance of IRF5 and produce a range of pro-inflammatory mediators including interleukin-23 (IL-23), IL-1β and TNF-α. IL-23 promotes T helper 17 (Th17) and Th1/Th17 cell differentiation and innate lymphoid type 3 (ILC3) infiltrate and production of Th1/Th17-type cytokines and also limits T regulatory (T_{reg}) cell induction by IL-33. IL-1β also contributes to pro-inflammatory ILC3 responses and epithelial, macrophage and dendritic cell (not depicted)-derived serum amyloid A proteins (SAAs) promote Th1/Th17 differentiation. IL-22 can induce STAT3 phosphorylation leading to proliferation, and neutrophil chemoattractant production in intestinal epithelial cells (IECs). Granulocyte-macrophage colony stimulating factor (GM-CSF) promotes pro-inflammatory eosinophilia and tumour necrosis factor-α (TNF-α) induces epithelial cell apoptosis. Figure and legend prepared by Rebecca Jeffery and used for publication in Current Opinion in Microbiology [1].

The microbiota plays a role in *H. hepaticus*-induced colitis. Susceptibility to *H. hepaticus*-induced colitis in *Il10*$^{-/-}$ mice has been shown to differ by vivarium, where mice with identical strain backgrounds display substantial differences in microbiome composition [151]. Differences in microbiome composition inevitably leads to differences in the metabolite milieu that is capable of shaping *H. hepaticus* growth and function. For example,

commensal-derived short chain fatty acid (SCFA) signalling through free fatty acid receptor 2 (FFAR2) limits *H. hepaticus* abundance. Additionally, hydrogen sulfide (H_2S), produced by sulfate reducing bacteria such as *Desulfovibrio* species, suppresses pro-inflammatory responses in *H. hepaticus*-induced innate colitis [152,153]. *H. hepaticus* also alters host responses towards other microbes, as prior infection with *H. hepaticus* leads to impaired control of *Mycobacterium tuberculosis* and *H. hepaticus* + aIL-10R treatment leads to differential IgA binding of other commensals [154,155].

1.4 Attributing causality to host-microbiota interactions in intestinal inflammation: Gnotobiotics

Specific pathogen free (SPF) is the gold standard practice for maintaining laboratory mice in commercial and institutional settings. Established in the 1960s, SPF refers to a state in which animals are maintained in an environment free of pathogens which would otherwise introduce experimental variability [156]. Commonly screened for and excluded pathogens in SPF facilities include *C. rodentium*, *Salmonella* spp. and *Mycoplasma pulomonis*. Nevertheless, the SPF microbiota is highly variable across animal vendors and in some cases can cause disparity in experimental results. For example, despite exerting clear influence over mucosal immune responses, *Helicobacter* spp. are not excluded by all commercial vendors [156]. Moreover, vendor-driven variability in microbiota composition leading to alterations in intestinal immune cell composition has led to the identification of individual bacterial species with immune-modulating properties. Indeed, SFB was discovered due to differences in small intestinal Th17 cell populations from Jackson Laboratory and Taconic Farms mice [119]. Of note, manipulation of the SPF microbiota is achieved through antibiotic administration. Although such studies have yielded important insights, antibiotic use does not facilitate study of bacteria in isolation and comes with the caveats of off-target effects and incomplete microbial depletion [157].

The rapid expansion in microbiome research over the past decade has led to increasing interest in i) studying bacteria, bacterial-derived products and/or bacterial interactions in isolation and ii) creating standardised, tractable microbial communities that retain functional capacities of the relatively complex SPF microbiota. “Gnotobiotic” in microbiome research refers to studies in which mice harbour a defined microbiota, extending from GF to curated diverse microbial communities. Importantly, gnotobiotic studies facilitate the transition from correlation to causation for bacterial species in physiological and disease processes [158].

1.4.1 Insights gained from GF mice

Germ-free mice are devoid of all microorganisms. Although the first GF mice were established in 1959, the ability to conduct GF experiments is only more recently becoming readily accessible, advancing the number of experiments done in GF and gnotobiotic conditions [158,159]. Characterisation of the GF mucosal immune system has highlighted the importance the microbiota plays in shaping intestinal function, with microbes observed to be involved in caecal and mLN anatomy as well as in the development of goblet cells and thus the mucus barrier [160]. In addition to barrier function, the microbiota plays a role in promoting and regulating innate immunity through increasing ILC3s and enabling hyporesponsiveness to lipopolysaccharide (LPS) stimulation [161]. Adaptive immune cells are also influenced by the microbiota, as GF mice have reduced numbers of colonic lamina propria iT_{reg} cells, and T_{reg} cells isolated from mLNs have impaired suppressive capacity [162,163]. Moreover, intestinal IgA responses are diminished in GF mice and systemic immunity is skewed to type 2 responses, including an increase in splenic Th2 cells and systemic IgE levels [63,164,165]. These have important implications on host physiology. For example, T_{reg} cells isolated from GF mice are partially impaired in their ability to ameliorate colitis induced by naïve T cell transfer into lymphodeplete severe combined immunodeficiency (SCID) mice [166]. Moreover, GF type 2 skewing corresponds to an increased susceptibility to allergic sensitisation [167,168].

In addition to demonstrating the role of the microbiota in homeostatic immunity, GF mice have been used to show the importance of the microbiota in IBD pathogenesis. Indeed, multiple animal models do not develop pathology in GF settings [125,166,169]. Both the role of the microbiota in promoting barrier function and driving inflammation is captured in the DSS model, where GF mice develop minimal colitis but high mortality rates due to exacerbated epithelial depletion [170]. Owing to the ability of the microbiota to confer colonization resistance, *C. rodentium* reaches higher levels in GF mice but induces colitis of comparable severity to that seen in SPF infected mice [116]. In contrast, in GF *Il10*$^{-/-}$ mice, *H. hepaticus* colonises but fails to induce colitis, suggesting a requirement for other commensals in disease development [171,172].

1.4.2 The Oligo-Mouse-Microbiota: A standardised and tractable model mouse microbiota

GF technology platforms can be exploited to interrogate the role of individual commensals in health and disease. Indeed, a number of strategies extending beyond GF mice have been adopted including the introduction of individual bacteria or bacterial-derived metabolites to further mechanistic understanding of host-bacteria interactions in isolation [158] (figure 1.3). For example, monocolonization studies have been used to establish the immunomodulatory properties of *B. fragilis* PSA [63,64]. In addition, curation of defined microbial communities has led to the establishment of gnotobiotic mice stably colonised with a minimal but functionally relevant gut microbiota. Early endeavours included the Altered Schaedler Flora (ASF), established in the late 1970s and comprising 8 bacterial species, which has been used in numerous studies assessing the influence of the microbiota on mucosal immune responses and interactions with enteropathogens [173,174]. However, ASF colonised animals have impaired colonisation resistance to *Salmonella enterica* serovar Typhimurium (*S*. Tm) suggesting it does not recapture complex microbiota functionality [175].

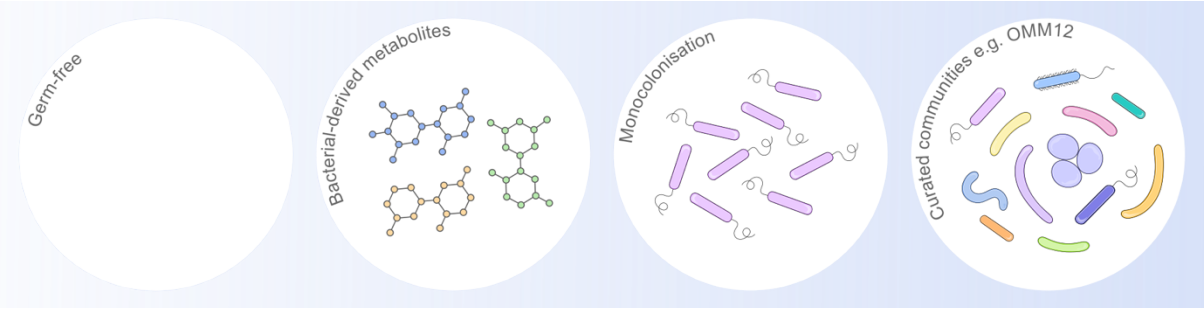


Figure 1.3. Gnotobiotic approaches to attributing causality to host-microbiota interactions. Approaches used in gnotobiotics to probe the role of the gut microbiota in modulating host physiology. This includes germ-free (GF) mice which lack any microorganisms, the introduction of bacterial-derived metabolites to GF mice, establishment of animals monocolonized with a bacterium of interest and the curation of minimal communities, such as the 12-member Oligo-Mouse-Microbiota (OMM12). Figure created using information from [158].

The Oligo-Mouse-Microbiota (OMM^{12}) comprises 12 bacteria which cover the 5 major phyla present in the murine gut [176]. Developed as a tractable, standardised mouse microbiota, its first usage was in demonstrating distinct microbial functions in mucus versus luminal dwelling bacterial populations [177]. Although other minimal communities have been developed [178], attributes that make the OMM^{12} an attractive model for microbiota research include its ability to confer partial colonisation resistance against *S*. Tm, which can reach conventional-like levels through the introduction of a single *E. coli* strain (Mt1B1) [176,179]. Moreover, the genome sequences of all OMM^{12} members are readily available and the OMM^{12} stably colonises mice across generations and research institutes [180,181]. In addition, the metabolic properties of OMM^{12} mice and *in vitro* bacterial interaction networks have been extensively characterised and *in vivo* tools are being developed and shared with the wider research community [182–184].

However, OMM^{12} mice display alterations in their intestinal immune system which places them as intermediates between GF and SPF mice in terms of mucosal immune development. For example, the OMM^{12} caecum is larger than that observed in SPF, but smaller than GF, mice [176,185]. Moreover, OMM^{12} mice have increased levels of iT_{reg} cells in the colonic lamina propria relative to GF mice, although to a lesser extent than those observed in SPF mice. As such immune populations have important roles in disease and

homeostasis, studies using OMM^{12} mice should consider the fact that OMM^{12} immune responses may not necessarily recapitulate those seen in SPF counterparts. These differences can be partially corrected through the introduction of an additional 9 bacterial strains [185]. However, such manipulations tread a fine line of achieving physiological relevance and increasing microbial complexity to a point that hinders interrogation of host-microbiota relationships. It should also be considered that even the phenotype of an SPF mouse, with relatively high microbial complexity, is more reflective of responses seen in neonates versus adult humans [158]. Curation of a complex (119 strains) but defined microbiota comprising human microbial strains represents another strategy to recapitulate microbiota function relevant to human physiology [186]. However, as the microbiota has coevolved with its host, it is unlikely that host-microbiota interactions between human-derived commensals and the mouse mucosal immune system are a true reflection of those seen in human physiology [187]. Thus, gnotobiotic microbiotas should be selected based on the research question they wish to address, which will in-turn inherit the caveats of the selected model.

1.5 Informing microbiota-based therapeutic strategies by attributing causality to microbiota members in animal colitis models

Delineating the role of the microbiota in host physiology has begun to unlock avenues into the development of microbiota-based therapeutics. At present, microbiota therapies most extensively pursued in clinical trials for IBD include faecal microbiota transplantation (FMT), antibiotics, probiotics (introduction of a single bacterium) and prebiotics (dietary intervention to promote growth of a given bacterial species). However, these interventions have thus far been met with limited success. For example, FMT outcomes are influenced by the composition of the donor microbiota in a manner that's hard to predict and colonisation resistance conferred by the recipient microbiota can impair engraftment, which is also an issue with probiotics. Antibiotics, whilst having reported benefits in IBD, have concerns with

off-target effects on beneficial microbiota constituents. Finally, whilst the most clinically feasible approach to altering the microbiota, dietary intervention strategies have problems with compliance and palatability [73,188,189]. Whilst it is clear that the microbiota plays a role in IBD pathogenesis, a more refined understanding of the host-microbial interactions underpinning disease is required for the development of more targeted therapeutics with translational potential [73].

1.5.1 Enterobacteriaceae expansion

Enterobacteriaceae expansion is perhaps the most robust signature of dysbiosis in IBD that has also led to the identification of AIEC [87,88,190]. This has led to substantial interest in pursuing the role of Enterobacteriaceae species in promoting disease development in animal colitis models [191]. An emerging theme in the literature is that Enterobacteriaceae, due to their flexible respiratory capacity, capitalise on host-derived changes in electron donor and acceptor availability to proliferate in the inflamed niche [192–197]. Most pertinently, this has led to the targeting of Enterobacteriaceae species with sodium tungstate, which targets molybdenum-dependent respiratory enzymes exclusively used by Enterobacteriaceae during gut inflammation [198]. As tungstate has no reported effects on other microbiota members or the host, this serves as a targeted method of inhibiting dysbiotic Enterobacteriaceae expansion which has been shown to ameliorate pathology in chemically-induced colitis models including the DSS model [198]. However, Enterobacteriaceae expansion is not limited to DSS-induced colitis and features in the *H. hepaticus* + aIL-10R model. Furthermore, in *H. hepaticus* + aIL-10R-induced colitis, an upregulation of tungstate transporter gene expression originating from other microbiota members precedes Enterobacteriaceae expansion and inflammation onset (Ilott *et al*, unpublished). Moreover, *C. rodentium* is a colitogenic Enterobacteriaceae which relies on similar respiratory capacities as commensal Enterobacteriaceae, including molybdenum-dependent respiratory enzymes, for optimal fitness *in vivo* [199,200]. Thus, targeting of Enterobacteriaceae species

through tungstate treatment may serve as a pan microbiota-based therapeutic strategy with application in multiple IBD-like contexts.

1.5.2 Complex microbial involvement underpins IBD pathogenesis

Despite extensive characterisation of the human gut microbiome, we have limited understanding of the metabolic and ecological interactions that occur both within the microbiota and between the microbiota and the host. Understanding such interaction networks is a daunting task but will likely lead to the development of novel therapeutic strategies [201]. For example, metabolic cross-feeding pathways may be used to inform methods to promote engraftment of beneficial species and alter community structure. Moreover, developing our understanding of bacterial cell-cell communication, namely quorum sensing, may be utilised to alter virulence and community phenotype [73]. An exemplar model to delineate bacteria-bacteria and host-bacteria interactions which influence disease pathogenesis is the *H. hepaticus* + aIL-10R model. For over 20 years, it has been known that *H. hepaticus* alone is not sufficient to induce colitis in IL-10 deficient mice [172]. Whilst studies have attempted to deduce the role of the microbiota in *H. hepaticus*-induced colitis, limited progress has been made to understand the mechanistic basis behind this observation [151,202]. More recently, it has been shown that OMM^{12} mice are susceptible to *H. hepaticus* + aIL-10R colitis [154]. Due to the tractable nature of the OMM^{12} and accessibility to individual OMM^{12} constituents [180], this facilitates the opportunity to interrogate colitogenic bacteria-bacteria and host-bacteria interactions in isolation.

1.6 Thesis aims

This thesis aims to underpin causal roles for microbiota species in the pathophysiology of IBD. This will encompass two biological questions. First, the role and targetability of molybdenum-dependent Enterobacteriaceae expansion in multiple animal colitis models.

Second, the influence of the microbiota in *H. hepaticus* + aIL-10R colitis. The specific aims of this thesis are:

1) Understand if tungstate treatment represents a reproducible and viable therapeutic option in DSS, *H. hepaticus* + aIL-10R and *C. rodentium* colitis
2) Characterise OMM^{12} community composition and functional changes over the course of *H. hepaticus* + aIL-10R colitis
3) Identify colitogenic OMM^{12} community members of interest and further explore the mechanistic basis of *H. hepaticus* + aIL-10R disease development.

Chapter 2 Materials and methods

2.1 Mice

C57BL/6 mice were sourced from Charles River or bred internally. OMM^{12} colonized mice were kindly provided by Prof. Andrew Macpherson. HH7-2 transgenic Rag$^{-/-}$ mice (HH7-2tgRag$^{-/-}$) were kindly provided by Prof. Dan Littman. All mice were maintained in SPF or GF conditions in an accredited animal facility at the University of Oxford. All procedures were conducted in accordance with the UK Animals (Scientific Procedures) Act with approval from the Home Office. Females and males aged over 6 weeks were used in experiments as indicated. Experimental groups were randomly assigned and split across cages.

2.1.1 Generation and maintenance of gnotobiotic colonies

Monocolonized mice were established through single gavage of 1x10^9 colony forming unit (CFU) bacteria of interest into GF breeding pairs. To confirm colonization, breeder stools were collected 1-day post-gavage, homogenized in 500 µL sterile PBS (Life Technologies, CA, US), 10-fold serially diluted and then plated according to bacteria of interest *in vitro* growth conditions (as detailed in section 2.2.4). Subsequent litters were used for all experiments or to maintain animal colonies. All gnotobiotic mice were maintained in flexible film isolators and screened regularly for contamination through culturing, metagenomic sequencing by Transnetyx (TN, US) and, in the case of GF mice, hematoxylin and eosin (H&E) imaging of animal and/or isolator samples.

2.2 Bacterial culture

2.2.1 *Citrobacter rodentium*

C. rodentium (strain ATCC51459) was grown routinely from glycerol stocks on LB agar (Merck, Darmstadt, Germany) supplemented with 50 µg/ml nalidixic acid (Merck, Darmstadt, Germany) overnight at 37°C. A single colony was then inoculated into LB broth (Merck, Darmstadt, Germany) supplemented with 50 µg/ml nalidixic acid and incubated overnight at 37°C shaking (200 rpm).

2.2.2 Endogenous Enterobacteriaceae

Stool samples obtained from SPF experimental mice were homogenised in 500 µL sterile PBS, 10-fold serially diluted and then plated onto MacConkey agar (Merck, Darmstadt, Germany) plates and incubated overnight at 37°C. Single representative colonies were inoculated into LB broth and grown overnight at 37°C in a shaking incubator. Cultures were then stored in 25% glycerol (Merck, Darmstadt, Germany) at -80°C. For *in vitro* assays, glycerol stocks were grown on LB agar plates overnight at 37°C. Single colonies were then inoculated into LB broth and incubated overnight at 37°C, shaking prior to experimental start.

2.2.3 *Helicobacter hepaticus*

H. hepaticus NCI-Frederick isolate 1A (strain ATCC51449) was grown from glycerol stocks on leaked horse blood agar plates (Oxoid,UK) supplemented with trimethoprim, vancomycin and polymyxin B (TVP) (Oxoid, Hampshire, UK) which were incubated at 37°C for 48-72 hours under microaerobic conditions (3-5% O_2, 10% CO_2, 10% H_2, balanced N_2) utilizing a CampyPak jar (Oxoid, Hampshire, UK). *H. hepaticus* was harvested with sterile swabs into trypticase soy broth (TSB) supplemented with 10% fetal bovine serum (FBS, Life Technologies, CA, US) and TVP. *H. hepaticus* was then grown under microaerobic conditions at 37°C shaking and split 1/10 every 24 hours.

2.2.4 Oligo-Mouse-Microbiota members

Clostridium innocuum (strain I46, DSM number 26113) and *Enterocloster clostridioformis* (strain YL32, DSM number 26114) were grown from glycerol stocks on Schaedler blood agar plates (Wilkins-Chalgren anaerobe agar (Merck, Darmstadt, Germany), 5 µg/mL hemin (Merck, Darmstadt, Germany), 5% leaked horse blood (Merck, Darmstadt, Germany), 0.4 mg/mL L-cystine (Merck, Darmstadt, Germany), 4 mg/mL glucose (Merck, Darmstadt, Germany)) at 37°C under anaerobic conditions (0% O_2, 10% CO_2, 10% H_2, 80% N_2) in a Coy vinyl anaerobic chamber (Coy Laboratory products, MI, US) for 2 and 3 days, respectively. Single colonies were inoculated into Schaedler blood media (Wilkins-Chalgren anaerobe media (Merck, Darmstadt, Germany), 5 µg/mL hemin, 5% leaked horse blood, 0.4 mg/mL L-cystine, 4 mg/mL glucose) and grown for 2 (*C. innocuum* I46) or 3 (*E. clostridioformis* YL32) days at 37°C under anaerobic conditions.

2.3 *In vitro* bacterial growth assays

2.3.1 Tungstate susceptibility assay

For anaerobic growth assays, bacteria were cultured in mucin broth comprised of no-carbon E medium [203] supplemented with 0.5% type III mucin from porcine stomach (Merck, Darmstadt, Germany), trace elements [204] with or without 40 mM sodium nitrate (Merck, Darmstadt, Germany). Aerobic assays were completed in LB broth. 100 mg/L sodium tungstate dihydrate (Merck, Darmstadt, Germany) was added to culture media as indicated. Bacteria were inoculated from overnight aerobic culture to 10^4 CFU/mL and incubated at 37ºC for 24 hours aerobically or anaerobically in the Coy vinyl anaerobic chamber. CFUs were enumerated at t = 0 and t = 24 by spot plating of 10-fold serially diluted culture samples.

2.3.2 Antibiotic susceptibility assay

Liquid cultures of *H. hepaticus* and *E. clostridioformis* YL32 were established as described in sections 2.2.3 and 2.2.4. At time 0, liquid cultures were inoculated 1/10 into TSB + 10% FBS or Schaedler blood media supplemented with 0.5 g/L, 50 mg/L or 5 mg/L vancomycin hydrochloride (Cambridge Bioscience, Cambridgeshire, UK). Bacteria were incubated under the appropriate conditions for 1-3 days. *H. hepaticus* and *E. clostridioformis* were enumerated from start and end-point experimental cultures through OD measurement and plating of 10-fold serially diluted culture samples to determine CFU, respectively.

2.4 Colitis induction and animal models

2.4.1 *C. rodentium*

C. rodentium was grown under the conditions described in section 2.2.1. On the day of infection, *C. rodentium* liquid culture was diluted to 0.1 OD in LB broth + 50 µg/ml nalidixic acid and grown to log phase (OD 1-1.5, ~3-3.5 hours) at 37°C, shaking. Animals were gavaged with $5x10^9$ CFU prepared in 200 µL sterile PBS, with CFUs being calculated using the following: CFU/mL = $5x10^8$ x log phase OD – $3x10^7$.

2.4.2 DSS

2.5% DSS (MP Biomedicals, CA, US) with or without the addition of 0.2% sodium tungstate was administered to mice in the drinking water for 5 days. After this point, mice were returned to normal drinking water or 0.2% sodium tungstate. Mouse weights were monitored daily throughout the experiment to ensure weight loss did not exceed 20%.

2.4.3 *H. hepaticus* + aIL-10R

H. hepaticus was grown and maintained in liquid culture as described in section 2.2.3. On infection days, *H. hepaticus* was prepared to $1x10^8$ CFU in 200 µL sterile PBS. CFU was calculated using the following conversion: 1 OD = $1x10^8$ CFU. For SPF experiments, animals were gavaged with *H. hepaticus* inoculum on experimental days 0 and 1. In gnotobiotic experiments, animals received a single *H. hepaticus* gavage on day 0. Both SPF and gnotobiotic mice received intraperitoneal injection of 1 mg aIL-10R (clone 1B1.3A, 2B Scientific, Oxfordshire, UK) on days 0 and then weekly for the duration of the experiment.

2.4.4 *H. hepaticus*-specific T cell transfer

Spleens were taken from sex-matched HH7-2tgRag$^{-/-}$ donors and collected into PBS supplemented with 0.1% BSA (Merck, Darmstadt, Germany), 1% penicillin-streptomycin (Merck, Darmstadt, Germany) and 5 mM EDTA (Life Technologies, CA, US) (PBS/BSA/EDTA/pen-strep). To minimize contamination risk, 3 sets of sterile tools were used for spleen collection, 1 to open the skin, 1 to open the peritoneum and 1 to remove the spleen. Spleens were processed by passing tissues through a 70 µM filter (Fisher Scientific, Leicestershire, UK) into PBS/BSA/EDTA/pen-strep. Red blood cells were lysed with 0.5 mL/spleen Ammonium-Chloride-Potassium (ACK) lysis buffer for 3 mins prior to quenching with 40 mL PBS/BSA/EDTA/pen-strep. Splenic preparations were then 20 uM filtered and stained with antibodies (table 2.1) prepared in PBS/BSA/EDTA/pen-strep for 30 mins on ice. Cells were washed with 40 mL PBS/BSA/EDTA/pen-strep before being prepared at 20 x 10^6 cells/mL in PBS/BSA/EDTA/pen-strep for sorting. Cells were sorted according to the following: lymphocytes (FSC-A vs SSC-A), single cells (FSC-H vs SSC-H), live CD45$^+$, CD3$^+$PerCP-Cy5.5$^-$, CD4$^+$CD25^{lo}, CD44CD62L, TCRVb6$^+$ and collected in FCS supplemented with 1% pen-strep. Cells were washed once and then prepared at 2,000 or 100,000 cells/200 µL in sterile 1X PBS.

Marker	Fluorophore	Company	Clone
L/D	APC-Cy7	Invitrogen	N/A
CD45	PE-Cy7	BioLegend	30-F11
CD3	PerCP-Cy5.5	BioLegend	17A2
CD4	BV785	BioLegend	RM4-5
CD25	eF450	eBioscience	Ebio3c7
TCRVB6	APC	BioLegend	RR4-7
CD44	AF700	BioLegend	IM7
CD62L	BV510	BD Biosciences	MEL-14
CD11c	BV605	BioLegend	N418
CD11b	BV605	BioLegend	M1/70
B220	BV605	BioLegend	RA3-6B2

Table 2.1. Antibodies used for *H. hepaticus*-specific T cell transfer

2.5 Histopathological scoring

Colon (proximal, distal and mid sections) and caecum tissues were fixed in 3.7% formalin for at least 4 days and stored in 70% ethanol for histological assessment. Triplicate sections of colonic and caecal samples were processed by in-house facilities and stained with hematoxylin and eosin (H&E). Samples were scored blindly according to the system in table 2.2. Colon histopathology scores were calculated according to the average obtained across proximal, mid and distal sections.

Area	Criteria	Score
Epithelium	None	0
	Mild hyperplasia (1.5x) and/or goblet cell depletion (25%)	1
	Moderate hyperplasia (2-3x) and/or goblet cell depletion (25-50%)	2
	Severe hyperplasia (>3x) and/or substantial goblet cell depletion (>50%)	3
Inflammation in the lamina propria	None – few leucocytes	0
	Mild – some increase in leucocytes at the tips of crypts or many lymphoid follicles	1
	Moderate – marked infiltrate (notable broadening of crypt)	2
	Severe – dense infiltrate throughout	3
Area affected	None	0
	Up to 25%	1
	25-50%	2
	>50%	3
Markers of severe inflammation	None	0
	Submucosal inflammation or few crypt abscesses (<5)	1
	• Submucosal inflammation and few crypt abscesses (<5) • Many crypt abscesses (>5) or extensive submucosal inflammation or crypt branching	2
	• Many crypt abscesses (>5) and extensive submucosal inflammation/crypt branching • Ulceration or extensive fibrosis	3

Table 2.2. Scoring system used for histopathological scoring of colitis models

2.6 Assessment of immune cell populations by flow cytometry

2.6.1 Processing of secondary lymphoid organs

Cell isolations were prepared from spleens and mesenteric lymph nodes (mLNs) by passing tissues through 70 μM filters into PBS/BSA. To lyse red blood cells, splenic preparations were resuspended in 1 mL ACK lysis buffer and incubated for 3 mins at room temperature before the reaction was quenched through the addition of 10 mL PBS/BSA. Entire mLN and 1/10 of splenic preparations were prepared in PBS/BSA for staining (section 2.6.3).

2.6.2 Isolation of colonic lamina propria leukocytes

Opened colonic sections were washed twice in RPMI-1640 medium (Merck, Darmstadt, Germany) supplemented with 5% FBS and 5 mM EDTA in a shaking incubator at 37ºC. Tissues were digested with 1 mg/mL type VIII collagenase (Merck, Darmstadt, Germany) prepared in RPMI-1640 medium supplemented with 5% FCS and 15 mM HEPES (Merck, Darmstadt, Germany) for 1 hour at 37ºC. Cells were filtered, resuspended in 4 mL 37.5% Percoll (VWR International, PA, US) and centrifuged at 1800 rpm for 5 mins. Debris was removed and pellets washed with and then resuspended in PBS/BSA for staining.

2.6.3 Staining and fixation

Samples were stained for surface markers using antibodies prepared in PBS/BSA for 15 mins at 4ºC. Stained samples were fixed with fix/perm (Invitrogen, MA, US) by incubating for 20 minutes at room temperature. Samples were then washed in 1X Perm Wash for 15 mins at room temperature (Invitrogen, MA, US). Intracellular antibodies were prepared in 1X Perm Wash and samples stained for 30 mins at room temperature. Samples were resuspended in PBS/BSA for acquisition.

Marker	Fluorophore	Clone	Provider	Staining Stage
Ly6G	AF488	RB6-8C5	BioLegend	Extracellular
CD3	PE-Cy7	17A2	BioLegend	Extracellular
CD8	PE-Dazzle	53-6.7	BioLegend	Extracellular
L/D	APC-Cy7	N/A	Invitrogen	Extracellular
CD4	BV711/BV510	RM4-5	BioLegend	Extracellular
CD45	BV605/BV711	30-F11	BioLegend	Extracellular
CD11b	BV510/BV605	M1/70	BioLegend	Extracellular
FOXP3	eF450	FJK-16s	Invitrogen	Intracellular
ROR-γt	PE	Q31-378	BD Bioscience	Intracellular
GATA3	eF660	TWAJ	Invitrogen	Intracellular

Table 2.3. Antibodies used for flow cytometric analysis of immune cell populations

2.6.4 Data acquisition

Data acquisition was performed on the Fortessa X-20 (BD Bioscience, Berkshire, UK) and analysis done using FlowJo10 software (BD Bioscience, Berkshire, UK).

2.7 Lipocallin-2 (LCN2) ELISA

Samples were homogenized in 1 mL cOmplete ULTRA tablets EDTA-free (Roche, Basel, Switzerland) using screw cap O-ring microcentrifuge tubes (ThermoFisher Scientific, MA, US) for 10 mins at 30 Hz using the Tissue Lyser II (Qiagen, Manchester, UK). Samples were centrifuged at 10,000 g for 5 minutes at 4°C. Supernatants were then analysed for LCN2 levels using the LCN2 Mouse ELISA Kit (ThermoFisher Scientific, MA, US) according to manufacturer's instructions.

2.8 Host RNA analysis

2.8.1 RNA extraction

Colon and caecum tissues were snap frozen in RNAlater (Qiagen, Manchester, UK) and stored at -80°C prior to extraction. Thawed samples were homogenized with a single steel bead (Qiagen, Manchester, UK) in RLT lysis buffer (Qiagen, Manchester, UK) containing 1% β-mercaptoethanol (Merck, Darmstadt, Germany) for 10 mins at 30 Hz using the Tissue Lyser II or 40s at 6.5m/s in a FASTPREP-24 (MP Biomedicals, CA, US). RNA was extracted using the RNeasy miniprep kit (Qiagen, Manchester, UK) according to manufacturer's instructions. Extracted RNA was stored at -80°C or immediately converted to cDNA.

2.8.2 qRT-PCR

1µg of RNA was reverse transcribed with the High-Capacity cDNA Reverse Transcription Kit with 5% RNase inhibitor (Applied Biosystems, MA, US) according to manufacturer's instructions. RT-PCR was performed in the C1000 TouchTM Thermal Cycler (Bio-Rad, CA, US). cDNA was diluted 1:5 using nuclease-free water prior to use in quantitative PCR (qPCR) which was done on the Viia7 Real-time PCR detection system (Applied Biosystems, MA, US) using Taqman assays (Applied Biosystems, MA, US, table 2.4) and PrecisionPlus mastermix (PrimerDesign, Hampshire, UK). *Hprt* served as the housekeeping gene, with gene of interest (GOI) relative expression levels calculated according to $2^{-\Delta CT}$ where ΔCT = GOI CT – *Hprt* CT.

Gene	Assay ID
Hprt	Mm01545399_m1
Nos2	Mm00440502_m1
Cxcl1	Mm04207460_m1
Cxcl2	Mm00436450_m1

Table 2.4. Taqman probes used for host qPCR

2.8.3 RNA Sequencing (RNA-seq)

Selection of PolyA+ mRNA, generation of double stranded cDNA and library construction were performed using NEBNext Poly(A) mRNA Magnetic Isolation Module (E7490) *(New England Biolabs,* MA, US*)* and NEBNext Ultra II Directional RNA Library Prep Kit for Illumina (E7760L) *(New England Biolabs,* MA, US*)* with Illumina adapters and barcode tags (dual indexing, based on [205]). The RNA-seq libraries were pooled and sequenced on an Illumina NovaSeq6000 (Illumina, CA, US) as 150bp paired end reads. This generated ~30 million paired reads per sample.

2.8.4 RNA-seq data processing

Raw data quality was assessed using fastqc v0.11.9 (https://www.bioinformatics.babraham.ac.uk/projects/fastqc/) and all samples displayed high quality (quality score > 31 over 100% of the length of the reads). Transcripts were quantified using kallisto v0.46.2 [206] which was run using a kallisto index (k=31) built using mouse genome build GRCm39 and annotated with Ensembl [207] build 106. Kallisto was run with default parameters. Gene-level counts were used for downstream analysis that were obtained using tximport [208].

2.8.5 RNA-seq downstream analysis

All downstream analysis was done in R 4.1.2. Initial analysis was done on a subset of data containing *H. hepaticus* colonized *E. clostridioformis* YL32 and *C. innocuum* I46 samples only. This dataset was filtered to retain genes that had a read count of 3 in at least 9 samples (corresponding to the lowest number of samples in an experimental group). Batch effects were removed using limma::removeBatchEffect version 3.50.0 [209] prior to principal component analysis (PCA). Differential gene expression was assessed through DESeq2 version 1.34.0 [210], with formula design taking into consideration extraction method and microbiota composition. ENSEMBL IDs were converted to gene names with the BioMart package version 2.50.0 [211]. Gene set enrichment analysis was done on DESeq2 results using fgsea version 1.20.0 [212]. Leading edge genes belonging to pathways of interest (TNFα via NF-κB signaling and inflammatory response) were then assessed in the whole dataset, which underwent rlog transformation and batch effect correction prior to statistical analysis by Kruskal Wallis with Dunn's post-hoc testing using the dunn.test package version 1.3.5 [213]. Both Kruskal Wallis and Dunn's p values were adjusted for multiple testing by the Benjamin-Hochberg approach. $P_{adj} < 0.05$ was considered statistically significant. Heatmaps were created using ComplexHeatmap version 2.10.0 [214] with clustering determined with dynamicTreeCut version 1.63-1 [215].

2.9 Bacterial DNA analysis

2.9.1 DNA extraction

DNA was extracted from stool, colon and/or caecum contents using the DNeasy PowerSoil Pro Kit (Qiagen, Manchester, UK) or ZymoBIOMICS DNA/RNA Miniprep Kit (Cambridge Bioscience, Cambridgeshire, UK) according to manufacturer's instructions, with homogenization step done at 30Hz for 10 mins in the Tissue Lyser II and kit supplied lysis buffer and bead beating tubes.

2.9.2 Quantification of Oligo-Mouse-Microbiota members

OMM^{12} members were quantified by qPCR using Takyon Low ROX Probe 2X MasterMix (Eurogentec, Seraing, Belgium) and primers and probes with individual OMM^{12} specificity as described previously [176] (table 2.5). A standard curve was generated from linearised plasmids harbouring 16S sequences of OMM^{12} members [176], which were a kind gift from Prof. Bärbel Stecher. Plasmid stocks were maintained through transformation of Subcloning Efficiency DH5α Competent Cells (ThermoFisher Scientific, MA, US) in SOC medium (ThermoFisher Scientific, MA, US) according to manufacturer's instructions. Transformed cells were selected through growth on LB agar supplemented with 100 µg/mL ampicillin (Merck, Darmstadt, Germany) overnight at 37 in standard aerobic conditions. A single colony was then inoculated into LB broth + 100 µg/mL ampicillin and grown overnight prior to DNA extraction using the Isolate II Plasmid Mini Kit (Meridian Bioscience, OH, US) according to manufacturer's instructions. Plasmid DNA was linearised through restriction digest with NotI, HindIII or NcoI enzymes (New England Biolabs, MA, US) as appropriate [176] and according to manufacturer's instructions. Plasmid standards were prepared in 10-fold serial dilutions from 2 x 10^8 copies/µL.

OMM[12] member	*Forward primer*	*Reverse primer*	*Probe*
C. innocuum I46	CGGATCGTAAAGCTCTGTTGTAAG	GCTACCGTCACTCCCATAGCA	AAGAACGGCTCATAGAGG
L. reuteri I49	GCACTGGCTCAACTGATTGATG	CCGCCACTCACTGGTGATC	CTTGCACCTGATTGACGA
B. coccoides YL58	GAAGAGCAAGTCTGATGTGAAAGG	CGGCACTCTAGAAAAACAGTTTCC	TAACCCCAGGACTGCAT
M. intestinale YL27	TCAAGTCAGCGGTAAAAATTCG	CCCACTCAAGAACATCAGTTTCAA	CAACCCCGTCGTGCC
F. plautii YL31	AGGCGGGATTGCAAGTCA	CCAGCACTCAAGAACTACAGTTTCA	CAACCTCCAGCCTGC
E. clostridioformis YL32	AATACCGCATAAGCGCACAGT	CCATCTCACACCACCAAAGTTTT	CGCATGGCAGTGTGT
E. faecalis KB1	CTTCTTTCCTCCCGAGTGCTT	CCCCTCTGATGGGTAGGTTACC	CACTCAATTGGAAAGAGGAG
B. animalis YL2	GGGTGAGTAATGCGTGACCAA	CGGAGCATCCGGTATTACCA	CGGAATAGCTCCTGGAAA

A. muris KB18	TGGCAAGTCAGTAGTG AAATCCA	TCACTCAAGCTCGACA GTTTCAA	CTTAACCCATGAAC TGC
A. muciniphil a YL44	CGGGATAGCCCTGGG AAA	GCGCATTGCTGCTTTA ATCTTT	TGGGATTAATACCG CATAGTA
T. muris YL45	AGACGGCCTTCGGGTT GTA	CGTCATCGTCTATCGG TATTATCAA	ACCACTTTTGTAGA GAACGA
B. caecimuri s I48	GGCAGCATGGGAGTTT GCT	TTATCGGCAGGTTGGA TACGT	CAAACTTCCGATG GCGAC

Table 2.5. Primer and probe sequences used to quantify OMM[12] members

2.9.3 Quantification of *H. hepaticus*

H. hepaticus colonization levels were determined by qPCR assessment of CdtB in stool, colon and/or caecum contents as described (table 2.6) [216]. *H. hepaticus* qPCR was done using PrecisionPlus Mastermix (PrimerDesign, Hampshire, UK) on the Viia7 Real-Time PCR detection system (Applied Biosystems, MA, US). Standard curves comprised 10-fold serially dilutions starting from 100 ng/µL *H. hepaticus* genomic DNA extracted from pure bacterial cultures using the DNeasy Kit (Qiagen, Manchester, UK).

Primers	Sequence
cdtB forward	CCGCAAATTGCAGCAATACTT
cdtB reverse	TCGTCCAAAATGCACAGGTG
cdtB fluorescent probe	AATATACGCGCACACCTCTCATCTGACCAT

Table 2.6. Primer and probe sequences used to quantify *H. hepaticus*

2.9.4 16S sequencing

Libraries were prepared from barcoded 515F/806R PCR amplified samples and sequenced by Oxford Genomics Centre on the Illumina Mi-Seq (Illumina, CA, US). Adaptor sequences were removed, reads trimmed for quality, with resulting lengths of 183bp and 179bp for forward and reverse reads, respectively. Amplicon sequence variants (ASVs) annotated according to the RefSeq RDP 16S database (v2 May 2018) using dada2 (v1.12.1) implemented in the OCMS_16S pipeline [217] using default parameters and 10M bases used to estimate error profiles. Genus-level annotation was able to distinguish between individual Oligo-MM^{12} members, with the exceptions of *A. muris* KB18 and *E. clostridioformis* YL32, which both belong to *Clostridium* XIVa [154]. Downstream analysis was done in R 4.1.2. PCA was done using phyloseq version 1.38.0 [218]. For stool samples, statistical analysis of OMM^{12} genera was done using linear modelling (Abundance ~ Condition * Time + (1|SampleID) with post-hoc estimated marginal means using the lmerTest version 3.1-3 [219] and emmeans version 1.7.5 [220] packages. Significance was driven by the interaction term of the model. For the contents, statistical analysis was done using Kruskal Wallis with Dunn's post-hoc testing using the dunn.test package version 1.3.5 [213]. All p values were adjusted according to Benjamin-Hochberg approach. $P_{adj} < 0.05$ was considered statistically significant.

2.10 Bacterial RNA analysis

2.10.1 RNA extraction

For SPF samples, samples were homogenized in DNA/RNA shield (Cambridge Bioscience, Cambridgeshire, UK) using ZR BashingBead Lysis Tubes (Cambridge Bioscience, Cambridgeshire, UK) at 30Hz for 10 mins using the Tissue Lyser II. RNA was then extracted using the ZymoBIOMICS DNA/RNA Miniprep Kit (Cambridge Bioscience, Cambridgeshire, UK) according to manufacturer's instructions with additional on-column DNAse I digest

treatment. For gnotobiotic experiments, samples were homogenized in Trizol (ThermoFisher Scientific, MA, US) using soft tissue homogenizing CK14 tubes (Stretton Scientific, Derbyshire, UK) for 2 minutes at 6.5m/s in a FASTPREP-24. Samples were then centrifuged for 10 mins at 16,000 g at 4°C to remove debris. Supernatant was transferred to a new tube, where 200 µL ice cold chloroform was added and samples were shaken vigorously for 30 seconds before being placed on ice for 1 minute. Samples were then centrifuged at 10,000g at 4°C for 15 mins. The clear phase was transferred to a new tube and chloroform separation was repeated as above. An equal volume of >99.5% ethanol (Merck, Darmstadt, Germany) was added to the final clear phase, mixed and then transferred to the Zymo-spin IIICG column (Cambridge Bioscience, Cambridgeshire, UK). Samples were then washed with 400 µL RNA wash buffer and treated with on-column DNAse I digest treatment (Cambridge Bioscience, Cambridgeshire, UK) according to manufacturer's instructions. Samples were then washed with 400 µL RNA prep buffer (30 second centrifugation), 700 µL RNA wash (30 second centrifugation) and then 400 µL RNA wash (2-minute centrifugation) (all Cambridge Bioscience, Cambridgeshire, UK) prior to elution with nuclease-free water.

2.10.2 Assessment of *C. rodentium* molybdenum-related gene expression

RNA was reverse transcribed as described for the host in section 2.8.2 cDNA was then analyzed by qPCR using primers designed on the *C. rodentium* genome [221] (table 2.7) and FastStart Universal SYBR Green with Rox (Roche, Basel, Switzerland) on the Viia7 Real-time PCR detection system. Expression of genes of interest were normalised to that of *rpoD* using the $2^{-\Delta CT}$ method as outlined in section 2.8.2.

Gene	Forward primer	Reverse primer	Reference
rpoD	ATCAAAGCGAAAGGTCGTAGCCAC	CCATCATCACGCGCATACTGTTCA	[222]
modB	CTGGTTTGGCGTCACCTTTG	CTGCTCCAGCTTCATGTCCA	This thesis
narH	GTCGGACGCATCCGTTATCT	ATTGAGGAACACGTCGCACT	This thesis
cydA	GGTTTGTCGCGGAATATGGC	ACATGGAGAACAGCAGGTCG	This thesis
fdoG	CTGGGGCAACTACCCGAAAT	ACACGTCGTACCCTTTGTCC	This thesis
moaA	GGTCAAAGTCAACACCGTGC	GATGAAGCGCAGCTGAATGG	This thesis
moaC	TTATTGACGGCAGCCACCAT	GCGTCCGCCTTAAAATCACC	This thesis

Table 2.7. Primer sequences to assess *C. rodentium* molybdenum-related gene expression

2.10.3 Assessment of *H. hepaticus* putative virulence gene expression

RNA was reverse transcribed as described for the host in section 2.8.2. cDNA was then analyzed by qPCR using primers designed based on the *H. hepaticus* genome [223] (table 2.8) and FastStart Universal SYBR Green with Rox on the Viia7 Real-time PCR detection system. Expression of genes of interest were normalised to the geometric mean of *secA*, *gyrA* and *gyrB* CT values using the $2^{-\Delta CT}$ method as outlined in section 2.8.2.

Gene	Forward primer	Reverse primer	Reference
secA	TGCCAAACAGCACACCAAAG	TAGCGATTGTTACTGCGCCT	This thesis
gyrA	TGTGCGTATGGCACAGGATT	TGCACTTGTCATACGTGCCT	This thesis
gyrB	ATCTTCCTGCAGCCACACTC	CCTACTCCGTGTAATCCGCC	This thesis
cdtB	CCGCAAATTGCAGCAATACTT	TCGTCCAAAATGCACAGGTG	[216]
HH0252	GCACGGAGTTACGTTTGAGC	ACGCCCATTCGCCACTATAA	This thesis
HH0260	AGGGGATAATAGCGGTTGCT	GTGGTTGGCAATTCCTGTGT	This thesis

Table 2.8. Primer sequences used to assess *H. hepaticus* putative virulence gene expression

2.11 Untargeted metabolomics

2.11.1 Sample preparation

Samples were collected in >99.5% ethanol, snap frozen on dry ice and stored at -80°C. The liquid fraction (ethanol) was then filtered (Amicon Ultra 0.0 mL, Millipore, UFC501096) (Merck, Darmstadt, Germany) according to the manufacturer's instructions. Briefly, filters were washed with MilliQ H2O and centrifuged (14000 g, 25 min, 4°C). Water was removed, sample was loaded and was centrifuged again using the same settings. Filtered samples were then transferred to total recovery mass spectrometry vials.

2.11.2 IC-MS and metabolite identification

IC-MS was performed by Dr. Mariya Misheva in the Department of Chemistry as described previously [224], with the exception of mass range, which was altered to 50-750 m/z to allow for SCFA detection. Metabolite identification was performed using Progenesis QI (Nonlinear Dynamics, Waters) to search for matches within an in-house database and The Human Metabolome Database (HMDB). The in-house metabolite standards database was constructed and identifications accepted as described previously [224], with the slight deviation of an accepted <60s differences between authentic standard and analyte retention

times. For HMDB, putative identifications were accepted when the following criteria were met: <3 ppm differences between measured and theoretical mass (based on chemical formula). Theoretical fragmentation was performed, and accepted when precursor tolerance was within 5 ppm.

2.11.3 Untargeted metabolomics downstream analysis

Data was filtered according to metabolite prevalence and abundance, with threshold cut-offs of 20% and average peak area of 100, respectively. Data was then log10 transformed prior to PCA. A separate dataset was created from the annotated metabolite fraction and used in all subsequent analysis. Outliers were removed from the annotated dataset informed by PCA clustering and the number of zeros present in a given sample. Stool and content data were analyzed separately. In both cases, statistical analysis comprised of linear mixed effects model analysis followed by post-hoc estimated marginal means using the lmerTest version 3.1-3 [219] and emmeans version 1.7.5 [220] packages. Models for stool and contents were Abundance ~ Time * Condition + (1|SampleID) and Abundance ~ Site * Condition + (1|SampleID). Significantly significant metabolites in the stool were determined by the interaction term of the model whereas condition alone led to the identification of metabolites significantly altered in intestinal contents. Heatmaps were created using the ComplexHeatmap package version 2.10.0 [214], with clustering determined with dynamicTreeCut version 1.63-1 [215]. A final set of metabolites of interest was generated as the intersection of clusters of interest in the stool and intestinal contents.

2.12 ICP-MS

Intestinal contents were autoclaved prior to microwave-assisted digestion in 5 mL ACS grade 70% nitric acid (Merck, Darmstadt, Germany) using the MARS 6 (12-minute ramp (900W) to 150-170ºC, 15 min hold) (CEM, Buckingham, UK). Digested samples were

prepared to 15 mL with 2% nitric acid (prepared in-house). Blank and control digests were done using empty tubes and bovine liver reference material NIST-1577C (LGC, Middlesex, UK), respectively. Tungstate and control water samples were diluted 1:100 in 2% nitric acid. All samples were run on the NexION 2000B ICP-MS (PerkinElmer, MA, USA). 10 ppm multi-element standard (Merck, Darmstadt, Germany) and QMx multi-element solution (QMX, Thaxted, UK) served as calibration and quality control standards, respectively.

2.13 General data analysis

All data was processed, and all graphs produced in RStudio using R 4.1.2 and tidyr version 1.2.0 [225], ggplot2 version 3.3.6 [226], ggpubr version 0.4.0 [227] and scales version 1.2.0 [228] packages. All statistical analysis was done in R 4.1.2 using mixed linear effects modelling with post-hoc estimated marginal means analysis, Kruskal-Wallis with post-hoc Dunn's or Wilcox testing as indicated. Packages lmerTest version 3.1-3 [219], emmeans version 1.7.5 [220] and dunn.test version 1.3.5 [213] were used in addition to base R statistics. When appropriate, p values were adjusted for multiple testing using the Benjamin-Hochberg approach (p_{adj}). In all analyses, p or p_{adj} values < 0.05 were statistically significant.

Chapter 3 Targeting molybdenum-dependent respiratory processes in colitis

3.1 Introduction

In health, the gut microbiota is dominated by obligate anaerobic members of the Firmicutes and Bacteroides phyla. Dysbiosis in IBD is characterised in-part by an expansion of facultative anaerobic Pseudomonadota, in particular those belonging to the Enterobacteriaceae family [191]. These inflammation-associated microbiota shifts underpin the oxygen hypothesis - the notion that inflammation leads to an increase in oxygen availability in the gut, in turn promoting facultative anaerobic expansion [190]. Indeed, in homeostasis colonocytes maintain a state of hypoxia which limits oxygen diffusion into the gut lumen [229]. In animal models, when intestinal homeostasis is disrupted, including following antibiotic administration, enteropathogenic infection and DSS colitis, colonocyte hypoxia is ablated [193,194,200]. In addition to increased epithelial oxygenation, alternative electron donors and acceptors also become more readily available [229]. For example, microbiota-derived formate, which functions as an electron donor upstream of aerobic respiration, is elevated in DSS colitis [230]. Moreover, nitrate, an electron acceptor whose redox potential is preceded only by oxygen [231], is elevated in colonic mucus obtained from DSS treated mice [192] and in IBD patient sera and stool [232,233].

Due to their respiratory capacity and proximity to the epithelium, Enterobacteriaceae are poised to capitalise on inflammation-associated disturbances in oxygen and alternative electron donor and acceptor availability. Indeed, mutants defective in the ability to respire oxygen, nitrate and/or formate have impaired fitness in the inflamed gut [192,230,234]. Moreover, Enterobacteriaceae enteropathogens have been shown to employ virulence factors to establish their own oxygenated niche. For example, *C. rodentium* fuels its own aerobic growth *in vivo* by utilising its T3SS to induce colonocyte proliferation, which in turn leads to oxygenation of the intestinal epithelium [200]. Notably, Enterobacteriaceae

association with the gut epithelium is consistent in IBD, as AIEC have been isolated from the mucosa of IBD patients [191,235,236].

The dependence of Enterobacteriaceae growth on oxygen, nitrate and formate respiration during intestinal inflammation has generated interest in targeting these pathways therapeutically. Maintenance of hypoxia and repression of *Nos2* expression, which encodes inducible nitric oxide synthase (iNOS), in epithelial cells is controlled by PPAR-γ signalling [194]. Administration of the PPAR-γ agonist, 5-aminosalicyclic acid (5-ASA), restores epithelial hypoxia, blunts Enterobacteriaceae expansion and ameliorates pathology in DSS colitis [237]. Importantly, 5-ASA is a current frontline therapeutic used in the clinic to induce and maintain remission in UC [238].

In addition to targeting host pathways, Enterobacteriaceae use of alternative respiratory enzymes during gut inflammation serves as a therapeutic target in colitis model systems [198]. Central to the catalytic activity of nitrate reductases and formate dehydrogenases is molybdenum, which is coordinated to molybdopterin to form a molybdenum cofactor (MoCo) [239]. Incorporation of the chemically similar metal, tungsten in place of molybdenum in molybdoenzymes generally renders them inactive, although enzymes with dual functionality exist [239]. Sodium tungstate, the naturally occurring salt form of tungsten, inhibits Enterobacteriaceae growth *in vitro* under conditions that favour the use of MoCo-dependent respiratory enzymes [198]. Moreover, tungstate administration *in vivo* reduces Enterobacteriaceae numbers and ameliorates pathology in DSS and piroxicam-accelerated *Il10*$^{-/-}$ colitis [198] (figure 3.1).

IBD encompasses a spectrum of pathologies, aspects of which are recapitulated in different animal models. DSS and piroxicam-accelerated *Il10*$^{-/-}$ colitis model acute disruption of

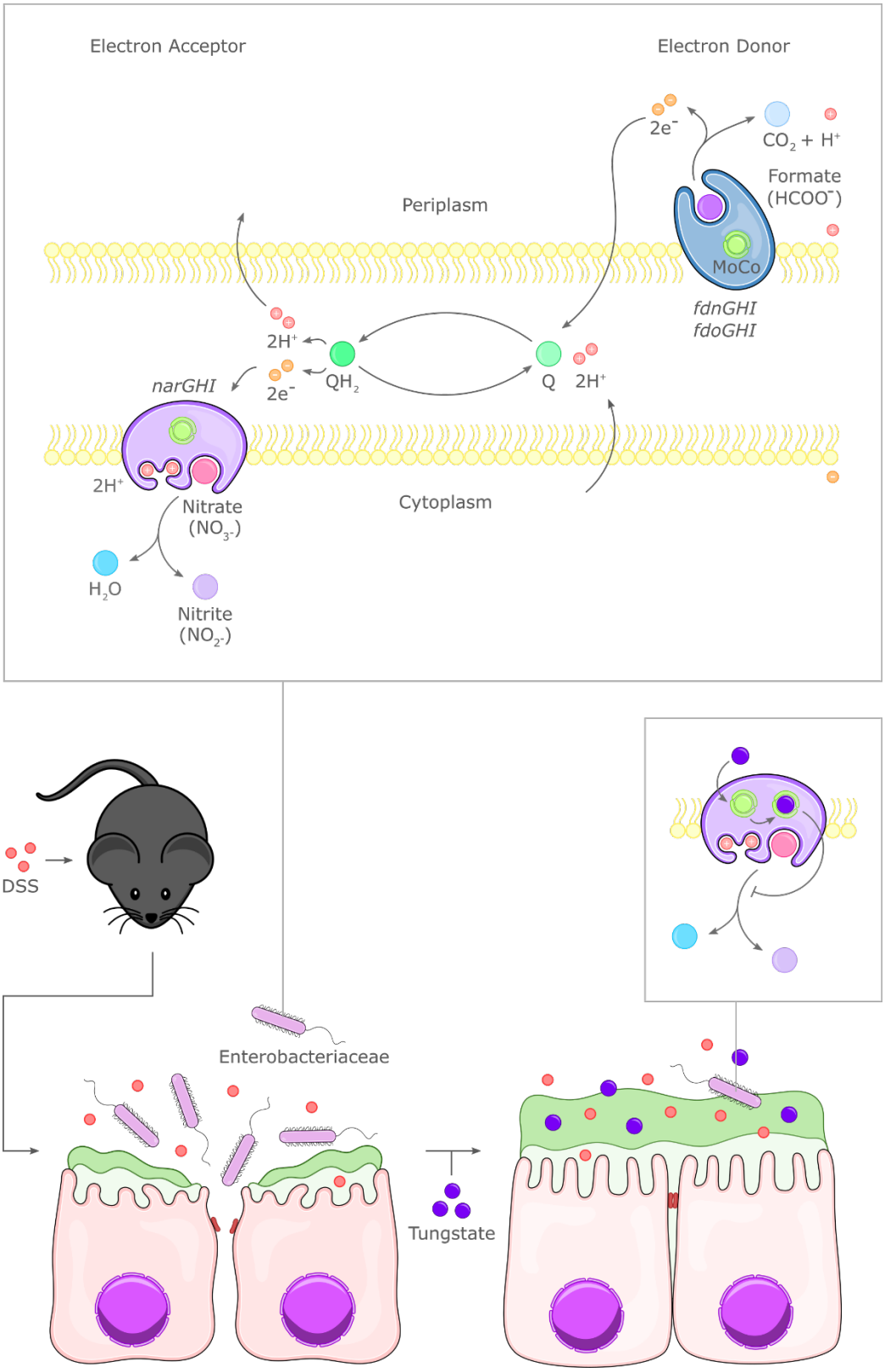


Figure 3.1 Enterobacteriaceae expansion in chemically-induced colitis is fuelled by molybdenum-dependent respiratory processes which are inhibited by sodium tungstate. (Top/left image) MoCo-dependent respiratory enzymes such as formate dehydrogenases (encoded by *fdnGHI* and fdoGHI genes) and nitrate reductase (encoded by *narGHI*) fuel Enterobacteriaceae growth in DSS-induced colitis. (Right) Preventative treatment with tungstate during DSS colitis limits Enterobacteriaceae growth and pathology by inhibiting MoCo-dependent respiratory enzyme activity. Created using information from [200].

mucosal barrier integrity [240,241], whereas pathology in *H. hepaticus* + aIL-10R and *C. rodentium* models is driven by colitis-promoting interactions between these particular bacteria and the host [1,115]. Whilst the therapeutic effects of tungstate have been demonstrated in DSS colitis, commensal Enterobacteriaceae expansion is also a feature of dysbiosis in *H. hepaticus* + aIL-10R colitis and *C. rodentium* fitness *in vivo* is reliant on MoCo synthesis [122,200] (figure 3.2A) (Ilott *et al*, unpublished). Moreover, in the *H. hepaticus* + aIL-10R model, transcriptomic analysis has shown that *Desulfovibrio* species upregulate tungstate transporter expression prior to Enterobacteriaceae expansion and disease onset (figure 3.2B) (Ilott *et al*, unpublished). This suggests that tungstate regulation by gut commensals may permit colitogenic Enterobacteriaceae expansion during *H. hepaticus* + aIL-10R colitis.

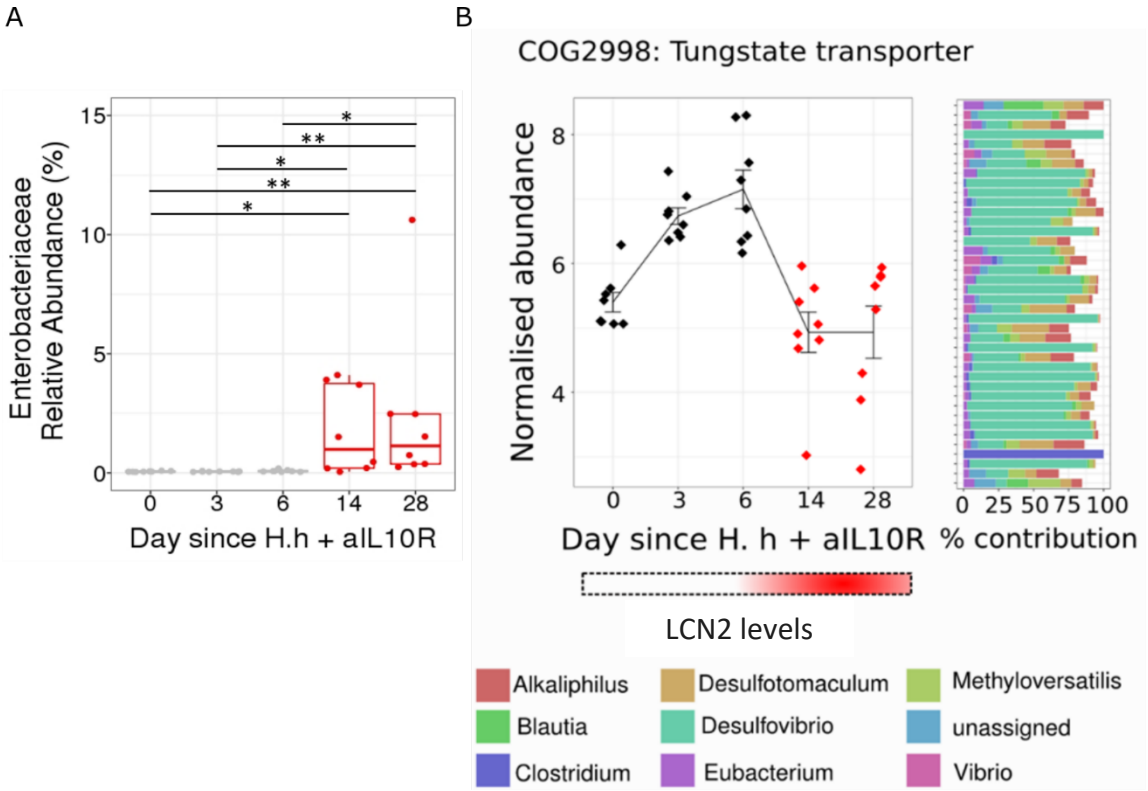


Figure 3.2. Tungstate transporter upregulation by *Desulfovibrio* species precedes Enterobacteriaceae expansion and colitis in the *H. hepaticus* + aIL-10R model. A) The relative abundance of DNA reads mapping to the Enterobacteriaceae family. Boxplots denote median + interquartile range and individual data points are shown. B) Normalized abundances (log10 cpm) of COG2998 (*tupA*) reads over time following *H. hepaticus* + aIL-10R treatment. Bars denote mean +/- SD. The bacterial genera and their contribution to this transcriptional signature are shown on the right. LCN2 levels are shown below time points on the x axis, with increasing levels corresponding to an increase in red intensity. Figure kindly provided by Dr. N.E. Ilott.

Due to the implication of Enterobacteriaceae in the above models, we aimed to replicate the finding that tungstate ameliorates Enterobacteriaceae expansion and pathology in the DSS model and further determine the therapeutic effects of tungstate in *H. hepaticus* + aIL-10R and *C. rodentium* colitis. This in turn would establish whether targeting of molybdenum-dependent respiratory pathways serves as a broad-spectrum microbiota-based therapeutic for IBD pathologies.

3.2 Results

3.2.1 Tungstate inhibits Enterobacteriaceae anaerobic, nitrate-dependent growth *in vitro*

In order to assess the effects of tungstate on Enterobacteriaceae growth *in vitro*, *C. rodentium* and *E. coli* K12 were cultured for 24 hours under aerobic and anaerobic conditions in the presence or absence of 100 mg/L sodium tungstate. When cultured aerobically in LB broth, tungstate had no effects on Enterobacteriaceae growth (figure 3.3). However, when cultured anaerobically in mucin broth supplemented with sodium nitrate, tungstate significantly reduced the growth of both *C. rodentium* and *E. coli* K12 (figure 3.3). This suggests that, in accordance with previously published data [198], sodium tungstate inhibits Enterobacteriaceae growth in conditions which promote molybdenum-dependent nitrate respiration.

3.2.2 Tungstate has limited effects on Enterobacteriaceae growth across multiple colitis models

As tungstate inhibition of Enterobacteriaceae molybdenum-dependent growth *in vitro* was a repeatable phenotype, we further sought to determine the effects of tungstate on Enterobacteriaceae growth in DSS, *H. hepaticus* + aIL-10R and *C. rodentium* colitis. In the latter, we assessed the effects of tungstate on levels of *C. rodentium* whereas

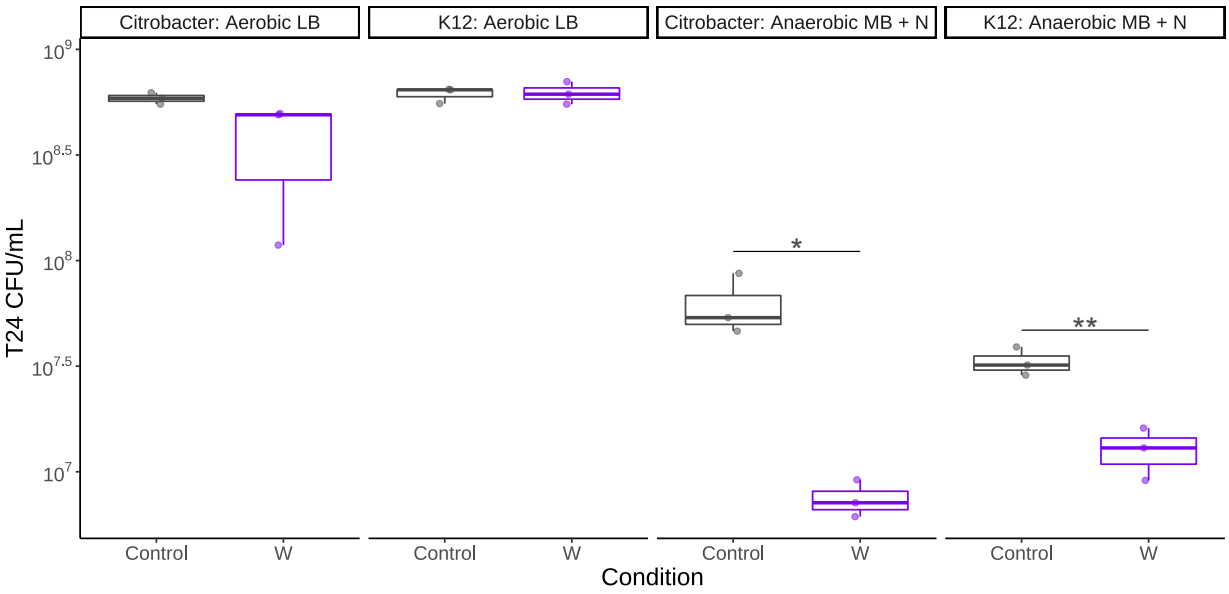


Figure 3.3. Tungstate inhibits Enterobacteriaceae nitrate-dependent anaerobic growth *in vitro*. *Citrobacter rodentium* and *Escherichia coli* K12 were cultured in LB or mucin broth supplemented with nitrate (MB + N) in the presence or absence of 100 mg/L sodium tungstate (W) aerobically or anaerobically for 24 hours. CFU = colony forming units. *p<0.05, **p<0.01 (Welch's t test). Data from 1 experiment. Boxplots denote median + interquartile range and individual data points shown.

Enterobacteriaceae of interest in DSS and *H. hepaticus* + aIL-10R-induced colitis were those endogenous to the SPF community. For all experiments, 0.2% sodium tungstate was administered in the drinking water, either at the point of, (*H. hepaticus* + aIL-10R and DSS) or 7 days prior to, (*C. rodentium*) model inception. Tungstate did not have any effects on water consumption across experimental set ups (figure 3.4A) and tungsten was readily detected in the stool, colon and caecum contents of tungstate treated mice, where it reached levels ~1000 times greater than that of molybdenum (figure 3.4B).

In steady state mice, faecal Enterobacteriaceae counts did not fluctuate from baseline values nor were influenced by tungstate administration at any time point (figure 3.5A). Moreover, tungstate did not influence Enterobacteriaceae loads in steady state intestinal contents and tissues (figure 3.5B). DSS treatment led to the progressive increase in control faecal Enterobacteriaceae counts which peaked at ~10^6 CFU/g at day 9. Coincident with the peak of Enterobacteriaceae load, tungstate administration led to a significant ~10-fold

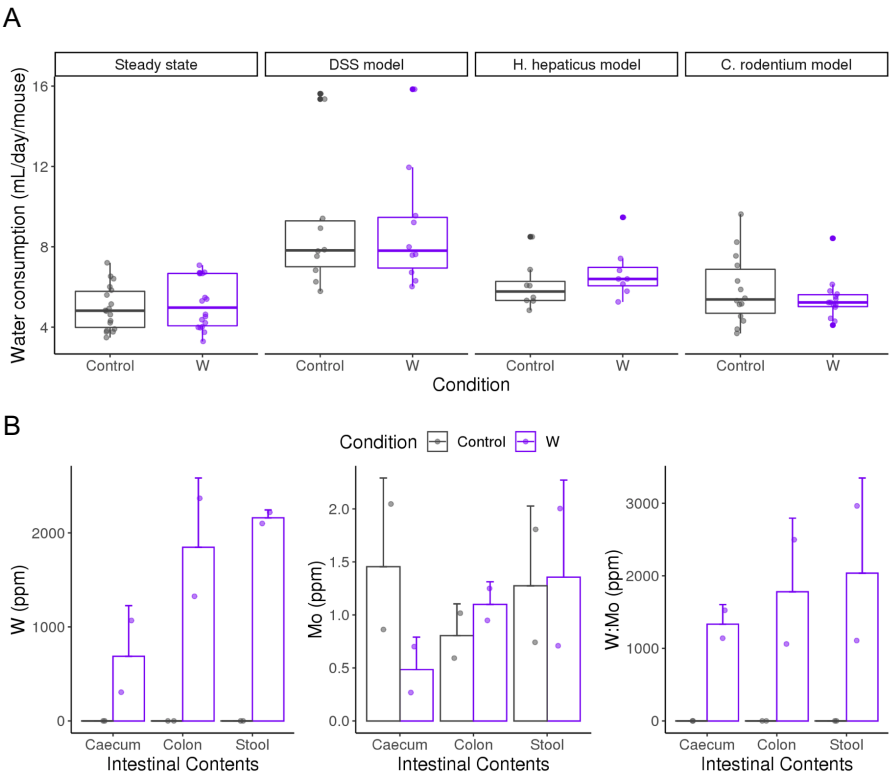


Figure 3.4. Tungstate administration in the drinking water leads to tungsten accumulation in the large intestine. A) Water consumption per day corrected for the number of animals per cage. Boxplots denote median + interquartile range and individual data points shown. B) Tungsten (W) and molybdenum (Mo) detected by ICP-MS in the caecum and colon contents and stool obtained from control or tungstate treated *C. rodentium* infected mice 14 dpi. Bars show mean + SD and individual data points are shown. All data obtained from 1 experiment.

reduction in faecal counts (figure 3.5A). However, these tungstate-mediated effects on Enterobacteriaceae levels were not reflected in day 9 large intestinal contents and tissues (figure 3.5B). In the *H. hepaticus* + aIL-10R model, no significant differences were seen in control faecal counts over disease time course although Enterobacteriaceae levels were ~10 times higher than baseline values at days 11 and 12 (figure 3.5A). Surprisingly, in tungstate treated *H. hepaticus* + aIL-10R mice, faecal Enterobacteriaceae counts were significantly elevated ~100 and ~$10^{1.5}$ fold from baseline levels at days 8 and 11, respectively. Moreover, at the day 8 peak, tungstate treated mice had ~100-fold higher faecal Enterobacteriaceae counts than their control counterparts (figure 3.5A). However, this significant elevation dissipated at day 11 and was not reflected in day 14 caecal or colonic content or tissues (figure 3.5A and B). Faecal *C. rodentium* load remained comparable between control and tungstate groups at all stages of infection (days 3-11), with peak burden reaching ~10^{11}

CFU/g stool in both groups at day 6 (figure 3.5C). Moreover, *C. rodentium* was recovered at comparable levels from day 7 and 14 intestinal contents in control and tungstate treated mice (figure 3.5D). Tungstate also did not have any statistically significant effects on *C. rodentium* dissemination dynamics to the liver and spleen (figure 3.5E). Thus, the inhibitory effects of tungstate were limited to a reduction in endogenous Enterobacteriaceae faecal load at the peak of DSS-induced Enterobacteriaceae expansion.

To ensure that the observed minimal effects of tungstate on Enterobacteriaceae growth was not due to an inability of tungstate to inhibit those endogenous to our SPF facility, we repeated our tungstate inhibition growth assay using representative colonies obtained from the stool of experimental mice. As we had surprisingly seen an increase in Enterobacteriaceae counts with tungstate treatment at day 8 in the *H. hepaticus* + aIL-10R model, we used these samples to assess tungstate susceptibility *in vitro*. As with *E. coli* K12 and *C. rodentium*, tungstate abolished nitrate-induced growth of SPF Enterobacteriaceae *in vitro* (figure 3.5F). Furthermore, no differences in growth dynamics were noted between Enterobacteriaceae obtained from control or tungstate treated stool (figure 3.5F). Thus, Enterobacteriaceae endogenous to the SPF microbiota were susceptible to tungstate inhibition *in vitro* in an identical manner to that observed by ourselves and others for *E. coli* K12, *C. rodentium* and other Enterobacteriaceae [198].

3.2.3 Tungstate fails to control pathology development in murine colitis models

Tungstate has been shown to have therapeutic effects in DSS and piroxicam-accelerated *Il10*$^{-/-}$ colitis and we saw an inhibitory effect of tungstate on Enterobacteriaceae growth at day 9 in the DSS model. Therefore, we further sought to characterise the effects of tungstate on pathology development in our experiments. In the DSS model, DSS treatment led to rapid weight loss 6-8 days post DSS administration that was comparable between control and

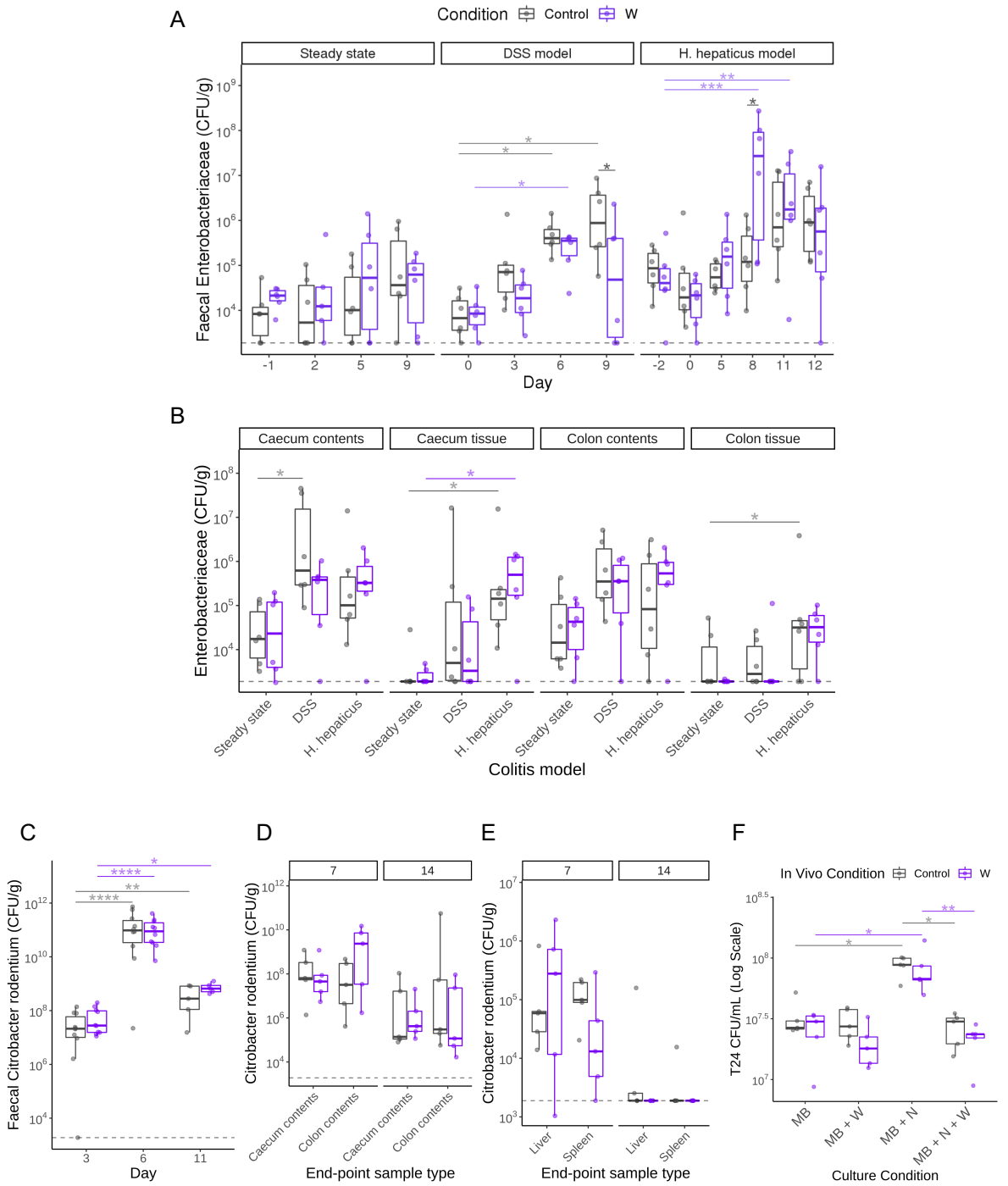


Figure 3.5. Tungstate has limited effects on Enterobacteriaceae growth across colitis models. A) Faecal and B) end-point Enterobacteriaceae colony forming units (CFU)/g sample obtained from steady state and DSS and *H. hepaticus* + aIL-10R treated mice given autoclaved DI (control) or 0.2% sodium tungstate (W) water. End-points are 9 days post tungstate administration for steady state mice and 9- and 14-days post model inception for DSS and *H. hepaticus* + aIL-10R treated mice, respectively. C) Faecal and D) 7 and 14 dpi *C. rodentium* CFU/g from control or W treated, *C. rodentium* infected mice. Dotted lines represent the detection limit. E) 24-hour *in vitro* growth of representative Enterobacteriaceae colonies obtained from *H. hepaticus* model day 8 faecal plates (A) in mucin broth (MB) supplemented with or without sodium nitrate (N) and 100 mg/L sodium tungstate (W). *p<0.05, **p<0.01, ***p<0.001, ****p<0.0001 A and C) Mixed linear effects modelling with post-hoc estimated marginal means analysis. B, D and E) Kruskal Wallis with Dunn's post hoc testing. All data obtained from 1 experiment. Boxplots denote median + interquartile range and individual data points are shown

tungstate treated groups. At 9 days post DSS administration, animal weights began to recover at comparable rates in both control and tungstate treated mice (figure 3.6). *H. hepaticus* + aIL-10R treated and *C. rodentium* infected mice did not lose weight, as is expected with these models, nor did tungstate influence animal weight at any time point. Similarly, tungstate did not alter steady state animal weights (appendix figure A.1).

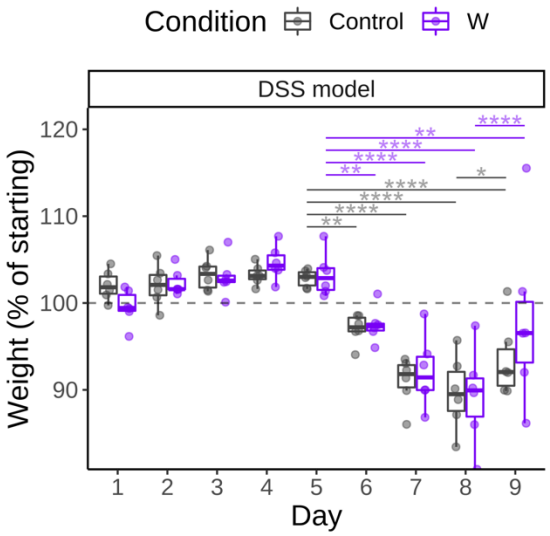


Figure 3.6. Tungstate does not influence animal weight loss or recovery in DSS colitis. Weights of DSS treated mice given autoclaved DI (control) or 0.2% tungstate (W) water. Weight is expressed relative to the starting weight. Data obtained from1 experiment. *p<0.05, **p<0.01, ****p<0.0001 mixed linear effects modelling with post-hoc estimated marginal means analysis. Boxplots denote median + interquartile range and individual data points are shown

To determine the effects of tungstate on colonic histopathology, H&E-stained colon tissues were assessed for evidence of disease. All colitis models displayed significantly elevated histopathology scores in comparison to steady state tissues. However, tungstate did not have any effects in any of the models tested (figure 3.7A and B). As tungstate has been reported to have therapeutic effects on caecum histopathology in DSS colitis [198] and *H. hepaticus* + aIL-10R leads to typhlitis [78], we further assessed caecum tissues from these models for evidence of tungstate-mediated amelioration of disease. In both models, disease scores were unaltered by tungstate administration (figure 3.7C and D). Thus, tungstate failed

to alter pathology development across DSS, *H. hepaticus* + aIL-10R and *C. rodentium* colitis.

To further determine if tungstate had any effects on systemic and mucosal immune responses, flow cytometric analysis was conducted on spleens, mLNs and colonic lamina propria leukocytes obtained from steady state and colitic mice. Gating strategies and representative colon plots are shown in appendix figure A.2. Colitis induced by DSS, *H. hepaticus* + aIL-10R and *C. rodentium* was characterised by an increase in the number of neutrophils and CD4 T cells in the lamina propria, which remained unaffected with tungstate treatment (figure 3.8A). Similarly, CD8 T cell expansion, which featured in DSS and *C. rodentium* colitis, was unaffected by tungstate treatment (figure 3.8A). Moreover, tungstate did not have any effect on colonic T cell or neutrophil frequencies within each model (appendix figure A.3A).

In *H. hepaticus* + aIL-10R and *C. rodentium* colitis, we further assessed Th17, T_{reg} and iT_{reg} cell subset distribution. In both models, Th17 cell proportions were increased, whilst iT_{reg} cells were reduced at comparable levels in control and tungstate treated mice (figure 3.8B). In *C. rodentium* colitis, RORγt$^-$ T_{reg} cells were also significantly reduced although this was unaffected by tungstate treatment (figure 3.8B). Total colonic Th17 cell numbers were increased in both colitis models, although tungstate administration did not have a significant impact on this expansion (figure 3.8C). Similarly, tungstate did not alter colonic iT_{reg} or T_{reg} cell counts in steady state or colitic mice (appendix figure A.3B). Tungstate also failed to alter neutrophil and T cell populations in the spleen and mLNs of colitic and steady state mice (appendix figure A.4). Thus, tungstate treatment did not influence the development of local or systemic immune responses across DSS, *H. hepaticus* + aIL-10R and *C. rodentium* colitis models.

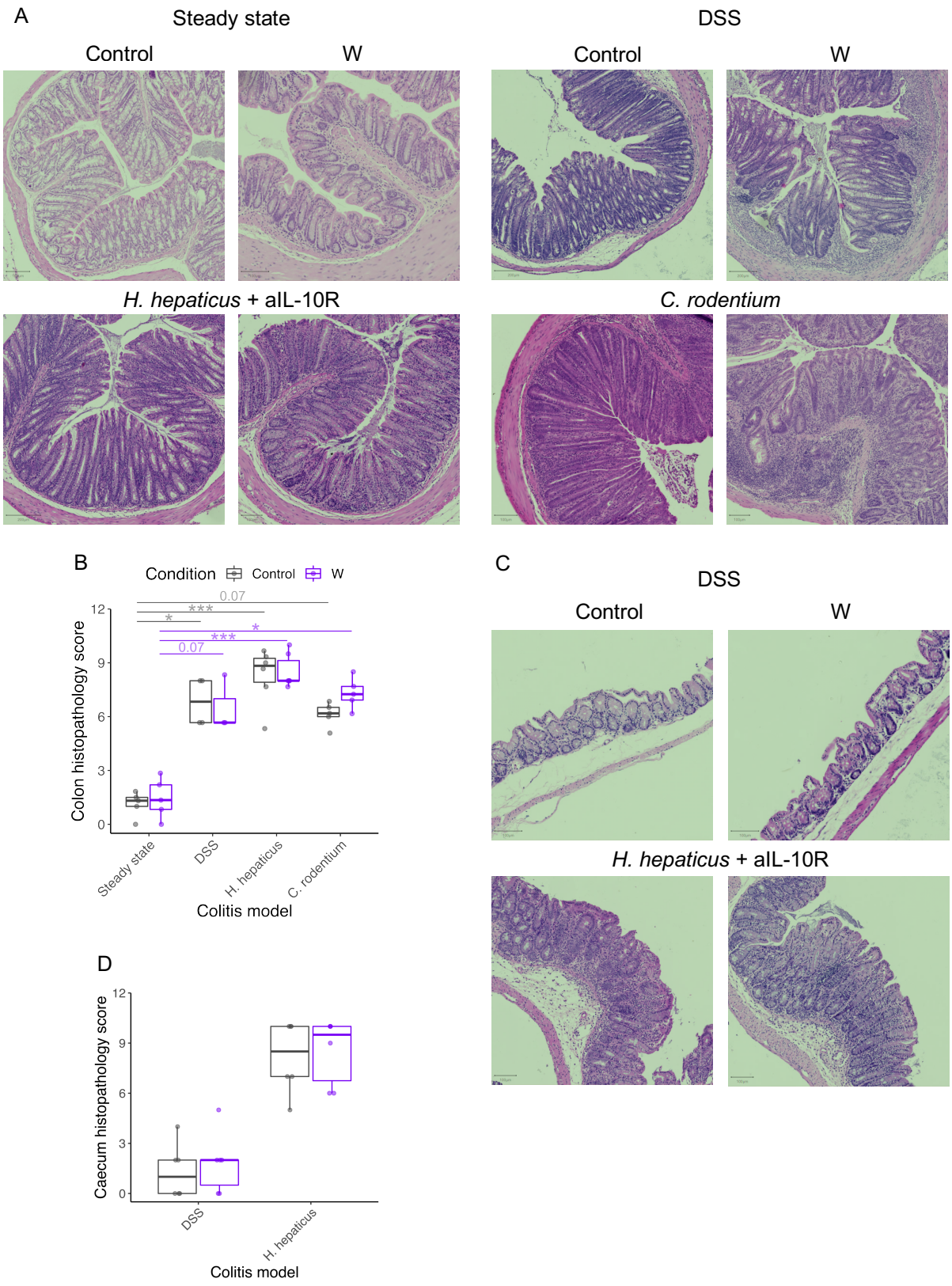


Figure 3.7. Tungstate does not alter pathology development in murine colitis models. A) Representative H&E images of mid colon tissues from steady state and DSS and *H. hepaticus* + aIL-10R treated and *C. rodentium* infected mice administered autoclaved DI (control) or 0.2% tungstate (W) water. B) Histopathology scoring of colon sections. C) Representative H&E images of caecum tissues from control and W treated DSS and H. hepaticus + aIL-10R colitic mice. D) Caecum histopathology scores. DSS tissues were obtained 9 days post model inception. *C. rodentium* and *H. hepaticus* + aIL-10R samples were obtained 14 days post model inception. Steady state values were obtained 14 days post tungstate treatment. **p<0.01 Kruskal Wallis with Dunn's post hoc testing. All data obtained from1 experiment. In B&D boxplots denote median + interquartile range and individual data points are shown

As nitrate respiration provides a competitive advantage to Enterobacteriaceae during gut inflammation [192], we analysed large intestinal tissues for expression of *Nos2*, which is implicated in the generation of nitrate during colitis. *Nos2* mRNA levels were significantly elevated in *H. hepaticus* + aIL-10R and *C. rodentium*, but not DSS, treated colonic and caecal tissues in comparison to steady state controls and in all groups unaltered by tungstate treatment (figure 3.8D). As tungstate has previously been shown to suppress *Cxcl1* and *Cxcl2* expression in DSS colitis [198], we further probed the expression of these genes. As with *Nos2*, large intestinal *Cxcxl1* expression was significantly elevated in *C. rodentium* and *H. hepaticus* + aIL-10R, but not DSS, colitis (figure 3.8E). However, tungstate failed to influence *Cxcl1* expression within groups across tissues (figure 3.8E). Colonic *Cxcl2* expression was significantly elevated from steady state levels in all colitis models. As with *Cxcl1* and *Nos2*, tungstate did not significantly alter colonic *Cxcl2* expression in *H. hepaticus* and *C. rodentium* colitis, although there was an observed reduction in DSS colitis which did not reach statistical significance (figure 3.8F). In the caecum, *Cxcl2* expression in *H. hepaticus* + aIL-10R and *C. rodentium* mice was significantly elevated from steady state values, but unaltered by tungstate treatment (figure 3.8F). Thus, despite model-dependent differences, tungstate largely did not modulate inflammatory gene expression in colonic and caecal tissues across DSS, *C. rodentium* and *H. hepaticus* + aIL-10R colitis. This was in line with flow cytometric and histopathology data in which tungstate did not influence disease across models.

3.2.4 *Citrobacter rodentium* expansion is independent of tungstate-mediated suppression of molybdenum-related gene expression

C. rodentium has previously been shown to rely on MoCo synthesis to achieve optimal fitness *in vivo* [200]. We therefore probed *C. rodentium* MoCo-related gene expression in colon contents obtained from control and tungstate treated mice. Due

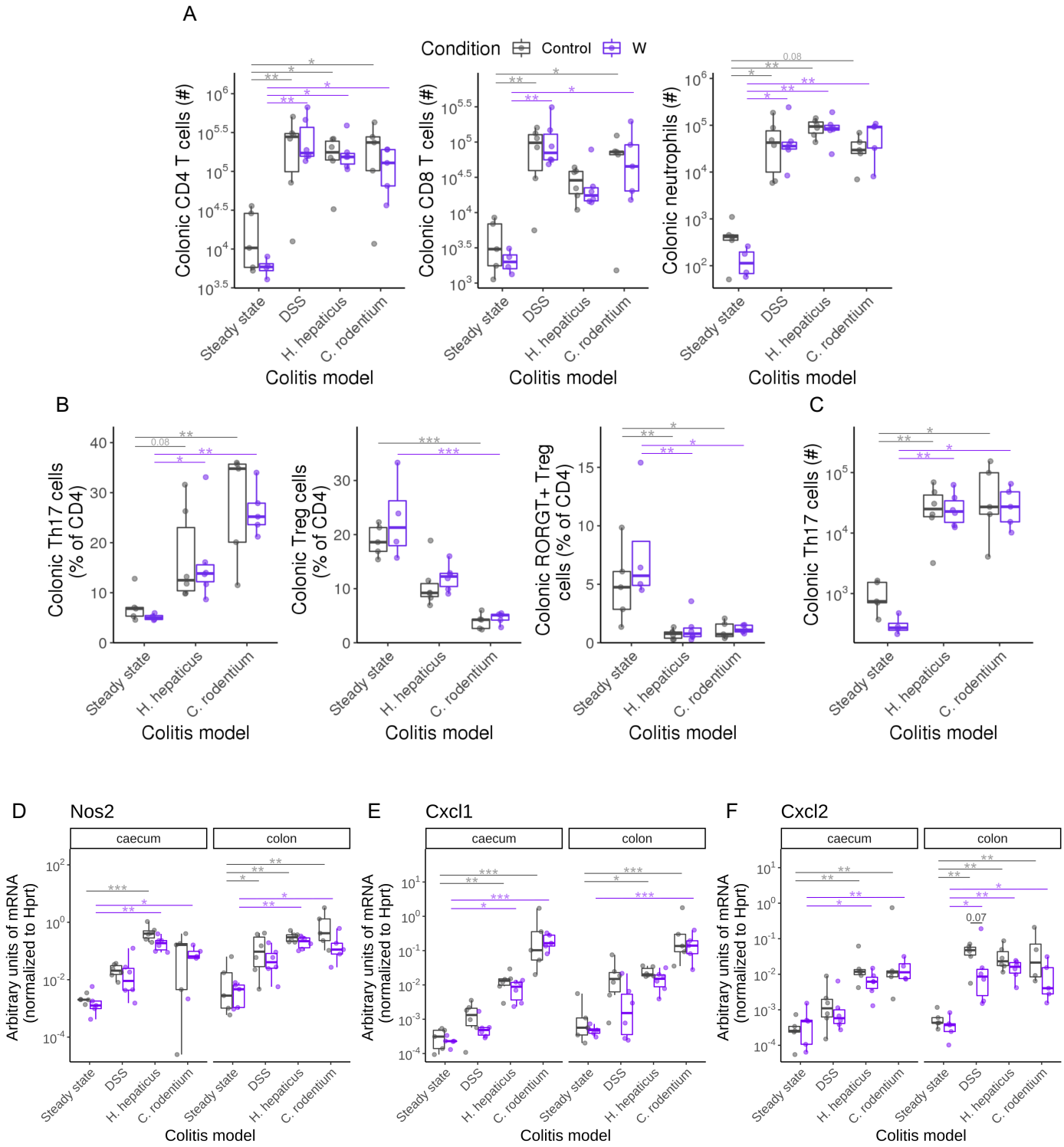


Figure 3.8. Tungstate fails to control inflammation in murine colitis models. A) Left-right CD4 and CD8 T cell and neutrophil counts in the colonic lamina propria of steady state and DSS, *H. hepaticus* + aIL-10R treated and *C. rodentium* infected mice given autoclaved DI (control) or tungstate (W) water. B) Left-right Th17, Treg and iTreg cell distribution within the colonic lamina propria CD4 T cell compartments of steady state and DSS, *H. hepaticus* + aIL-10R treated and *C. rodentium* infected mice receiving control or W water. C) Th17 cell counts in the colon of control or W treated steady state and *H. hepaticus* + aIL-10R and *C. rodentium* treated mice. D) Left-right *Nos2*, *Cxcl1*, *Cxcl2* gene expression expressed relative to *Hprt* in large intestinal tissues obtained from control and W treated steady state and colitic mice. DSS values were obtained 9 days post model inception. *C. rodentium* and *H. hepaticus* values were obtained 14 days post model inception. Steady state values were obtained 14 days post tungstate treatment. *p<0.05, **p<0.01, ***p<0.001 Kruskal Wallis with Dunn's post hoc testing. All data obtained from1 experiment. Boxplots denote median + interquartile range and individual data points are shown

to i) the availability of tungstate induced expression patterns in *E. coli* [242–244] and ii) the dependence of *C. rodentium* on formate dehydrogenase O (Fdh-O) and cytochrome *bd*-I oxidase, but not nitrate reductase respiratory enzymes [200], genes of interest were those involved in molybdate transport (*modB*), molybdenum cofactor synthesis (*moaA/C*) and Fdh-O (*fdoG*), cytochrome *bd*-I oxidase (*cydA*) and nitrate reductase (*narH*) activity. Primers were designed against *C. rodentium* sequences and tested on *C. rodentium* and *E. coli* K12 genomic DNA and DNA extracted from naïve SPF colon contents to ensure specificity. Expression levels were normalized to that of *rpoD* [222].

Consistent with *in vitro* expression patterns documented in *E. coli* [242,243], tungstate administration led to a significant reduction in *C. rodentium modB* gene expression at 7 and 14 dpi (figure 3.9). Expression of *moaC* was significantly increased in tungstate treated mice at 14 dpi, consistent with failed repression of the *moaABC* operon by a tungsten-complexed molybdopterin cofactor [244]. However, it should be noted that no significant changes were noted in *moaA* expression (figure 3.9). As expected, and in contrast to *narH* - *fdoG* and *cydA* transcripts were readily detected in colon contents. However, levels remained comparable between control and tungstate treated groups (figure 3.9). Together, these data suggest that tungstate administration led to altered expression of molybdate transport and MoCo synthesis genes, but not key respiratory genes employed by *C. rodentium in vivo*. This coincided with a failure to influence *C. rodentium* infection dynamics and the development of host inflammation and pathology.

3.3 Discussion

Tungstate has been shown to reduce Enterobacteriaceae expansion and ameliorate pathology during DSS and piroxicam-accelerated *Il10*$^{-/-}$ colitis [198]. However, we failed to reproduce these findings in the DSS model and moreover did not note any preventative effects of tungstate in *C. rodentium* and *H. hepaticus* + aIL-10R colitis. We readily detected

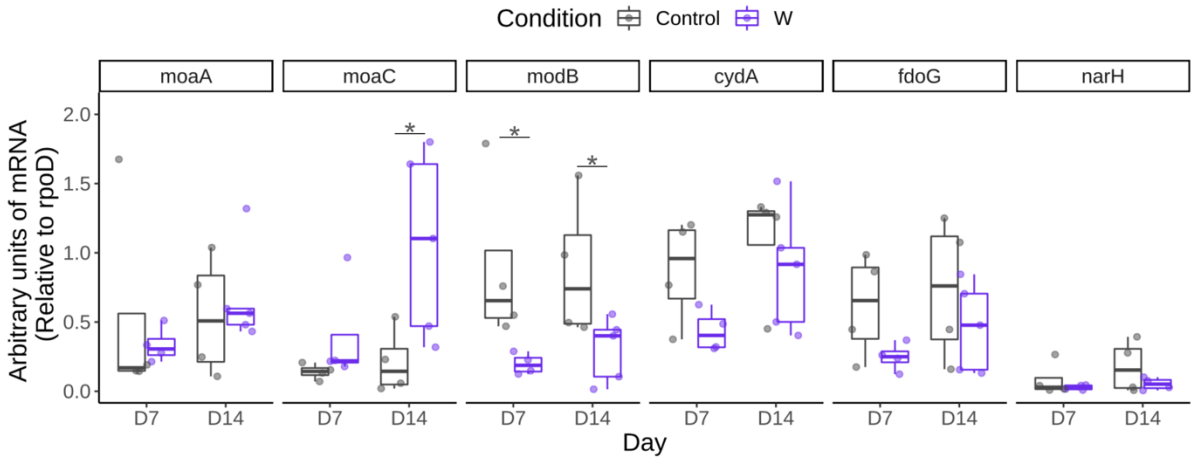


Figure 3.9. *C. rodentium* growth *in vivo* is independent of tungstate mediated suppression of molybdenum cofactor related gene expression. Expression of *C. rodentium* genes involved in molybdenum cofactor synthesis (*moaA* and *moaC*), molybdate transport (*modB*) and cytochrome *bd*-I oxidase (*cydA*), formate dehydrogenase (*fdoG*) and nitrate reductase (*narH*) activity. Expression values are normalized to that of the housekeeping gene *rpoD* and obtained from the colon contents of mice given autoclaved DI (control) or 0.2% tungstate (W) water 7- or 14-days post infection with *C. rodentium*. *p<0.05 Kruskal Wallis with Dunn's post hoc testing. All data obtained from1 experiment. Boxplots denote median + interquartile range and individual data points are shown

tungsten accumulation in the caecum, colon and stool of tungstate treated animals using ICP-MS and thus conclude that tungstate administration was successful and there are alternative explanations for a lack of effect.

The DSS treatment regimen employed by Zhu *et al* differs from that utilized in this study. To avoid excessive animal weight loss (>80%) in line with ethical considerations set on our home office license, we administered DSS for 5 days in the drinking water followed by a 4-day recovery period, whereas Zhu *et al* had a lengthened DSS treatment period of 8 days with 1-day recovery. Interestingly it has been suggested shorter periods (4-5 days) of DSS treatment may serve as a more physiologically relevant colitis model as they induce levels of intestinal permeability that are comparable to those observed in IBD patients [245]. Irrespective of DSS treatment duration, experimental outcomes in the DSS model are highly variable, which has been linked to the presence or absence of non-Enterobacteriaceae bacterial species that can alter disease severity [109,246]. In contrast to that seen by Zhu *et al*, disease induced by DSS in our study predominantly materialized in the colon, with low

histopathology scores achieved in caecal tissues. Moreover, in our experiments, colitis was accompanied by limited (<10-fold) induction of *Nos2* and *Cxcl1* gene expression, whereas levels were 100-fold higher in DSS tissues in the study done by Zhu *et al*. Despite these discrepancies, DSS treatment led to rapid weight lost, as is characteristic of this model, and animals developed colitis as evidenced by histopathological and flow cytometric analysis.

Whilst we did observe Enterobacteriaceae counts that were significantly elevated from baseline levels in DSS and *H. hepaticus* + aIL-10R colitis, this was on a modest scale (~10-100 fold) in comparison to that observed by Zhu *et al*, where the endogenous Enterobacteriaceae population was 10^4 times greater in DSS versus steady state caecal contents [198]. In our DSS experiment this low-level expansion may be due to blunted *Nos2* induction, as Enterobacteriaceae inflammatory fitness has been shown to be dependent on host iNOS [192]. As we failed to substantially inhibit Enterobacteriaceae growth in our *in vivo* experiments, we cannot deduce the contribution of Enterobacteriaceae species to disease development in these settings. However, it should be noted that gnotobiotic mice stably colonized with the OMM^{12}, which is void of Enterobacteriaceae, are susceptible to *H. hepaticus* + aIL-10R colitis [154].

In the case of *C. rodentium*, a reliance on MoCo synthesis to achieve optimal growth has been demonstrated *in vivo*. However, this reliance is independent of nitrate reductase activity and manifests in a gene cluster (*fdoGHI*) encoding Fdh-O [200]. Whilst *E. coli* Fdh-O is described as a molybdoenzyme, formate dehydrogenases are an exemplar family of tungstoenzymes, which in certain species have been described to have dual Mo/W function [247,248]. We observed alterations in *C. rodentium* molybdenum-related gene expression that were consistent with expression patterns induced by tungstate uptake in *E. coli* [242–244]. *C. rodentium* and other Enterobacteriaceae species have been shown to employ multiple upstream and terminal components of the electron transport chain to proliferate effectively during inflammation, including hydrogenases, cytochrome c peroxidase and

microaerobic cytochrome *bd*-I and *bd*-II oxidases [199,200,230,234,249]. Moreover, the fitness advantage conferred by molybdenum cofactor synthesis in *C. rodentium* is influenced by other microbiota members as it is lost in GF mice [200]. Thus, the failing of tungstate to inhibit *C. rodentium* growth and pathology may be due to multiple factors, including dual tungsten and molybdenum functionality of Fdh-O, *C. rodentium* respiratory adaptation or vivarium discrepancies in microbiota composition.

In this chapter, we aimed to determine the therapeutic effects of tungstate over a range of colitis models that capture different aspects of IBD pathophysiology. Whilst our results were obtained from one experimental run-through and thus repeats are required for conclusive interpretation, we found that tungstate did not prevent colitis development in any of the models tested. Likely this is reflective of the variable nature of the DSS model and differing disease mechanisms in *H. hepaticus* + aIL-10R and *C. rodentium*-induced colitis. Regardless, targeting of molybdenum-dependent Enterobacteriaceae expansion does not appear to be a broadly applicable microbiota-based therapy in IBD and instead serves as a tailored strategy dependent on disease context.

Chapter 4 Characterising Oligo-Mouse-Microbiota community dynamics over the course of *Helicobacter hepaticus*-induced colitis

4.1 Introduction

Mechanistic insight on how inflammation-associated changes in bacterial community structure play a role in IBD can be informed by linking dysbiosis to alterations in intestinal metabolite availability [250]. Indeed, shifts in faecal metabolite profiles are often observed in IBD patients and bacterial-derived metabolites in particular are increasingly appreciated as regulators of epithelial and mucosal immune responses [251]. For example, advances in mass spectrometry analysis platforms have led to the identification of IBD-associated reductions in microbiota-derived SCFAs, SBAs and tryptophan derivatives [250,251]. These metabolites have been shown to exert multiple homeostatic functions including maintenance of epithelial hypoxia, control over the Th17/T_{reg} cell axis and induction of barrier protective IL-22 production by RORγt^{+} ILC3s, respectively [57,252,253]. Notably, whilst links between the microbiota, metabolites and IBD are being established in the literature, studies are often hindered by the interindividual variability seen in complex microbiotas [254]. As is applicable to understanding the role of dysbiotic community compositional shifts, minimal model microbiotas, such as the OMM^{12}, are institutionally standardised and remove substantial variability and microbial complexity [181]. In doing so such models can be used to further our understanding of how individual bacteria and metabolites influence disease process.

H. hepaticus is a member of the murine mouse microbiota that can cause disease in various immune deficiencies and is thus termed a pathobiont. Ablation of the anti-inflammatory cytokine IL-10 in *H. hepaticus* colonised mice leads to a failure of the homeostatic T_{reg} cell response and pathogenic Th1/Th17 cell outgrowth [78,131]. Both responses are *H. hepaticus* specific and their differential development is dependent on context determined by the immune status of the infected host [32]. Thus, pathology in the *H. hepaticus* + aIL-10R model arises due to maladaptation of the host response to *H. hepaticus*, which itself is highly

specialised in its ability to influence mucosal immunity [1]. Colitis in the *H. hepaticus* + aIL-10R model is associated with dysbiosis and increased expression of oxidative stress response genes predominantly in lactic acid bacteria, including *Lactobacillus* and *Enterococcus* [255].

Other commensal bacteria influence *H. hepaticus* colitis model outcome. Disease level differs in mice with identical genetic backgrounds but substantial vivaria-driven differences in microbiota composition [151]. Most pertinently, various strains of GF *Il10*$^{-/-}$ mice do not develop colitis when monoassociated with *H. hepaticus*, despite evidence of *H. hepaticus* colonization [171,172,202]. However, inoculation of GF adult mice with a single strain of human derived *Lactobacillus reuteri* or stable colonisation with the OMM^{12} renders mice susceptible to *H. hepaticus* colitis in the context of IL-10 deficiency [154,202]. Thus, *H. hepaticus* is dependent on other commensal bacteria for disease development. Although specific features of this dependence are not currently known, it is somewhat unsurprising given that in other contexts bacterial interactions have been shown to modulate virulence factor gene expression, niche establishment and ultimately host physiology [179,256].

Given the ability of *H. hepaticus* + aIL-10R treatment to cause colitis in OMM^{12} mice, it represents a good model to dissect the roles of commensal bacteria in colitis development. Major properties of a diverse microbiota are retained in this minimal community that includes coverage of the 5 major phyla present in the conventional mouse gut [176]. Moreover, the OMM^{12} stably colonizes germ-free animals across generations and vivaria, making it a useful tool in microbiota research [176,181]. Indeed, it has been used by others to delineate the role of the microbiota in conferring protection from pathogens [179,257,258], the biogeography of the microbiota in discrete intestinal niches [177] and how this fosters distinct bacteria-bacteriophage interactions [259]. As the *H. hepaticus* + aIL-10R OMM^{12} colitis model is a novel model, the first step in its utilisation is characterisation. Thus, the aim

of this thesis chapter was to characterise changes in the OMM^{12} over the course of *H. hepaticus* + aIL-10R colitis, focusing on community composition and metabolic output.

4.2 Results

4.2.1 *H. hepaticus* + aIL-10R-induced inflammation coincides with dysbiosis in OMM^{12} gnotobiotic mice

To first confirm that *H. hepaticus* requires OMM^{12} members to cause disease in the context of IL-10 deficiency, we colonised GF and stably colonized OMM^{12} mice with *H. hepaticus* and treated them with aIL-10R. Steady state (no *H. hepaticus* nor aIL-10R), aIL-10R treated and *H. hepaticus* colonised mice served as controls. After 14 days post model inception, colon and caecum tissues were collected and subjected to histopathological scoring. As expected, GF mice administered *H. hepaticus* + aIL-10R failed to develop signs of colon pathology (figure 4.1A) and disease levels were comparable to that of controls (figure 4.1B). In contrast, *H. hepaticus* + aIL-10R treatment in OMM^{12} mice led to clear signs of colitis (figure 4.1A), with histopathological scores significantly elevated from control and GF *H. hepaticus* + aIL-10R treated mice (figure 4.1B). Moreover, disease levels were significantly elevated in *H. hepaticus* + aIL-10R OMM^{12} caecum tissues relative to OMM^{12} controls (figure 4.2A and B). Thus, as we and others have shown, *H. hepaticus* fails to induce colitis in GF IL-10 deficient mice and requires other commensals to cause disease, including those belonging to the OMM^{12}.

To characterise OMM^{12} community dynamics over the course of colitis, we conducted 16S ribosomal RNA (rRNA) amplicon sequencing on longitudinal stool and end-point colon and caecum content samples obtained from the above mice. To relate community compositional changes to colitis development, we first assessed matched samples for levels of LCN2, a neutrophil-derived protein that serves as a marker of intestinal inflammation. As expected, *H. hepaticus* + aIL-10R treatment led to a significant ~400-fold increase in faecal LCN2

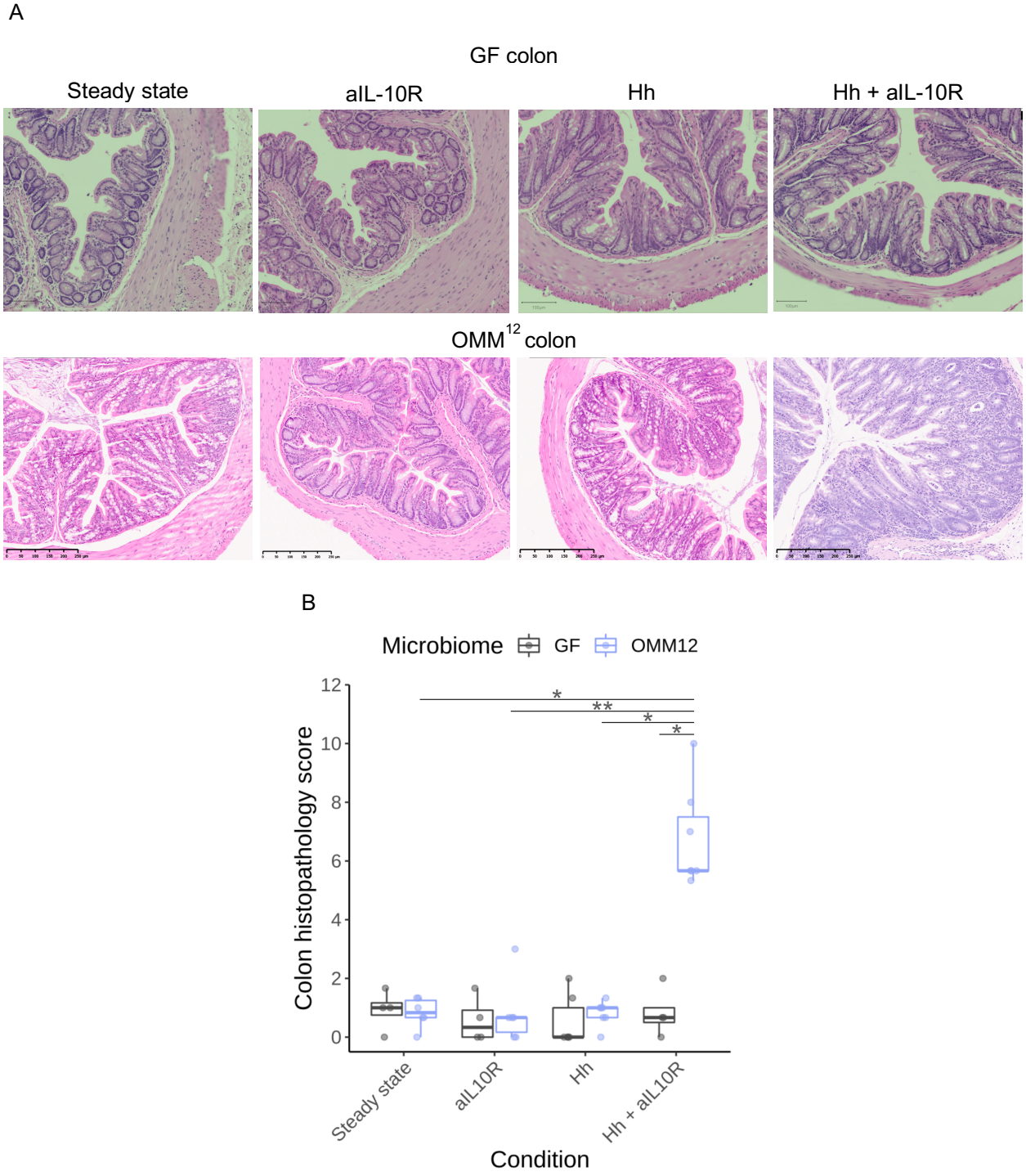


Figure 4.1. *H. hepaticus* requires other commensals to induce colitis in IL-10 deficiency. A) Representative images from H&E-stained mid colon sections obtained from germ-free (GF) or Oligo-Mouse-Microbiota 12 (OMM^{12}) mice in the steady state (untreated) or administered anti-interleukin-10 receptor (aIL-10R), *Helicobacter hepaticus*, or both *H. hepaticus* + aIL-10R. B) Quantification of histopathology scoring of proximal, mid and distal colon sections. * p_{adj}<0.05, ** p_{adj}<0.01 Kruskal Wallis with Dunn's posthoc testing. All data obtained from one experiment. Boxplots show median and interquartile range and individual data points are shown

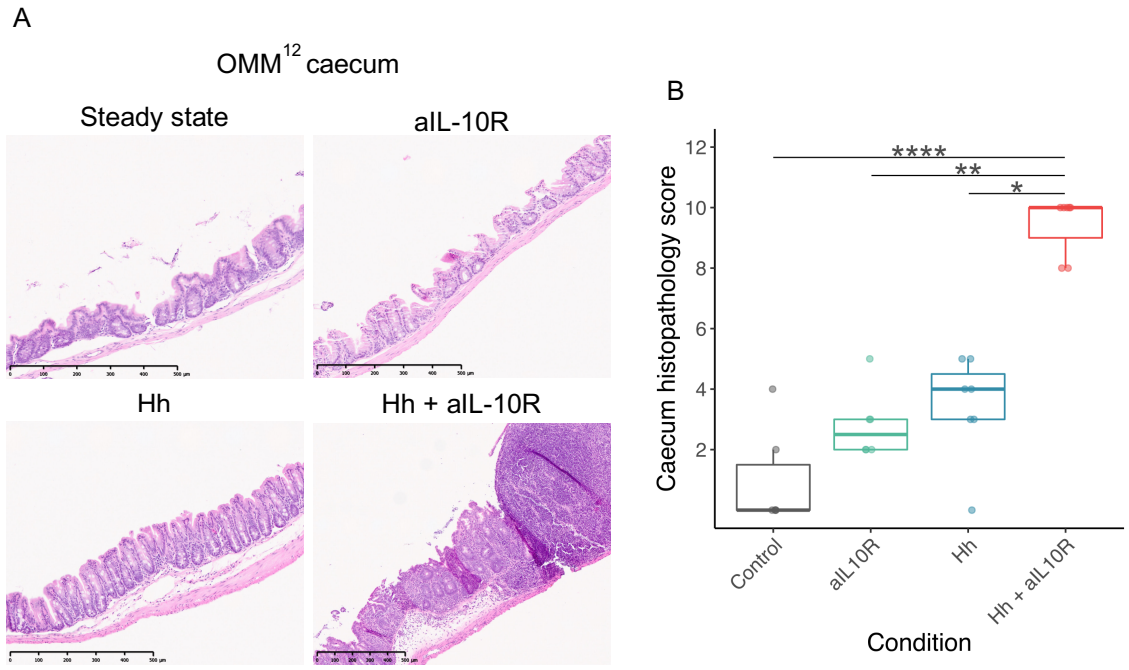


Figure 4.2. OMM[12] mice develop typhlitis following *H. hepaticus* + aIL-10R treatment. A) Representative images from H&E-stained caecum sections obtained from Oligo-Mouse-Microbiota 12 (OMM[12]) mice in the steady state (untreated) or administered anti-interleukin-10 receptor (aIL-10R), *Helicobacter hepaticus*, or both *H. hepaticus* + aIL-10R. B) Quantification of histopathology scoring of caecum sections. * p_{adj}<0.05, ** p_{adj}<0.01, ***p_{adj} < 0.001. Kruskal Wallis with Dunn's posthoc testing. Boxplots show median and interquartile range and individual data points are shown. All data obtained from one experiment.

levels 7 days post model inception that was maintained until day 10. Interestingly, *H. hepaticus* controls also showed a significant elevation in LCN2 levels at day 7, although this increase was of ~200-fold lower magnitude and no longer significant at day 10 (figure 4.3A). Similarly, LCN2 levels were significantly elevated ~350-fold in *H. hepaticus* + aIL-10R caecum contents relative to steady state and aIL-10R controls. *H. hepaticus* colonized mice also displayed a significant albeit lesser ~100-fold elevation from control groups (figure 4.3A). As *H. hepaticus* treated mice did not develop histopathology (figures 4.1 and 4.2), these small increases in faecal and caecum content LCN2 levels likely reflect a sub-pathological response to *H. hepaticus* colonization. Regardless, *H. hepaticus* + aIL-10R treatment led to an elevation in faecal LCN2 levels at day 7 that was maintained until experimental end-point.

In 16S sequencing, within each sample ~99.7% of reads corresponded to OMM^{12} genera. Genus-level annotation was able to distinguish between individual OMM^{12} members, with the exceptions of *A. muris* KB18 and *E. clostridioformis* YL32, which were both assigned as *Clostridium* XIVa in the dada2 classifier [154]. *H. hepaticus* + aIL-10R samples clustered distinctly from other groups from day 7 in the stool and in both caecum and colon contents by PCA analysis (figure 4.3B). Moreover, community shifts unique to the *H. hepaticus* + aIL-10R group were strikingly apparent from day 7 in the stool and in caecum and colon contents (figure 4.3C). Importantly, the onset of faecal compositional changes coincided with the rise in faecal LCN2 levels (figure 4.3A). Notably, one *H. hepaticus* + aIL-10R caecum content sample had a lot of "other" reads (accounting for ~45% abundance), the majority of which (~75%) were classified to the *Prevotella* genus (figure 4.3C). As this was not seen in any other samples including those obtained from experimental cage mates, it is unlikely that this originated from an *in vivo* contamination and thus this sample was excluded from further analysis. Finally, Helicobacter reads were present in *H. hepaticus* and *H. hepaticus* + aIL-10R mice at comparable levels from day 5 in the stool and in caecum and colon contents (figure 4.3D). Thus, *H. hepaticus* + aIL-10R treatment in OMM^{12} mice led to dysbiosis that coincided with colitis development, which did not affect *H. hepaticus* abundance levels.

4.2.2 *H. hepaticus* + aIL-10R-induced OMM^{12} dysbiosis coinciding with inflammation development is characterised by changes in 5 OMM^{12} members

To identify OMM^{12} members that defined community dysbiosis, we performed statistical analysis on faecal relative abundances utilizing linear modelling, in which the interaction term was used to define bacteria of interest. Following this we conducted estimated marginal means analysis to identify 8 bacterial signatures that were manifesting over time exclusively in the *H. hepaticus* + aIL-10R group. Significant increases in *Enterococcus* (*Enterococcus faecalis* KB1), *Lactobacillus* (*Lactobacillus reuteri* I49) and *Parasutterella* (*Turicimonas muris* YL45) were seen at days 7 and 10 relative to baseline (day 0) values (figure 4.4A-C).

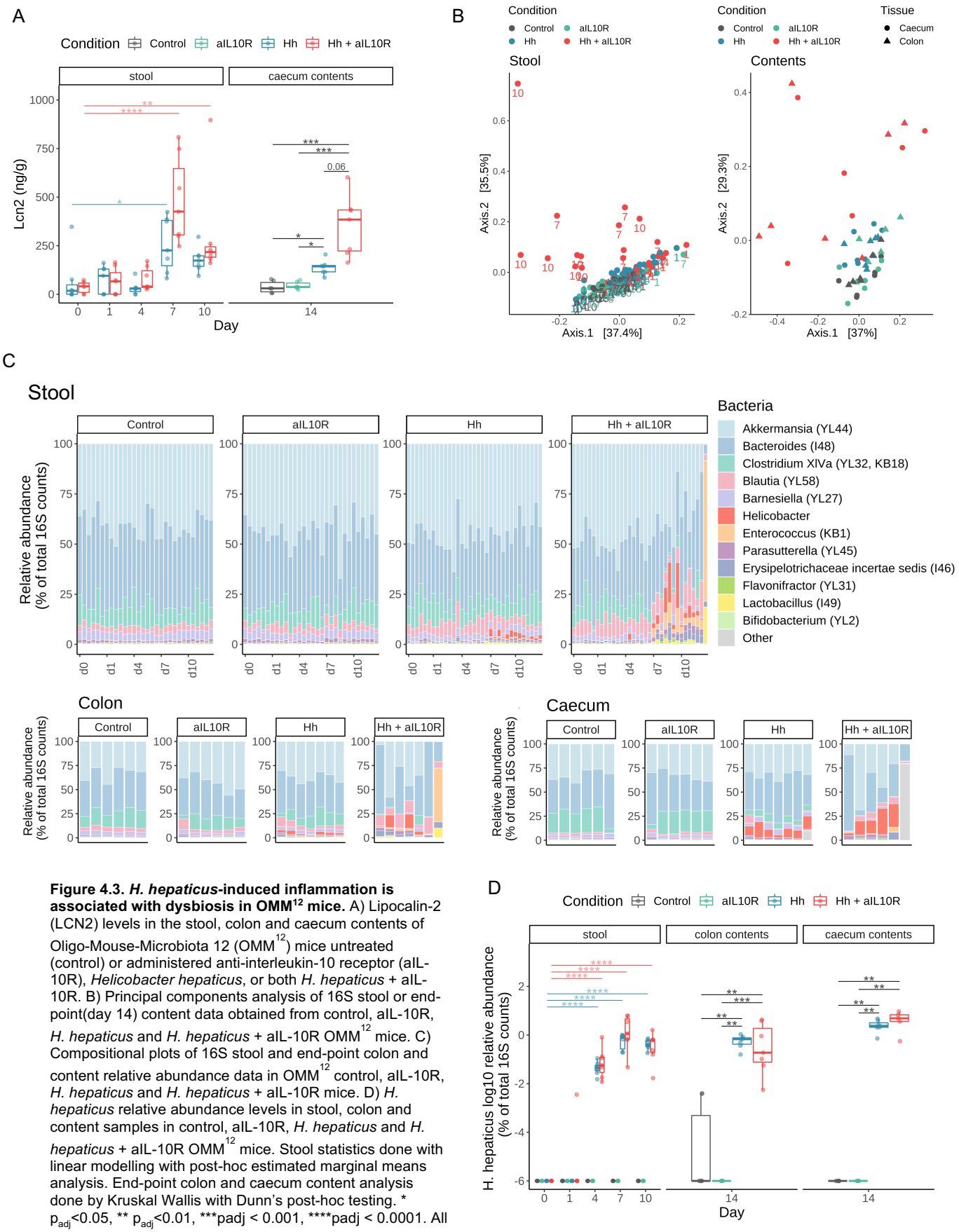


Figure 4.3. *H. hepaticus*-induced inflammation is associated with dysbiosis in OMM[12] mice. A) Lipocalin-2 (LCN2) levels in the stool, colon and caecum contents of Oligo-Mouse-Microbiota 12 (OMM[12]) mice untreated (control) or administered anti-interleukin-10 receptor (aIL-10R), *Helicobacter hepaticus*, or both *H. hepaticus* + aIL-10R. B) Principal components analysis of 16S stool or end-point(day 14) content data obtained from control, aIL-10R, *H. hepaticus* and *H. hepaticus* + aIL-10R OMM[12] mice. C) Compositional plots of 16S stool and end-point colon and content relative abundance data in OMM[12] control, aIL-10R, *H. hepaticus* and *H. hepaticus* + aIL-10R mice. D) *H. hepaticus* relative abundance levels in stool, colon and content samples in control, aIL-10R, *H. hepaticus* and *H. hepaticus* + aIL-10R OMM[12] mice. Stool statistics done with linear modelling with post-hoc estimated marginal means analysis. End-point colon and caecum content analysis done by Kruskal Wallis with Dunn's post-hoc testing. * p_{adj}<0.05, ** p_{adj}<0.01, ***padj < 0.001, ****padj < 0.0001. All data obtained from one experiment. In A&D boxplots show median and interquartile range and individual data points are shown

Additionally, *Erysipelotrichaceae* (*Clostridium innocuum* I46) was significantly elevated in *H. hepaticus* + aIL-10R stool, although the onset of this was not until day 10 (figure 4.4D). In contrast, *Clostridium* XIVa (*Enterocloster clostridioformis* YL32 or *Acutalibacter muris* K18), *Barnesiella* (*Muribaculum intestinale* YL27) and *Akkermansia* (*Akkermansia muciniphila* YL44) genera were reduced, although only the former two materialized from day 7, with the latter seen exclusively at day 10 (figure 4.4E-G). *Blautia* (*Blautia coccoides* YL58) showed a significant increase in *H. hepaticus* + aIL-10R stool, although this was at days 1 and 10 relative to baseline (figure 4.4H). As inflammation reached detectable levels from day 7 onwards (figure 4.3A), *E. faecalis* KB1, *L. reuteri* I49, *T. muris* YL45, *E. clostridioformis* YL32 or *A. muris* KB18 dysbiotic signatures therefore coincided with colitis development (figure 4.4A-C and 4.4E). In contrast, increased *C. innocuum* I46 and reduced *A. muciniphila* YL44 abundances represented delayed community compositional responses to inflammation (figure 4.4D and 4.4G). *B. coccoides* YL58 abundances appeared to be influenced by *H. hepaticus* colonization alone as levels were elevated prior to inflammation development in the *H. hepaticus* + aIL-10R group and reduced at day 10 relative to baseline in the *H. hepaticus* group (figure 4.4H). Interestingly, *E. faecalis* KB1, *L. reuteri* I49 and *T. muris* YL45 abundances were also significantly increased at days 7 or 10 from baseline values in the *H. hepaticus* group (figure 4.4A-C), suggestive of potential non-colitogenic interactions between these bacteria and *H. hepaticus*.

To determine if longitudinal signatures of dysbiosis were seen in end-point samples, we further performed statistical analysis on caecum and colon content 16S profiles. *E. faecalis* KB1 was significantly increased in *H. hepaticus* + aIL-10R relative to at least one control group in both caecum and colon contents. In contrast, *E. clostridioformis* YL32 or *A. muris* K18 and *M. intestinale* YL27 were significantly reduced in both caecum and colon contents relative to controls (figure 4.5A and B). Interestingly, *T. muris* YL45 showed site dependent differences, as it was only significantly altered in the caecum contents, where it was elevated in *H. hepaticus* + aIL-10R and *H. hepaticus* mice relative to controls (figure 4.5B). Additional

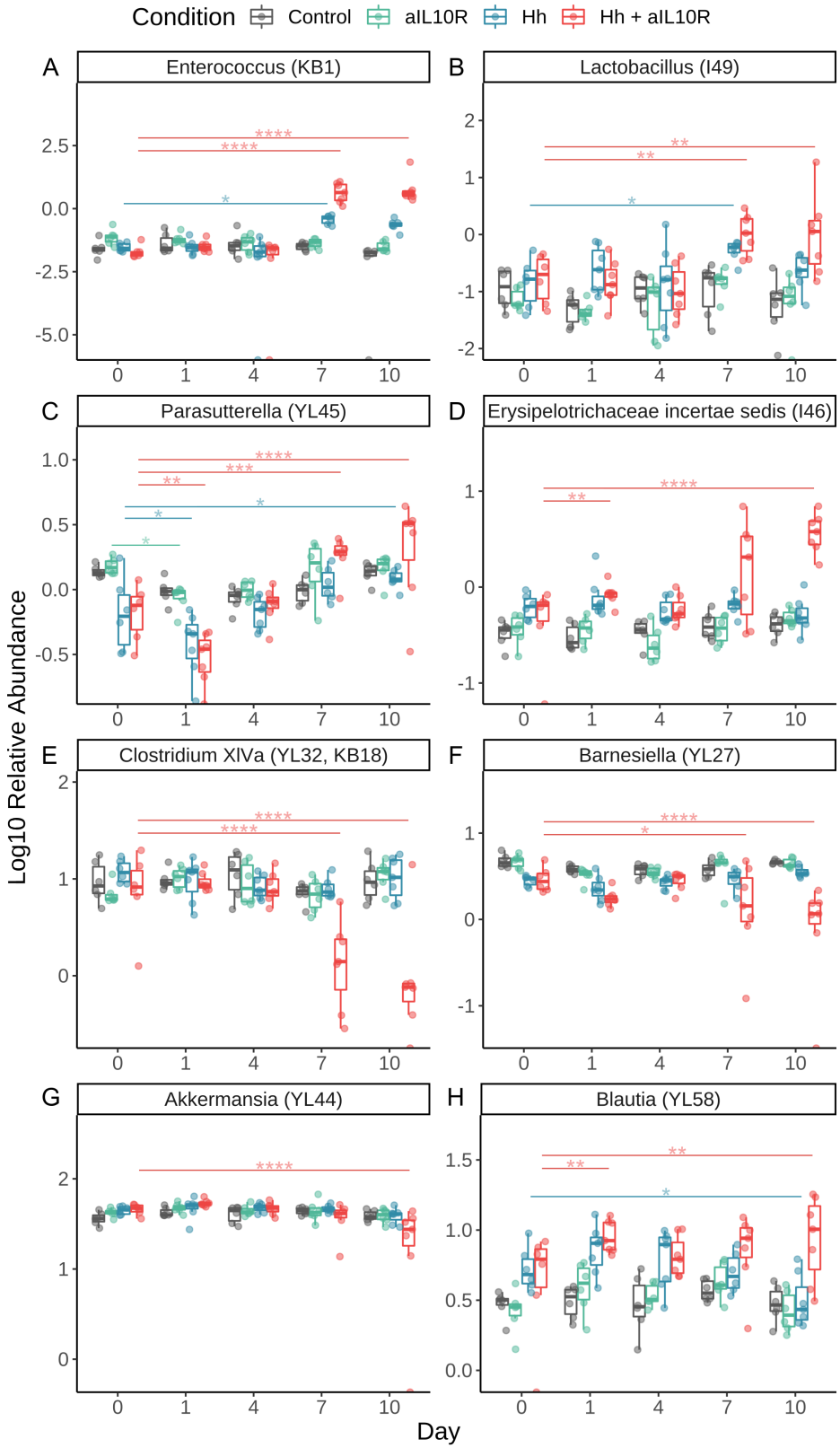


Figure 4.4. *H. hepaticus*-induced colitis is associated with alterations in the relative abundance profiles of 8 OMM[12] members. Relative abundances of A) *E. faecalis* KB1, B) *L. reuteri* I49, C) *T. muris* YL45, D) *C. innocuum* I46, E) *E. clostridioformis* YL32 or *A. muris* KB18, F) *M. intestinale* YL27, G) *A. muciniphila* YL44 and H) *B. coccoides* YL58 in longitudinal stool samples obtained from control, anti-interleukin-10 receptor (aIL-10R), *Helicobacter hepaticus*, or *H. hepaticus* + aIL-10R treated OMM[12] mice. Bacterial identification derived from genus-level annotation, which cannot distinguish between *E. clostridioformis* YL32 and A. muris KB18. * p_{adj}<0.05, ** p_{adj}<0.01, ***padj < 0.001, ****padj < 0.0001. Linear modelling with post-hoc estimated marginal means analysis. Boxplots show median and interquartile range and individual data points are shown. All data obtained from one experiment.

potential *H. hepaticus* interaction signatures were noted for *E. faecalis* KB1 and *M. intestinale* YL27, which were increased in both caecum and colon contents and caecum contents alone relative to controls, respectively (figure 4.5A and B). Thus, *H. hepaticus* + aIL-10R treatment led to dysbiosis in OMM^{12} mice that coincided with inflammation onset, characterized by an increase in *E. faecalis* KB1, *L. reuteri* I49 and *T. muris* YL45, and reductions in *E. clostridioformis* YL32/*A. muris* KB18 and *M. intestinale* YL27 abundances. With the exception of *L. reuteri* I49, these dysbiotic signatures translated to those seen in either colon or caecum contents at experimental end-point.

4.2.3 Reductions of *E. clostridioformis* YL32 and *M. intestinale* YL27 and an expansion of *E. faecalis* KB1 are robust signatures of OMM^{12} dysbiosis coinciding with *H. hepaticus* + aIL-10R colitis

As we had established that *H. hepaticus* + aIL-10R induced inflammation in OMM^{12} mice led to alterations in the abundances of 5 OMM^{12} members, we further sought to understand whether these served as consistent signatures of dysbiosis in this model. Thus, we repeated *H. hepaticus* + aIL-10R treatment in OMM^{12} mice. As we had seen evidence of interactions with *H. hepaticus* alone but no differences with aIL-10R treatment, and longitudinal sample collection ensured we had steady state values for each individual animal, *H. hepaticus* treated mice served as controls.

As with the first experiment, *H. hepaticus* + aIL-10R treatment, but not colonization with *H. hepaticus* alone, led to disease induction in the caecum and colon as assessed by histopathological analysis (figure 4.6A and B). Moreover, LCN2 analysis of faecal and caecum and colon content samples showed significant increases in *H. hepaticus* + aIL-10R LCN2 levels from day 5 in the stool that was maintained until experimental end-point (figure 4.7A). Interestingly, we again noted a small but significant, likely sub-pathological, increase from baseline values in faecal LCN2 levels at day 10 in *H. hepaticus* alone samples (figure 4.7A). Unsurprisingly, *H. hepaticus* was detected in both groups at comparable levels from

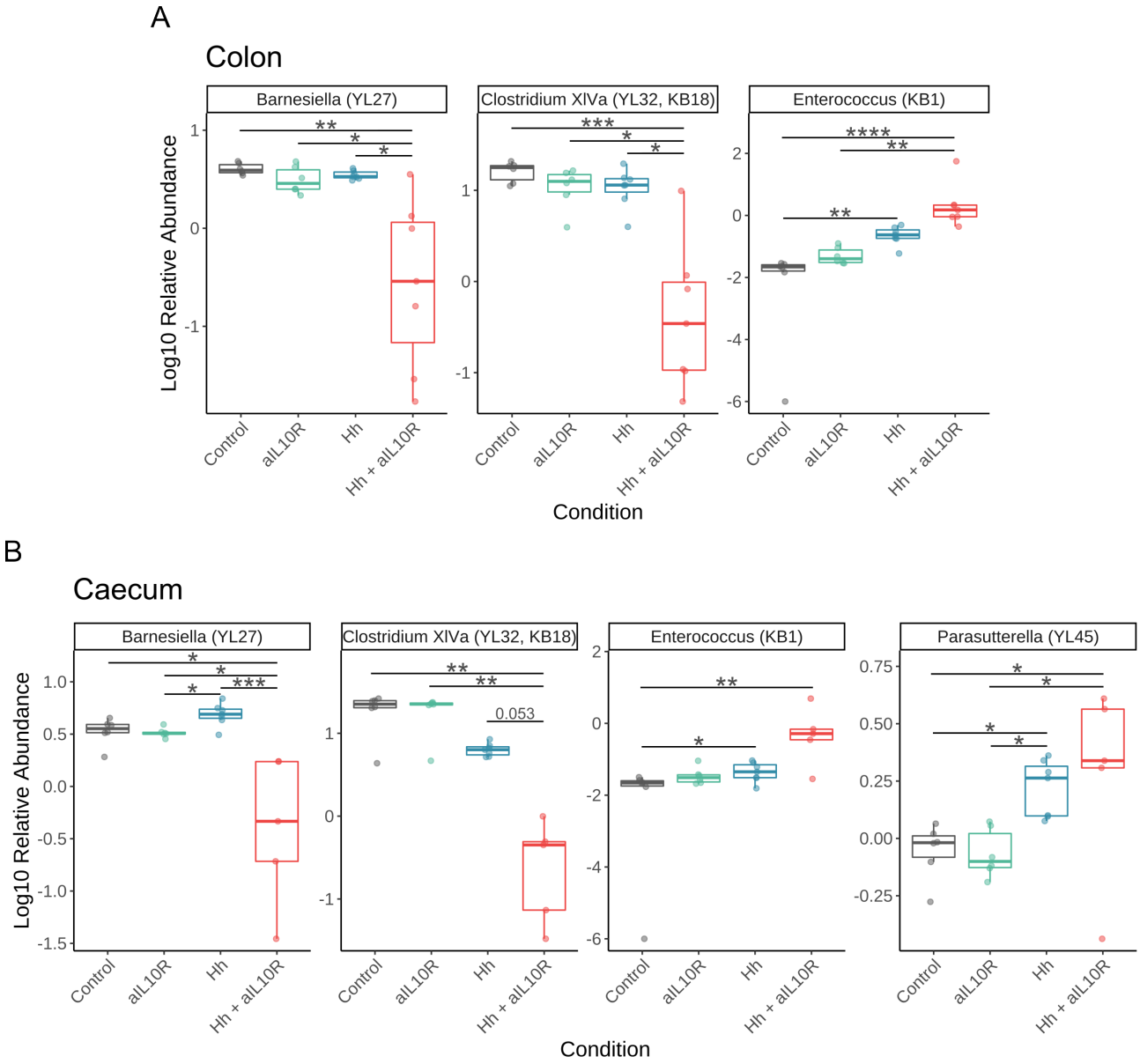


Figure 4.5. OMM[12] longitudinal dysbiotic signatures are shared in end-point caecum and colon contents. Relative abundance profiles of *M. intestinale* YL27 (genus Barnesiella), *E. clostridioformis* YL32 or *A. muris* KB18 (Clostridium XlVa), *E. faecalis* KB1 (Enterococcus) and *T. muris* YL45 (Parasutterella) in end-point A) colon and B) caecum contents of control, anti-interleukin-10 receptor (aIL-10R), *H. hepaticus* (Hh) and Hh + aIL-10R treated OMM[12] mice * p_{adj}<0.05, ** p_{adj}<0.01, ***p_{adj} < 0.001, ****p_{adj} < 0.0001 Kruskal Wallis with Dunn's posthoc testing. Boxplots show median and interquartile range and individual data points are shown. All data obtained from one experiment.

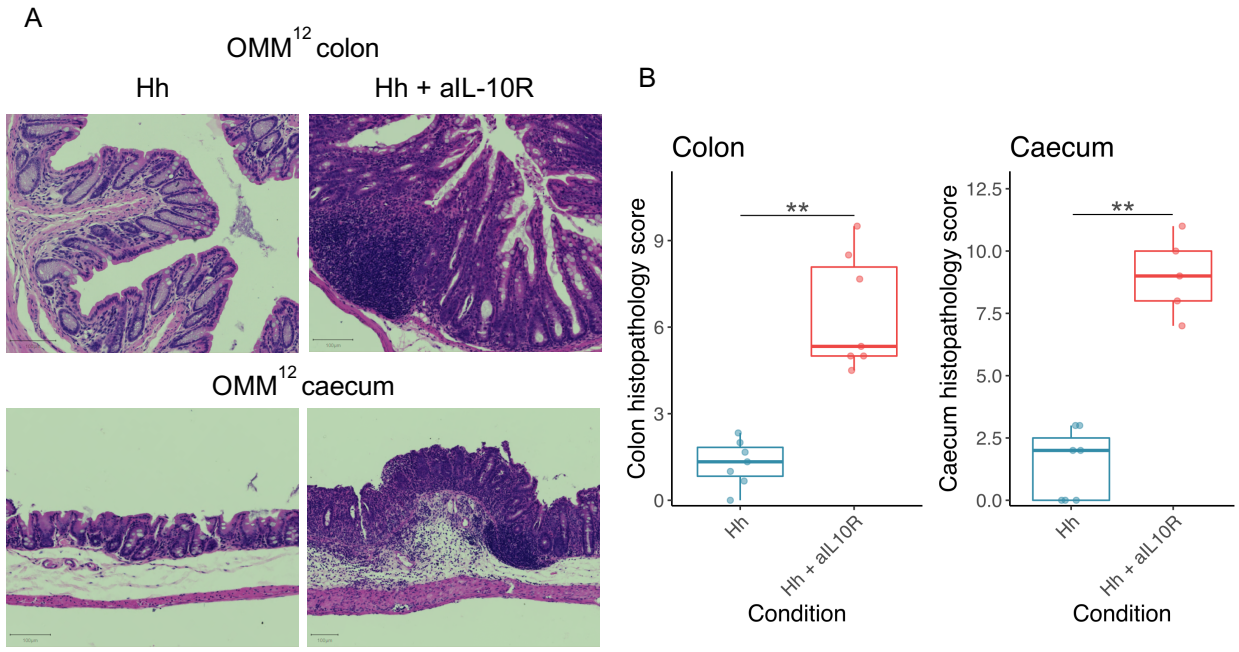


Figure 4.6. OMM[12] mice reproducibly develop inflammation in the colon and caecum following *H. hepaticus* + aIL-10R treatment. A) Representative images from H&E-stained colon and caecum sections obtained from Oligo-Mouse-Microbiota 12 (OMM[12]) mice colonized with *Helicobacter hepaticus*, or colonized with *H. hepaticus* and administered anti-interleukin-10 receptor (aIL-10R). B) Quantification of histopathology scoring of colon and caecum sections. ** p<0.01 Wilcoxon test. Boxplots show median and interquartile range and individual data points are shown. Data obtained from one experiment.

day 1 in the stool and in end-point colon and caecum contents (figure 4.7B).

16S analysis is a useful tool in determining changes in microbial community composition. However, it does so by describing relative abundances as opposed to quantifying absolute changes in a given bacterial species. Thus, we proceeded with qPCR utilizing OMM[12] specific primers, probes and standards to further refine our understanding of dysbiosis in the *H. hepaticus* + aIL-10R OMM[12] model. Notably, *A. muris* KB18 was variably detected in all samples and thus removed from subsequent analysis. Consistent with 16S analysis, *E. faecalis* KB1 was significantly increased in *H. hepaticus* + aIL-10R mice at days 5, 7 and 12 in comparison to baseline (days -13) values (figure 4.8A). Similarly, *E. clostridioformis* YL32 and *M. intestinale* YL27 were significantly reduced at days 5, 7 and 12 in comparison to baseline levels (figure 4.8B and C). *A. muciniphila* YL44 again showed reductions in

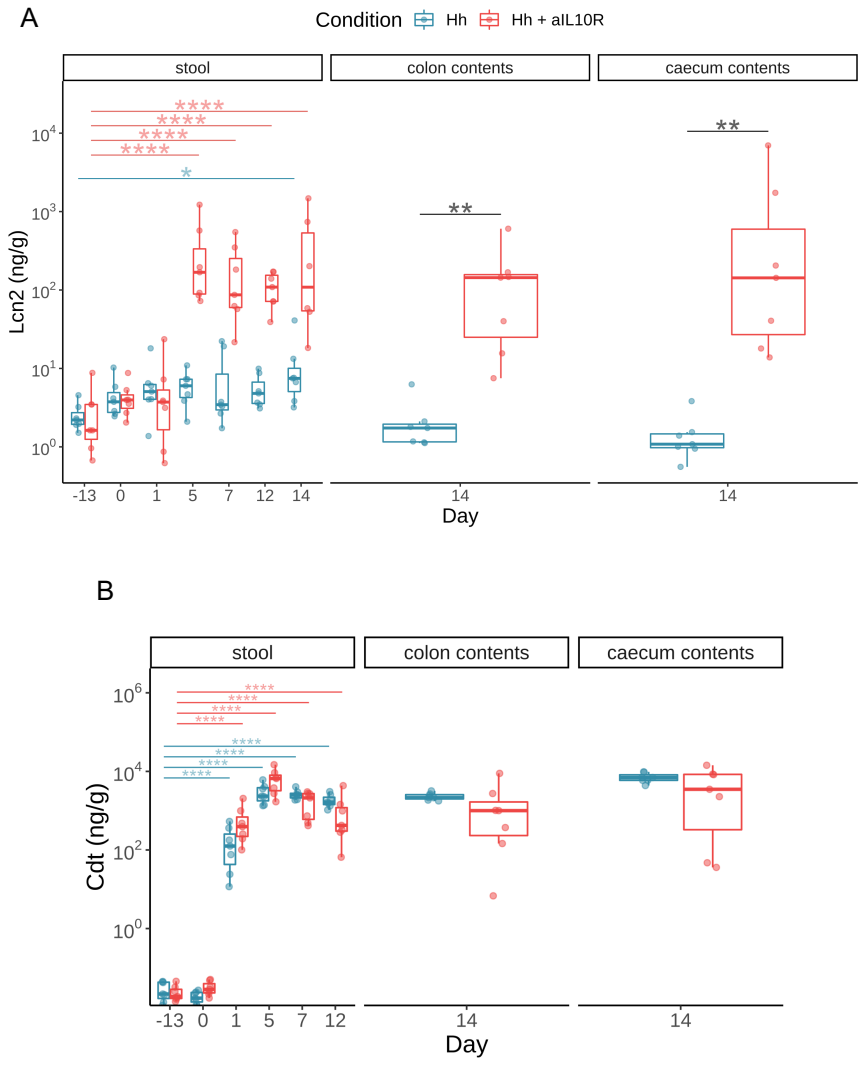


Figure 4.7. Inflammation develops robustly around day 5 after *H. hepaticus* + aIL-10R treatment in OMM^{12} mice and is not associated with a drop in *H. hepaticus* levels. A) Lipocalin-2 levels in longitudinal stool and end-point colon and caecum contents obtained from Oligo-Mouse-Microbiota (OMM^{12}) mice treated with *Helicobacter hepaticus* (Hh) or Hh + anti-interleukin-10 receptor (aIL-10R). B) *H. hepaticus* levels determined by qPCR analysis of Cytolethal distending toxin B (CdtB) DNA in stool, colon and caecum contents of Hh and Hh + aIL-10R OMM^{12} mice. Longitudinal stool statistics done with linear modelling followed by post-hoc estimated marginal means. End-point contents assessed by Wilcoxon test. * p_{adj}<0.05, ** p_{adj}<0.01, ****p_{adj} < 0.0001. Boxplots show median and interquartile range and individual data points are shown. Data obtained from one experiment.

established inflammation as it was significantly reduced in *H. hepaticus* + aIL-10R stool at day 12 (figure 4.8D). In contradiction to the increased abundance detected in 16S profiling, *T. muris* YL45 was significantly reduced at days 5, 7 and 12 in contrast to baseline values (figure 4.8E). Unique *H. hepaticus* + aIL-10R signatures identified by qPCR were significant reductions in *B. caecimuris* I48, *F. plautii* YL31 and *B. coccoides* YL58, although only the

former materialized from day 5 onwards whilst *B. coccoides* YL58 appeared to fluctuate transiently prior to day 5 (figure 4.8F-H).

To establish whether these signatures were maintained in end-point samples, we repeated qPCR analysis on caecum and colon contents. In line with that seen in the stool, *E. faecalis* KB1 was significantly increased whilst *E. clostridioformis* YL32, *M. intestinale* YL27, *A. muciniphila* YL44, *T. muris* YL45, *F. plautii* YL31 and *B. caecimuris* I48 were significantly reduced in *H. hepaticus* + aIL-10R caecum and colon contents (figure 4.9A-G). Interestingly, despite not changing in stool samples, *Bifidobacterium animalis* YL2 was significantly increased in *H. hepaticus* + aIL-10R caecum and colon contents (figure 4.9H). Regardless, changes in caecum and colon contents largely reflected those seen in longitudinal faecal samples.

4.2.4 Discrepancies in dysbiotic signatures inferred by 16S sequencing and qPCR analysis are largely due to relative versus absolute quantification

As our experiments had discrepancies inherent to each analysis type, we utilised OMM^{12} relative abundance profiles calculated from qPCR derived copy numbers to explore if inconsistent bacterial signatures were due to experimental or analytical disparity. *B. coccoides* YL58, *C. innocuum* I46 and *L. reuteri* I49 abundance levels inferred by qPCR were significantly elevated in *H. hepaticus* + aIL-10R mice relative to baseline at days 5, 7 and 12 (figure 4.10A-C). These changes were in accordance with those noted by 16S sequencing, although all coincided with the elevation of faecal LCN2, whereas by 16S this was only the case for *L. reuteri* I49. *B. caecimuris* I48 and *F. plautii* YL31 qPCR determined abundances displayed significant alterations in *H. hepaticus* + aIL-10R mice, although this was limited to transient reductions at days 5 and 12, respectively (figure 4.10D and E). These inferred abundance profiles were more consistent with 16S analysis, in which no significant changes were noted in either bacterium. In contrast to the increase seen by 16S

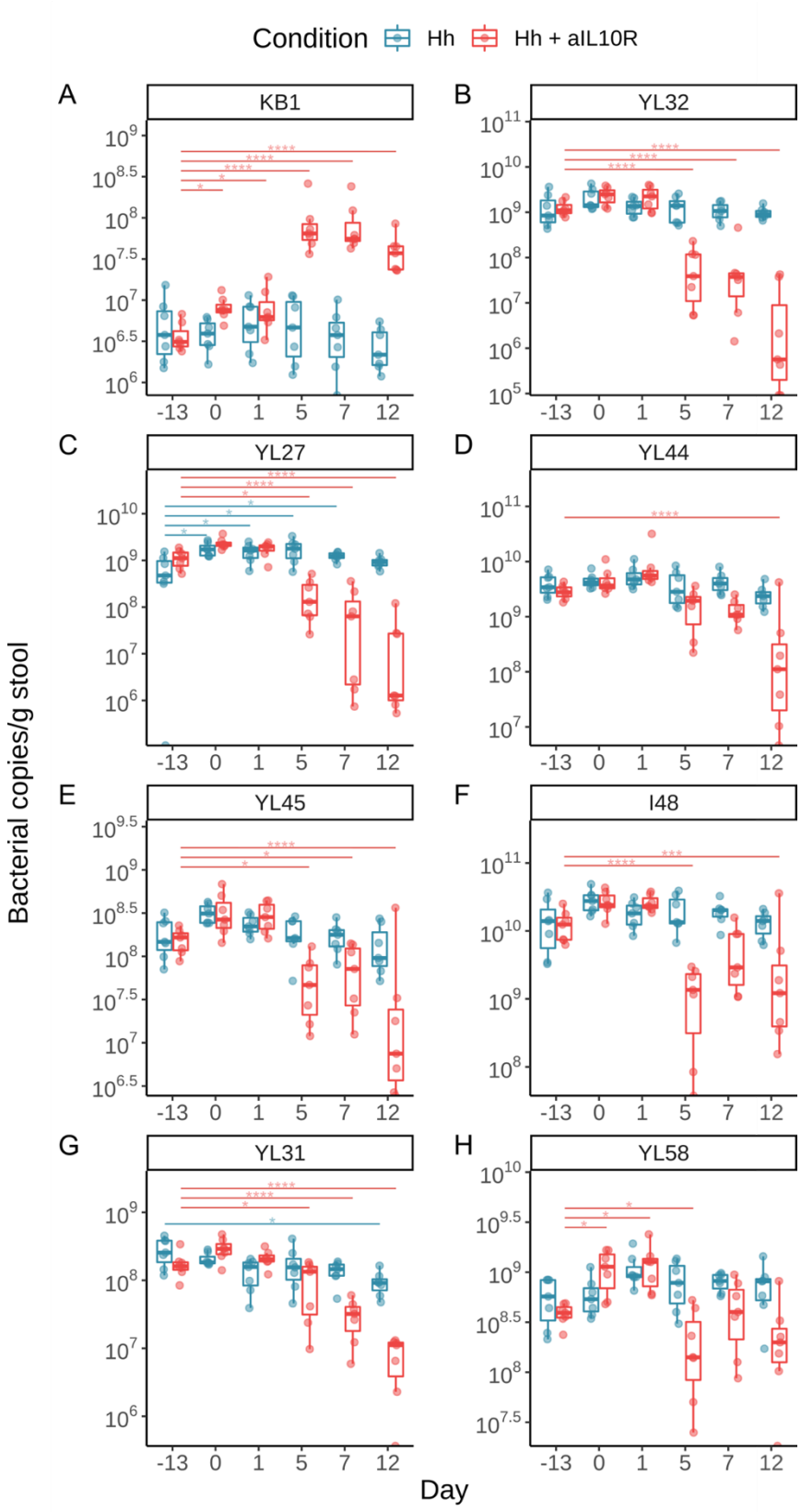


Figure 4.8. An expansion *of E. faecalis* KB1 and reductions in *E. clostridioformis* YL32, *M. intestinale* YL27 and *A. muciniphila* YL44 are robust signatures of *H. hepaticus*-induced OMM^{12} dysbiosis. Absolute values of A) *Enterococcus faecalis* KB1, B) *Enterocloster clostridioformis* YL32, C) *Muribaculum intestinale* YL27, D) *Akkermansia muciniphila* YL44, E) *Turicimonas muris* YL45, F) *Bacteroides caecimuris* I48, G) *Flavonifractor plautii* YL31 and H) *Blautia coccoides* YL58 in *Helicobacter hepaticus* (Hh) and Hh + anti-interleukin-10 receptor (aIL-10R) treated Oligo-Mouse-Microbiota 12 (OMM12) stool. * p_{adj}<0.05, *** p_{adj}<0.001, ****p_{adj} < 0.0001 Linear modelling with post-hoc estimated marginal means analysis. Boxplots display median and interquartile range and individual data points are shown. Data from one experiment

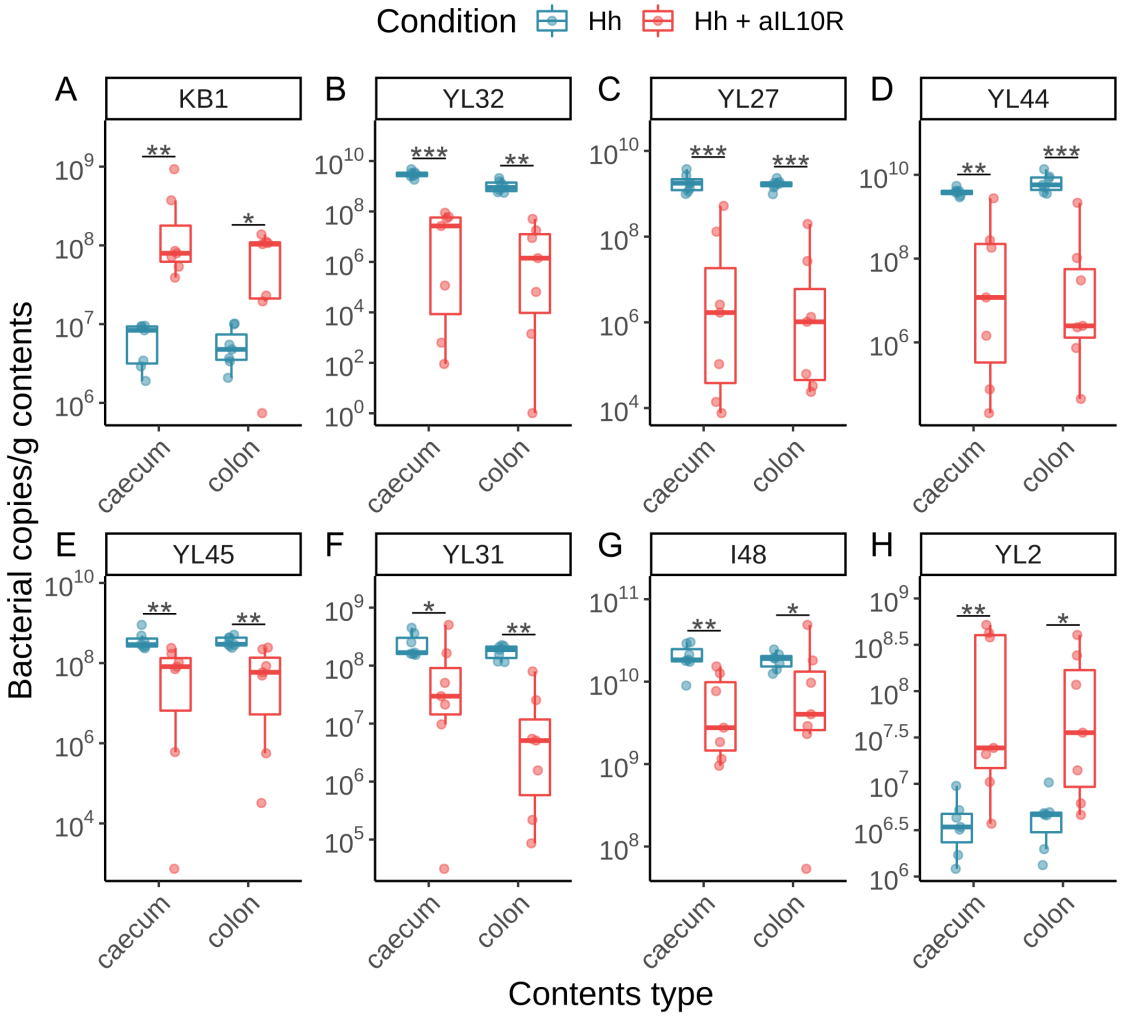


Figure 4.9. Longitudinal signatures of *H. hepaticus*-induced OMM^{12} dysbiosis are present in end-point intestinal contents. Absolute values of A) *Enterococcus faecalis* KB1, B) *Enterocloster clostridioformis* YL32, C) *Muribaculum intestinale* YL27, D) *Akkermansia muciniphila* YL44, E) *Turicimonas muris* YL45, F) *Flavonifractor plautii* YL31, G) *Bacteroides caecimuris* I48 and H) *Bifidobacterium longum* subsp. *animalis* YL2 in *Helicobacter hepaticus* (Hh) and Hh + anti-interleukin-10 receptor (aIL-10R) treated Oligo-Mouse-Microbiota 12 (OMM12) caecum or colon contents. * p_{adj}<0.05, **p_{adj} < 0.01, *** p_{adj}<0.001. Kruskal Wallis with Dunn's post-hoc testing. Boxplots show median and interquartile range and individual data points are shown. Data from one experiment

sequencing, *T. muris* YL45 abundance levels inferred by qPCR were unaltered in both *H. hepaticus* and *H. hepaticus* + aIL-10R groups across timepoints (figure 4.10F). Thus, conversion of absolute to relative abundance profiles corrected dysbiotic signature discrepancies for *B. coccoides* YL58, *C. innocuum* I46, *L. reuteri* I49, *B. caecimuris* I48 and *F. plautii* YL31.

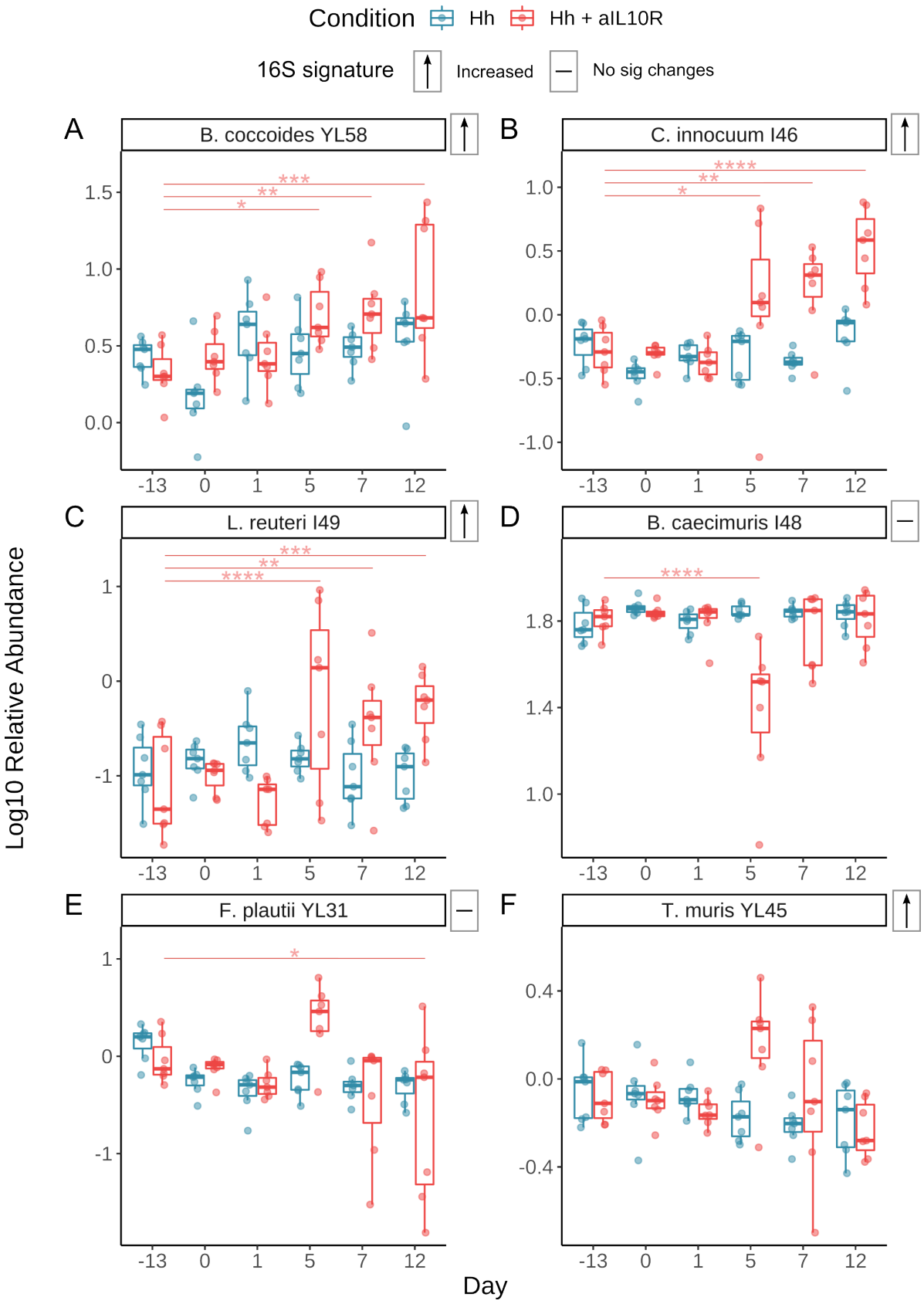


Figure 4.10. Contradictory signatures obtained by 16S versus qPCR analysis are due to discrepancies between relative versus absolute quantification. Relative abundance profiles inferred from qPCR quantification of A) *Blautia coccoides* YL58, B) *Clostridium innocuum* I46, C) *Lactobacillus reuteri* I49, D) *Bacteroides caecimuris* I48, *Flavonifractor plautii* YL31 and *Turicimonas muris* YL45 in Helicobacter hepaticus (Hh) and Hh + anti-interleukin-10 receptor (aIL-10R) Oligo-Mouse-Microbiota 12 (OMM12) stool. Previous dysbiotic signature determined through 16S analysis is dictated to the right of each individual plot. * p_{adj}<0.05, **p_{adj} < 0.01, *** p_{adj}<0.001, ****p_{adj} < 0.0001. Linear modelling with post-hoc estimated marginal means analysis. Boxplots show median and interquartile range and individual datapoints are shown. Data from one experiment.

4.2.5 *H. hepaticus* + aIL-10R colitis is associated with alterations in intestinal metabolite composition

As bacterial derived metabolites have increasingly important roles in gut health, we further sought to understand intestinal metabolite disturbances that developed alongside *H. hepaticus* + aIL-10R colitis and OMM^{12} dysbiosis. Thus, we conducted untargeted mass spectrometry on longitudinal stool and end-point caecum and colon content samples from *H. hepaticus* and *H. hepaticus* + aIL-10R mice.

IC-MS detected ~5600 metabolites per sample (stool: 5405±1234, contents: 6307±1725, mean±SD), with comparable numbers detected between groups across timepoints and intestinal sites (figure 4.11A). Of the total metabolites detected, ~3.1% (stool: 3.2%±0.6%, contents: 2.8%±0.6%, mean±SD) were assigned a putative identification. In stool samples, this was comparable between groups across timepoints (figure 4.11B). In the intestinal contents, 2% of *H. hepaticus* caecum samples held an identification, which was significantly increased to 2.5% in inflamed *H. hepaticus* + aIL-10R mice (figure 4.11B). However, these differences were not seen in colon content samples where annotated fractions were ~3.25% in both experimental groups (figure 4.11B). Despite low identification coverage, abundances derived from annotated metabolites accounted for ~27.0% (stool: 26.0%±6.8%, contents: 30.5%±8.3%) of the total pool. Interestingly, annotated metabolite abundance coverages in stool samples were significantly elevated ~1.5 fold at days 5-14 in *H. hepaticus* + aIL-10R relative to *H. hepaticus* mice (figure 4.11C) which coincided with inflammation onset (figure 4.7A). Moreover, this increase in abundances derived from annotated metabolites in colitic mice was also seen in caecum and colon contents, where differences were 1.3 and 1.4-fold, respectively (figure 4.11C). Thus, IC-MS analysis of longitudinal stool and end-point colon and caecum samples led to the detection of ~5500 metabolites per sample of which ~3% held a putative identification. Nonetheless, the combined abundance levels of annotated metabolites accounted for ~25% of the total metabolite pool. Whilst differences in detection

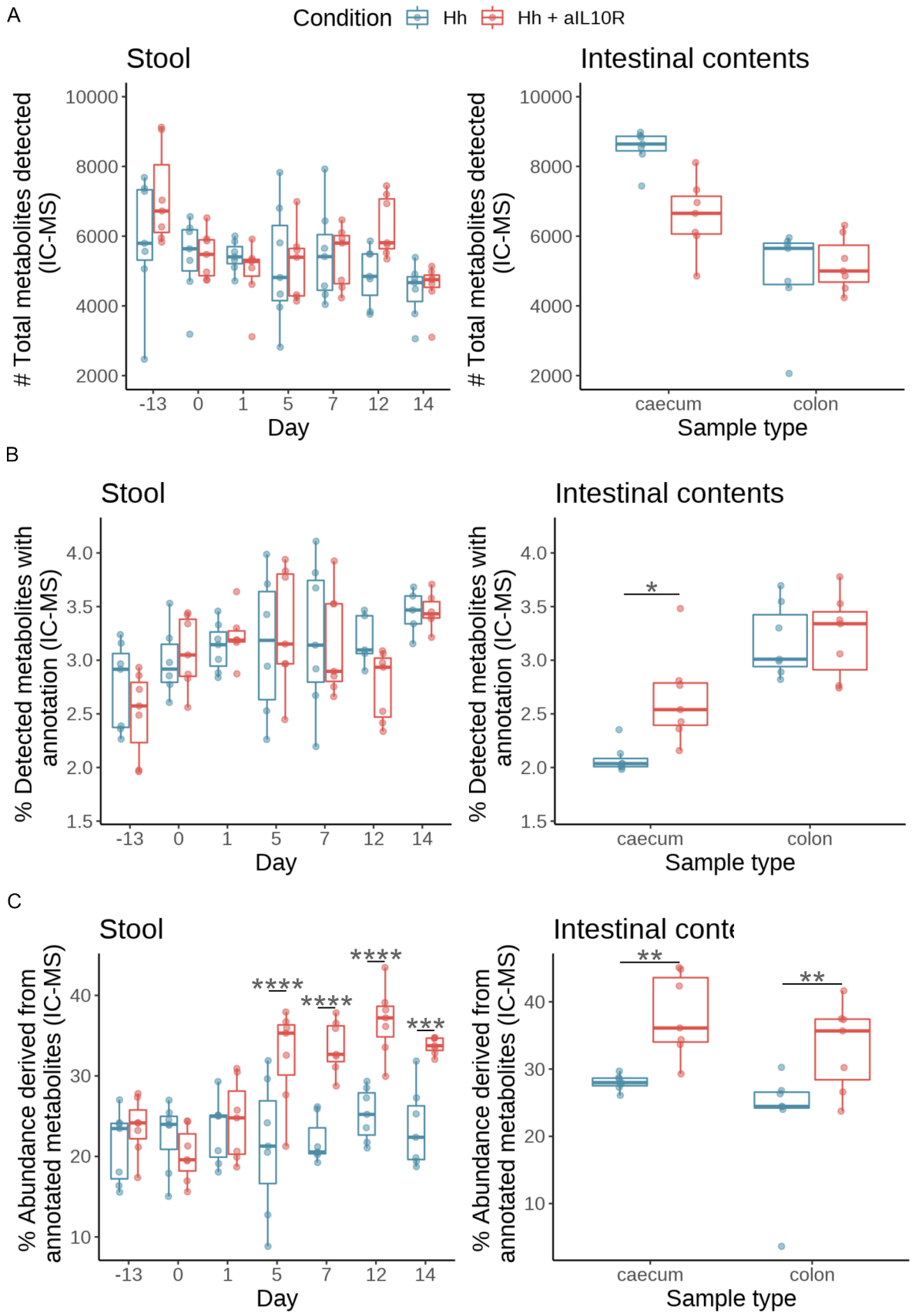


Figure 4.11. Metabolites with a putative identification are at low count but high abundance in untargeted IC-MS data. A) Total number of metabolites detected by ion chromatography mass spectrometry (IC-MS) in stool and intestinal contents obtained from *Helicobacter hepaticus* (Hh) and Hh + anti-interleukin-10 receptor (aIL-10R) treated Oligo-Mouse-Microbiota 12 (OMM^{12}) mice. B) The percentage of total metabolites detected (A) that hold a putative identification form HMDB. C) The abundances derived from annotated metabolite fraction. * p_{adj}<0.05, ** p_{adj} < 0.01, **** p_{adj} < 0.0001. Kruskal Wallis with Dunn's post-hoc testing. Boxplots show median and interquartile range and individual data points are shown. Data from one experiment

level and identification coverage were not explicitly linked to biological reasoning, inflammation consistently led to an increase in annotated metabolite abundance regardless of intestinal sampling site.

From the raw metabolite data, we performed a filtering step to remove metabolites of low abundance (<100 average peak area across samples) and sample prevalence (<20%) (figure 4.12). Prevalence was set at this conservative level based on the rationale that a unique colitic metabolite would have a prevalence of ~33% if presenting in stool samples from day 5 onwards (28/98 samples) and end-point caecum and colon contents (14/28 samples). We then log10 transformed data to normalise distribution profiles (figure 4.13A). In transformed faecal data, *H. hepaticus* + aIL-10R samples began to separate from others from day 5 onwards by PCA (figure 4.13B). Similarly, PCA of end-point caecum and colon data showed clear separation of *H. hepaticus* and *H. hepaticus* + aIL-10R groups. Interestingly, separation of samples according to intestinal site was also apparent within each experimental condition (figure 4.13C).

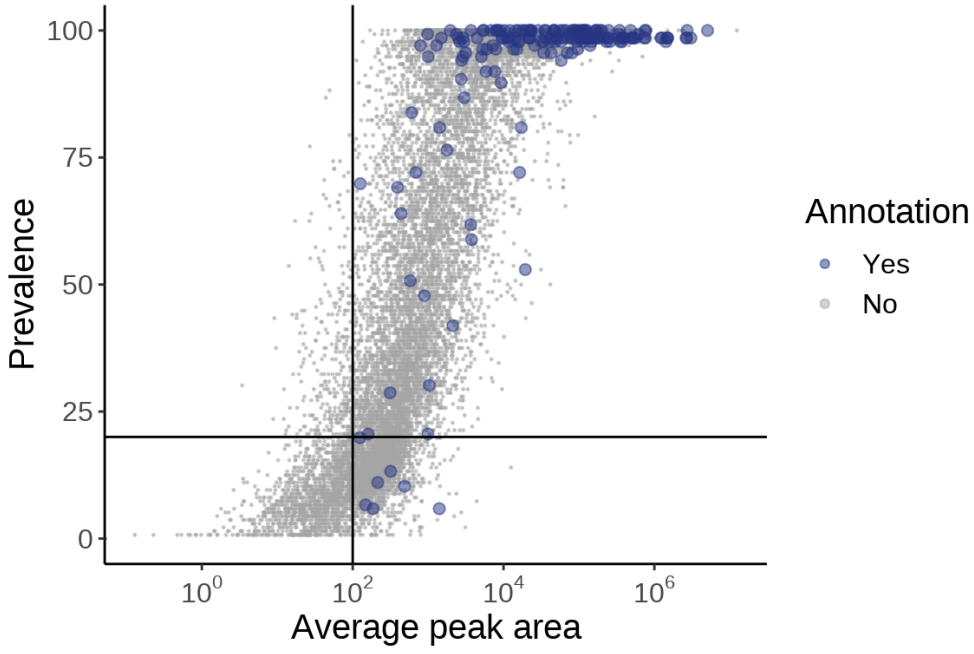


Figure 4.12. Abundance versus prevalence profiles of faecal and intestinal content metabolite data. Metabolites detected by ion chromatography mass spectrometry (IC-MS) in stool and intestinal contents obtained from *Helicobacter hepaticus* (Hh) and Hh + anti-interleukin-10 receptor (aIL-10R) treated Oligo-Mouse-Microbiota 12 (OMM^{12}) mice. Plotted according to prevalence (% of samples present) and abundance (average peak area). Colored according to whether the metabolite holds a putative identification. Data obtained from one experiment

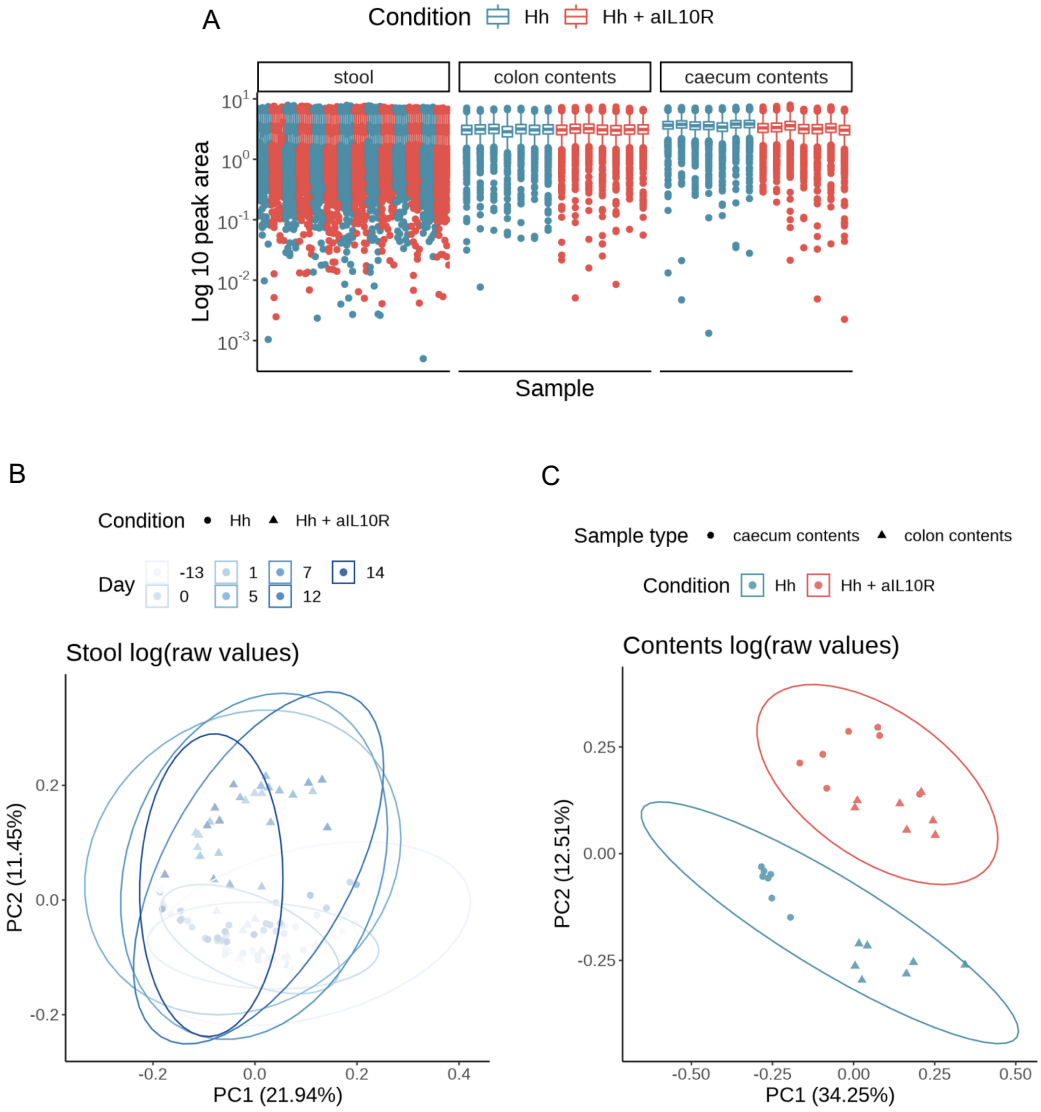


Figure 4.13. Metabolite data from OMM[12] mice displays distinct clustering according to colitic status. A) Distribution plots of log10 transformed metabolites detected by ion chromatography mass spectrometry (IC-MS) in stool and intestinal contents obtained from *Helicobacter hepaticus* (Hh) and Hh + anti-interleukin-10 receptor (aIL-10R) treated Oligo-Mouse-Microbiota 12 (OMM[12]) mice. B) Principal components analysis (PCA) of faecal metabolites coloured by day, with shape depicting experimental condition. C) PCA of intestinal content metabolites coloured by day, with shape depicting intestinal site. Data obtained from one experiment

As annotated metabolites were of most immediate interest, we subsetted metabolites that held a putative identification (177 metabolites). Repeat PCA of these annotated metabolites led to the identification of 7 outliers (6 faecal and 1 colon content) (figure 4.14A), removal of which restored data clustering patterns seen in the whole dataset by PCA (figure 4.14B). Outliers were obtained from mixed animals at altering time points across treatment groups and displayed excessive zero counts in either total or annotated metabolite fractions

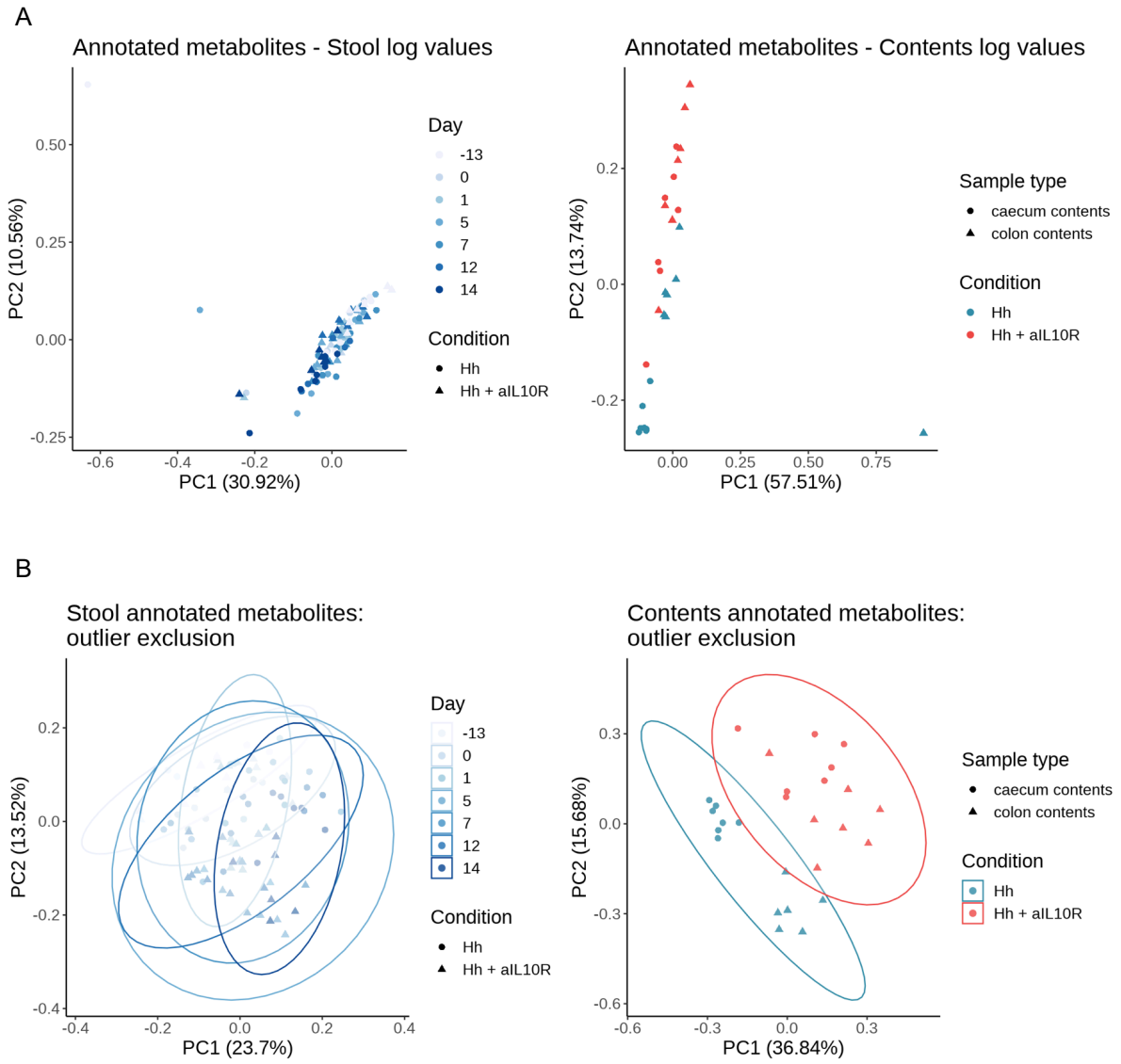


Figure 4.14. Annotated metabolite fractions show clear separation according to colitic status following outlier removal. A) Principal components analysis (PCA) of annotated metabolites detected by ion chromatography mass spectrometry (IC-MS) in stool and intestinal contents obtained from *Helicobacter hepaticus* (Hh) and Hh + anti-interleukin-10 receptor (aIL-10R) treated Oligo-Mouse-Microbiota 12 (OMM^{12}) mice. For the stool, samples are coloured by day, with shape depicting condition. For intestinal contents, samples are coloured by condition with shape depicting intestinal site. B) Repeat PCA of annotated metabolite fraction data with clear outliers from A) removed. Data obtained from one experiment.

suggesting technical as opposed to biological reasoning for their outlier status (appendix figure A.5). Following outlier exclusion, we applied linear mixed effects modelling to identify metabolites with inflammatory-associated changes in abundance. In the stool, the model was identical to that used for community compositional analysis. Faecal metabolites of interest were those with significance driven by the interaction term of this model, implying

differing changes over time in each experimental group (66 metabolites). Significant faecal metabolites fell into 2 distinct clusters, which appeared to be upregulated (cluster 1) or downregulated (cluster 2) over time predominantly in the *H. hepaticus* + aIL-10R group (figure 4.15A). Caecum and colon content end-point data was assessed by a similar model, although as pathology developed in both the caecum and colon, intestinal site influences were less important when determining metabolite significance. Thus, metabolites of interest were those driven by experimental condition alone (98 metabolites). Significant content metabolites fell into 3 distinct clusters, those upregulated (cluster 0) or downregulated (cluster 1) to a similar extent across intestinal sites predominantly in *H. hepaticus* + aIL-10R mice and those where reductions were restricted to colitic caecum contents (cluster 2) (figure 4.15B).

4.2.6 Metabolite disturbances in OMM^{12} mice recapture signatures seen in IBD

Metabolomic analysis of IBD patient samples has led to the identification of key bacterial-derived metabolites with overt influence over intestinal physiology. Those featured heavily in the field include SCFAs, secondary bile acids, tryptophan metabolites and tricarboxylic acid (TCA) cycle intermediates, predominantly succinate [251]. Moreover, dietary-derived MCFAs, although less of a focus than SCFAs, have also been reportedly reduced in IBD patients [251,260,261]. Thus, we proceeded to interrogate our significant faecal and intestinal content datasets to determine if alterations in any of the above featured in OMM^{12} colitis. Notably, we were not able to identify a number of metabolites in our annotated fraction, including propionate, acetate or any primary or secondary bile acids. However, we did readily detect butyrate, and hydroxy-isobutyrate, indoles, kynurenine, MCFAs and TCA cycle intermediates. In the stool, there were significant reductions in several MCFAs, namely nonate, pimelic acid, suberic acid and hydroxyoctanoic acid, and the tryptophan metabolite indolelactic acid (ILA) at the point of inflammation development in *H. hepaticus* + aIL-10R treated mice. Moreover, metabolites relating to the TCA cycle, namely succinate, pyruvate

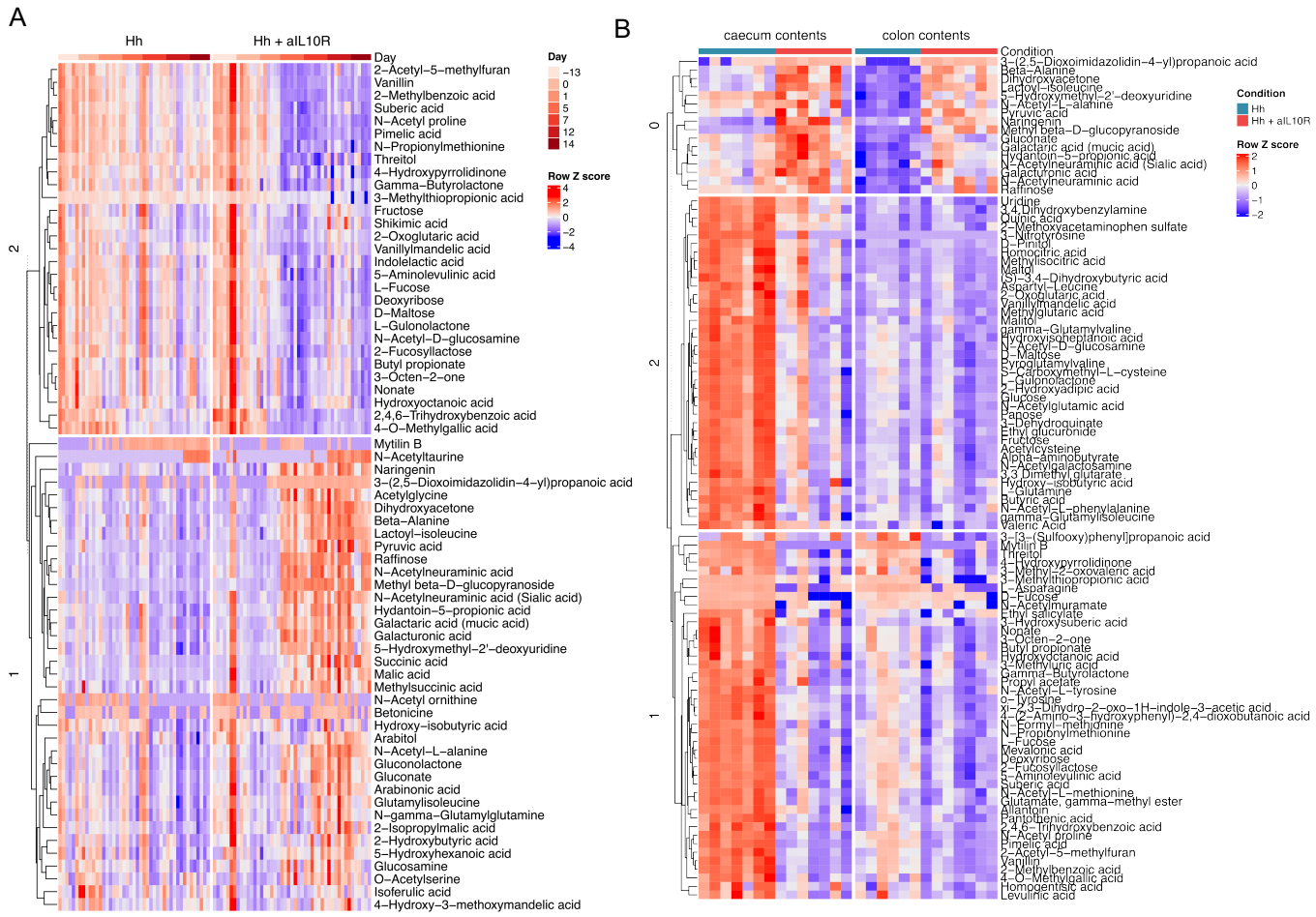


Figure 4.15. *H. hepaticus*-induced colitis in OMM[12] mice is associated with shifts in faecal and intestinal metabolite composition. Heatmaps displaying metabolites with significant inflammation-associated alterations in A) faecal and B) intestinal content samples obtained from *Helicobacter hepaticus* (Hh) and Hh + anti-interleukin-10 receptor (aIL-10R) treated Oligo-Mouse-Microbiota 12 (OMM[12]) mice. Data obtained from one experiment

and malate were increased in *H. hepaticus* + aIL-10R colitic faecal samples (figure 4.16). Inflammatory-associated reductions in nonate, pimelic acid and suberic acid were also seen in end-point caecum and colon contents. In the caecum we also detected reduced levels of the MCFAs valeric acid and hydroxyoctanoic acid, and SCFAs butyrate and hydroxy-isobutyrate. In colon contents and reflective of the profile seen in faecal samples, pyruvate levels were significantly elevated in *H. hepaticus* + aIL-10R mice (figure 4.17). Thus, metabolite disturbances induced by *H. hepaticus* + aIL-10R colitis in OMM[12] mice shared features common to human IBD. Namely, these included increases in TCA cycle metabolites and reductions in SCFAs, MCFAs and tryptophan derivatives.

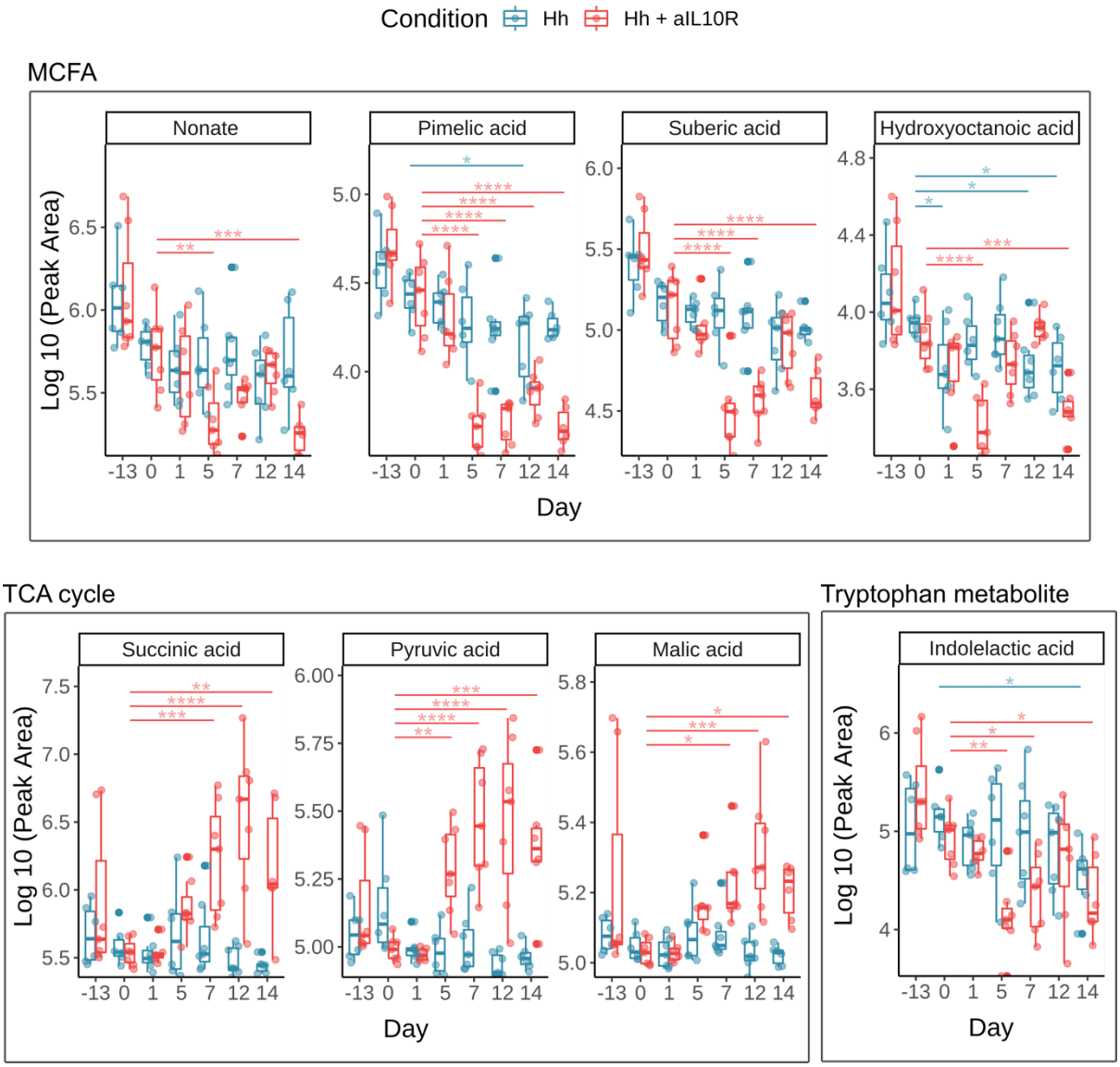


Figure* 4.16. Inflammatory-associated shifts in faecal metabolite profiles recapitulates signatures seen in human IBD.** Metabolites identified as significantly altered in *H. hepaticus* (Hh)-induced inflammation in Oligo-Mouse-Microbiota 12 (OMM^{12}) faecal samples with putative identification relating to medium chain fatty acid (MCFAs), tricarboxylic acid (TCA) cycle intermediates and tryptophan metabolites. Plots denoted relative abundances in Hh and Hh + anti-interleukin-10 receptor (aIL-10R) OMM^{12} mice. *p_{adj} < 0.05, **p_{adj} < 0.01, ***p_{adj} < 0.001, *p_{adj} < 0.0001. Linear modelling with post-hoc estimated marginal means analysis. Boxplots show median and interquartile range and individual data points are shown. Data obtained from one experiment

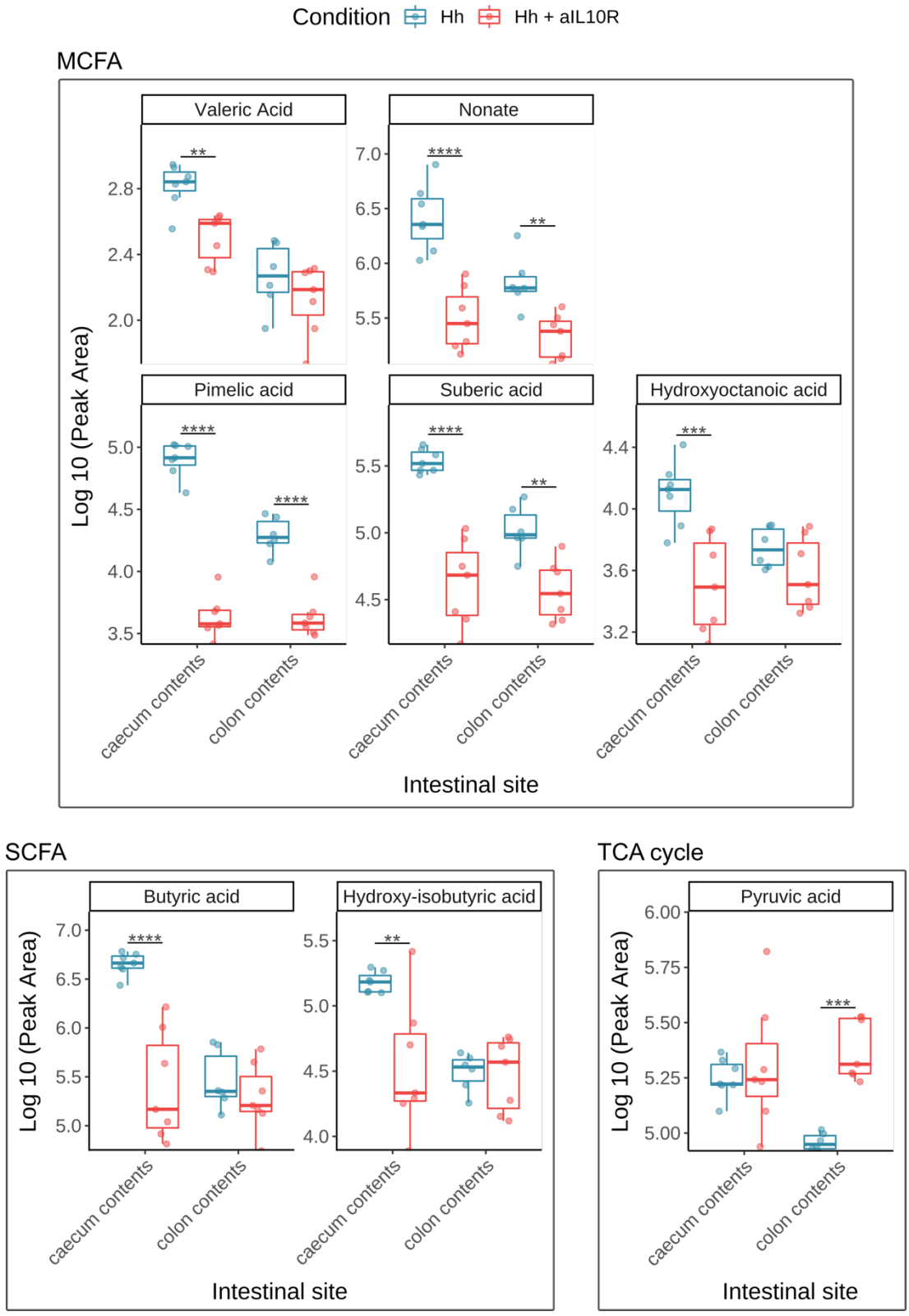


Figure 4.17. Inflammatory-associated shifts in intestinal content metabolite profiles recapitulate signatures seen in human IBD. Metabolites identified as significantly altered in *H. hepaticus* (Hh)-induced inflammation in Oligo-Mouse-Microbiota 12 (OMM^{12}) intestinal contents with putative identification relating to medium chain fatty acid (MCFAs), short chain fatty acids (SCFAs) or tricarboxylic acid (TCA) cycle intermediates. Plots denoted relative abundances in Hh and Hh + anti-interleukin-10 receptor (aIL-10R) OMM^{12} mice. **p_{adj} < 0.01, ***p_{adj} < 0.001, ****p_{adj} < 0.0001. Kruskal Wallis with Dunn's post-hoc testing. Boxplots show median and interquartile range and individual data points are shown. Data obtained from one experiment.

4.2.7 Benzenoids are a unique chemical class downregulated across all intestinal sampling sites in *H. hepaticus* + aIL-10R colitis

To further unbiasedly define a subset of metabolites significantly upregulated or downregulated across all colic samples in OMM^{12} mice, we overlaid metabolites belonging to cluster 1 and 0 or cluster 2 and 1 in faecal and content analysis, respectively. This led to the identification of 37 annotated metabolites spanning 7 chemical classes that were significantly upregulated (16) or downregulated (21) during *H. hepaticus* induced inflammation (table 4.1). Interestingly, in addition to the previously identified MCFAs, benzenoids represented a chemical class unique to and enriched in the downregulated metabolite fraction. In the stool, 2-methylbenzoic acid, 2, 4, 6-trihydroxybenzoic acid, 4-O-methylgallic acid (4-OMGA) and vanillin levels appeared to reduce over time in both *H. hepaticus* and *H. hepaticus* + aIL-10R groups, although, with the exception of 4-OMGA, reductions were greater and more significant in *H. hepaticus* + aIL-10R samples (figure 4.18A). In intestinal contents, 2-methylbenzoic acid and vanillin were significantly reduced across both the caecum and colon, whereas 4-OMGA and 2,4,6-trihydroxybenzoic acid were only significantly reduced in the caecum (figure 4.18B). Thus, we further identified several metabolites belonging to the benzenoids chemical class that were significantly downregulated in *H. hepaticus* + aIL-10R colitis.

Metabolite	Group
2,4,6-Trihydroxybenzoic acid	Down: Benzenoids
2-Methylbenzoic acid	Down: Benzenoids
4-O-Methylgallic acid	Down: Benzenoids
Vanillin	Down: Benzenoids
3-Methylthiopropionic acid	Down: Lipids and lipid-like molecules
Hydroxyoctanoic acid	Down: Lipids and lipid-like molecules
Nonate	Down: Lipids and lipid-like molecules
Pimelic acid	Down: Lipids and lipid-like molecules
Suberic acid	Down: Lipids and lipid-like molecules
5-Aminolevulinic acid	Down: Organic acids and derivatives
Butyl propionate	Down: Organic acids and derivatives
N-Acetyl proline	Down: Organic acids and derivatives
N-Propionylmethionine	Down: Organic acids and derivatives
2-Acetyl-5-methylfuran	Down: Organic oxygen compounds
2-Fucosyllactose	Down: Organic oxygen compounds
3-Octen-2-one	Down: Organic oxygen compounds
Deoxyribose	Down: Organic oxygen compounds
L-Fucose	Down: Organic oxygen compounds
Threitol	Down: Organic oxygen compounds
Gamma-Butyrolactone	Down: Organoheterocyclic compounds
4-Hydroxypyrrolidinone	Down: Organoheterocyclic compounds
5-Hydroxymethyl-2'-deoxyuridine	Increased: Nucleosides, nucleotides and analogues
Beta-Alanine	Increased: Organic acids and derivatives
Lactoyl-isoleucine	Increased: Organic acids and derivatives
N-Acetyl-L-alanine	Increased: Organic acids and derivatives
Pyruvic acid	Increased: Organic acids and derivatives
Dihydroxyacetone	Increased: Organic oxygen compounds
Galactaric acid (mucic acid)	Increased: Organic oxygen compounds
Galacturonic acid	Increased: Organic oxygen compounds
Gluconate	Increased: Organic oxygen compounds
Methyl beta-D-glucopyranoside	Increased: Organic oxygen compounds
N-Acetylneuraminic acid	Increased: Organic oxygen compounds
N-Acetylneuraminic acid (Sialic acid)	Increased: Organic oxygen compounds
Raffinose	Increased: Organic oxygen compounds
3-(2,5-Dioxoimidazolidin-4-yl)propanoic acid	Increased: Organoheterocyclic compounds
Hydantoin-5-propionic acid	Increased: Organoheterocyclic compounds
Naringenin	Increased: Phenylpropanoids and polyketides

Table 4.1. *H. hepaticus* + aIL-10R colitis in OMM^{12} mice is associated with shifts of distinct metabolites across intestinal sites. Metabolites identified as significantly altered in faecal and intestinal content samples in colitic *H. hepaticus* + anti-interleukin-10 receptor (aIL-10R) treated Oligo-Mouse-Microbiota 12 (OMM^{12}) mice. Group given as chemical class and upregulation or downregulation pattern. Data obtained from one experiment

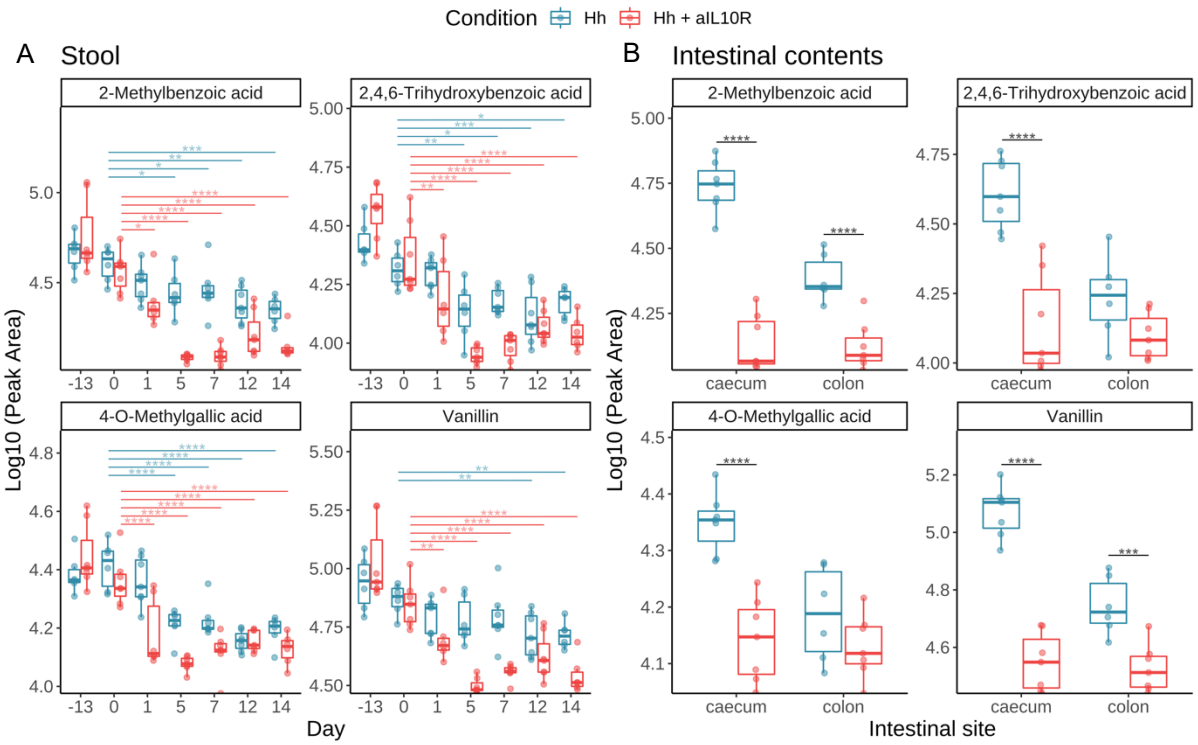


Figure 4.18. Benzenoids represents a chemical class uniquely downregulated in *H. hepaticus* + aIL-10R colitis in OMM^{12} mice. Profiles of individual metabolites pertaining to the benzenoids class in A) stool and B) intestinal content samples obtained from H. hepaticus (Hh) and Hh + anti-interleukin-10 receptor (aIL-10R) treated Oligo-Mouse-Microbiota 12 (OMM^{12}) mice. *p_{adj}<0.05, **p_{adj} < 0.01, ***p_{adj} < 0.001, ****p_{adj} < 0.0001 A) Linear modelling with post-hoc estimated marginal means analysis and B) Kruskal Wallis with Dunn's post-hoc testing. Boxplots show median and interquartile range and individual data points are shown. Data obtained from one experiment

4.3 Discussion

Defined microbial communities offer the ability to identify causative microbes in the pathogenesis of IBD. We have utilised the OMM^{12} to decipher the role of the microbiota in *H. hepaticus* induced colitis in the context of IL-10 deficiency. GF mice administered aIL-10R alongside *H. hepaticus* infection failed to develop pathology as is consistent with previously published findings [171,172,202]. OMM^{12} colonized mice developed colitis only when administered aIL-10R alongside *H. hepaticus* infection, but not from aIL-10R treatment nor *H. hepaticus* infection alone, recapitulating what is seen in SPF mice [78]. As this is a repeatable phenotype, *H. hepaticus* + aIL-10R colitis in OMM^{12} mice is a robust model in which to dissect causal roles for commensals in the development of intestinal inflammation.

Omic technology platforms have been widely employed in human studies to implicate the gut microbiota in IBD [84]. We carried out extensive characterisation of OMM^{12} community and intestinal metabolite dynamics over the course of *H. hepaticus* + aIL-10R colitis, performing LCN2 analysis on matched samples to link information about population and metabolite shifts with that of the developing host inflammatory response. In regards to population shifts, we utilised 16S sequencing and qPCR to describe relative and absolute changes in bacterial levels. Dysbiosis in the OMM^{12} community robustly comprised an expansion of *E. faecalis* KB1 and reductions in *E. clostridioformis* YL32, *M. intestinale* YL27 and *A. muciniphila* YL44. Whilst the former signatures coincided with rising faecal LCN2 levels, *A. muciniphila* YL44 reductions were only seen at later disease stages and thus reflective of a response to established inflammation. These changes were maintained across 2 independent experiments regardless of analysis type, inferring that changes in abundances were driven by absolute increases or reductions in each bacterial population.

In addition to robust signatures of OMM^{12} dysbiosis, we also observed bacterial changes that were inconsistent between 16S sequencing and qPCR analysis. Inferring relative abundances from absolute values corrected signature inconsistencies in the majority of cases. *C. innocuum* I46, *L. reuteri* I49 and *B. coccoides* YL58 increased in abundance across experiments. However, whilst *C. innocuum* I46 and *L. reuteri* I49 coincided with inflammation, *B. coccoides* YL58 dynamics differed between experiments, suggesting this does not robustly correlate with inflammation in this model. As absolute levels of these bacteria were stable across the disease time course, these increased abundances appear to be due to contractions in the OMM^{12} community. Interestingly, qPCR-inferred relative abundance levels masked inflammation associated reductions in the absolute levels of *B. caecimuris* I48 and *F. plautii* YL31. However, it is not clear whether these changes also occurred in the 16S experiment due to our inability to delineate absolute values from 16S sequencing data. Moreover, *T. muris* YL45, whilst significantly altered in both experiments, had contradictory signatures that could not be explained by absolute versus relative

quantification. Thus, this bacterium did not display consistent shifts over the course of *H. hepaticus* + aIL-10R induced inflammation.

Dysbiosis observed in IBD is characterised by the emergence of facultative anaerobic bacteria from a community that in health is dominated by obligate anaerobic members [262]. Often this expansion is attributed to bacteria pertaining to the Pseudomonadota phylum, in particular mucosa associated members of the Enterobacteriaceae family, which has led to a growing body of work pursuing the exacerbation of colitis by Enterobacteriaceae species [49,190,194,235,252]. Interestingly, dysbiosis in OMM^{12} mice was characterised in-part by absolute and/or relative increases of *E. faecalis* KB1 and *L. reuteri* I49, which are the only facultative anaerobic members of the OMM^{12} community. Notably, *E. faecalis* has previously been shown to induce colitis in GF *Il10*$^{-/-}$ mice although disease severity is dependent on the infecting strain [263,264]. *E. faecalis* KB1 has been identified as a dominant driver in shaping OMM^{12} community composition *in vitro* and produces antimicrobials effective against *E. clostridioformis* YL32, *F. plautii* YL31, *C. innocuum* I46, *L. reuteri* I49 and *B. animalis* YL2 [183], although only *E. clostridioformis* YL32 and *F. plautii* YL31 showed reductions during inflammation and *E. faecalis* KB1 outgrowth in our model. Whilst *L. reuteri* strains are generally considered anti-inflammatory and are reported to have therapeutic effects in animal colitis models [265,266], *L. reuteri* ATCC PTA 6475 has been shown to promote *H. hepaticus* colitis in monoassociated *Il10*$^{-/-}$ mice [202]. Regardless of causal implications, an outgrowth of facultative anaerobic bacteria in this highly reductionist model free of Enterobacteriaceae family members suggests dysbiotic signatures that mimic those seen in complex murine and human settings. Interestingly, the development of dysbiosis and disease in the absence of Enterobacteriaceae family members highlights other commensals as disease drivers in this context.

In addition to an increase in facultative anaerobic OMM^{12} members, *C. innocuum* I46 showed consistent inflammation-associated increases in relative abundance. Interestingly,

this bacteria has been implicated in antibiotic-associated diarrhoea and the development of "creeping fat" in CD patients due to its ability to translocate to and modulate mesenteric adipose tissue [267,268]. We also noted reductions in the absolute and relative abundance levels of *A. muciniphila* YL44, *M. intestinale* YL27 and *E. clostridioformis* YL32 coinciding with developing or established inflammation. *M. intestinale* YL27 has been found to be reduced in the ileal contents of mice with spontaneous CD-like ileitis [269]. In contrast, *A. muciniphila* expands and promotes colitis in the context of dual NOD-like receptor family pyrin domain-containing 6 (NLRP6) and IL-10 deficiency and renders mice maintained on a fibre-free diet susceptible to *C. rodentium* colitis due to its ability to degrade the host mucus barrier [7,139]. However, in DSS colitis *A. muciniphila* has been shown to ameliorate or exacerbate pathology depending on the infecting strain [270].

E. clostridioformis YL32 was historically assigned to the *Clostridium* XIVa cluster, a group of *Clostridium* species associated with butyrate production [271]. Butyrate has been shown to mediate multiple homeostatic functions within the intestine, including T_{reg} cell generation, in turn promoting interest in developing this SCFA as a microbiota-based therapeutic [53]. However, *E. clostridioformis* YL32, recently reclassified from *Clostridium clostridioforme* based on 16S rRNA gene phylogeny, does not produce butyrate [183,271]. Notably, *F. plautii* YL31 and *C. innocuum* I46 are the butyrate producing members of the OMM^{12} [179,183], of which we found *F. plautii* YL31 to be reduced in *H. hepaticus* + aIL-10R colitis. SCFA levels in OMM^{12} mice are lower than that of their SPF counterparts, with butyrate in particular being present at very low concentrations in OMM^{12} caecal content (<1 μmol/g) [179,182]. Despite this, we were able to detect butyrate and hydroxy-isobutyrate in our annotated metabolite fraction, where they showed significant reductions in the caecum contents of *H. hepaticus* + aIL-10R mice. Dysbiotic reductions in butyrate-producing bacteria is a feature of human IBD and butyrate levels are lower in UC patients with active disease [272,273]. Thus, reductions in butyrate producers and corresponding reductions in butyrate levels is an IBD signature recaptured in the *H. hepaticus* + aIL-10R OMM^{12} model.

In addition to SCFAs, we identified several medium chain fatty acids (MCFAs) that were reduced during *H. hepaticus* + aIL-10R-induced colitis in OMM^{12} mice. This signature is shared in human IBD, as MCFA levels are consistently reported to be reduced in IBD faecal samples [260,261]. In addition to fatty acids, bile acids, tryptophan metabolites and succinate have been implicated in IBD pathogenesis [251]. Notably OMM^{12} members do not have the capacity for 7α-dehydroxylation and thus cannot generate SBAs DCA and LCA [257]. Whilst these are undetectable in OMM^{12} mice, PBAs, predominantly cholic acid (CA) and β-muricholic acid (BMCA), have been identified in steady state caecal content [257]. CA, when administered with derivatives also present in OMM^{12} caeca, has been shown to have therapeutic effects on T_{reg} cell differentiation *in vitro* [58,257]. However, we were unable to detected CA, BMCA or other primary bile acids in our annotated metabolite fraction.

Tryptophan metabolites serve as ligands for the aryl hydrocarbon receptor (AHR), which modulates various homeostatic functions in CD4 T cells, IECs, intraepithelial lymphocytes (IELs) and ILCs [54]. Whilst we were able to identify several tryptophan metabolites in our annotated dataset, only ILA was significantly reduced in colitic OMM^{12} stool. *Lactobacillus* and *Bifidobacterium* species have been shown to produce ILA, which acts via the AHR to inhibit Th17 cell polarization, induce the differentiation of barrier protective $CD4^+CD8\alpha\alpha^+$ IELs and suppress pro-inflammatory IL-8 production by IECs *in vitro* [274–276]. *Ahr*$^{-/-}$ deficient mice are susceptible to chronic intestinal inflammation and rectal prolapse, which interestingly in turn is associated with *H. hepaticus* infection [277]. Moreover, AHR signalling promotes colonic IL-22 production and Th17 cell differentiation *in vivo*, which confers protection in various colitis models including that induced by DSS and infection with *C. rodentium* [55,278]. Notably, AHR is reduced on IBD patient intestinal tissues and the traditional Chinese medicine Inidigo naturalise, which contains AHR ligands including indole, has been shown to promote mucosal healing in UC patients although with extraintestinal adverse effects [278–280].

Succinate is a TCA cycle intermediate that, in addition to being produced by host mitochondria, is produced by the gut microbiota where it is actively transported across the epithelium into the intestinal lamina propria [251,281]. Succinate levels, and that of its receptor, are increased in IBD patients and deletion of the succinate receptor protects mice from chemically induced colitis [282,283]. This dysbiotic metabolic signature was shared by OMM^{12} mice as succinate was significantly elevated in colitic *H. hepaticus* + aIL-10R faecal samples. Moreover, pyruvate, which is converted to acetyl-CoA for entry into the TCA cycle, was also significantly upregulated in OMM^{12} colitic faecal, colon and caecal content samples. Although less prominently implicated in IBD than succinate, levels of M2-pyruvate kinase, which catalyses the generation of pyruvate, are increased in IBD patients [284].

In addition to metabolites with established links to IBD in the literature, we identified a number of metabolites that did not fall into the above groups. Most strikingly, benzenoids served as a chemical class unique to and enriched in metabolites downregulated in *H. hepaticus* + aIL-10R colitis. Namely, we saw significant reductions across faecal and intestinal sites of vanillin, 4-OMGA, 2, 4, 6-trihydroxybenzoic acid and 2-methylbenzoic acid. Interestingly, vanillin has antioxidant activity and is protective in chemically-induced colitis [285–287]. Moreover, 4-OMGA has been shown to inhibit NF-κB activity and ROS production in endothelial cells *in vitro* [288]. Thus, the identification of benzenoids in our model and described anti-inflammatory action in the literature warrants further investigation into the therapeutic potential of these metabolites in experimental colitis.

Importantly, we only conducted statistical analysis on our annotated metabolite dataset, which accounted for ~3% of the total number detected. This metabolomic “dark matter” therefore represents a major limitation of our study and one that is shared by the field [289]. Moreover, it is important to note that even where metabolites held an identification, this was putative and targeted approaches would be required to validate our experimental findings.

This would also inform as to the absolute values of a given metabolite and remove the reliance on relative data. Whilst the microbiome field has been dependent on conducting compositional analysis utilising relative abundance measures, absolute versus relative changes likely have significant biological importance [290]. Indeed, within our own study we found the relative increases of *L. reuteri* I49 and *C. innocuum* I46 were not driven by absolute expansion of these bacteria, thus questioning the relevance of these bacterial signatures. Moreover, the spatial distribution of bacteria within the intestine likely plays a role in their influence over host responses [1]. For example, residence within the colonic mucus layer in close association with the epithelium likely plays a role in the ability of bacteria to influence host physiology, as is the case with *H. hepaticus* [1,291]. As our compositional analysis utilised intestinal contents representative of luminal bacterial populations [292], this is therefore another limitation of our study that overlooks both population and metabolic changes likely at the forefront of host-microbiota interactions.

Despite our experimental limitations, we were able identify signatures of inflammatory associated population and metabolite disturbances that shared similarities with those described in complex murine and human data. Thus, although the OMM^{12} reflects a highly reductionist approach to understanding the role of the microbiota in colitis, it is one that captures aspects relevant to human physiology. Whilst our characterisation experiments are important first steps in understanding the role of OMM^{12} members in the *H. hepaticus* + aIL-10R colitis model, functional validation of all disease association signatures is required to confirm the importance of these findings. Thus, further experiments focusing on causal as opposed to correlative relationships between OMM^{12} members and *H. hepaticus* + aIL-10R colitis are critical to understand disease promoting host-bacteria and bacteria-bacteria interactions in this model.

Chapter 5 *Enterocloster clostridioformis* YL32 is a key facilitator of *H. hepaticus*-induced colitis

5.1 Introduction

Descriptive analyses have dominated the microbiota research field and implicated dysbiosis in IBD pathogenesis. Naturally, the field is evolving to understand whether such associations are causal of, or consequential to, disease development. This understanding in turn will feed into the development of microbiota-based therapeutics. At present, the microbiota represents a relatively untapped resource in the clinic. Indeed, current applications comprise relatively crude microbiota therapies including FMT, antibiotics and probiotics, all of which have had limited effects in clinical trials of patients with UC or CD [293–295]. The reasons for lack of effect using these methods remains undetermined yet likely involve donor microbiota composition and non-engraftment due to colonisation resistance conferred by the recipient microbiota, depletion of beneficial bacteria and inability to withstand the harsh environment of the stomach, respectively [188,189]. More targeted approaches may be more beneficial as they are capable of modulating specific bacteria and/or metabolic pathways that are dysregulated in subsets of patients. For example, phage therapy offers novel therapeutic opportunities as they can selectively deplete pathobionts without altering other microbial species due to their host specificity [296]. Indeed, a phage cocktail targeting IBD-associated *Klebsiella pneumoniae* attenuates disease severity in animal models and demonstrates safe engraftment in humans [297]. Notably, the use of a phage consortium as opposed to a single phage avoids the development of phage-resistance [297]. In contrast to targeting pathogenic species, the delivery of rationally designed consortia with homeostatic functions in animal models has gained commercial interest and phase 2 trials are ongoing [298,299]. However, as with FMTs and probiotics, prolonged engraftment of such live biotherapeutic products (LBPs) remains a challenge, which will likely require personalised approaches to overcome [299,300].

Research focused on exploiting bacterial function as opposed to targeting a given bacterial species will likely contribute to the development of novel microbiota-based treatments. SCFAs are perhaps the most well studied bacterial-derived metabolites with abilities to promote intestinal health. In particular butyrate, produced from microbial fermentation of indigestible dietary fibre, has been shown to modulate regulatory B and T cells and boost macrophage antimicrobial function [51,53,301]. Butyrate and butyrate-producing bacteria are consistently reduced in IBD patients, which supports enhancing butyrate production as a potential therapeutic strategy. However, butyrate supplementation is limited by its low palatability, which in turn has led to the exploration of butyrate-producing LBPs [302]. Additional examples of immune-modulating microbial metabolites include SBAs and the pomegranate-derived metabolite urolithin-A, which are capable of ameliorating experimental colitis through control of the T_{reg}-Th17 cell axis and enhancing barrier function, respectively [57,94,303,304]. In combination with characterisation of metabolite biosynthetic pathways, understanding biological functions of microbial metabolites in-turn opens up opportunities to engineer commensal species with enhanced anti-inflammatory function [303].

In addition to bacterial metabolites, cell surface or secreted bacterial molecules can also be used to modulate mucosal immunity. For example, vaccination with the antigenic protein flagellin, leads to the induction of flagellin-specific IgA which limits penetration of the mucosa by motile bacteria and protects against IL-10 deficient colitis [12]. Moreover, polysaccharides produced by multiple bacterial species can induce regulatory properties of mucosal immune cells including, for example, OMVs-derived PSA from *B. fragilis* and a large polysaccharide from *H. hepaticus* which are capable of inducing IL-10 producing T_{reg} cells [64] and an anti-inflammatory program in macrophages, respectively [67].

In our previous studies, we have shown that *H. hepaticus* requires other commensals to cause disease in IL-10 deficiency and that the gnotobiotic OMM^{12} community is sufficient to support pathology in this model. This warrants further investigation into the roles of individual

OMM^{12} members in colitis development, with the view that identifying inter-bacteria and host-bacteria interactions underpinning disease in this setting may inform microbiota-based therapeutics. As seen in SPF mice, other colitis models and IBD patients, the development of inflammation in *H. hepaticus* + aIL-10R treated OMM^{12} mice is associated with dysbiosis and alterations in intestinal metabolite composition. Previously, the lab has also shown that *H. hepaticus* + aIL-10R colitis leads to differential IgA binding of OMM^{12} members [154]. Based on this finding and preliminary unpublished analysis into *H. hepaticus* + aIL-10R-induced OMM^{12} dysbiosis, previous work in the lab led by Lilian Lam established gnotobiotic mice colonised with OMM^{12} members of interest. Namely, i) *A. muciniphila* YL44 which is increasingly bound by IgA in *H. hepaticus* + aIL-10R colitis, ii) *L. reuteri* I49 that displays reduced IgA binding in colitis, iii) *E. faecalis* KB1 which increases in abundance during colitis, and iv) *E. clostridioformis* YL32 and *C. innocuum* I46 as members that reduce in abundance during colitis. Notably, results presented in this thesis support the rationale for *E. faecalis* KB1 and *E. clostridioformis* YL32 and adds that *A. muciniphila* YL44 is also reduced in *H. hepaticus* + aIL-10R established colitis. Interestingly, animals that are dual colonized with *E. clostridioformis* YL32 and *C. innocuum* I46 are susceptible to *H. hepaticus* + aIL-10R colitis, whereas *A. muciniphila* YL44, *L. reuteri* I49 and *E. faecalis* KB1 monocolonized mice do not develop disease (figure 5.1). Thus, OMM^{12} members display differential abilities to support *H. hepaticus* + aIL-10R colitis, with the combination of *E. clostridioformis* YL32 and *C. innocuum* I46 seemingly key to disease development.

The aims of this final results chapter were to build on these observations and i) determine the individual contributions of *E. clostridioformis* YL32 and *C. innocuum* I46 to *H. hepaticus* + aIL-10R disease pathogenesis, and ii) leverage differential phenotypes to delineate disease mechanism.

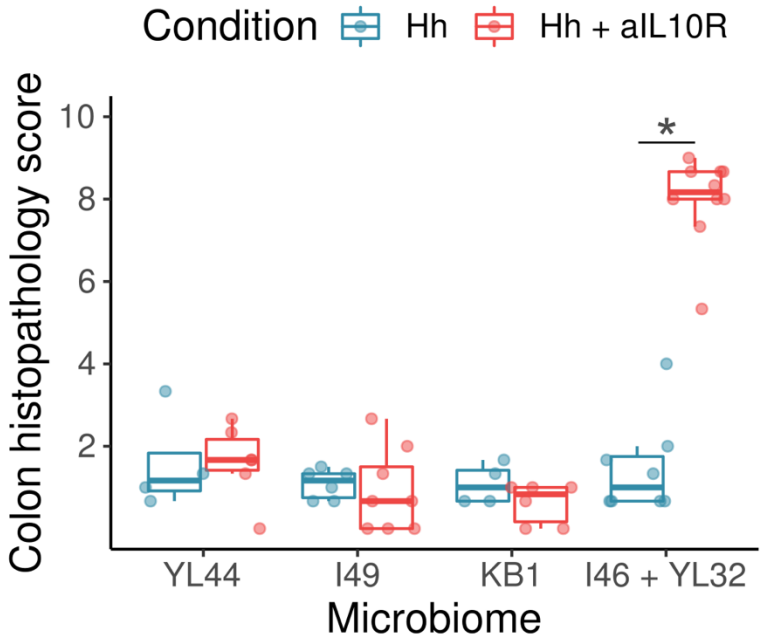


Figure 5.1. Susceptibility to *H. hepaticus* + aIL-10R colitis is not ubiquitous to OMM[12] members and instead requires *C. innocuum* I46 and *E. clostridioformis* YL32. Histopathology scores obtained from the colons of mice stably colonized with *Akkermansia muciniphila* YL44 (YL44), *Lactobacillus reuteri* I49 (I49), Enterococcus faecalis KB1 (KB1) or *Clostridium innocuum* I46 + *Enterocloster clostridioformis* YL32 (I46 + YL32) 14 days after *Helicobacter hepaticus* (Hh) or Hh + anti-interleukin-10 receptor (aIL-10R) treatment. *p_{adj}<0.05, Kruskal Wallis with Dunns post-hoc test. Boxplots denote median and interquartile range and individual data points are shown. Lam et al, unpublished.

5.2 Results

5.2.1 *E. clostridioformis* is a key colitogenic member of the OMM[12]

As animals dual-colonized with *E. clostridioformis* YL32 and *C. innocuum* I46 are susceptible to *H. hepaticus* + aIL-10R colitis (figure 5.1), we established animal colonies that were monocolonized with each bacterium. Plating of stool samples obtained from breeding pairs 1 day post gavage with either bacterium confirmed initial colonisation (figure 5.2A). Further metagenomic sequencing of faecal samples obtained from subsequent litters showed that mice were free from contamination and stably colonised with *E. clostridioformis* YL32 or *C. innocuum* I46 (figure 5.2B).

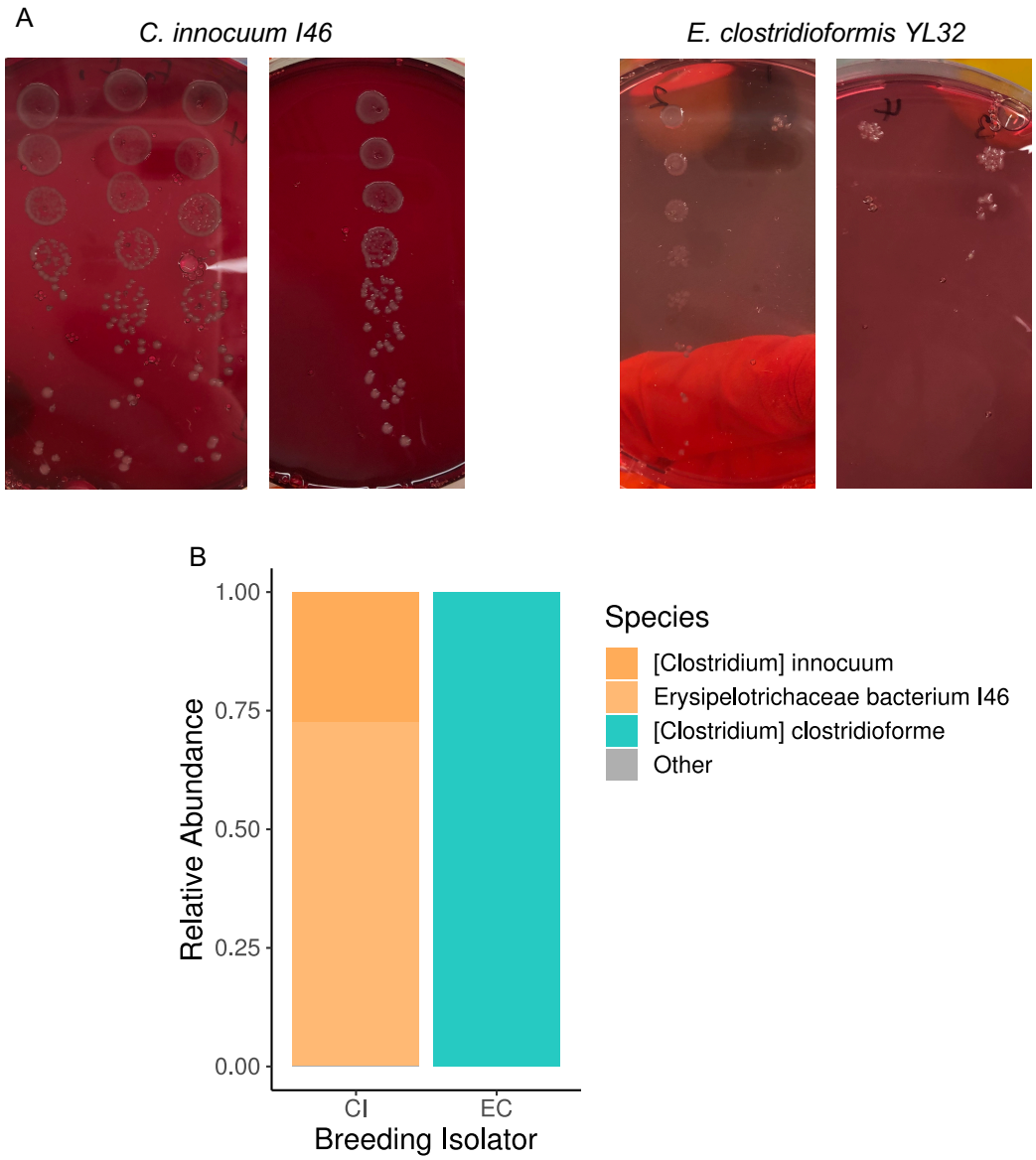


Figure 5.2. Generation of stably colonised *E. clostridioformis* YL32 and *C. innocuum* I46 mice. A) Faecal samples plated from breeding pairs 1 day after gavage with *Clostridium innocuum* I46 or *Enterocloster clostridioformis* YL32. B) Shotgun metagenomic sequencing of faecal samples obtained from offspring born to colonised breeding pairs.

To determine if *E. clostridioformis* YL32 or *C. innocuum* I46 supported the development of *H. hepaticus*-induced colitis, we administered *H. hepaticus* + aIL-10R treatment to stably colonised mice, with steady state, aIL-10R only and *H. hepaticus* only mice serving as controls. In addition, we included GF and OMM^{12} *H. hepaticus* and *H. hepaticus* + aIL-10R mice to assess disease levels relative to these groups. Moreover, we co-housed adult *E. clostridioformis* YL32 and *C. innocuum* I46 mice to re-establish a dual-colonised line and

determine if early life exposure to either bacterium altered disease outcome. Large intestinal tissues were collected at 14 days post treatment and assessed for evidence of pathology. In the colon, *C. innocuum* I46 mice displayed low levels of pathology that were comparable across treatment groups (figure 5.3A and B). In contrast, *H. hepaticus* + aIL-10R treatment led to an increase in histopathology scoring in *E. clostridioformis* YL32 mice, which were significantly elevated from control *E. clostridioformis* YL32 groups (figure 5.3A and B). Moreover, disease levels in *H. hepaticus* + aIL-10R treated *E. clostridioformis* YL32 colonic tissues were comparable to those seen in OMM^{12} mice (figure 5.3A and B) and significantly elevated from *H. hepaticus* + aIL-10R *C. innocuum* I46 samples. Interestingly, we saw similar levels of pathology in co-housed *E. clostridioformis* YL32 and *C. innocuum* I46 mice regardless of which bacterium they were colonised with from birth (figure 5.3A and B). These levels were comparable to *E. clostridioformis* YL32 and OMM^{12} *H. hepaticus* + aIL-10R mice and ~3-fold higher than *C. innocuum* I46 groups (figure 5.3B).

Similarly, *H. hepaticus* + aIL-10R treatment led to significantly elevated disease levels in *E. clostridioformis* YL32 caecal tissues that were comparable to those seen in *H. hepaticus* + aIL-10R OMM^{12} mice (figure 5.4A and B). In contrast, whilst *H. hepaticus* + aIL-10R *C. innocuum* I46 treated caecal tissues showed significantly increased histopathology scores relative to steady state control groups, levels were significantly lower than those seen in *E. clostridioformis* YL32 and OMM^{12} mice and not significantly altered from GF tissues (figure 5.4A and B). Moreover, co-housed *E. clostridioformis* YL32 and *C. innocuum* I46 mice displayed similar levels of pathology that were comparable to OMM^{12} and *E. clostridioformis* YL32 *H. hepaticus* + aIL-10R mice. Notably, disease severity appeared slightly more variable in animals colonised with *C. innocuum* I46 at birth (figure 5.4A and B). Regardless, *E. clostridioformis* YL32 mice were susceptible to *H. hepaticus*-induced colitis and displayed pathology levels that were comparable to those seen in OMM^{12} colon and caecal tissues. In contrast, *C. innocuum* I46 mice did not develop disease in the colon following *H. hepaticus* +

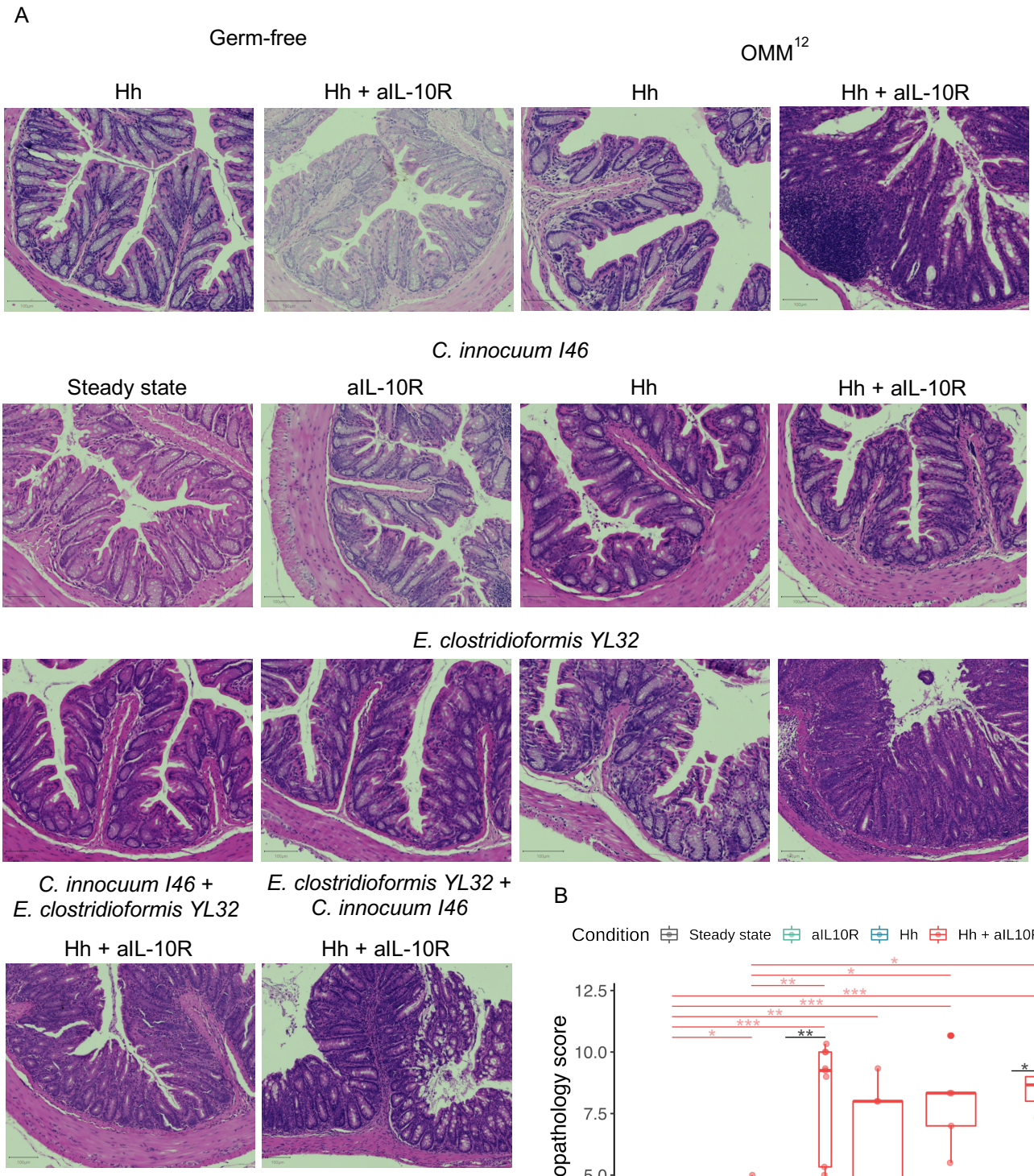


Figure 5.3. *E. clostridioformis* YL32 mice are susceptible to *H. hepaticus* + aIL-10R-induced colon pathology. A) Representative images of H&E-stained colon tissues obtained from Germ-free, Oligo-Mouse-Microbiota 12 (OMM^{12}), *Clostridium innocuum* I46, *Enterocloster clostridioformis* YL32 or co-housed *C. innocuum* I46 and *E. clostridioformis* YL32 adult mice. Experimental groups are steady state, anti-interleukin-10 receptor (aIL-10R), *Helicobacter hepaticus* (Hh) and Hh + aIL-10R. For co-housed adult mice starting microbiota is the bacteria listed first. Tissues obtained 14 days after aIL-10R, Hh or Hh + aIL-10R treatment. B) Quantification of histopathology scores obtained from the average of proximal, mid and distal colon section scores. *p_{adj} <0.05, **p_{adj} < 0.01, ***p_{adj} < 0.001. Kruskal Wallis with Dunn's post-hoc testing. Boxplots denote median and interquartile range and individual data points are shown. For CI I46 and EC YL32 Hh and Hh + aIL-10R – data obtained from 2 experiments. For all other groups data obtained from 1 experiment

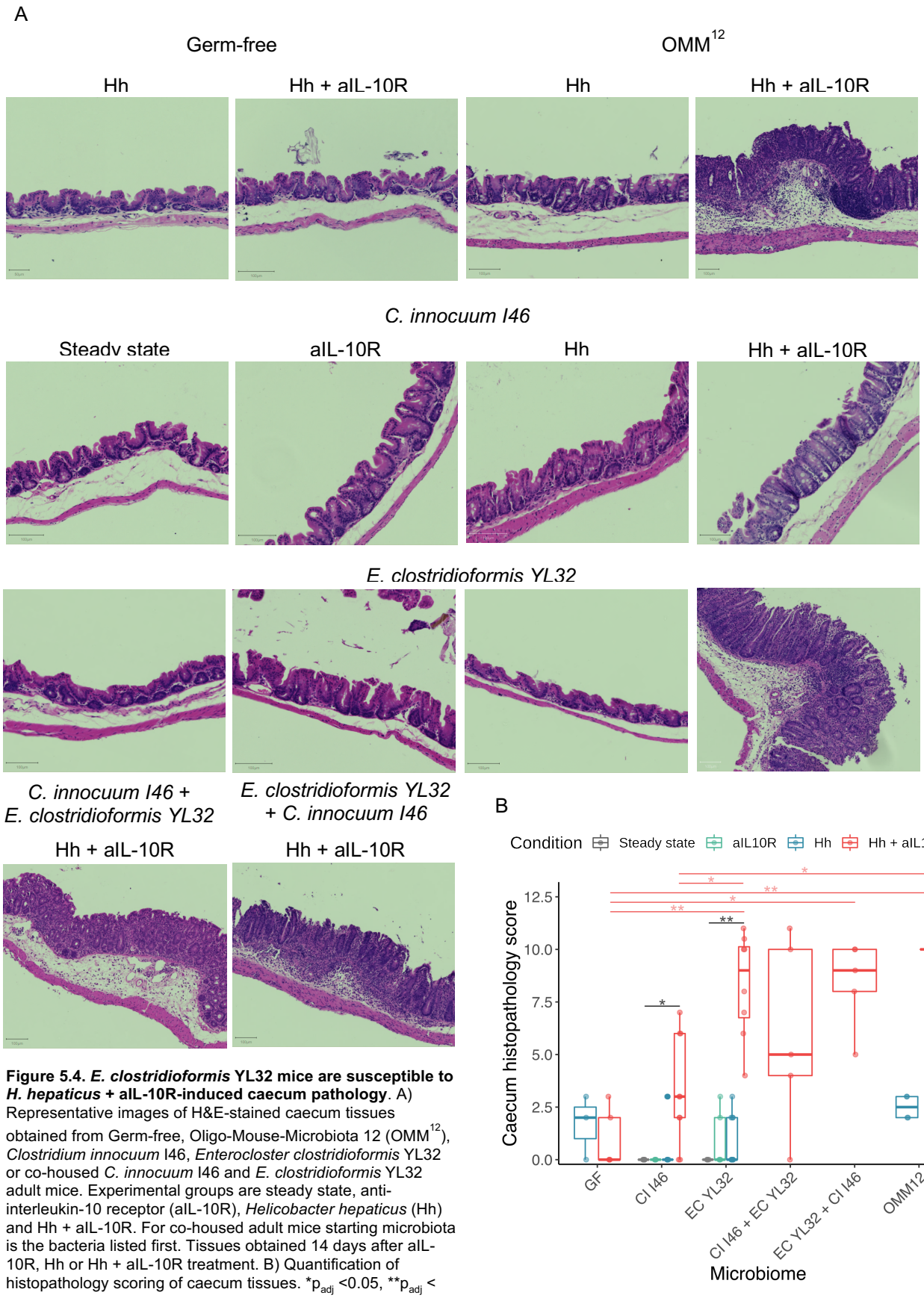


Figure 5.4. *E. clostridioformis* YL32 mice are susceptible to *H. hepaticus* + aIL-10R-induced caecum pathology. A) Representative images of H&E-stained caecum tissues obtained from Germ-free, Oligo-Mouse-Microbiota 12 (OMM[12]), *Clostridium innocuum* I46, *Enterocloster clostridioformis* YL32 or co-housed *C. innocuum* I46 and *E. clostridioformis* YL32 adult mice. Experimental groups are steady state, anti-interleukin-10 receptor (aIL-10R), *Helicobacter hepaticus* (Hh) and Hh + aIL-10R. For co-housed adult mice starting microbiota is the bacteria listed first. Tissues obtained 14 days after aIL-10R, Hh or Hh + aIL-10R treatment. B) Quantification of histopathology scoring of caecum tissues. *p_{adj} <0.05, **p_{adj} < 0.01. Kruskal Wallis with Dunn's post-hoc testing. Boxplots show median and interquartile range and individual data points are shown. For CI I46 and EC YL32 Hh and Hh + aIL-10R – data obtained from 2 experiments. For all other groups data obtained from 1 experiment

aIL-10R treatment. Pathology in the caecum was minimal, comparable to GF mice and substantially less severe than OMM^{12} and *E. clostridioformis* YL32 counterparts. Moreover, dual-colonised adult *E. clostridioformis* YL32 and *C. innocuum* I46 mice developed disease regardless of birth microbiota. Thus, *E. clostridioformis* YL32 is a key colitogenic member of the OMM^{12} and this attribute appears independent of early life exposure.

As Th17 cell expansion is a hallmark of *H. hepaticus* + aIL-10R pathology, we further investigated CD4 T cell changes in the colonic lamina propria by flow cytometry. In both *E. clostridioformis* YL32 and *C. innocuum* I46 mice, *H. hepaticus* + aIL-10R treatment led to significantly higher colonic Th17 cell counts in comparison to the respective steady state, *H. hepaticus* and aIL-10R controls. However, *H. hepaticus* + aIL-10R-induced Th17 cell expansion in *E. clostridioformis* YL32 mice was ~100-fold greater than that seen in *C. innocuum* I46 mice and comparable to counts recovered from colitic *H. hepaticus* + aIL-10R treated OMM^{12} mice (figure 5.5A). This ~100-fold increase was also shared by *E. clostridioformis* YL32 and *C. innocuum* I46 co-housed adult mice regardless of starting microbiota composition (figure 5.5A).

Interestingly, RORγt^{+} iT$_{reg}$ cell counts were elevated in *C. innocuum* I46 and *E. clostridioformis* YL32 mice colonised with *H. hepaticus* relative to respective steady state and/or aIL-10R treated controls. Notably, in both settings iT$_{reg}$ cell counts were elevated to those seen in *H. hepaticus* colonised GF mice and comparable to counts recovered from *H. hepaticus* colonised OMM^{12} mice (figure 5.5B). This suggests an induction of *H. hepaticus* responsive iT$_{reg}$ cells as is seen in SPF mice [32]. Highest iT$_{reg}$ cell counts were recovered from colitic *H. hepaticus* + aIL-10R *E. clostridioformis* YL32, OMM^{12} and dual-colonised *C. innocuum* I46 and *E. clostridioformis* YL32 mice, consistent with a general increase in immune cell counts with *H. hepaticus*-induced colitis (figure 5.5B).

When looking at CD4 T cell subset distributions, iT_{reg} cell frequencies were reduced by ~15% and ~10% in *E. clostridioformis* YL32 and OMM^{12} *H. hepaticus* + aIL-10R relative to *H. hepaticus* mice, respectively (figure 5.5C). Moreover, in-line with count data, Th17 cells frequencies were significantly elevated by ~25% in *E. clostridioformis* YL32 *H. hepaticus* + aIL-10R mice relative to steady state, aIL-10R and/or *H. hepaticus* controls. This was also noted in OMM^{12} *H. hepaticus* + aIL-10R mice relative to *H. hepaticus* controls (figure 5.5D). These alterations in CD4 T cell subset distributions led to a significant elevation in Th17:iT_{reg} cell ratios in *E. clostridioformis* YL32 and OMM^{12} *H. hepaticus* + aIL-10R mice relative to *H. hepaticus* controls. These shifts were not reflected in *C. innocuum* I46 nor GF mice, but shared by co-housed *C. innocuum* I46 and *E. clostridioformis* YL32 mice irrespective of birth microbiota, receiving *H. hepaticus* + aIL-10R treatment (figure 5.5E). Thus, *H. hepaticus* + aIL-10R treatment in *E. clostridioformis* YL32 mice led to an expansion of Th17 cells and reduction in iT_{reg} cell subset distribution as is characteristic of this model. This was comparable to signatures seen in OMM^{12} and co-housed *C. innocuum* I46 and *E. clostridioformis* YL32 mice and not reflected in *C. innocuum* I46 nor GF mice. This corresponded with histopathological data in which *E. clostridioformis* YL32 but not *C. innocuum* I46 mice develop colitis following *H. hepaticus* + aIL-10R treatment.

5.2.2 *H. hepaticus* colonization alone does not determine disease outcome

As *E. clostridioformis* YL32 but not *C. innocuum* I46 supported *H. hepaticus* + aIL-10R colitis, we further sought to understand the mechanistic basis of this finding. Previously, *H. hepaticus* has been shown to colonise GF *Il10*$^{-/-}$ mice although quantification as to how levels relate to those seen in SPF counterparts is limited [171,172]. Moreover, *H. hepaticus* has been shown to influence *L. reuteri* colonisation levels in the context of dual colonisation leading to disease development [202]. Thus, we assessed levels of *H. hepaticus*, *E. clostridioformis* YL32 and *C. innocuum* I46 in the caecum contents of GF, *E. clostridioformis* YL32, *C. innocuum* I46, co-housed *E. clostridioformis* YL32 and *C. innocuum* I46 and/or

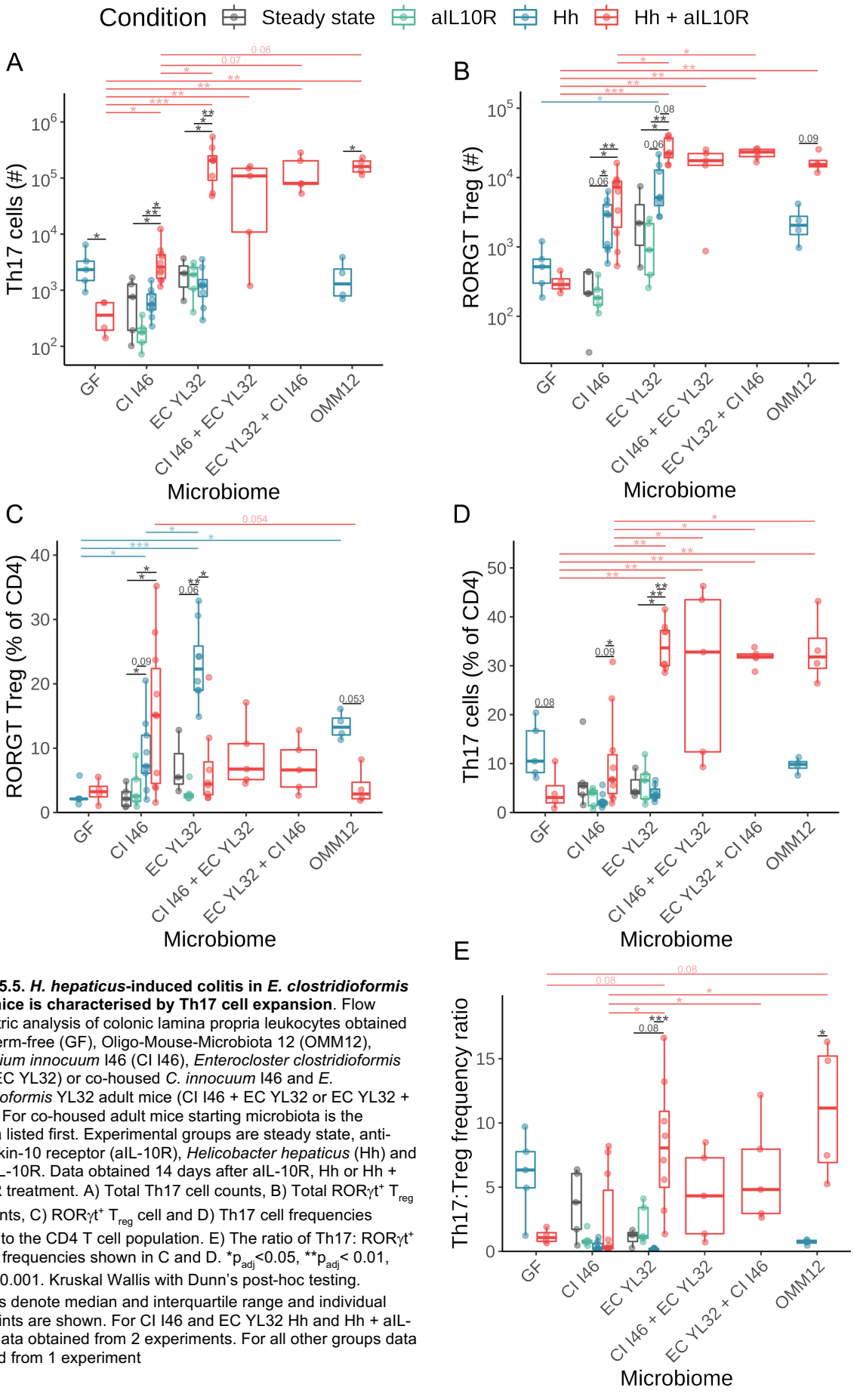


Figure 5.5. *H. hepaticus*-induced colitis in *E. clostridioformis* YL32 mice is characterised by Th17 cell expansion. Flow cytometric analysis of colonic lamina propria leukocytes obtained from Germ-free (GF), Oligo-Mouse-Microbiota 12 (OMM12), *Clostridium innocuum* I46 (CI I46), *Enterocloster clostridioformis* YL32 (EC YL32) or co-housed *C. innocuum* I46 and *E. clostridioformis* YL32 adult mice (CI I46 + EC YL32 or EC YL32 + CI I46). For co-housed adult mice starting microbiota is the bacteria listed first. Experimental groups are steady state, anti-interleukin-10 receptor (aIL-10R), *Helicobacter hepaticus* (Hh) and Hh + aIL-10R. Data obtained 14 days after aIL-10R, Hh or Hh + aIL-10R treatment. A) Total Th17 cell counts, B) Total RORγt$^+$ T_{reg} cell counts, C) RORγt$^+$ T_{reg} cell and D) Th17 cell frequencies relative to the CD4 T cell population. E) The ratio of Th17: RORγt$^+$ T_{reg} cell frequencies shown in C and D. *p_{adj}<0.05, **p_{adj}< 0.01, ***p_{adj}< 0.001. Kruskal Wallis with Dunn's post-hoc testing. Boxplots denote median and interquartile range and individual data points are shown. For CI I46 and EC YL32 Hh and Hh + aIL-10R – data obtained from 2 experiments. For all other groups data obtained from 1 experiment

OMM^{12} mice colonised with *H. hepaticus* with and without aIL-10R treatment.

H. hepaticus colonisation was substantially reduced in GF mice, with levels ~10-30 times lower than seen in *C. innocuum* I46, *E. clostridioformis* YL32 and OMM^{12} groups. Importantly, *H. hepaticus* colonised to comparable levels in *C. innocuum* I46 and *E. clostridioformis* YL32 mice (~10^4 ng/g contents) (figure 5.6A). Similar levels were also reached in co-housed *C. innocuum* I46 and *E. clostridioformis* YL32 mice regardless of starting microbiota (figure 5.6A). Thus, whilst *H. hepaticus* required the presence of commensals to colonise effectively, this alone did not explain the differential susceptibility of *C. innocuum* I46 and *E. clostridioformis* YL32 to support *H. hepaticus*-induced colitis in the context of IL-10 deficiency.

Levels of *C. innocuum I46* were comparable in the context of dual-colonised *C. innocuum* I46 + *H. hepaticus* mice relative to the *H. hepaticus* OMM^{12} group. Interestingly, *C. innocuum* I46 levels were reduced ~10-fold in OMM^{12} *H. hepaticus* + aIL-10R mice, whereas levels were maintained in non-inflamed dual-colonised *C. innocuum* I46 + *H. hepaticus* mice treated with aIL-10R (figure 5.6B). These reduced *C. innocuum* I46 levels were also seen in colitic co-housed *E. clostridioformis* YL32 and *C. innocuum* I46 mice regardless of birth microbiota (figure 5.6B). Notably this inflammation-associated drop in *C. innocuum* I46 in OMM^{12} mice was not present in previous characterisation experiments and thus does not appear to be a consistent signature of OMM^{12} dysbiosis in our hands.

As expected, *E. clostridioformis* YL32 levels were significantly reduced in OMM^{12} *H. hepaticus* + aIL-10R mice relative to *H. hepaticus* groups. Interestingly, *E. clostridioformis* YL32 levels dropped ~10-fold in dual-colonised *H. hepaticus* + *E. clostridioformis* YL32 mice administered aIL-10R. These reduced levels were also seen in co-housed *E. clostridioformis* YL32 and *C. innocuum* I46 mice regardless of pre-weaning exposure. No differences were seen in *E. clostridioformis* YL32 colonisation levels between OMM^{12} and *E. clostridioformis*

YL32 *H. hepaticus* groups (figure 5.6B). Thus, *E. clostridioformis* YL32 and *C. innocuum* I46 colonisation levels in a dual-colonised setting with *H. hepaticus* were comparable to those in the context of the full OMM^{12} community. Inflammation-associated reductions in *E. clostridioformis* YL32 were somewhat recapitulated in mice harbouring only *E. clostridioformis* YL32 and *H. hepaticus*, whilst *C. innocuum* I46 levels were unaffected by aIL-10R treatment.

5.2.3 The ability of commensals to promote homeostatic *H. hepaticus*-specific T cell responses is not indicative of disease development in IL-10 deficiency

As *H. hepaticus* colonisation leads to the induction of *H. hepaticus*-specific iT_{reg} and Tfh cells in animals harbouring a complex microbiota [32] and we had seen hints of iT_{reg} cell generation in both *C. innocuum* I46 and *E. clostridioformis* YL32 *H. hepaticus* colonised mice, we next sought to characterise the *H. hepaticus*-specific response in these settings. To this end we colonised both gnotobiotic lines with *H. hepaticus* and after 1 week adoptively transferred in naïve transgenic T cells that harbour a *H. hepaticus*-specific TCR [32]. We then assessed i) the recovery of *H. hepaticus* specific cells from the spleen, mLNs, caecal patch, colon and caecum and ii) transcription factor and cell surface receptor expression on recovered cells by flow cytometry (figure 5.7A).

We were able to recover *H. hepaticus*-specific T cells in both *C. innocuum* I46 and *E. clostridioformis* YL32 mice at comparable numbers in the spleen, mLN, caecal patch and pooled colonic and caecal tissues (figure 5.7B). The majority (~50%) of *H. hepaticus*-specific CD4 T cells differentiated into FOXP3^{+}RORγt^{+} iT_{reg} cells in the colon/caecum, regardless of whether they were transferred into *E. clostridioformis* YL32 or *C. innocuum* I46 mice (figure 5.7C). Moreover, in both settings a further ~20% of *H. hepaticus*-specific cells in the tissue

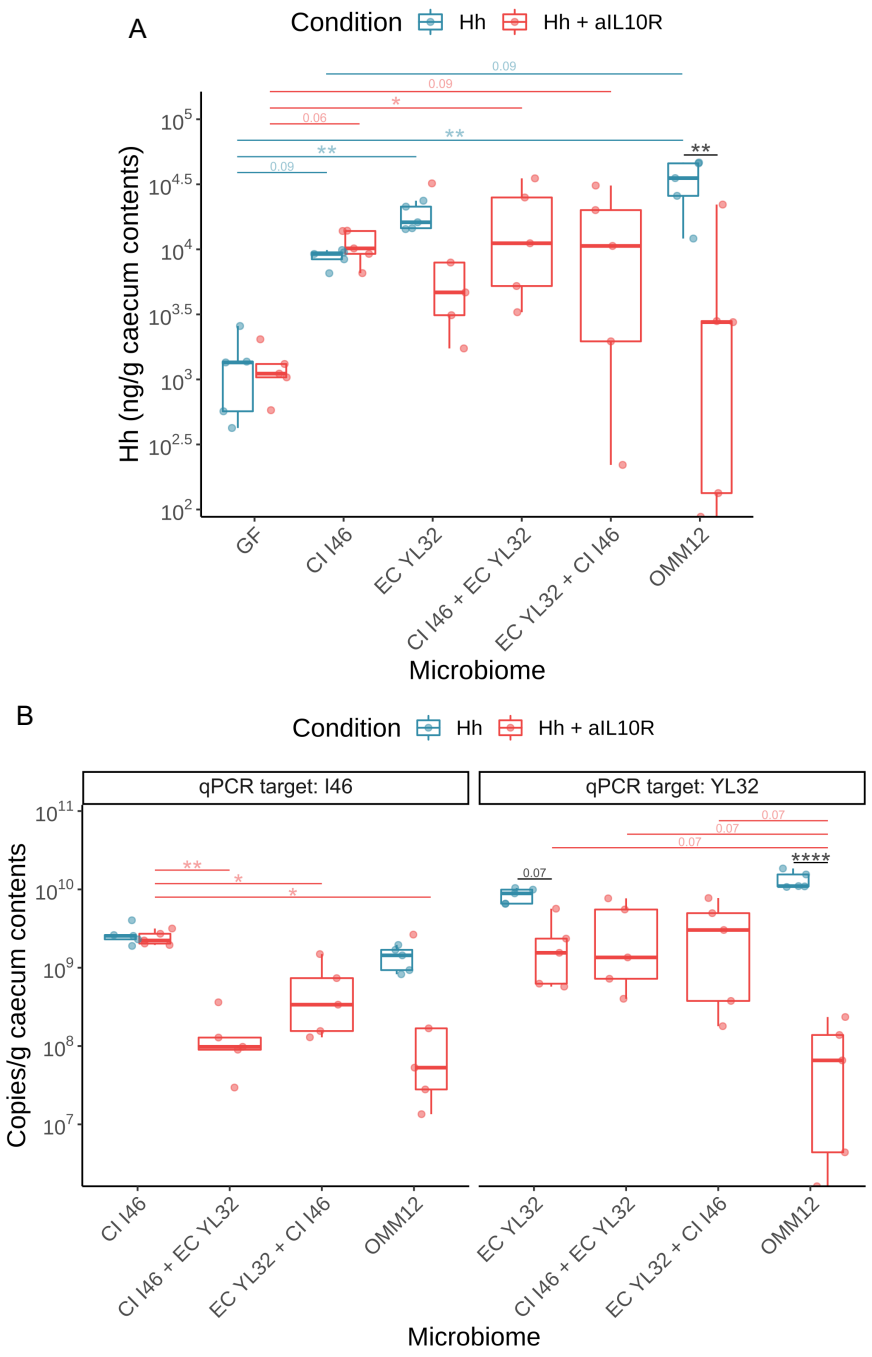


Figure 5.6. *H. hepaticus* colonisation is microbiota-dependent but does not determine disease outcome in IL-10 deficiency. qPCR analysis of A) *Helicobacter hepaticus* (Hh) and B) *C. innocuum* I46 and *E. clostridioformis* YL32 in Hh colonised germ-free (GF), Oligo-Mouse-Microbiota 12 (OMM12), *Clostridium innocuum* I46 (CI I46), *Enterocloster clostridioformis* YL32 (EC YL32) or co-housed *C. innocuum* I46 and *E. clostridioformis* YL32 (CI I46 + EC YL32 or EC YL32 + CI I46) adult mice with or without anti-interleukin-10 receptor (aIL-10R) treatment. For co-housed adult mice starting microbiota is the bacteria listed first. Bacterial quantities assessed in caecum contents 14 days after Hh or Hh + aIL-10R. *p_{adj}<0.05, **p_{adj}< 0.01, ****p_{adj}< 0.0001. Kruskal Wallis with Dunn's post-hoc testing. Boxplots denote median and interquartile range and individual data points are shown. All data obtained from 1 experiment

differentiated into RORγt^{+} Th17 cells (figure 5.7D). In the spleen, caecal patch and mLNs, ~50-80% adopted a PD-1^{+}CXCR5^{+} Tfh cell phenotype independent of gnotobiotic background (figure 5.7E). Thus, both microbial contexts were permissive to the generation of *H. hepaticus*-specific T cell responses, which were characterised predominantly by iT$_{reg}$ and Tfh cell differentiation in intestinal tissues and lymphoid structures, respectively. Notably this is in line with results reported by others in SPF mice [32]. Thus, in addition to comparable levels of *H. hepaticus* colonisation, differential disease outcomes in *E. clostridioformis* YL32 versus *C. innocuum* I46 mice following IL-10R blockade was not due to an inability of the host to generate a *H. hepaticus*-specific regulatory response.

5.2.4 *E. clostridioformis* YL32 promotes *H. hepaticus* expression of a putative T6SS component

Despite its widespread use in colitis models, comparatively little is known about the factors underpinning *H. hepaticus* virulence. The most well characterised is its cytolethal distending toxin (CDT), deletion of which reduces its ability to elicit colitis in *Il10*$^{-/-}$ mice presumably by impairing its ability to induce DNA damage in intestinal epithelial cells [305,306]. In addition to CDT, the *H. hepaticus* genome contains a potential pathogenicity island (HHIG1), encoding 70 putative genes (HH0233-HH0302) including those with homology to type 6 secretion system (T6SS) components, such as IcmF (HH0252), and type 4 secretion system (T4SS) components such as VirB4 (HH0260) [223,307]. Partial deletion of the pathogenicity island (HH0250-HH0268) ameliorates *H. hepaticus* ability to elicit colitis in *Il10*$^{-/-}$ mice [308], although a protective role of the T6SS in the T cell transfer colitis model has also been proposed [307]. As the unique ability of *E. clostridioformis* YL32 to support *H. hepaticus*-induced colitis could not be explained by our previous lines of investigation, we further probed whether expression of HHIG1 putative (HH0252 and HH0260) and CDT (*CdtB*) genes were altered in the presence of *E. clostridioformis* YL32 or *C. innocuum* I46. We

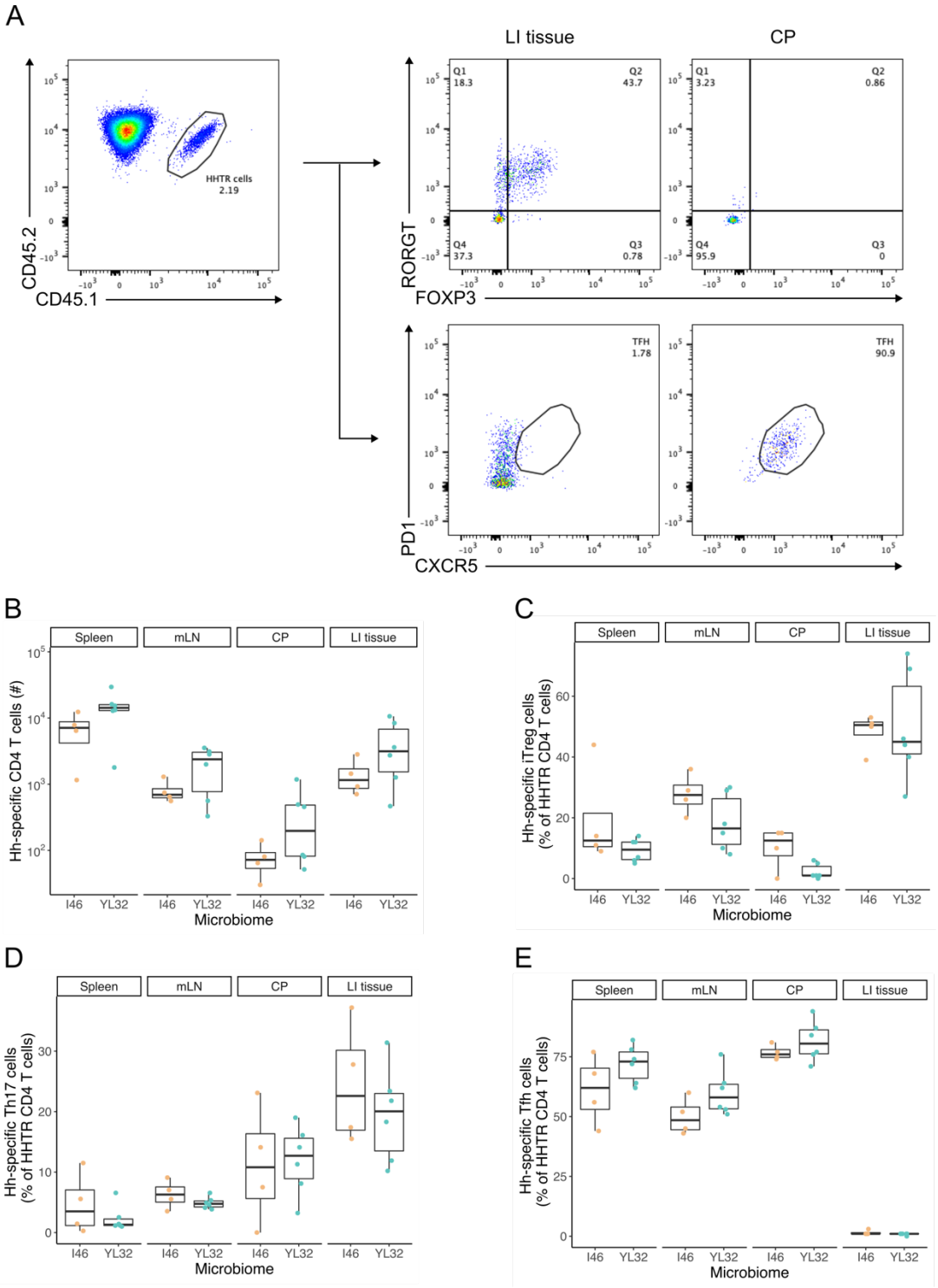


Figure 5.7. OMM[12] members promote the generation of *H. hepaticus*-specific responses regardless of pathology development in IL-10 deficiency. Flow cytometric analysis of Helicobacter hepaticus (Hh)-specific transgenic T cells transferred into Hh colonised *Clostridium innocuum* I46 (I46) or *Enterocloster clostridioformis* YL32 (YL32) adult mice. Hh was allowed to colonise for 7 days prior to T cell transfer. Flow cytometric analysis conducted 11 days post transfer. A) Representative gating strategy showing CD45.1^{+}CD45.2^{+} Hh-specific T cell recovery from the large intestinal (pooled colon and caecum) lamina propria (LI tissue) followed by gating of T helper type 17 (Th17) and RORγt^{+} T regulatory (T_{reg}) cells or CXCR5^{+}PD1^{+} T follicular helper (Tfh) cells in LI tissue or the caecal patch (CP). B) total Hh-specific T cell counts and C) RORγt^{+} T_{reg}, D) Th17 and E) Tfh cell frequencies as a % of the recovered Hh-specific T cell population across the spleen, mesenteric lymph nodes (mLN), CP and LI tissue of Hh colonised I46 and YL32 mice. Boxplots denote median and interquartile range and individual data points are shown. Data obtained from 1 experiment.

conducted RT-qPCR on caecum contents of *H. hepaticus* colonised *E. clostridioformis* YL32, *C. innocuum* I46 and OMM^{12} mice with or without aIL-10R treatment. Primer sequences were designed on the *H. hepaticus* ATCC51449 genome [223] or obtained from the literature in the case of *CdtB* [216] . All were tested on monocolonized *E. clostridioformis* YL32 and *C. innocuum* I46 and OMM^{12} contents to ensure specificity. *H. hepaticus gyrB*, *gyrA* and *secA* served as housekeeping controls from which we calculated the geometric mean to serve as a single reference [309].

H. hepaticus expression of *CdtB* showed no significant differences when in the presence of *E. clostridioformis* YL32 versus *C. innocuum* I46 with or without aIL-10R treatment (figure 5.8A). In addition, HH0260 showed highly variable expression across experiments although was increased in OMM^{12} versus *C. innocuum* I46 mice both with and without aIL-10R treatment, although more pronounced in homeostasis (figure 5.8B). Most strikingly, *H. hepaticus* expression of HH0252 was significantly elevated in *E. clostridioformis* YL32 relative to *C. innocuum* I46 mice in immunocompetent mice. Interestingly, this increase in HH0252 expression was comparable to that observed in steady state OMM^{12} mice (figure 5.8C). In aIL-10R treated mice, HH0252 expression showed slightly more variable expression patterns. Regardless, *H. hepaticus* appeared to increase expression of the putative virulence gene HH0252 in the presence of *E. clostridioformis* YL32 to levels that were comparable to those seen in the full OMM^{12} community. Importantly, this was in a homeostatic context in the absence of colitis but expression patterns reflected differential disease outcomes following aIL-10R blockade in gnotobiotic *C. innocuum* I46 versus *E. clostridioformis* YL32 mice.

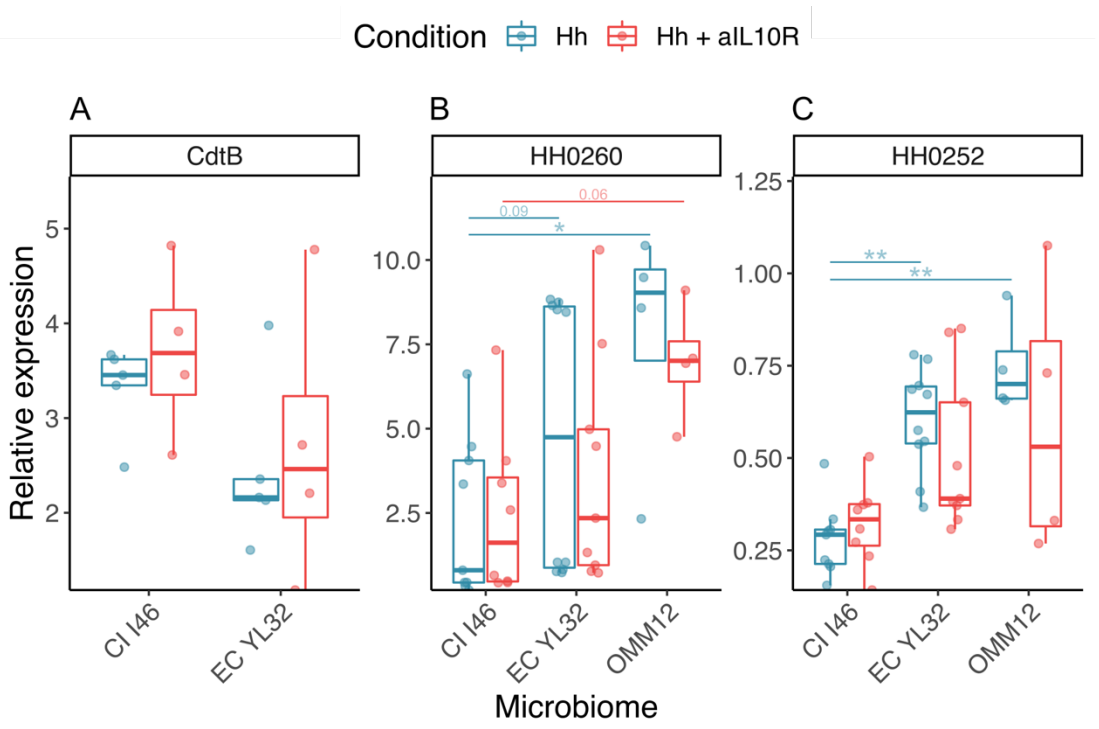


Figure 5.8. *H. hepaticus* upregulates putative gene expression in the presence of *E. clostridioformis* YL32. qPCR analysis of Helicobacter hepaticus (Hh) expression of A) Cytolethal distending toxin B (CdtB), B) HH0260 and C) HH0252 in *Clostridium innocuum* I46 (I46), *Enterocloster clostridioformis* YL32 (YL32) and Oligo-Mouse-Microbiota 12 (OMM12) adult mice with or without anti-interleukin-10-receptor (aIL-10R) treatment. Expression levels are normalised to the geometric mean of 3 Hh housekeeping genes, *secA*, *gyrA* and *gyrbB*. All expression data obtained from caecum contents of mice after 14 days of Hh or Hh + aIL-10R. *p_{adj}<0.05, **p_{adj}< 0.01. Kruksal Wallis with Dunn's post-hoc testing. Boxplots denote median and interquartile range and individual data points are shown. For HH0260 and HH0252 in Cl I46 and EC YL32 Hh and Hh + aIL-10R mice – data obtained from 2 experiments. All other data obtained from 1 experiment

5.2.5 *H. hepaticus* colonisation in *E. clostridioformis* YL32 mice leads to increased expression of molecular inflammatory signatures in the absence of disease

As we had observed a potential increase in *H. hepaticus* putative virulence gene expression in *E. clostridioformis* YL32 versus *C. innocuum* I46 mice during homeostasis, we hypothesised that this would lead to differential host gene expression in these two microbial contexts. Moreover, any differences in host responses in the absence of colitis may then inform as to why IL-10R blockade in *E. clostridioformis* YL32 but not *C. innocuum* I46 mice results in disease development. To address this, we performed RNA-sequencing of host caecal tissues in *H. hepaticus* colonised *E. clostridioformis* YL32 and *C. innocuum* I46 mice, with steady state, aIL-10R and *H. hepaticus* + aIL-10R treated groups serving as controls.

In order to determine host-responses to different gnotobiotic conditions, we first conducted analysis on *H. hepaticus* colonised *E. clostridioformis* YL32 and *C. innocuum* I46 groups. By PCA, gene expression variation attributable to microbiome composition was subtle (R2 = 0.086 and P = 0.11) (appendix figure A.6). However, differential expression analysis showed that a total of 2275 genes were significantly altered between the two groups. Of these, 1459 and 816 were significantly elevated and reduced in expression in *H. hepaticus* colonised *E. clostridioformis* YL32, relative to *C. innocuum* I46, mice, respectively (figure 5.9A). Pathway enrichment analysis revealed a total of 23 pathways that were significantly altered in *E. clostridioformis* YL32 versus *C. innocuum* I46 mice colonised with *H. hepaticus*. Within the top 5 significantly upregulated pathways were TNFα/NF-κB signalling and inflammatory response genes whilst those downregulated were involved in oxidative phosphorylation and fatty acid metabolism (figure 5.9B).

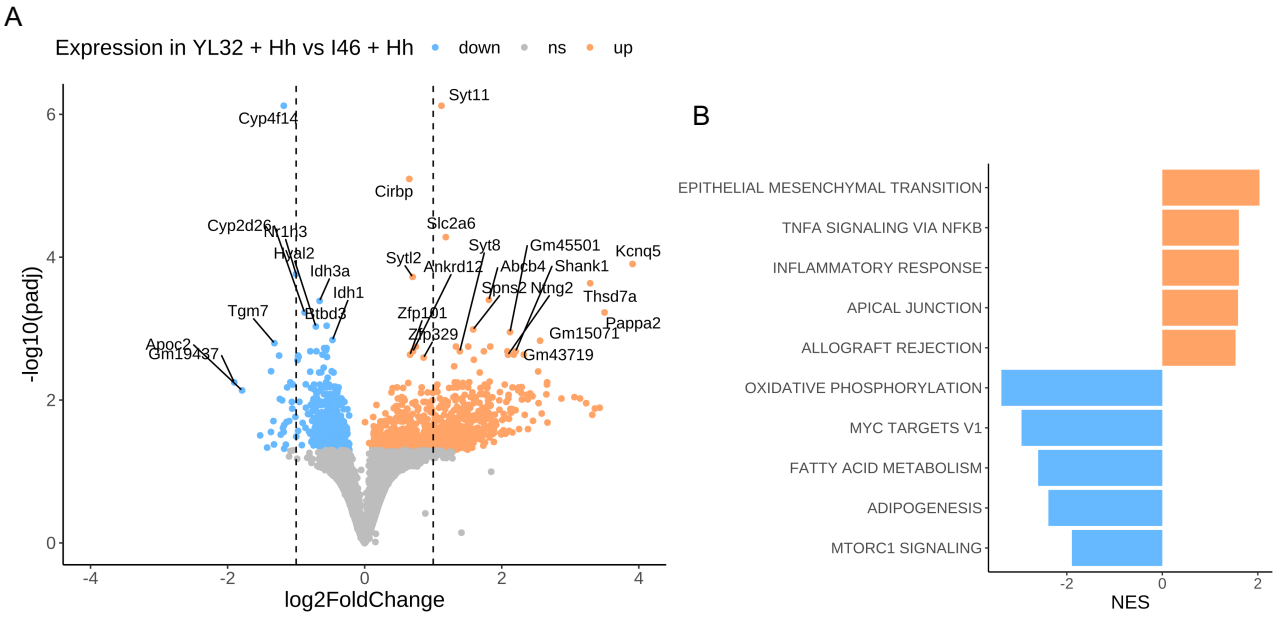


Figure 5.9. *H. hepaticus* colonisation in *E. clostridioformis* YL32 mice alters host gene expression. A) Differential expressed genes in the caecum tissues of *Enterocloster clostridioformis* YL32 (YL32) versus *Clostridium innocuum* I46 (I46) mice colonised with *Helicobacter hepaticus* for 14 days. Values are plotted according to Log2 fold change in YL32 + Hh vs I46 + Hh and –log10(p_{adj} value) and coloured by significance. B) Pathway enrichment analysis of significantly altered genes shown in A. Data obtained from 2 experiments

As a heightened inflammatory state in *E. clostridioformis* YL32 mice colonised with *H. hepaticus* may be linked to their susceptibility to colitis in IL-10 deficiency, we further probed

the expression of TNFα/NF-κB signalling and inflammatory response pathway leading-edge genes obtained from our focused analysis across all conditions (i.e. steady state, aIL-10R and *H. hepaticus* + aIL-10R). Interestingly, significantly altered TNFα/NF-κB genes fell into two distinct clusters which appeared upregulated in *H. hepaticus* colonised *E. clostridioformis* YL32 mice either predominantly in disease context (+ aIL-10R) (cluster 1) or in both disease and homeostasis (*H. hepaticus* colonisation alone) (cluster 0). In contrast, the majority of inflammatory response genes fell into a single cluster which appeared upregulated in *H hepaticus* colonised *E. clostridioformis* YL32 mice regardless of aIL-10R treatment (figure 5.10A). Notably, there was some overlap between significant TNFα/NF-κB and inflammatory pathway genes, with 11 shared between the two (figure 5.10B).

Interestingly, IL-23α was a significant hit pertaining to TNFα/NF-κB signalling. As IL-23 is critical for colitis development in the *H. hepaticus* + aIL-10R model [78], we further conducted post-hoc testing to assess expression levels across groups. Strikingly, IL-23 was significantly elevated in *E. clostridioformis* YL32 mice in *H. hepaticus* and *H. hepaticus* + aIL-10R, but not aIL-10R, groups relative to steady state controls. Moreover, levels remained unaltered in *C. innocuum* I46 mice regardless of treatment group and were significantly lower than *E. clostridioformis* YL32 *H. hepaticus* and *H. hepaticus* + aIL-10R counterparts (figure 5.10C). Thus, *H. hepaticus* colonisation in *E. clostridioformis* YL32 mice in the absence of pathology led to an altered host transcriptional response characterised in-part by an increase in inflammatory response genes. Indeed, IL-23α was induced in *E. clostridioformis* YL32 mice following *H. hepaticus* colonisation, a response that was not reflected in *C. innocuum* I46 mice. Given an observed coordinated increased expression of *H. hepaticus* virulence factors and host inflammatory response genes in *H. hepaticus* colonised *E. clostridioformis* YL32 mice, the data support inter-bacterial interactions that promote pro-inflammatory responses that predispose mice to colitis through IL-10R blockade.

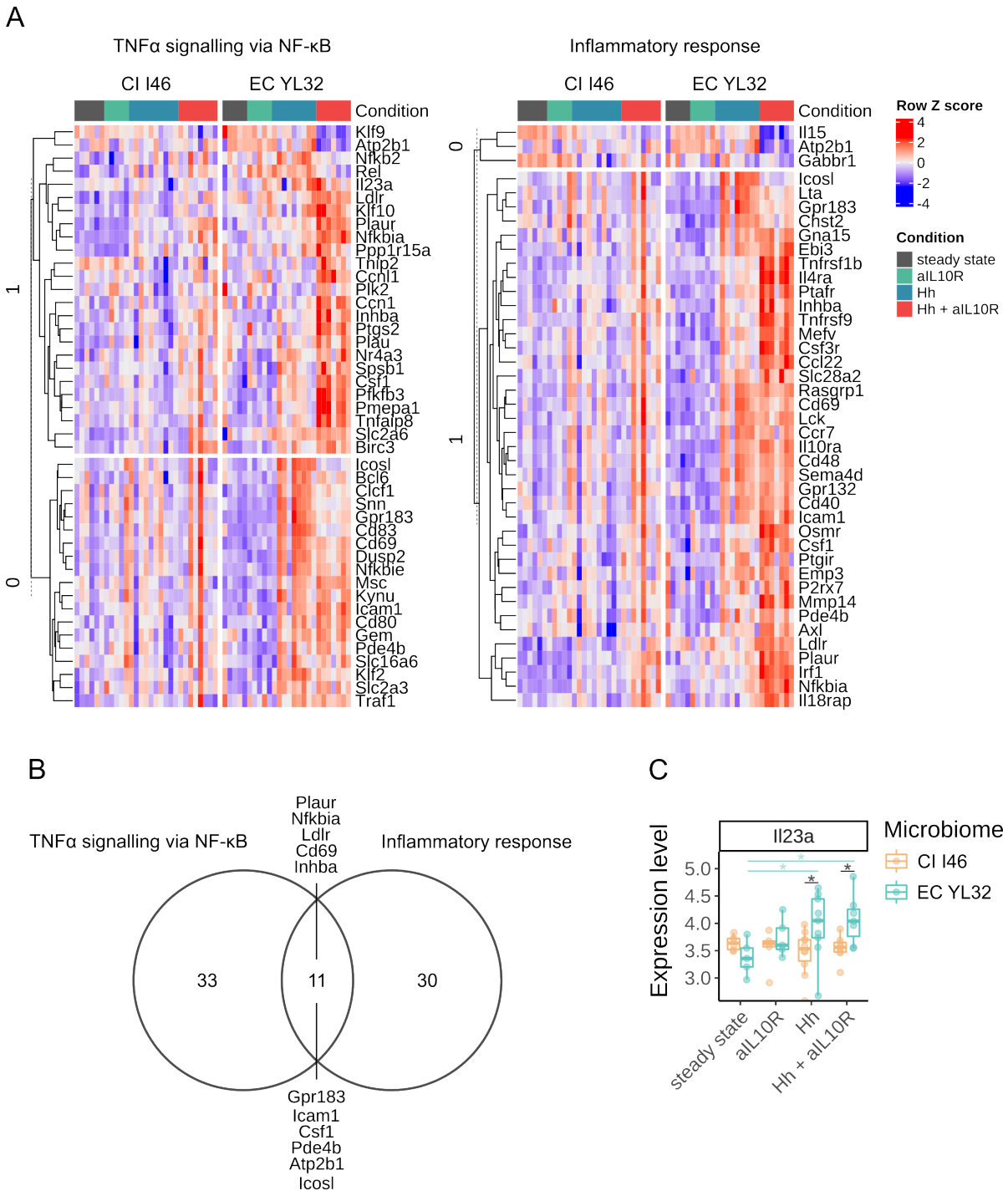


Figure 5.10. *H. hepaticus* colonisation in *E. clostridioformis* YL32 mice leads to the induction of a molecular inflammatory signature in the absence of disease. A) Heatmaps showing leading edge genes pertaining to the tumor necrosis factor α (TNFα) signalling via nuclear factor-κB (NF-κB) and inflammatory pathways identified as significantly enriched in caecum tissues obtained from *Enterocloster clostridioformis* YL32 (YL32) versus *Clostridium innocuum* I46 (I46) mice colonised with *Helicobacter hepaticus* for 14 days. Gene expression shown in caecum tissues obtained from all experimental groups i.e. CI I46 and EC YL32 steady state, anti-interleukin 10 receptor (aIL-10R), Hh and Hh + aIL-10R mice. B) Overlap of genes belonging to TNFα signalling and inflammatory response pathways. C) Expression of *Il23a* in caecum tissues of steady state, aIL-10R, Hh and Hh + aIL-10R CI I46 and EC YL32 mice. *p_{adj}<0.05 Kruskal Wallis with Dunn's post-hoc testing.

Boxplots denote median and interquartile range and individual data points are shown. For CI I46 and EC YL32 Hh and Hh + aIL-10R – data obtained from 2 experiments. For all other groups data obtained from 1 experiment

5.2.6 Selective targeting of *E. clostridioformis* YL32 reverts established colitis

As we hypothesised that *E. clostridioformis* YL32 and *H. hepaticus* interactions were critical for colitis development, we aimed to determine if we could target these therapeutically. Vancomycin is a commonly used antibiotic broadly effective against gram-positive bacteria [157]. As *E. clostridioformis* YL32 is a gram-positive bacterium whilst *H. hepaticus* is gram-negative, resistant to and routinely cultured in vancomycin [310], we sought to utilise vancomycin to selectively deplete *E. clostridioformis* YL32 in *H. hepaticus* + aIL-10R colitis. First, we assessed the susceptibility of each bacterium to vancomycin *in vitro*. As expected, *H. hepaticus* growth was unaltered, whereas *E. clostridioformis* YL32 was no longer detectable, when grown in the presence of 0.5 g/L vancomycin (figure 5.11A).

Next, we assessed whether depletion of *E. clostridioformis* YL32 prior to *H. hepaticus* + aIL-10R would serve as a preventative colitis treatment. We administered vancomycin to *E. clostridioformis* YL32 mice from 10 days prior to *H. hepaticus* + aIL-10R treatment (figure 5.11B). As expected, 10-day preventative vancomycin treatment led to the depletion of *E. clostridioformis* YL32, which was maintained until experimental end-point (figure 5.11C). *H. hepaticus* levels in the stool were significantly reduced in vancomycin treated mice at day 7. In addition, *H. hepaticus* colonisation levels were significantly reduced in end-point caecum contents, although comparable in colon contents, with vancomycin treatment (figure 5.11D). To assess the impact vancomycin preventative treatment had on pathology, we conducted histopathological analysis of colon and caecum tissues and broadly assessed colonic lamina propria populations by flow cytometry. Strikingly, pre-treatment with vancomycin led to substantially reduced pathology scores in the caecum and colon of *H. hepaticus* + aIL-10R treated mice (figure 5.12A and B). Moreover, neutrophil and CD4 and CD8 T cell infiltration was substantially reduced in vancomycin treated mice (figure 5.12C). Thus, pre-treatment with vancomycin leading to the removal of *E. clostridioformis* YL32 led to reduced levels of

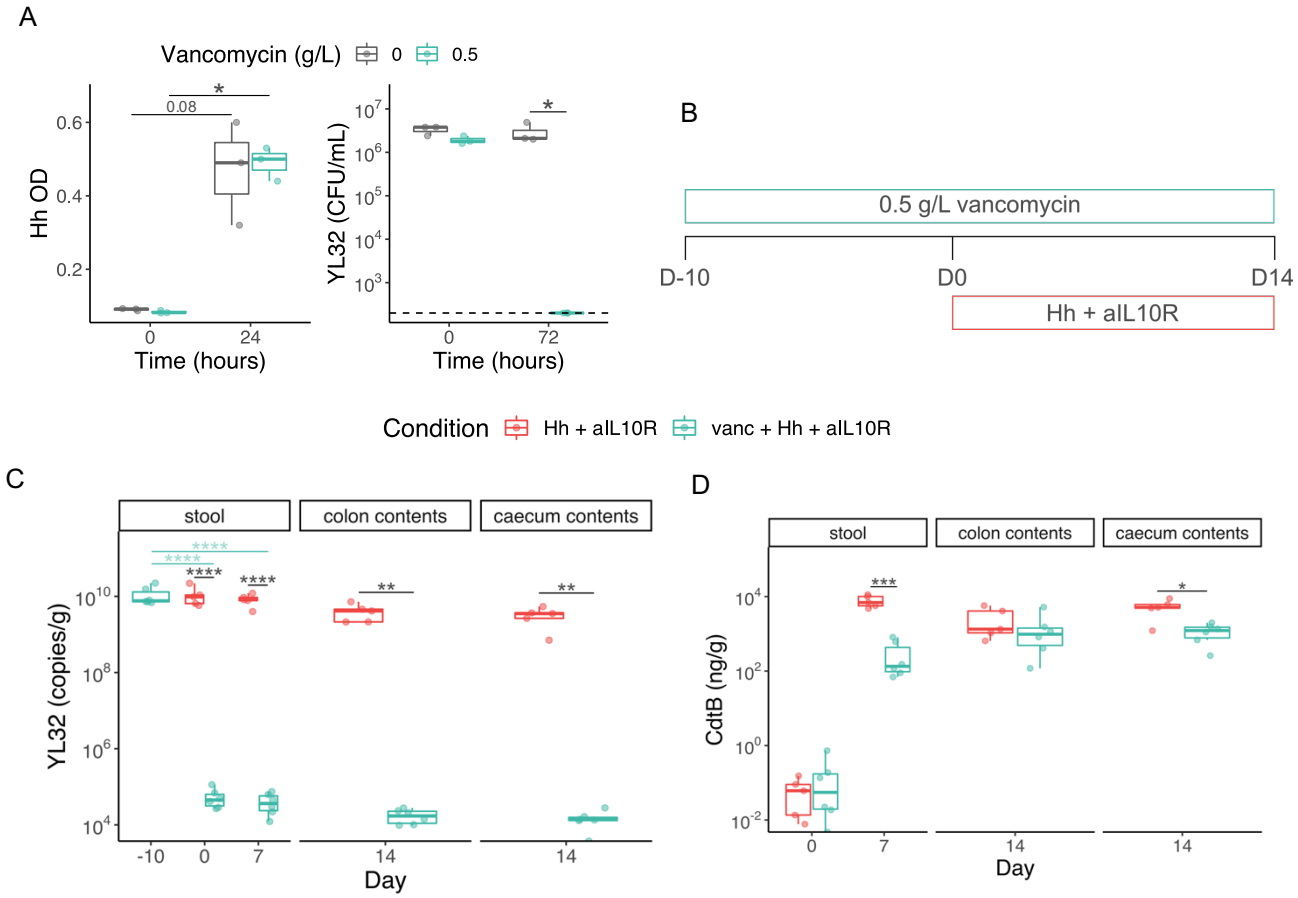


Figure 5.11. Preventative treatment with vancomycin leads to select targeting of *E. clostridioformis* YL32 and impaired *H. hepaticus* colonisation. A) *In vitro* growth of *Helicobacter hepaticus* (Hh) and *Enterocloster clostridioformis* YL32 (YL32) in the presence or absence of 0.5 g/L vancomycin. B) Experimental timings for preventative vancomycin therapy. C) *E. clostridioformis* YL32 and D) Hh levels in the stool, colon and caecum contents as determined by qPCR in EC YL32 mice treated with Hh + anti-interleukin-10 receptor (aIL-10R) with or without preventative vancomycin therapy. *p_{adj}< 0.05, **p_{adj} < 0.01, ***p_{adj}< 0.001, ****p_{adj} < 0.0001. For A Kruskal Wallis with Dunn's post-hoc testing. For C & D stool statistics lmer analysis with estimated marginal means post-hoc testing. Contents statistics wilcox test. For A, C & D boxplots denote median and interquartile range and individual data points are shown. Data obtained from 1 experiment

H. hepaticus colonisation early in the stool and in end-point caecum contents. Importantly, this prevented colitis development in normally susceptible *E. clostridioformis* YL32 mice in the context of IL-10 deficiency.

As pre-treatment with vancomycin led to amelioration of pathology, we next sought to establish whether vancomycin could serve as an intervention treatment. Thus, we induced *H. hepaticus* + aIL-10R colitis in *E. clostridioformis* YL32 mice and then at day 14 treated half of the animals with vancomycin for an additional two weeks (figure 5.13A). Notably we continued to administer aIL-10R weekly until experimental end-point to all mice. Again, vancomycin depleted *E. clostridioformis* YL32 *in vivo*, from day 21 until experimental end-point as determined by plating of faecal samples (figure 5.13B). *H. hepaticus* levels in the

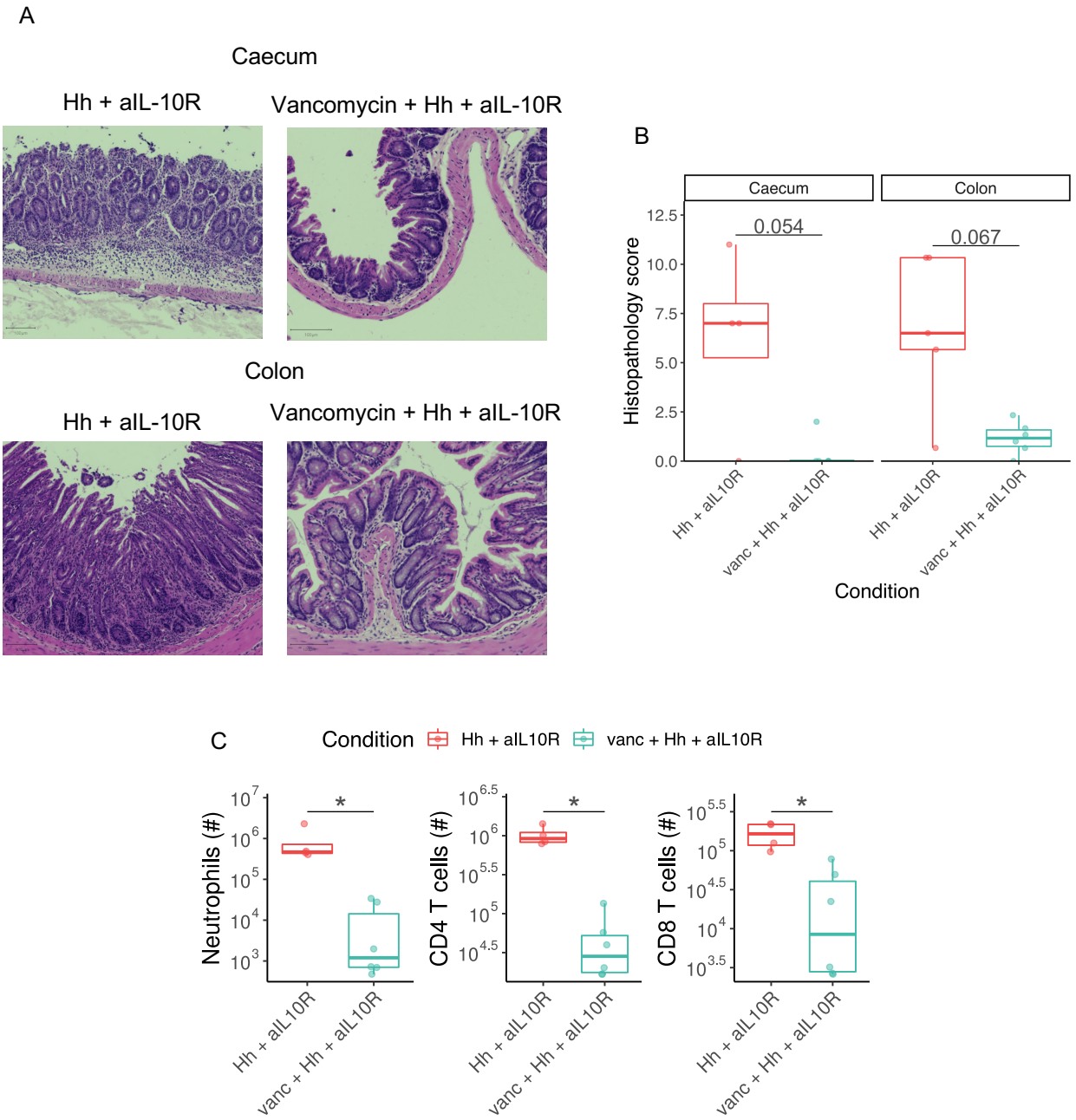


Figure 5.12. Preventative treatment with vancomycin ameliorates *H. hepaticus*-induced colitis in *E. clostridioformis* YL32 mice. A) Representative images of day 14 H&E-stained colon and caecum sections obtained from *Enterocloster clostridioformis* YL32 mice treated with Helicobacter hepaticus + anti-interleukin-10 receptor (aIL-10R) with or without preventative vancomycin therapy. B) Quantification of histopathology scores, where colon scores are the average obtained across proximal, mid and distal colonic sections. C) Day 14 neutrophil, CD4 and CD8 T cell counts in the colonic lamina propria of EC YL32 Hh + aIL-10R mice with or without preventative vancomycin treatment. *p<0.05 Wilcox test. For B&C boxplots denote median and interquartile range and individual data points are shown. Data obtained from 1 experiment.

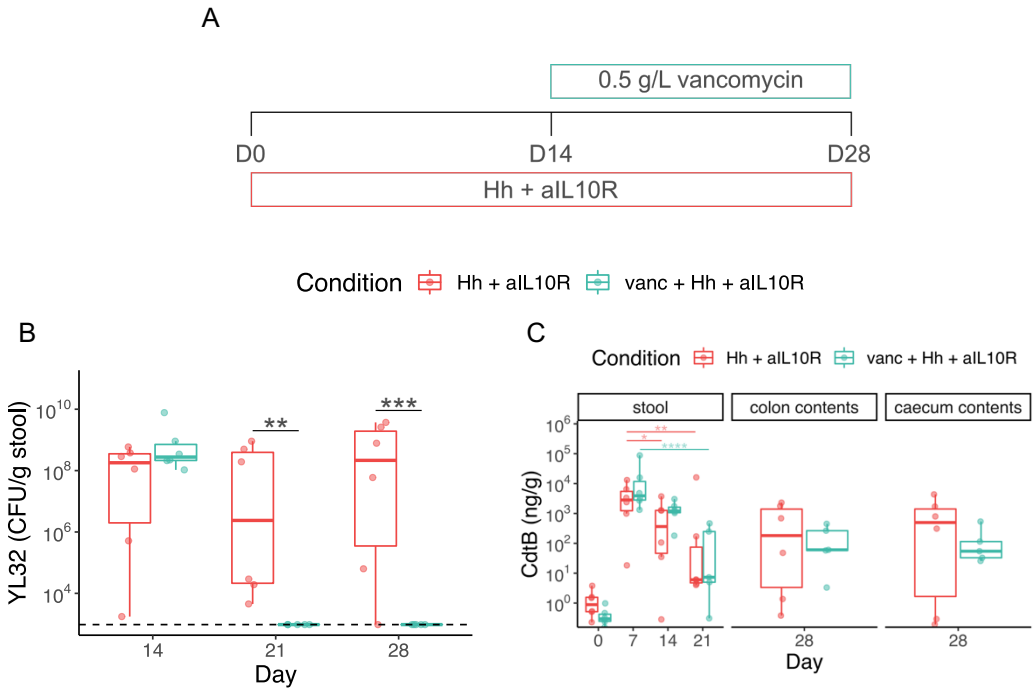


Figure 5.13. Intervention treatment with vancomycin leads to select targeting of *E. clostridioformis* YL32 without altering *H. hepaticus* colonisation. A) Experimental timings for intervention vancomycin therapy B) *Enterocloster clostridioformis* YL32 and C) Helicobacter hepaticus levels in the B) stool or C) stool and/or colon and caecum contents as determined by B) plating or C) qPCR in EC YL32 mice treated with Hh + anti-interleukin-10 receptor (aIL-10R) with or without intervention vancomycin therapy. *p_{adj}< 0.05, **p_{adj} < 0.01, ***p_{adj}< 0.001, ****p_{adj} < 0.0001. For B & C stool statistics lmer analysis with estimated marginal means post-hoc testing. For C contents statistics by wilcox test. For B&C boxplots denote median and interquartile range and individual data points are shown. Data obtained from 1 experiment.

stool and end-point colon and caecum contents were unaffected by vancomycin intervention treatment although faecal levels dropped in both groups over time (figure 5.13C).

To track inflammation development, we assessed LCN2 levels in longitudinal faecal samples. As expected, in both groups, *H. hepaticus* + aIL-10R led to a significant elevation in faecal LCN2 levels at day 7, which peaked at day 14. Strikingly, vancomycin administration from this point onwards led to a drop in faecal LCN2 at day 21, to values that were comparable to baseline levels. In contrast, significantly elevated faecal LCN2 levels were maintained in mice that did not receive vancomycin alongside continuous aIL-10R administration. Moreover, this vancomycin-induced significant reduction in LCN2 levels was reflected in day 28 colon and caecum contents, where levels were ~10-fold higher in mice that did not receive vancomycin treatment (figure 5.14A). Histopathological assessment

showed that therapeutic intervention with vancomycin led to significantly reduced pathology levels in both the colon and caecum of *H. hepaticus* + aIL-10R mice (figure 5.14B and C). We also observed a significant 10-fold reduction in total immune infiltrate in the colonic lamina propria, as well as a substantial ~300-fold drop in colonic neutrophilia. Th17 cell counts were also ~10-fold reduced in vancomycin treated mice (figure 5.14D). Thus, vancomycin administration at the peak of inflammation led to the reversal of *H. hepaticus* + aIL-10R colitis in *E. clostridioformis* YL32 mice. Interestingly, in contrast to that seen in our preventative treatment strategy, this was independent of a drop in *H. hepaticus* colonisation levels following vancomycin treatment. This suggests that selective targeting of *E. clostridioformis* YL32 may disrupt colitogenic interactions between this bacterium and *H. hepaticus*, in doing so extinguishing bacterial drivers of pathology resulting in the reversal of established colitis.

5.3 Discussion

The inability of *H. hepaticus* to cause colitis in IL-10 deficient mice in the absence of other commensals highlights the role of extrinsic microbial factors in disease development in this model. Interestingly, whilst OMM^{12} mice are susceptible to *H. hepaticus* + aIL-10R colitis, individual members display differential colitogenic abilities. Of those tested to date, *E. clostridioformis* YL32 is the only OMM^{12} member to support *H. hepaticus*-induced colitis, whereas *E. faecalis* KB1, *A. muciniphila* YL44, *L. reuteri* I49 and *C. innocuum* I46 do not. Of these innocuous bacteria, *E. faecalis* KB1 features as a robust signature of dysbiosis in the *H. hepaticus* + aIL-10R OMM^{12} model, where it is consistently increased at the point of and during inflammation. This highlights that correlative signatures do not necessarily inform a causative role for a given bacterium. Indeed, somewhat paradoxically, *E. clostridioformis* YL32 reduces during inflammation in *H. hepaticus* + aIL-10R treated OMM^{12} mice, despite that fact that it is a key colitogenic member of the community.

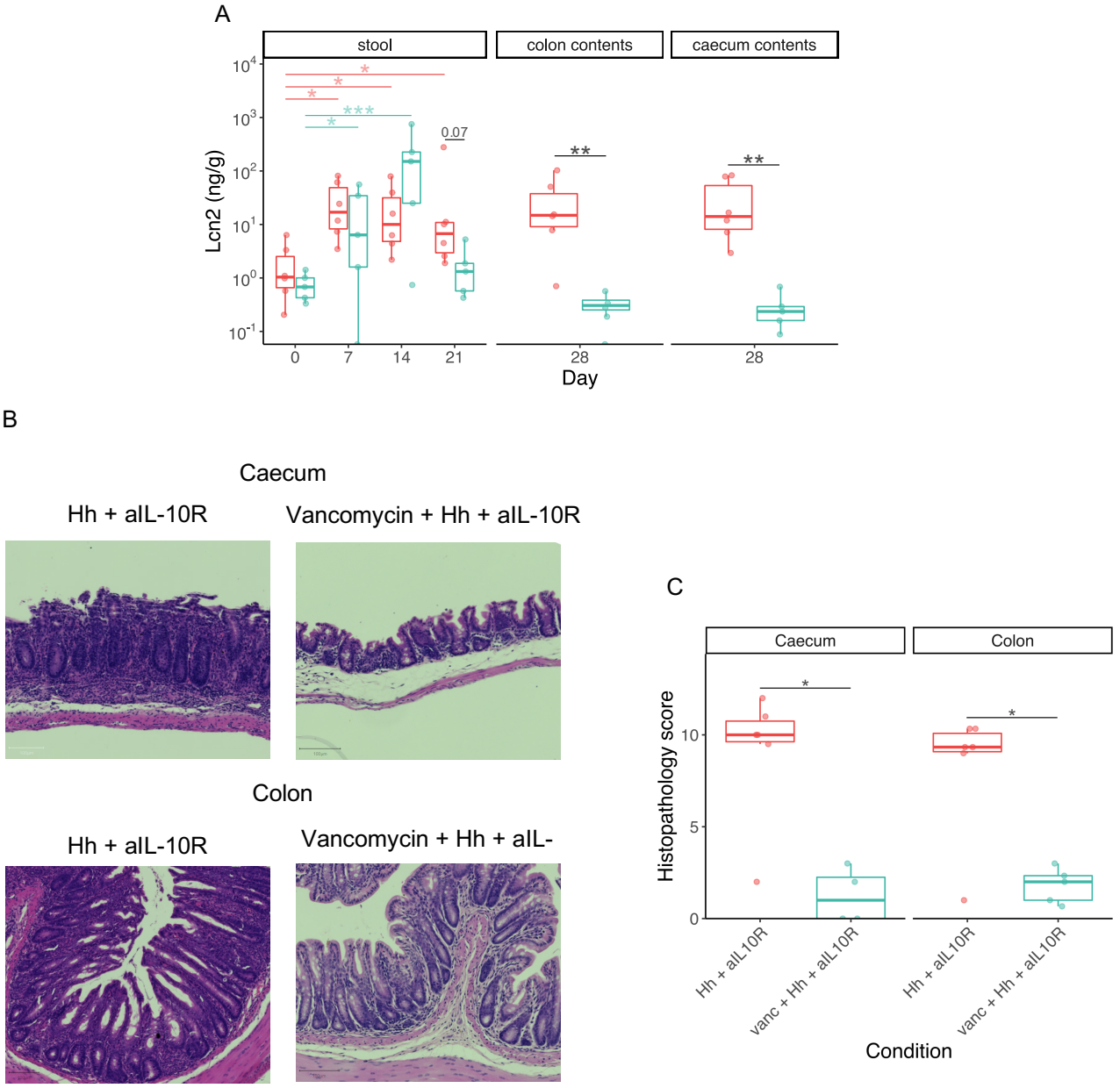


Figure 5.14. Selective depletion of *E. clostridioformis* YL32 reverts established *H. hepaticus*-induced colitis. A) Lipocalin-2 (LCN2) levels in the stool, colon and caecum contents of *Enterocloster clostridioformis* YL32 mice treated with *Helicobacter hepaticus* + anti-interleukin-10 receptor (Hh + aIL-10R) with or without intervention vancomycin therapy. B) Representative images of day 28 H&E-stained colon and caecum sections obtained from *Enterocloster clostridioformis* YL32 mice treated with Hh + aIL-10R with or without intervention vancomycin therapy. C) Quantification of histopathology scores, where colon scores are the average obtained across proximal, mid and distal colonic sections. D) Total immune ($CD45^+$), neutrophil and T helper type 17 (Th17) cell counts in day 28 colonic lamina propria of EC YL32 Hh + aIL-10R mice with or without intervention vancomycin treatment. *p<0.05, **padj<0.01, ***padj<0.001. For LCN2 stool lmer analysis with estimated marginal means post-hoc testing. Wilcox test used for all other statistics. For A, C&D boxplots denote median and interquartile range and individual data points are shown. Data obtained from 1 experiment

Differential phenotypes can be leveraged to delineate disease mechanism. We utilised *E. clostridioformis* YL32 and *C. innocuum* I46 stably monocolonized mice to probe mechanisms of disease susceptibility and resistance, respectively. One explanation of differential disease susceptibility could be differences in microbial influence on immune development as it is well established that the microbiota plays an important role in shaping aspects of immunity. Indeed, GF mice have defective lymphoid follicle formation, reduced mucosal intraepithelial lymphocyte and IgA responses and systemic skewing to type 2 immunity [4,63,311]. In addition, GF mice have an expansion of gut iNKT cells, which is linked to increased mortality rates in oxazalone-induced colitis. Importantly, these effects can be reversed through colonisation at birth but not during adulthood [312]. Thus, microbiota influence during early life can operate as a critical window in which to modulate gut physiology. Interestingly, we found that the ability of *E. clostridioformis* YL32 to promote *H. hepaticus*-induced colitis is independent of early life exposure as *C. innocuum* I46 mice developed colitis following introduction to *E. clostridioformis* YL32 at adulthood. Moreover, the ability of both *C. innocuum* I46 and *E. clostridioformis* YL32 to generate *H. hepaticus*-specific iT_{reg} and Tfh cell responses upon *H. hepaticus* colonization suggests comparable immune developmental profiles, at least in those contributing to the ability to generate bacterial specific homeostatic responses. Finally, selective targeting of *E. clostridioformis* YL32 through antibiotic depletion can revert established colitis, suggesting that indirect long-standing effects on host immunity do not contribute to *E. clostridioformis* YL32 colitogenic potential. Thus, it is unlikely that *E. clostridioformis* YL32 developmentally programs the host immune system to a pro-colitogenic state.

In IL-10 deficient SPF mice, *H. hepaticus* colonisation leads to an expansion of pathogenic *H. hepaticus*-specific Th17 cells that produce IL-17 and IFN-γ [32,78]. IL-23 is a key driver of this Th17 cell response, blockade of which ameliorates *H. hepaticus*-induced pathology [78]. $CD11c^{+}$ macrophages are the cellular source of IL-23 and their differentiation from $Ly6C^{hi}$ monocytes is dependent on the transcription factor IRF5 [141,142]. IRF5 is activated

downstream of signalling events following PRR activation. PRRs, such as those belonging to the TLR family recognise a range of both PAMPs and DAMPs.

The upstream triggers leading to this monocyte-IL-23-Th17 cascade are unclear as little is known about *H. hepaticus* biology. Indeed, previous work has focused on deciphering immunological, as opposed to microbial, drivers of disease, including those derived from *H. hepaticus* [1]. There are some exceptions to this, as *H. hepaticus* CDT has been shown to induce epithelial dysplasia and promote colitis development in IL-10 deficient and *Rag*$^{-/-}$ mice [305,313]. Even less well characterised is the candidate pathogenicity island HHIG1, a 71.0 kb region on the *H. hepaticus* genome that harbours genes with homology to T4SS and/or T6SS components [223,308]. Partial deletion of HHIG1 ameliorates *H. hepaticus* ability to cause colitis in IL-10 deficient mice [308], whilst contradictory information exists on the removal of individual putative virulence genes including HH0252 [307,314].

Interestingly, we found that *H. hepaticus* expression of CDT and HH0260 was comparable between *E. clostridioformis* YL32 and *C. innocuum* I46 mice in both healthy and disease states. In contrast, *H. hepaticus* upregulated expression of HH0252 in the presence of *E. clostridioformis* YL32 relative to *C. innocuum* I46. Differential expression patterns were also reflected in the host, as *E. clostridioformis* YL32 mice colonised with *H. hepaticus* upregulated expression of inflammatory response pathway genes including *Il23a*. Importantly, both *H. hepaticus* and host alterations in gene expression were in the context of homeostasis without IL-10R blockade and disease development. Thus, we hypothesise that interactions between *E. clostridioformis* YL32 and *H. hepaticus*, resulting in altered *H. hepaticus* virulence, lead to the induction of a “low-level” inflammatory response that is restrained from becoming pathological by IL-10.

Understanding the nature of the interbacterial interactions leading to disease development in the context of IL-10 deficiency requires further experimentation. Whilst we assessed 3 *H.*

hepaticus putative virulence genes, this serves as a preliminary investigation into the *H. hepaticus* response in differential microbial contexts. Moreover, *E. clostridioformis* YL32 may modulate direct effects on host physiology as well as indirect effects through *H. hepaticus*. All of the above aspects would be informed by RNA sequencing of caecal contents to unbiasedly assess bacterial transcriptional activity. This in turn would inform mutagenesis of either bacterium, which could then be employed *in vivo* to assess effects on *Il23a* expression and disease development. Nonetheless, our observation that *H. hepaticus* upregulates HH0252 expression in the presence of *E. clostridioformis* YL32 serves as an indication of inter-species relationships that can alter host physiology. Interestingly HH0252 is homologous to *icmF*, a conserved transmembrane structural component of T6SSs [307], which regulates adhesion, motility, biofilm formation and macrophage survival in other species such as *Aeromonas hydrophila* and *Vibrio parahaermolyticus* [315,316]. In *H. hepaticus*, HH0252/*icmF* has been consistently shown to limit colonisation levels, although this has been suggested to have both modest pro-inflammatory and anti-inflammatory effects in the T cell transfer model of colitis [307,314]. T6SSs are common to gram-negative bacteria, where they mediate inter-bacterial competition through the delivery of toxins to target cells [317]. Indeed, *S*. Tm utilises its T6SS to establish itself in the murine gut through targeted killing of commensal *Klebsiella* species [318]. However, gram-positive bacteria are often resistant to T6SS assaults [317], suggesting that HH0252 upregulation would not necessarily impact on *E. clostridioformis* YL32.

Strikingly, we were able to revert established *H. hepaticus* + aIL-10R colitis through targeted depletion of *E. clostridioformis* YL32 with vancomycin. Interestingly, vancomycin treatment in SPF mice does not influence *H. hepaticus*-induced disease severity in *Il10*$^{-/-}$ mice [171]. Thus, it is unlikely that vancomycin ability to ameliorate disease resulted from indirect effects on the host or *H. hepaticus* and that in our dual-colonised setting *E. clostridioformis* YL32 is key to disease development. It is unclear whether this ability of *E. clostridioformis* YL32 to promote disease in the *H. hepaticus* + aIL-10R model is shared by other OMM^{12} members,

namely *M. intestinale* YL27, *B. coccoides* YL58, *A. muris* KB18, *B. caecimuris* I48, *F. plautii* YL31, *T. muris* YL45 and *B. longum* YL2. Of these *M. intestinale* YL27 also shows inflammation-associated reductions in *H. hepaticus* + aIL-10R treated OMM^{12} mice. *E. clostridioformis* YL32 has been shown to be a key consumer of C5 and C6 sugars, in doing so limiting substrate availability and facilitating *E. coli*-mediated colonisation resistance against *S*. Tm infection. Notably, C5 and C6 sugar consumption conferring *S*. Tm colonisation resistance is a feature shared by *B. coccoides* YL58, suggesting potential metabolic overlap between these two bacteria *in vivo* [179]. Indeed, *E. clostridioformis* YL32 and *B. coccoides* YL58 exhibit the highest metabolic overlap when cultured *in vitro* [183]. Thus, *B. coccoides* YL58 and *M. intestinale* YL27 serve as high priority candidates for further monocolonization experiments. Alternatively, the requirement for an *E. clostridioformis* YL32-harboring microbiome to support *H. hepaticus* + aIL-10R colitis could be assessed through creation of an OMM^{11} lacking *E. clostridioformis* YL32.

Through the use of gnotobiotics, we have uncovered novel interactions between *H. hepaticus* and the commensal *E. clostridioformis* YL32 that are critical to disease development in IL-10 deficiency. Importantly, these potentially operate upstream of host pathways that are well established drivers of immunopathology in the *H. hepaticus* + aIL-10R model. Further work is required to delineate the exact nature of these inter-bacterial interactions and the important colitogenic attributes of each bacterium. Nonetheless, we demonstrate that microbial and host contexts are key to the development of IBD-like pathologies and attribute causality to *E. clostridioformis* YL32 in *H. hepaticus* + aIL-10R disease pathogenesis. Finally, we show that these pathways not only exist but can be targeted to revert established colitis. This serves as proof of concept that microbiota inter-bacteria and host-bacteria interactions serve as novel therapeutic strategies for IBD.

Chapter 6 General discussion

The gut microbiome is gaining increasing interest as having a pivotal role in human health and disease. The field is rapidly expanding, with the annual number of papers published on the microbiome increasing from 2,000 to 25,000 within the past decade. In addition to nutrition, development, metabolic, neurodegenerative and infectious diseases, a major field of study has been uncovering the role of the gut microbiome in IBD [319–321]. Importantly, the microbiome serves as a space in which to develop new IBD therapeutics, which will likely compliment and build upon current and ongoing efforts to target host immunopathological pathways [322]. However, the current scope of microbiota-based therapeutics is limited, with strategies such as FMT being impacted by donor composition heterogeneity and engraftment resistance by the recipient [189]. In more targeted approaches, academic research has highlighted the mechanisms by which gut commensals and derived products can promote health by reinforcing various aspects of intestinal homeostasis [57,59,64,323]. This inevitably has fuelled the growth of several biotechnology companies, with those such as Seres, Vedanta and Microbiotica securing multi-million pound investments to pursue the development of rationally-designed microbiota therapeutics including those aimed at IBD [324]. However, we still have limited understanding of the fundamental aspects of bacteria-bacteria and host-bacteria interactions that operate in the gut microbiota, which could be utilised to design better therapeutics (figure 6.1) [73].

6.1 Unravelling human dysbiotic signatures in animal models

The HMP spearheaded the rapid expansion of our knowledge on the microbiota [43]. Undertaking the mammoth task of characterising the microbiome in health and disease including IBD, the HMP highlighted inter-individual and niche-driven variability in microbial communities [41,42]. This complexity both within and between individuals somewhat hinders

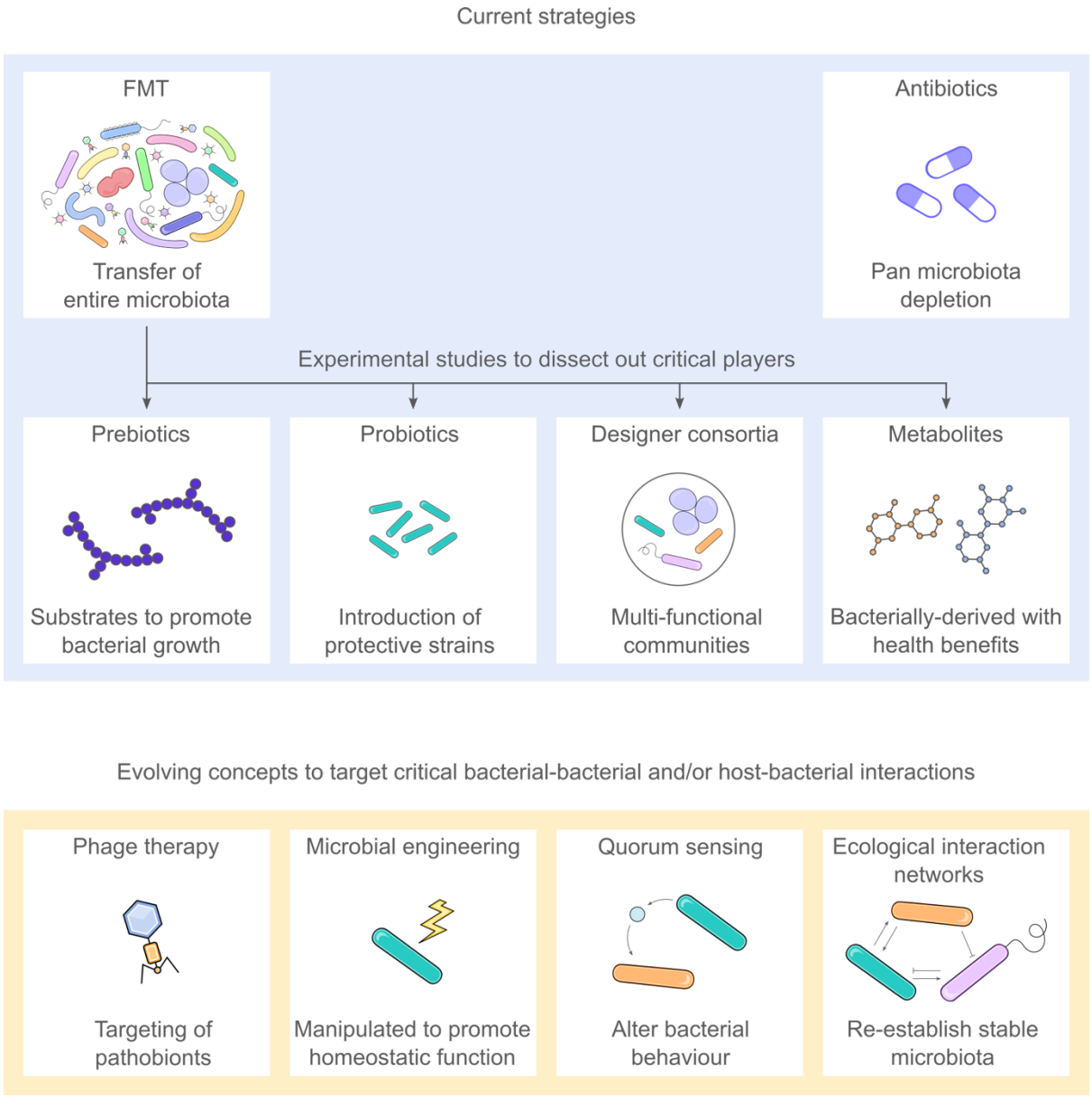


Figure 6.1. Microbiota-based therapeutic strategies. Current and evolving concepts to target the microbiota in IBD to re-establish a healthy microbiota composition, inhibit anti-inflammatory function or promote homeostatic functions encoded by microbiota constituents. Created using information from [72]

functional interrogation of physiologically relevant microbial taxa. However, despite this, reproducible disease-associated signatures have emerged from microbiota characterisation studies in IBD [319]. These include increases in Pseudomonadota, including members of the Enterobacteriaceae family [190,319]. Such associations have led to an interest in exploring the exacerbation of inflammation by facultative anaerobic Enterobacteriaceae species [192,194,229]. This body of work has highlighted the respiratory flexibility of

Enterobacteriaceae as a major contributor to their ability to expand during inflammation and exacerbate disease pathogenesis [192–197].

The importance of alternative respiratory pathways to inflammation-associated Enterobacteriaceae expansion has been delineated with animal models where therapeutic targeting by sodium tungstate has been demonstrated to alleviate DSS colitis through inhibiting molybdenum-dependent nitrate respiration and Enterobacteriaceae outgrowth [198]. In this thesis, we aimed to replicate and extend research into the role of tungstate on Enterobacteriaceae-driven experimental colitis. While we were able to inhibit *in vitro* growth of both commercially obtained and endogenous Enterobacteriaceae species using sodium tungstate, the extent of inhibition was limited *in vivo* and we were not able to replicate previous findings of tungstate-driven amelioration of pathology in DSS colitis. We speculate that this is due to the heterogeneity of the DSS model, outcomes of which are thought to be dictated by the presence or absence of key bacterial species not pertaining to the Enterobacteriaceae family [109].

In addition to DSS colitis, we extended our assessment of the therapeutic potential of tungstate in *C. rodentium* and *H. hepaticus* + aIL-10R colitis. However, tungstate did not have any effects on pathology development, endogenous Enterobacteriaceae and/or *C. rodentium* growth in these models. Collectively, the current data suggest that context-dependent targeting of molybdenum-dependent respiratory pathways can ameliorate Enterobacteriaceae growth and pathology. However, this does not serve as a broadly applicable microbiota-based therapeutic strategy and supports the development of personalised approaches to targeting the microbiota through, for example, assessing the extent of Enterobacteriaceae load prior to intervention. This mirrors the likely shift that will need to take place in host-targeted approaches where characterising disease pathotype prior to administering cytokine blockade treatments may be more beneficial for individual patients [72].

In complex, heterogeneous diseases such as IBD, it is unlikely that a single bacterium, or family of bacteria, are the only causal triggers. Indeed, OMM^{12} mice that lack any Enterobacteriaceae develop colitis following *H. hepaticus* colonisation and aIL-10R treatment. Whether this is through functional redundancy between distantly related members of the microbiome or through entirely different mechanisms is currently unknown. We aimed to explore the relationship between the host and OMM^{12} member changes in terms of abundance and absolute quantities and metabolism by 16S sequencing and IC-MS of longitudinal stool and end-point intestinal contents samples. We found that *H. hepaticus* + aIL-10R-induced dysbiosis could be robustly described through the expansion of *E. faecalis* KB1 and reduction in *M. intestinale* YL27, *E. clostridioformis* YL32 and *A. muciniphila* YL44. Moreover, colitis was associated with alterations in intestinal metabolite composition that recapitulated human IBD signatures, including reductions of MCFAs and butyrate.

The direction of associations in correlative microbiome analyses typically determine hypotheses of cause-and-effect relationships i.e. putative protective bacteria are identified as being lower in abundance in disease and putative harmful bacteria are increased. For example, members of the Firmicutes phylum reduced in human IBD are considered anti-inflammatory. Perhaps most pertinently, the study of Firmicutes, in particular members of the *Clostridium* XIVa and IV clusters, has led to the identification and implication of butyrate in promoting gut homeostasis, including conferring anti-microbial function to macrophages, maintaining epithelial barrier integrity and inducing T_{reg} cells [51,323,325].

However, this does not hold true in our studies. For example, we identified an inflammation-associated increase in facultative anaerobic bacteria, as *E. faecalis* KB1 expansion was a feature of *H. hepaticus*-induced OMM^{12} dysbiosis, a feature that is consistent with previous observations of increased facultative anaerobic bacteria and responses to oxidative stress in SPF mice using the same model [255]. However, *E. faecalis* KB1 monocolonized mice do not develop pathology following *H. hepaticus* colonisation and aIL-10R treatment (Lam *et al*,

unpublished). Thus, it is unlikely that *E. faecalis* KB1 plays a causal role in the *H. hepaticus* + aIL-10R model at least in initiating disease development. This may inform on the role facultative anaerobes play in disease pathogenesis. Indeed, given the fact that Enterobacteriaceae respiratory processes provide a fitness advantage only in the context of inflammation and not homeostasis [192], their role in colitis development is likely to exacerbate a developing or developed inflammatory response as opposed to being the initiating drivers of disease. This is supported by the fact that integrated transcriptional profiling of the host and microbiota during inflammation implicates an expansion and oxidative stress response of facultative anaerobic bacteria in response to the induction of environmental stresses in the inflamed environment [255]. Moreover, gram-negative bacteria have been shown to exacerbate already diseased states in other settings, such as chronic obstructive pulmonary disease [326].

Other robust signatures of OMM^{12} dysbiosis in *H. hepaticus* + aIL-10R treated mice were reductions in *M. intestinale* YL27 and *E. clostridioformis* YL32 at disease onset and decreases in *A. muciniphila* YL44 at late disease stages. Whilst the ability of *M. intestinale* YL27 to support *H. hepaticus*-induced colitis in a monocolonized setting has not yet been established, *A. muciniphila* YL44 monocolonized mice are not susceptible to *H. hepaticus*-induced pathology (Lam *et al*, unpublished). In contrast, we found *E. clostridioformis* YL32 to be a key colitogenic member of the OMM^{12}. This is somewhat contradictory to the role implied by its dysbiotic signature in experimental colitis and suggests that while it is capable of conspiring with *H. hepaticus* in colitis development, it is also sensitive to the inflammatory environment. The reasons for this sensitivity may involve susceptibility to increased levels of oxygen, ROS and RNS i.e., the same factors promoting the increase of facultative anaerobic bacteria, or bacterial-driven or host-driven increases in AMPs. Our data support the requirement for detailed investigations into members of the microbiota that change in colitis, regardless of direction, and while reductions in some may be indicative of a loss of anti-inflammatory properties, we have shown that a reduction of a particular taxon in disease

does not exclude it from being involved in disease progression. While we did not explore homeostatic function of *E. clostridioformis* YL32 in isolation and thus cannot draw conclusions on any anti-inflammatory functions this bacterium may have, our data suggests that colitogenic interactions between *E. clostridioformis* YL32 and *H. hepaticus* are key to pathology development in IL-10 deficiency.

6.2 IBD as the perfect host-microbial storm

Due to low disease penetrance in genetically susceptible individuals and disease heterogeneity, it has long been speculated that IBD arises from the culmination of genetic and environmental risk factors, including microbiome influences in genetically susceptible people [327]. Transitioning from associations between the microbiota and disease into causal roles for commensal species has been facilitated through the use of gnotobiotics. Leveraging such techniques, we found that that disease induction required the combination of *E. clostridioformis* YL32, *H. hepaticus* and IL-10 deficiency. Thus, our experiments support the notion that IBD pathologies develop due to a synergy of inter-bacterial interactions within the microbiota and maladaptation of the host.

The requirement of other commensals for *H. hepaticus* to elicit disease has been established in the literature for over two decades [172], which is at least in-part due to an impaired colonisation of *H. hepaticus* in the absence of other commensal bacteria. However, *H. hepaticus* colonisation alone does not dictate disease development as *H. hepaticus* colonised to comparable levels in *C. innocuum* I46 and *E. clostridioformis* YL32 mice, which were resistant and susceptible to pathology following aIL-10R treatment, respectively. Interestingly, we found that *H. hepaticus* upregulated putative virulence factor gene expression in the presence of *E. clostridioformis* YL32 relative to *C. innocuum* I46 and to levels seen in the full OMM^{12} community. These altered bacterial interactions between *H. hepaticus* and *E. clostridioformis* YL32 were associated with changes in host gene

expression, including increases in TNFα/NF-κB signalling and inflammatory response pathways and downregulation of genes involved in oxidative phosphorylation and fatty acid metabolism. Of note, we found *Il23a* to be upregulated in *E. clostridioformis* YL32 mice following *H. hepaticus* colonisation, whilst this response was not reflected in *C. innocuum* I46 mice. Importantly, these bacterial and host transcriptional responses were seen without aIL-10R treatment and thus in the absence of disease. We hypothesise that bacterial interactions between *H. hepaticus* and *E. clostridioformis* YL32 lead to the adoption of an increased *H. hepaticus* virulence phenotype which elicits a sub-pathological response in the host, including the induction of IL-23. In homeostasis these responses are restrained from becoming pathogenic through IL-10 signalling, where disease results from IL-10 blockade (figure 6.2).

It is of particular interest to further delineate the interactions between *E. clostridioformis* YL32 and *H. hepaticus* and how these influence the host during homeostasis as these will reflect predisposition to disease and will not be influenced by IL-10-regulated pro-inflammatory pathways. Although *H. hepaticus* is a murine pathobiont, enteric *Helicobacter* species have been reportedly enriched in paediatric CD patients [328–330]. Although resident in the stomach as opposed to the intestine, *H. hepaticus* shares similarities with the human pathogen *H. pylori,* including the ability to induce antigen-specific T_{reg} cells, pathogenicity island-encoded virulence factors and the ability to closely associate with the host epithelia [331–334]. In addition to environmental cues such as temperature, iron availability and exposure to reactive oxygen species, virulence gene expression can be modulated by inter-species interactions [335,336]. Interestingly, *H. pylori* expression of virulence factors mediating cell adhesion is inhibited by spent supernatants obtained from *Lactobacillus* species *in vitro*, which is associated with reduced epithelial adherence *in vitro* and *in vivo* [337]. Moreover, *H. pylori* switches to a coccoid form when grown with *Streptococcus mitis* and alters its metabolic profile [338]. Thus, inter-bacterial interactions leading to alterations in virulence and bacterial behaviour is common to other pathobiont

species such as *H. pylori* which is highly relevant to human gastric disease. Further experimentation is required to understand the inter-species interactions between *E. clostridioformis* YL32 and *H. hepaticus*. These should first focus on characterising transcriptional profiles of the two bacteria *in vivo* and then manipulating selected pathways through mutagenesis of gene targets. Determining whether such interaction networks can be recapitulated *in vitro*, e.g., assessing HH0252 expression in *H. hepaticus* cultured with *E. clostridioformis* YL32 or derived supernatant, will aid in mutagenesis screening.

In addition to further understanding the colitic interactions between *E. clostridioformis* YL32 and *H. hepaticus*, it is important to place these within the context of the host. IL-23 is an obvious target for future studies as it is critical for *H. hepaticus* + aIL-10R colitis development and the *IL23R* serves as genetic risk loci in human IBD [78,339]. Although we cannot deduce the source of IL-23 from our bulk RNA-sequencing data, $CD11c^{+}$ monocyte/macrophages are the key cellular sources of IL-23 in the SPF *H. hepaticus* + aIL-10R model [142]. However, it is not clear how *H. hepaticus* and/or other microbial factors interact with this population to induce IL-23 production. Interestingly, IRF5, a transcription factor operational downstream of PRRs, mediates the differentiation of recruited monocytes into IL-23 producing macrophages in *H. hepaticus* + aIL-10R colitis [141]. However, as PRRs can respond to both PAMPs and DAMPs, it is not clear whether monocyte differentiation is in response to contact with bacterial or host-derived factors. For example, *H. hepaticus* could interact directly with monocytes in the lamina propria through release of OMVs, which are commonly produced by most gram-negative bacteria [340]. Indeed, this is a strategy used by the pathobiont *Bacteroides thetaiotaomicron*, whose OMVs translocate the gut mucosal barrier to influence lamina propria macrophages [341]. In contrast, microbial influence over lamina propria populations may be indirect through interactions with the epithelium (figure 6.2). Regardless, understanding how *E. clostridioformis* YL32 and *H. hepaticus* interact with the host to induce IL-23 production amongst other responses will be critical to understanding disease development in the absence of IL-10.

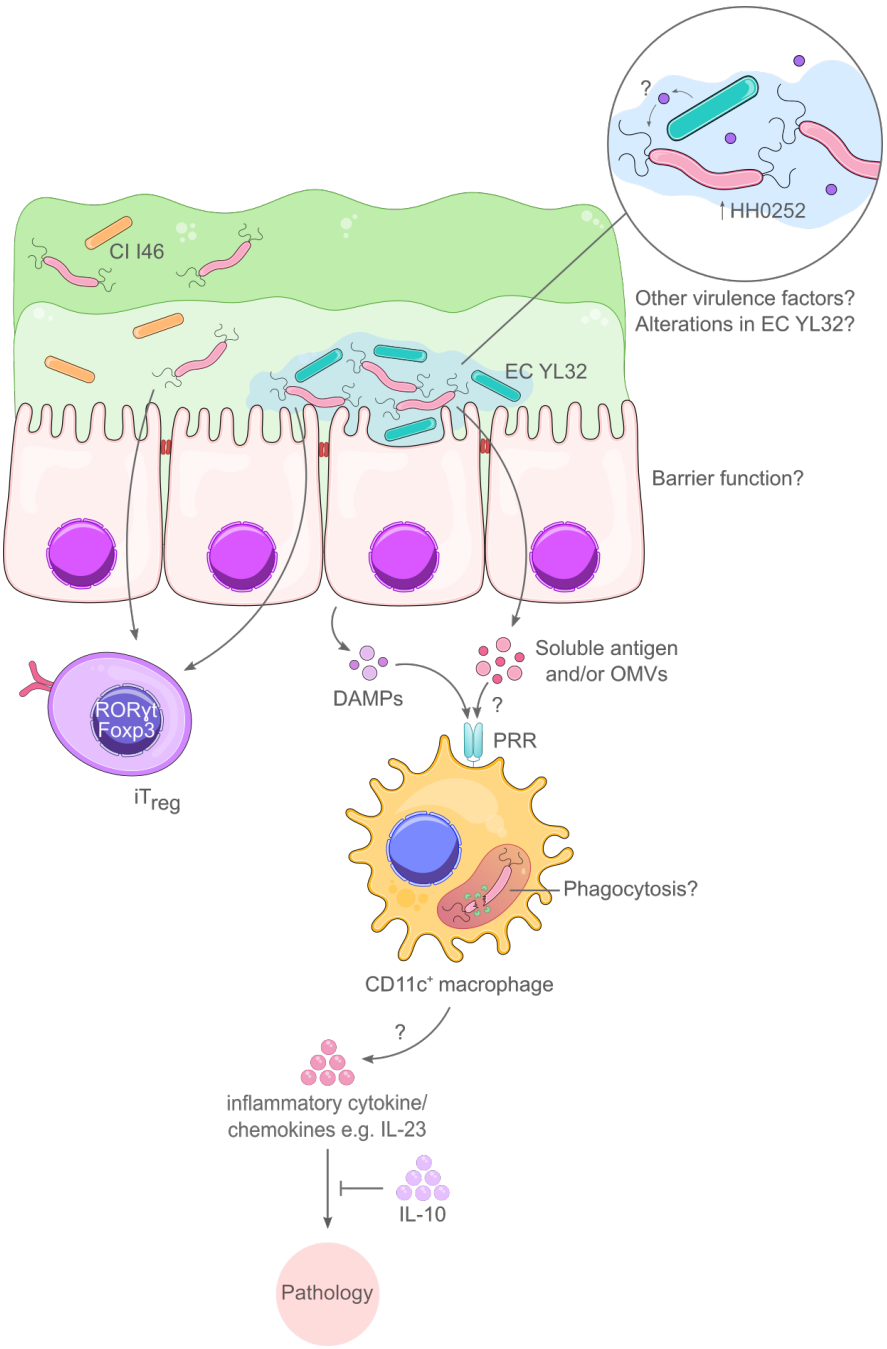


Figure 6.2. Proposed mechanism for the role of *E. clostridioformis* YL32-*H. hepaticus* interactions leading to disease in IL-10 deficiency. Bacterial-bacterial interactions between *E. clostridioformis* YL32 and *H. hepaticus* lead to an increase in bacterial behaviour, at least in-part characterised by an increase in *H, hepaticus* putative virulence gene expression. This leads to a "low-level" induction of inflammatory response gene expression including IL-23. Such responses are restrained from becoming pathological by IL-10. (Left) Interactions between *C. innocuum* I46 and H. *hepaticus* do not promote *H. hepaticus* virluence gene expression, thus leading to a lack of host pro-inflammtory transcriptional response. In both settings, the host retains the ability to generate a *H. hepaticus*-specific T_{reg} cell response. Critical questions to further our understanding and the therapeutic potential of this work include unbiasedly assessing responses of both *H. hepaticus* and *E. clostridioformis* YL32 to understand bacterial networks underpinning a change in pathogenic potential. Understanding how such changes may impact on the host, for example through effects on the epithelium leading to damage-associated molecular pattern (DAMP) production. Factors modulating access of bacterial stimuli to the lamina propria e.g. alterations to barrier function leading to outer membrane vesicle (OMV), soluble antigen or whole bacterium delivery (i.e. phagocytosis). Whether as in SPF mice, these factors converge to drive IL-23 production by CD11c+ macrophages which drives pathology in the absence of IL-10 signalling.

6.3 Targeting of the microbiota to ameliorate established disease

We identified bacterial interactions as key drivers of pathology during IL-10 deficiency. Of note, we were able to revert established colitis by selectively depleting *E. clostridioformis* YL32 with vancomycin. Vancomycin treatment has been shown to alleviate clinical symptoms in paediatric IBD patients, in particular those with concomitant primary sclerosing cholangitis [342–345]. Although vancomycin has been suggested to exert direct anti-inflammatory effects on the host [343], it has previously been shown that vancomycin treatment does not alter disease severity in *H. hepaticus* colonised *Il10*$^{-/-}$ SPF mice [171]. Specific targeting of *E. clostridioformis* YL32 in our system, through use of phage or bacteriocins, which are gaining increasing commercial and clinical interest [297,346], would mitigate potential off-target effects. However, understanding the functional implication of *E. clostridioformis* YL32 is more likely to increase the translational potential of this work. Indeed, we have already documented metabolite disturbances in *H. hepaticus* + aIL-10R OMM^{12} mice that recapitulate those seen in human IBD. Targeting of transcriptional and/or metabolic *E. clostridioformis* YL32 responses as opposed to the bacterium itself will also remove the need to identify a human *E. clostridioformis* YL32 equivalent. Moreover, as microbiome composition, but not of encoded functions [39], is so heterogenous between individuals [41], this serves as a more rational approach in identifying therapeutically targetable pathways in human IBD.

6.4 Conclusion

Although it is readily accepted that the microbiota plays a role in IBD, mechanisms behind pathogenesis are still not understood. The rapid expansion of the microbiome research field, fuelled by technological advancements in multi-omic analysis approaches and the increasing capacity for gnotobiotic research, has facilitated our understanding of the causal role bacteria play in disease development. We have leveraged such techniques to demonstrate that inter-bacterial interactions operational upstream of host immunomodulatory circuits are

therapeutically targetable. Notably, these serve not only as prevention strategies but as means to revert established disease. There are multiple challenges in translating these findings to a clinically relevant space and whether such interactions remain targetable in the setting of a complex microbiota remains to be determined. Nonetheless, we provide proof of concept that targeting of bacterial-bacterial interactions operating in the microbiota is a relevant strategy that may inform the development of highly targeted therapeutics with significant clinical impact.

References

1. Jeffery R, Ilott NE, Powrie F: **Genetic and environmental factors shape the host response to Helicobacter hepaticus: insights into IBD pathogenesis**. *Curr Opin Microbiol* 2022, **65**:145–155.
2. Belkaid Y, Harrison OJ: **Homeostatic immunity and the microbiota**. *Immunity* 2017, **46**:562–576.
3. Uhlig HH, Powrie F: **Translating immunology into therapeutic concepts for inflammatory bowel disease**. *Annu Rev Immunol* 2018, **36**:755–781.
4. Hooper L V., Littman DR, Macpherson AJ: **Interactions between the microbiota and the immune system**. *Science (80-)* 2012, **336**:1268–1273.
5. Johansson MEV, Phillipson M, Petersson J, Velcich A, Holm L, Hansson GC: **The inner of the two Muc2 mucin-dependent mucus layers in colon is devoid of bacteria**. *Proc Natl Acad Sci USA* 2008, **105**:15064–15069.
6. Bergstrom KSB, Kissoon-Singh V, Gibson DL, Ma C, Montero M, Sham HP, Ryz N, Huang T, Velcich A, Finlay BB, et al.: **Muc2 protects against lethal infectious colitis by disassociating pathogenic and commensal bacteria from the colonic mucosa**. *PLoS Pathog* 2010, **6**:e1000902.
7. Desai MS, Seekatz AM, Koropatkin NM, Kamada N, Hickey CA, Wolter M, Pudlo NA, Kitamoto S, Terrapon N, Muller A, et al.: **A dietary fiber-deprived gut microbiota degrades the colonic mucus barrier and enhances pathogen susceptibility**. *Cell* 2016, **167**:1339–1353.
8. Bergstrom K, Shan X, Casero D, Batushansky A, Lagishetty V, Jacobs JP, Hoover C, Kondo Y, Shao B, Gao L, et al.: **Proximal colon-derived O-glycosylated mucus encapsulates and modulates the microbiota**. *Science (80-)* 2020, **370**:467–472.
9. Okumura R, Kurakawa T, Nakano T, Kayama H, Kinoshita M, Motooka D, Gotoh K, Kimura T, Kamiyama N, Kusu T, et al.: **Lypd8 promotes the segregation of flagellated microbiota and colonic epithelia**. *Nature* 2016, **532**:117–121.

10. Pabst O, Slack E: **IgA and the intestinal microbiota: the importance of being specific**. *Mucosal Immunol 2019 131* 2019, **13**:12–21.

11. Melo-Gonzalez F, Kammoun H, Evren E, Dutton EE, Papadopoulou M, Bradford BM, Tanes C, Fardus-Reid F, Swann JR, Bittinger K, et al.: **Antigen-presenting ILC3 regulate T cell-dependent IgA responses to colonic mucosal bacteria**. *J Exp Med* 2019, **216**:728–742.

12. Tran HQ, Ley RE, Gewirtz AT, Chassaing B: **Flagellin-elicited adaptive immunity suppresses flagellated microbiota and vaccinates against chronic inflammatory diseases**. *Nat Commun 2019 101* 2019, **10**:1–15.

13. Gálvez EJC, Iljazovic A, Gronow A, Flavell R, Strowig T: **Shaping of intestinal microbiota in Nlrp6- and Rag2-deficient mice depends on community structure**. *Cell Rep* 2017, **21**:3914–3926.

14. Levy M, Thaiss CA, Zeevi D, Dohnalová L, Zilberman-Schapira G, Mahdi JA, David E, Savidor A, Korem T, Herzig Y, et al.: **Microbiota-modulated metabolites shape the intestinal microenvironment by regulating NLRP6 inflammasome signaling**. *Cell* 2015, **163**:1428–1443.

15. Harrison OJ, Srinivasan N, Pott J, Schiering C, Krausgruber T, Ilott NE, Maloy KJ: **Epithelial-derived IL-18 regulates Th17 cell differentiation and Foxp3^{+} Treg cell function in the intestine**. *Mucosal Immunol* 2015, **8**:1226–1236.

16. Heuberger C, Pott J, Maloy KJ: **Why do intestinal epithelial cells express MHC class II?** *Immunology* 2021, **162**:357–367.

17. Bain CC, Mowat AM: **Intestinal macrophages – specialised adaptation to a unique environment**. *Eur J Immunol* 2011, **41**:2494–2498.

18. Kim M, Galan C, Hill AA, Wu WJ, Fehlner-Peach H, Song HW, Schady D, Bettini ML, Simpson KW, Longman RS, et al.: **Critical role for the microbiota in CX3CR1+ intestinal mononuclear phagocyte regulation of intestinal T cell responses**. *Immunity* 2018, **49**:151-163.e5.

19. Niess JH, Brand S, Gu X, Landsman L, Jung S, McCormick BA, Vyas JM, Boes M,

Ploegh HL, Fox JG, et al.: **CX3CR1-mediated dendritic cell access to the intestinal lumen and bacterial clearance**. *Science* 2005, **307**:254–258.

20. Zigmond E, Bernshtein B, Friedlander G, Walker CR, Yona S, Kim KW, Brenner O, Krauthgamer R, Varol C, Müller W, et al.: **Macrophage-restricted interleukin-10 receptor deficiency, but not IL-10 deficiency, causes severe spontaneous colitis**. *Immunity* 2014, **40**:720–733.
21. Coombes JL, Powrie F: **Dendritic cells in intestinal immune regulation**. *Nat Rev Immunol 2008 86* 2008, **8**:435–446.
22. Monteleone I, Platt AM, Jaensson E, Agace WW, Mowat AMI: **IL-10-dependent partial refractoriness to Toll-like receptor stimulation modulates gut mucosal dendritic cell function**. *Eur J Immunol* 2008, **38**:1533–1547.
23. Russler-Germain E V., Yi J, Young S, Nutsch K, Wong HS, Ai TL, Chai JN, Durai V, Kaplan DH, Germain RN, et al.: **Gut *Helicobacter* presentation by multiple dendritic cell subsets enables context-specific regulatory T cell generation**. *Elife* 2021, **10**:1–29.
24. Eberl G, Colonna M, Santo JPD, McKenzie ANJ: **Innate lymphoid cells: A new paradigm in immunology**. *Science (80-)* 2015, **348**.
25. Mortha A, Chudnovskiy A, Hashimoto D, Bogunovic M, Spencer SP, Belkaid Y, Merad M: **Microbiota-dependent crosstalk between macrophages and ILC3 promotes intestinal homeostasis**. *Science (80-)* 2014, **343**:1249288.
26. Lyu M, Suzuki H, Kang L, Gaspal F, Zhou W, Goc J, Zhou L, Zhou J, Zhang W, Artis D, et al.: **ILC3s select microbiota-specific regulatory T cells to establish tolerance in the gut**. *Nature* 2022, **610**:744–751.
27. Hepworth MR, Monticelli LA, Fung TC, Ziegler CGK, Grunberg S, Sinha R, Mantegazza AR, Ma HL, Crawford A, Angelosanto JM, et al.: **Innate lymphoid cells regulate CD4+ T-cell responses to intestinal commensal bacteria**. *Nature* 2013, **498**:113–117.
28. Hegazy AN, West NR, Stubbington MJT, Wendt E, Suijker KIM, Datsi A, This S,

Danne C, Campion S, Duncan SH, et al.: **Circulating and tissue-resident CD4$^+$ T cells with reactivity to intestinal microbiota are abundant in healthy individuals and function is altered during inflammation**. *Gastroenterology* 2017, **153**:1320–1337.

29. Whibley N, Tucci A, Powrie F: **Regulatory T cell adaptation in the intestine and skin**. *Nat Immunol* 2019, **20**:386–396.

30. Zegarra-Ruiz DF, Kim D V., Norwood K, Kim M, Wu WJH, Saldana-Morales FB, Hill AA, Majumdar S, Orozco S, Bell R, et al.: **Thymic development of gut-microbiota-specific T cells**. *Nature* 2021, **594**:413–417.

31. Chai JN, Peng Y, Rengarajan S, Solomon BD, Ai TL, Shen Z, Perry JSA, Knoop KA, Tanoue T, Narushima S, et al.: ***Helicobacter* species are potent drivers of colonic T cell responses in homeostasis and inflammation**. *Sci Immunol* 2017, **2**:eaal5068.

32. Xu M, Pokrovskii M, Ding Y, Yi R, Au C, Harrison OJ, Galan C, Belkaid Y, Bonneau R, Littman DR: **C-MAF-dependent regulatory T cells mediate immunological tolerance to a gut pathobiont**. *Nature* 2018, **554**:373–377.

33. Wegorzewska MM, Glowacki RWP, Hsieh SA, Donermeyer DL, Hickey CA, Horvath SC, Martens EC, Stappenbeck TS, Allen PM: **Diet modulates colonic T cell responses by regulating the expression of a *Bacteroides thetaiotaomicron* antigen**. *Sci Immunol* 2019, **4**:eaau9079.

34. Cong Y, Feng T, Fujihashi K, Schoeb TR, Elson CO: **A dominant, coordinated T regulatory cell-IgA response to the intestinal microbiota**. *Proc Natl Acad Sci* 2009, **106**:19256–19261.

35. Hand TW, Dos Santos LM, Bouladoux N, Molloy MJ, Pagán AJ, Pepper M, Maynard CL, Elson CO, Belkaid Y: **Acute gastrointestinal infection induces long-lived microbiota-specific T cell responses**. *Science (80-)* 2012, **337**:1553–1556.

36. Chiaranunt P, Tometich JT, Ji J, Hand TW: **T cell proliferation and colitis are initiated by defined intestinal microbes**. *J Immunol* 2018, **201**:243–250.

37. Lynch S V., Pedersen O: **The Human Intestinal Microbiome in Health and Disease**. *N Engl J Med* 2016, **375**:2369–2379.

38. Sender R, Fuchs S, Milo R: **Revised Estimates for the Number of Human and Bacteria Cells in the Body**. *PLOS Biol* 2016, **14**:e1002533.

39. Li J, Jia H, Cai X, Zhong H, Feng Q, Sunagawa S, Arumugam M, Kultima JR, Prifti E, Nielsen T, et al.: **An integrated catalog of reference genes in the human gut microbiome**. *Nat Biotechnol* 2014, **32**:834–841.

40. Pertea M, Shumate A, Pertea G, Varabyou A, Breitwieser FP, Chang YC, Madugundu AK, Pandey A, Salzberg SL: **CHESS: A new human gene catalog curated from thousands of large-scale RNA sequencing experiments reveals extensive transcriptional noise**. *Genome Biol* 2018, **19**:1–14.

41. Huttenhower C, Gevers D, Knight R, Abubucker S, Badger JH, Chinwalla AT, Creasy HH, Earl AM, Fitzgerald MG, Fulton RS, et al.: **Structure, function and diversity of the healthy human microbiome**. *Nature* 2012, **486**:207–214.

42. Qin J, Li R, Raes J, Arumugam M, Burgdorf KS, Manichanh C, Nielsen T, Pons N, Levenez F, Yamada T, et al.: **A human gut microbial gene catalogue established by metagenomic sequencing**. *Nature* 2010, **464**:59–65.

43. Turnbaugh PJ, Ley RE, Hamady M, Fraser-Liggett CM, Knight R, Gordon JI: **The Human Microbiome Project**. *Nature* 2007, **449**:804–810.

44. Lloyd-Price J, Abu-Ali G, Huttenhower C: **The healthy human microbiome**. *Genome Med* 2016, **8**:1–11.

45. Eckburg PB, Bik EM, Bernstein CN, Purdom E, Dethlefsen L, Sargent M, Gill SR, Nelson KE, Relman DA: **Microbiology: Diversity of the human intestinal microbial flora**. *Science (80-)* 2005, **308**:1635–1638.

46. Miller BM, Baumler AJ: **The Habitat Filters of Microbiota-Nourishing Immunity**. *Annu Rev Immunol* 2021, **39**:1–18.

47. Morrison DJ, Preston T: **Formation of short chain fatty acids by the gut microbiota and their impact on human metabolism**. *Gut Microbes* 2016, **7**:189–

200.

48. Roediger WEW: **Utilization of Nutrients by Isolated Epithelial Cells of the Rat Colon**. *Gastroenterology* 1982, **83**:424–429.

49. Litvak Y, Byndloss MX, Bäumler AJ: **Colonocyte metabolism shapes the gut microbiota**. *Science (80-)* 2018, **362**:eaat9076.

50. Wang HB, Wang PY, Wang X, Wan YL, Liu YC: **Butyrate enhances intestinal epithelial barrier function via up-regulation of tight junction protein claudin-1 transcription**. *Dig Dis Sci* 2012, **57**:3126–3135.

51. Schulthess J, Pandey S, Capitani M, Rue-Albrecht KC, Arnold I, Franchini F, Chomka A, Ilott NE, Johnston DGW, Pires E, et al.: **The Short Chain Fatty Acid Butyrate Imprints an Antimicrobial Program in Macrophages**. *Immunity* 2019, **50**:432-445.e7.

52. Scott NA, Andrusaite A, Andersen P, Lawson M, Alcon-Giner C, Leclaire C, Caim S, Le Gall G, Shaw T, Connolly JPR, et al.: **Antibiotics induce sustained dysregulation of intestinal T cell immunity by perturbing macrophage homeostasis**. *Sci Transl Med* 2018, **10**:eaao4755.

53. Furusawa Y, Obata Y, Fukuda S, Endo TA, Nakato G, Takahashi D, Nakanishi Y, Uetake C, Kato K, Kato T, et al.: **Commensal microbe-derived butyrate induces the differentiation of colonic regulatory T cells**. *Nature* 2013, **504**:446–450.

54. Stockinger B, Shah K, Wincent E: **AHR in the intestinal microenvironment: safeguarding barrier function**. *Nat Rev Gastroenterol Hepatol* 2021, **18**:559–570.

55. Schiering C, Wincent E, Metidji A, Iseppon A, Li Y, Potocnik AJ, Omenetti S, Henderson CJ, Wolf CR, Nebert DW, et al.: **Feedback control of AHR signalling regulates intestinal immunity**. *Nature* 2017, **542**:242–245.

56. Guzior D V., Quinn RA: **Review: microbial transformations of human bile acids**. *Microbiome* 2021, **9**:1–13.

57. Hang S, Paik D, Yao L, Kim E, Jamma T, Lu J, Ha S, Nelson BN, Kelly SP, Wu L, et al.: **Bile acid metabolites control TH17 and Treg cell differentiation**. *Nature* 2019,

576:143–148.

58. Song X, Sun X, Oh SF, Wu M, Zhang Y, Zheng W, Geva-Zatorsky N, Jupp R, Mathis D, Benoist C, et al.: **Microbial bile acid metabolites modulate gut RORγ$^+$ regulatory T cell homeostasis**. *Nature* 2020, **577**:410–415.
59. Campbell C, McKenney PT, Konstantinovsky D, Isaeva OI, Schizas M, Verter J, Mai C, Jin WB, Guo CJ, Violante S, et al.: **Bacterial metabolism of bile acids promotes generation of peripheral regulatory T cells**. *Nature* 2020, **581**:475–479.
60. Buffie CG, Bucci V, Stein RR, McKenney PT, Ling L, Gobourne A, No D, Liu H, Kinnebrew M, Viale A, et al.: **Precision microbiome reconstitution restores bile acid mediated resistance to Clostridium difficile**. *Nature* 2014, **517**:205–208.
61. Kang JD, Myers CJ, Harris SC, Kakiyama G, Lee IK, Yun BS, Matsuzaki K, Furukawa M, Min HK, Bajaj JS, et al.: **Bile Acid 7α-Dehydroxylating Gut Bacteria Secrete Antibiotics that Inhibit Clostridium difficile: Role of Secondary Bile Acids**. *Cell Chem Biol* 2019, **26**:27-34.e4.
62. McKenney PT, Yan J, Vaubourgeix J, Becattini S, Lampen N, Motzer A, Larson PJ, Dannaoui D, Fujisawa S, Xavier JB, et al.: **Intestinal Bile Acids Induce a Morphotype Switch in Vancomycin-Resistant Enterococcus that Facilitates Intestinal Colonization**. *Cell Host Microbe* 2019, **25**:695-705.e5.
63. Mazmanian SK, Cui HL, Tzianabos AO, Kasper DL: **An Immunomodulatory Molecule of Symbiotic Bacteria Directs Maturation of the Host Immune System**. *Cell* 2005, **122**:107–118.
64. Mazmanian SK, Round JL, Kasper DL: **A microbial symbiosis factor prevents intestinal inflammatory disease**. *Nature* 2008, **453**:620–625.
65. Shen Y, Torchia MLG, Lawson GW, Karp CL, Ashwell JD, Mazmanian SK: **Outer membrane vesicles of a human commensal mediate immune regulation and disease protection**. *Cell Host Microbe* 2012, **12**:509–520.
66. Round JL, Lee SM, Li J, Tran G, Jabri B, Chatila TA, Mazmanian SK: **The toll-like receptor 2 pathway establishes colonization by a commensal of the human**

microbiota. *Science (80-)* 2011, **332**:974–977.

67. Danne C, Ryzhakov G, Martínez-López M, Ilott NE, Franchini F, Cuskin F, Lowe EC, Bullers SJ, Arthur JSC, Powrie F: **A large polysaccharide produced by *Helicobacter hepaticus* induces an anti-inflammatory gene signature in macrophages**. *Cell Host Microbe* 2017, **22**:733–745.

68. Kaser A, Zeissig S, Blumberg RS: **Inflammatory Bowel Disease**. *Annu Rev Immunol* 2010, **28**:573–621.

69. Bernell O, Lapidus A, Hellers G: **Risk Factors for Surgery and Postoperative Recurrence in Crohn's Disease**. *Ann Surg* 2000, **231**:38.

70. Hendrickson BA, Gokhale R, Cho JH: **Clinical aspects and pathophysiology of inflammatory bowel disease**. *Clin Microbiol Rev* 2002, **15**:79–94.

71. King D, Reulen RC, Thomas T, Chandan JS, Thayakaran R, Subramanian A, Gokhale K, Bhala N, Nirantharakumar K, Adderley NJ, et al.: **Changing patterns in the epidemiology and outcomes of inflammatory bowel disease in the United Kingdom: 2000-2018**. *Aliment Pharmacol Ther* 2020, **51**:922–934.

72. Friedrich M, Pohin M, Jackson MA, Korsunsky I, Bullers SJ, Rue-Albrecht K, Christoforidou Z, Sathananthan D, Thomas T, Ravindran R, et al.: **IL-1-driven stromal–neutrophil interactions define a subset of patients with inflammatory bowel disease that does not respond to therapies**. *Nat Med* 2021, **27**:1970–1981.

73. Plichta DR, Graham DB, Subramanian S, Xavier RJ: **Therapeutic Opportunities in Inflammatory Bowel Disease: Mechanistic Dissection of Host-Microbiome Relationships**. *Cell* 2019, **178**:1041–1056.

74. Jostins L, Ripke S, Weersma RK, Duerr RH, McGovern DP, Hui KY, Lee JC, Philip Schumm L, Sharma Y, Anderson CA, et al.: **Host–microbe interactions have shaped the genetic architecture of inflammatory bowel disease**. *Nature* 2012, **491**:119–124.

75. Neurath MF: **Current and emerging therapeutic targets for IBD**. *Nat Rev Gastroenterol Hepatol 2017 145* 2017, **14**:269–278.

76. Cohen BL, Sachar DB: **Update on anti-tumor necrosis factor agents and other new drugs for inflammatory bowel disease**. *BMJ* 2017, **357**:j2505.

77. Noviello D, Mager R, Roda G, Borroni RG, Fiorino G, Vetrano S: **The IL23-IL17 Immune Axis in the Treatment of Ulcerative Colitis: Successes, Defeats, and Ongoing Challenges**. *Front Immunol* 2021, **12**:611256.

78. Kullberg MC, Jankovic D, Feng CG, Hue S, Gorelick PL, McKenzie BS, Cua DJ, Powrie F, Cheever AW, Maloy KJ, et al.: **IL-23 plays a key role in *Helicobacter hepaticus*-induced T cell-dependent colitis.** *J Exp Med* 2006, **203**:2485–2494.

79. Hueber W, Sands BE, Lewitzky S, Vandemeulebroecke M, Reinisch W, Higgins PDR, Wehkamp J, Feagan BG, Yao MD, Karczewski M, et al.: **Secukinumab, a human anti-IL-17A monoclonal antibody, for moderate to severe Crohn's disease: unexpected results of a randomised, double-blind placebo-controlled trial**. *Gut* 2012, **61**:1693–1700.

80. Sands BE, Sandborn WJ, Panaccione R, O'Brien CD, Zhang H, Johanns J, Adedokun OJ, Li K, Peyrin-Biroulet L, Van Assche G, et al.: **Ustekinumab as Induction and Maintenance Therapy for Ulcerative Colitis**. *N Engl J Med* 2019, **381**:1201–1214.

81. Feagan BG, Sandborn WJ, Gasink C, Jacobstein D, Lang Y, Friedman JR, Blank MA, Johanns J, Gao L-L, Miao Y, et al.: **Ustekinumab as Induction and Maintenance Therapy for Crohn's Disease**. *N Engl J Med* 2016, **375**:1946–1960.

82. Parigi TL, Iacucci M, Ghosh S: **Blockade of IL-23: What is in the Pipeline?** *J Crohns Colitis* 2022, **16**:ii64–ii72.

83. Khera A V., Chaffin M, Aragam KG, Haas ME, Roselli C, Choi SH, Natarajan P, Lander ES, Lubitz SA, Ellinor PT, et al.: **Genome-wide polygenic scores for common diseases identify individuals with risk equivalent to monogenic mutations**. *Nat Genet* 2018, **50**:1219–1224.

84. Ni J, Wu GD, Albenberg L, Tomov VT: **Gut microbiota and IBD: causation or correlation?** *Nat Rev Gastroenterol Hepatol 2017 1410* 2017, **14**:573–584.

85. Carlsson AH, Yakymenko O, Olivier I, Håkansson F, Postma E, Keita Å V.,

Söderholm JD: **Faecalibacterium prausnitzii supernatant improves intestinal barrier function in mice DSS colitis**. *Scand J Gastroenterol* 2013, **48**:1136–1144.

86. Sokol H, Pigneur B, Watterlot L, Lakhdari O, Bermúdez-Humarán LG, Gratadoux JJ, Blugeon S, Bridonneau C, Furet JP, Corthier G, et al.: **Faecalibacterium prausnitzii is an anti-inflammatory commensal bacterium identified by gut microbiota analysis of Crohn disease patients**. *Proc Natl Acad Sci USA* 2008, **105**:16731–16736.

87. Baumgart M, Dogan B, Rishniw M, Weitzman G, Bosworth B, Yantiss R, Orsi RH, Wiedmann M, McDonough P, Kim SG, et al.: **Culture independent analysis of ileal mucosa reveals a selective increase in invasive Escherichia coli of novel phylogeny relative to depletion of Clostridiales in Crohn's disease involving the ileum**. *ISME J* 2007, **1**:403–418.

88. Darfeuille-Michaud A, Neut C, Barnich N, Lederman E, Di Martino P, Desreumaux P, Gambiez L, Joly B, Cortot A, Colombel JF: **Presence of adherent Escherichia coli strains in ileal mucosa of patients with Crohn's disease**. *Gastroenterology* 1998, **115**:1405–1413.

89. Marchesi JR, Holmes E, Khan F, Kochhar S, Scanlan P, Shanahan F, Wilson ID, Wang Y: **Rapid and noninvasive metabonomic characterization of inflammatory bowel disease**. *J Proteome Res* 2007, **6**:546–551.

90. Bjerrum JT, Wang Y, Hao F, Coskun M, Ludwig C, Günther U, Nielsen OH: **Metabonomics of human fecal extracts characterize ulcerative colitis, Crohn's disease and healthy individuals**. *Metabolomics* 2015, **11**:122.

91. Ji J, Shu D, Zheng M, Wang J, Luo C, Wang Y, Guo F, Zou X, Lv X, Li Y, et al.: **Microbial metabolite butyrate facilitates M2 macrophage polarization and function**. *Sci Rep* 2016, **6**:24838.

92. Hallert C, Björck I, Nyman M, Pousette A, Grännö C, Svensson H: **Increasing fecal butyrate in ulcerative colitis patients by diet: controlled pilot study**. *Inflamm Bowel Dis* 2003, **9**:116–121.

93. Valcheva R, Koleva P, Martínez I, Walter J, Gänzle MG, Dieleman LA: **Inulin-type fructans improve active ulcerative colitis associated with microbiota changes and increased short-chain fatty acids levels**. *Gut Microbes* 2019, **10**:334–357.

94. Sinha SR, Haileselassie Y, Nguyen LP, Tropini C, Wang M, Becker LS, Sim D, Jarr K, Spear ET, Singh G, et al.: **Dysbiosis-Induced Secondary Bile Acid Deficiency Promotes Intestinal Inflammation**. *Cell Host Microbe* 2020, **27**:659-670.e5.

95. Palm NW, de Zoete MR, Cullen TW, Barry NA, Stefanowski J, Hao L, Degnan PH, Hu J, Peter I, Zhang W, et al.: **Immunoglobulin A coating identifies colitogenic bacteria in inflammatory bowel disease**. *Cell* 2014, **158**:1000–1010.

96. Armstrong H, Alipour M, Valcheva R, Bording-Jorgensen M, Jovel J, Zaidi D, Shah P, Lou Y, Ebeling C, Mason AL, et al.: **Host immunoglobulin G selectively identifies pathobionts in pediatric inflammatory bowel diseases**. *Microbiome* 2019, **7**:1.

97. Rengarajan S, Vivio EE, Parkes M, Peterson DA, Roberson EDO, Newberry RD, Ciorba MA, Hsieh CS: **Dynamic immunoglobulin responses to gut bacteria during inflammatory bowel disease**. *Gut Microbes* 2020, **11**:405–420.

98. Goyal N, Rana A, Ahlawat A, Bijjem KR V., Kumar P: **Animal models of inflammatory bowel disease: A review**. *Inflammopharmacology* 2014, **22**:219–233.

99. Perše M, Cerar A: **Dextran Sodium Sulphate Colitis Mouse Model: Traps and Tricks**. *J Biomed Biotechnol* 2012, **2012**:718617.

100. Okayasu I, Hatakeyama S, Yamada M, Ohkusa T, Inagaki Y, Nakaya R: **A Novel Method in the Induction of Reliable Experimental Acute and Chronic Ulcerative Colitis in Mice**. *Gastroenterology* 1990, **98**:694–702.

101. Dieleman LA, Ridwan BU, Tennyson GS, Beagley KW, Bucy RP, Elson CO: **Dextran sulfate sodium-induced colitis occurs in severe combined immunodeficient mice**. *Gastroenterology* 1994, **107**:1643–1652.

102. Laroui H, Ingersoll SA, Liu HC, Baker MT, Ayyadurai S, Charania MA, Laroui F, Yan Y, Sitaraman S V., Merlin D: **Dextran Sodium Sulfate (DSS) Induces Colitis in Mice by Forming Nano-Lipocomplexes with Medium-Chain-Length Fatty Acids**

in the Colon. *PLoS One* 2012, **7**:32084.

103. Wirtz S, Neufert C, Weigmann B, Neurath MF: **Chemically induced mouse models of intestinal inflammation**. *Nat Protoc 2007 23* 2007, **2**:541–546.

104. Antoni L, Nuding S, Wehkamp J, Stange EF: **Intestinal barrier in inflammatory bowel disease**. *World J Gastroenterol* 2014, **20**:1165.

105. Heller F, Florian P, Bojarski C, Richter J, Christ M, Hillenbrand B, Mankertz J, Gitter AH, Bürgel N, Fromm M, et al.: **Interleukin-13 is the key effector Th2 cytokine in ulcerative colitis that affects epithelial tight junctions, apoptosis, and cell restitution**. *Gastroenterology* 2005, **129**:550–564.

106. Luettig J, Rosenthal R, Barmeyer C, Schulzke JD: **Claudin-2 as a mediator of leaky gut barrier during intestinal inflammation**. *Tissue Barriers* 2015, **3**:1–2.

107. Nagalingam NA, Kao JY, Young VB: **Microbial ecology of the murine gut associated with the development of dextran sodium sulfate-induced colitis**. *Inflamm Bowel Dis* 2011, **17**:917–926.

108. Munyaka PM, Rabbi MF, Khafipour E, Ghia JE: **Acute dextran sulfate sodium (DSS)-induced colitis promotes gut microbial dysbiosis in mice**. *J Basic Microbiol* 2016, **56**:986–998.

109. Forster SC, Clare S, Beresford-Jones BS, Harcourt K, Notley G, Stares MD, Kumar N, Soderholm AT, Adoum A, Wong H, et al.: **Identification of gut microbial species linked with disease variability in a widely used mouse model of colitis**. *Nat Microbiol 2022 74* 2022, **7**:590–599.

110. Chang CS, Liao YC, Huang CT, Lin CM, Cheung CHY, Ruan JW, Yu WH, Tsai YT, Lin IJ, Huang CH, et al.: **Identification of a gut microbiota member that ameliorates DSS-induced colitis in intestinal barrier enhanced Dusp6-deficient mice**. *Cell Rep* 2021, **37**:110016.

111. Schauer DB, Falkow S: **Attaching and effacing locus of a Citrobacter freundii biotype that causes transmissible murine colonic hyperplasia.** *Infect Immun* 1993, **61**:2486.

112. Collins JW, Keeney KM, Crepin VF, Rathinam VAK, Fitzgerald KA, Finlay BB, Frankel G: **Citrobacter rodentium: infection, inflammation and the microbiota**. *Nat Rev Microbiol* 2014, **12**:612–623.

113. Gaytán MO, Martínez-Santos VI, Soto E, González-Pedrajo B: **Type Three Secretion System in Attaching and Effacing Pathogens**. *Front Cell Infect Microbiol* 2016, **6**:129.

114. Koroleva EP, Halperin S, Gubernatorova EO, Macho-Fernandez E, Spencer CM, Tumanov A V.: **Citrobacter rodentium-induced colitis: A robust model to study mucosal immune responses in the gut**. *J Immunol Methods* 2015, **421**:61–72.

115. Mullineaux-Sanders C, Sanchez-Garrido J, Hopkins EGD, Shenoy AR, Barry R, Frankel G: **Citrobacter rodentium–host–microbiota interactions: immunity, bioenergetics and metabolism**. *Nat Rev Microbiol* 2019, **17**:701–715.

116. Kamada N, Kim YG, Sham HP, Vallance BA, Puente JL, Martens EC, Núñez G: **Regulated virulence controls the ability of a pathogen to compete with the gut microbiota**. *Science (80-)* 2012, **336**:1325–1329.

117. Stockinger B, Omenetti S: **The dichotomous nature of T helper 17 cells**. *Nat Rev Immunol 2017 179* 2017, **17**:535–544.

118. Osbelt L, Thiemann S, Smit N, Lesker TR, Schröter M, Gálvez EJC, Schmidt-Hohagen K, Pils MC, Mühlen S, Dersch P, et al.: **Variations in microbiota composition of laboratory mice influence Citrobacter rodentium infection via variable short-chain fatty acid production**. *PLoS Pathog* 2020, **16**:e1008448.

119. Ivanov II, Atarashi K, Manel N, Brodie EL, Shima T, Karaoz U, Wei D, Goldfarb KC, Santee CA, Lynch S V., et al.: **Induction of intestinal Th17 cells by segmented filamentous bacteria**. *Cell* 2009, **139**:485.

120. Mullineaux-Sanders C, Collins JW, Ruano-Gallego D, Levy M, Pevsner-Fischer M, Glegola-Madejska IT, Sågfors AM, Wong JLC, Elinav E, Crepin VF, et al.: **Citrobacter rodentium Relies on Commensals for Colonization of the Colonic Mucosa**. *Cell Rep* 2017, **21**:3381.

121. Hoffmann C, Hill DA, Minkah N, Kirn T, Troy A, Artis D, Bushman F: **Community-wide response of the gut microbiota to enteropathogenic Citrobacter rodentium infection revealed by deep sequencing**. *Infect Immun* 2009, **77**:4668–4678.

122. Hopkins EGD, Roumeliotis TI, Mullineaux-Sanders C, Choudhary JS, Frankel G: **Intestinal Epithelial Cells and the Microbiome Undergo Swift Reprogramming at the Inception of Colonic Citrobacter rodentium Infection**. *MBio* 2019, **10**:e00062-19.

123. Fox JG, Dewhirst FE, Tully JG, Paster BJ, Yan L, Taylor NS, Collins MJ, Gorelick PL, Ward JM: ***Helicobacter hepaticus*** **sp. nov., a microaerophilic bacterium isolated from livers and intestinal mucosal scrapings from mice**. *J Clin Microbiol* 1994, **32**:1238–1245.

124. Ward JM, Anver MR, Haines DC, Melhorn JM, Gorelick P, Yan L, Fox JG: **Inflammatory large bowel disease in immunodeficient mice naturally infected with *Helicobacter hepaticus***. *Lab Anim Sci* 1996, **46**:15–20.

125. Cahill RJ, Foltz CJ, Fox JG, Dangler CA, Powrie F, Schauer DB: **Inflammatory bowel disease: An immunity-mediated condition triggered by bacterial infection with *Helicobacter hepaticus***. *Infect Immun* 1997, **65**:3126–3131.

126. Kullberg MC, Ward JM, Gorelick PL, Caspar P, Hieny S, Cheever A, Jankovic D, Sher A: ***Helicobacter hepaticus*** **triggers colitis in specific-pathogen-free interleukin-10 (IL-10)-deficient mice through an IL-12- and gamma interferon-dependent mechanism.** *Infect Immun* 1998, **66**:5157–5166.

127. Boulard O, Kirchberger S, Royston DJ, Maloy KJ, Powrie FM: **Identification of a genetic locus controlling bacteria-driven colitis and associated cancer through effects on innate inflammation**. *J Exp Med* 2012, **209**:1309–1324.

128. Buonocore S, Ahern PP, Uhlig HH, Ivanov II, Littman DR, Maloy KJ, Powrie F: **Innate lymphoid cells drive IL-23 dependent innate intestinal pathology**. *Nature* 2010, **464**:1371.

129. Morrison PJ, Bending D, Fouser LA, Wright JF, Stockinger B, Cooke A, Kullberg MC:

Th17-cell plasticity in *Helicobacter hepaticus*-induced intestinal inflammation. *Mucosal Immunol* 2013, **6**:1143–1156.

130. Kullberg MC, Andersen JF, Gorelick PL, Caspar P, Suerbaum S, Fox JG, Cheever AW, Jankovic D, Sher A: **Induction of colitis by a CD4$^+$ T cell clone specific for a bacterial epitope**. *Proc Natl Acad Sci USA* 2003, **100**:15830–15835.

131. Kullberg MC, Jankovic D, Gorelick PL, Caspar P, Letterio JJ, Cheever AW, Sher A: **Bacteria-triggered CD4$^+$ T regulatory cells suppress *Helicobacter hepaticus*-induced colitis**. *J Exp Med* 2002, **196**:505–515.

132. Friedrich V, Forné I, Matzek D, Ring D, Popper B, Jochum L, Spriewald S, Straub T, Imhof A, Krug A, et al.: ***Helicobacter hepaticus* is required for immune targeting of bacterial heat shock protein 60 and fatal colitis in mice**. *Gut Microbes* 2021, **13**:1–20.

133. Atherly T, Mosher C, Wang C, Hostetter J, Proctor A, Brand MW, Phillips GJ, Wannemuehler M, Jergens AE: ***Helicobacter bilis* infection alters mucosal bacteria and modulates colitis development in defined microbiota mice**. *Inflamm Bowel Dis* 2016, **22**:2571–2581.

134. Gomes-Neto JC, Kittana H, Mantz S, Segura Munoz RR, Schmaltz RJ, Bindels LB, Clarke J, Hostetter JM, Benson AK, Walter J, et al.: **A gut pathobiont synergizes with the microbiota to instigate inflammatory disease marked by immunoreactivity against other symbionts but not itself**. *Sci Rep* 2017, **7**:17701.

135. Powell N, Walker AW, Stolarczyk E, Canavan JB, Gökmen MR, Marks E, Jackson I, Hashim A, Curtis MA, Jenner RG, et al.: **The transcription factor T-bet regulates intestinal inflammation mediated by interleukin-7 receptor$^+$ innate lymphoid cells**. *Immunity* 2012, **37**:674–684.

136. Chichlowski M, Sharp JM, Vanderford DA, Myles MH, Hale LP: ***Helicobacter typhlonius* and *Helicobacter rodentium* differentially affect the severity of colon inflammation and inflammation-associated neoplasia in IL10-deficient mice**. *Comp Med* 2008, **58**:534–541.

137. Bloom SM, Bijanki VN, Nava GM, Sun L, Malvin NP, Donermeyer DL, Dunne WM, Allen PM, Stappenbeck TS: **Commensal *Bacteroides* species induce colitis in host-genotype-specific fashion in a mouse model of inflammatory bowel disease**. *Cell Host Microbe* 2011, **9**:390–403.

138. Caruso R, Mathes T, Martens EC, Kamada N, Nusrat A, Inohara N, Núñez G: **A specific gene-microbe interaction drives the development of Crohn's disease–like colitis in mice**. *Sci Immunol* 2019, **4**:eaaw4341.

139. Seregin SS, Golovchenko N, Schaf B, Chen J, Pudlo NA, Mitchell J, Baxter NT, Zhao L, Schloss PD, Martens EC, et al.: **NLRP6 protects Il10$^{-/-}$ mice from colitis by limiting colonization of *Akkermansia muciniphila***. *Cell Rep* 2017, **19**:733–745.

140. Chassaing B, Koren O, Carvalho FA, Ley RE, Gewirtz AT: **AIEC pathobiont instigates chronic colitis in susceptible hosts by altering microbiota composition**. *Gut* 2014, **63**:1069–1080.

141. Corbin AL, Gomez-Vazquez M, Berthold DL, Attar M, Arnold IC, Powrie FM, Sansom SN, Udalova IA: **IRF5 guides monocytes toward an inflammatory CD11c^{+} macrophage phenotype and promotes intestinal inflammation**. *Sci Immunol* 2020, **5**:eaax6085.

142. Arnold IC, Mathisen S, Schulthess J, Danne C, Hegazy AN, Powrie F: **CD11c^{+} monocyte/macrophages promote chronic *Helicobacter hepaticus*-induced intestinal inflammation through the production of IL-23**. *Mucosal Immunol* 2016, **9**:352–363.

143. Griseri T, Arnold IC, Pearson C, Mckenzie BS, Crocker PR, Correspondence FP: **Granulocyte macrophage colony-stimulating factor-activated eosinophils promote interleukin-23 driven chronic colitis**. *Immunity* 2015, **43**:187–199.

144. Coccia M, Harrison OJ, Schiering C, Asquith MJ, Becher B, Powrie F, Maloy KJ: **IL-1β mediates chronic intestinal inflammation by promoting the accumulation of IL-17A secreting innate lymphoid cells and CD4^{+} Th17 cells.** *J Exp Med* 2012, **209**:1595–1609.

145. Bain CC, Oliphant CJ, Thomson CA, Kullberg MC, Mowat AM: **Proinflammatory role of monocyte-derived CX3CR1^{int} macrophages in *Helicobacter hepaticus*-induced colitis.** *Infect Immun* 2018, **86**:e00579-17.

146. Bernshtein B, Curato C, Ioannou M, Thaiss CA, Gross-Vered M, Kolesnikov M, Wang Q, David E, Chappell-Maor L, Harmelin A, et al.: **IL-23-producing IL-10Rα-deficient gut macrophages elicit an IL-22-driven proinflammatory epithelial cell response**. *Sci Immunol* 2019, **4**:eaau6571.

147. Kirchberger S, Royston DJ, Boulard O, Thornton E, Franchini F, Szabady RL, Harrison O, Powrie F: **Innate lymphoid cells sustain colon cancer through production of interleukin-22 in a mouse model**. *J Exp Med* 2013, **210**:917–931.

148. Kedmi R, Najar TA, Mesa KR, Grayson A, Kroehling L, Hao Y, Hao S, Pokrovskii M, Xu M, Talbot J, et al.: **A RORγt+ cell instructs gut microbiota-specific Treg cell differentiation**. *Nat 2022 6107933* 2022, **610**:737–743.

149. Lee JY, Hall JA, Kroehling L, Wu L, Najar T, Nguyen HH, Lin WY, Yeung ST, Silva HM, Li D, et al.: **Serum amyloid A proteins induce pathogenic Th17 cells and promote inflammatory disease**. *Cell* 2020, **180**:79–91.

150. Kullberg MC, Rothfuchs AG, Jankovic D, Caspar P, Wynn TA, Gorelick PL, Cheever AW, Sher A: ***Helicobacter hepaticus*-induced colitis in interleukin-10-deficient mice: Cytokine requirements for the induction and maintenance of intestinal inflammation**. *Infect Immun* 2001, **69**:4232–4241.

151. Yang I, Eibach D, Kops F, Brenneke B, Woltemate S, Schulze J, Bleich A, Gruber AD, Muthupalani S, Fox JG, et al.: **Intestinal microbiota composition of interleukin-10 deficient C57BL/6J mice and susceptibility to *Helicobacter hepaticus*-induced colitis**. *PLoS One* 2013, **8**:e70783.

152. De Cicco P, Sanders T, Cirino G, Maloy KJ, Ianaro A: **Hydrogen sulfide reduces myeloid-derived suppressor cell-mediated inflammatory response in a model of *Helicobacter hepaticus*-induced colitis**. *Front Immunol* 2018, **9**:499.

153. Sivaprakasam S, Gurav A, Paschall A V, Coe GL, Chaudhary K, Cai Y, Kolhe R,

Martin P, Browning D, Huang L, et al.: **An essential role of Ffar2 (Gpr43) in dietary fibre-mediated promotion of healthy composition of gut microbiota and suppression of intestinal carcinogenesis**. *Oncogenesis* 2016, **5**:e238.

154. Jackson MA, Pearson C, Ilott NE, Huus KE, Hegazy AN, Webber J, Finlay BB, Macpherson AJ, Powrie F, Lam LH: **Accurate identification and quantification of commensal microbiota bound by host immunoglobulins**. *Microbiome* 2021, **9**:33.

155. Majlessi L, Sayes F, Bureau JF, Pawlik A, Michel V, Jouvion G, Huerre M, Severgnini M, Consolandi C, Peano C, et al.: **Colonization with *Helicobacter* is concomitant with modified gut microbiota and drastic failure of the immune control of *Mycobacterium tuberculosis***. *Mucosal Immunol* 2017, **10**:1178–1189.

156. Dobson GP, Letson HL, Biros E, Morris J: **Specific pathogen-free (SPF) animal status as a variable in biomedical research: Have we come full circle?** *EBioMedicine* 2019, **41**:42.

157. Kennedy EA, King KY, Baldridge MT: **Mouse microbiota models: Comparing germ-free mice and antibiotics treatment as tools for modifying gut bacteria**. *Front Physiol* 2018, **9**:1534.

158. Thomson CA, Morgan SC, Ohland C, McCoy KD: **From germ-free to wild: modulating microbiome complexity to understand mucosal immunology**. *Mucosal Immunol* 2022, **15**:1085–1094.

159. Yi P, Li LJ: **The germfree murine animal: An important animal model for research on the relationship between gut microbiota and the host**. *Vet Microbiol* 2012, **157**:1–7.

160. Sommer F, Bäckhed F: **The gut microbiota — masters of host development and physiology**. *Nat Rev Microbiol 2013 114* 2013, **11**:227–238.

161. Ueda Y, Kayama H, Jeon SG, Kusu T, Isaka Y, Rakugi H, Yamamoto M, Takeda K: **Commensal microbiota induce LPS hyporesponsiveness in colonic macrophages via the production of IL-10**. *Int Immunol* 2010, **22**:953–962.

162. Östman S, Rask C, Wold AE, Hultkrantz S, Telemo E: **Impaired regulatory T cell**

function in germ-free mice. *Eur J Immunol* 2006, **36**:2336–2346.

163. Geuking MB, Cahenzli J, Lawson MAE, Ng DCK, Slack E, Hapfelmeier S, McCoy KD, Macpherson AJ: **Intestinal Bacterial Colonization Induces Mutualistic Regulatory T Cell Responses**. *Immunity* 2011, **34**:794–806.

164. Bunker JJ, Erickson SA, Flynn TM, Henry C, Koval JC, Meisel M, Jabri B, Antonopoulos DA, Wilson PC, Bendelac A: **Natural polyreactive IgA antibodies coat the intestinal microbiota**. *Science* 2017, **358**:eaan6619.

165. Cahenzli J, Köller Y, Wyss M, Geuking MB, McCoy KD: **Intestinal microbial diversity during early-life colonization shapes long-term IgE levels**. *Cell Host Microbe* 2013, **14**:559–570.

166. Singh B, Read S, Asseman C, Malmström V, Mottet C, Stephens LA, Stepankova R, Tlaskalova H, Powrie F: **Control of intestinal inflammation by regulatory T cells**. *Immunol Rev* 2001, **182**:190–200.

167. Stefka AT, Feehley T, Tripathi P, Qiu J, McCoy K, Mazmanian SK, Tjota MY, Seo GY, Cao S, Theriault BR, et al.: **Commensal bacteria protect against food allergen sensitization**. *Proc Natl Acad Sci USA* 2014, **111**:13145–13150.

168. Kozakova H, Schwarzer M, Tuckova L, Srutkova D, Czarnowska E, Rosiak I, Hudcovic T, Schabussova I, Hermanova P, Zakostelska Z, et al.: **Colonization of germ-free mice with a mixture of three lactobacillus strains enhances the integrity of gut mucosa and ameliorates allergic sensitization**. *Cell Mol Immunol 2016 132* 2015, **13**:251–262.

169. Sellon RK, Tonkonogy S, Schultz M, Dieleman LA, Grenther W, Balish E, Rennick DM, Sartor RB: **Resident enteric bacteria are necessary for development of spontaneous colitis and immune system activation in interleukin-10-deficient mice**. *Infect Immun* 1998, **66**:5224–5231.

170. Hernández-Chirlaque C, Aranda CJ, Ocón B, Capitán-Cañadas F, Ortega-González M, Carrero JJ, Suárez MD, Zarzuelo A, de Medina FS, Martínez-Augustin O: **Germ-free and antibiotic-treated mice are highly susceptible to epithelial injury in DSS**

colitis. *J Crohn's Colitis* 2016, **10**:1324–1335.

171. Nagalingam NA, Robinson CJ, Bergin IL, Eaton KA, Huffnagle GB, Young VB: **The effects of intestinal microbial community structure on disease manifestation in IL-10$^{-/-}$ mice infected with *Helicobacter hepaticus***. *Microbiome* 2013, **1**:15.

172. Dieleman LA, Arends A, Tonkonogy SL, Goerres MS, Craft DW, Grenther W, Sellon RK, Balish E, Sartor RB: **Helicobacter hepaticus does not induce or potentiate colitis in interleukin-10-deficient mice**. *Infect Immun* 2000, **68**:5107–5113.

173. Brand MW, Wannemuehler MJ, Phillips GJ, Proctor A, Overstreet AM, Jergens AE, Orcutt RP, Fox JG: **The Altered Schaedler Flora: Continued Applications of a Defined Murine Microbial Community**. *ILAR J* 2015, **56**:169.

174. Dewhirst FE, Chien CC, Paster BJ, Ericson RL, Orcutt RP, Schauer DB, Fox JG: **Phylogeny of the defined murine microbiota: altered Schaedler flora**. *Appl Environ Microbiol* 1999, **65**:3287–3292.

175. Stecher B, Chaffron S, Käppeli R, Hapfelmeier S, Freedrich S, Weber TC, Kirundi J, Suar M, McCoy KD, Von Mering C, et al.: **Like Will to Like: Abundances of Closely Related Species Can Predict Susceptibility to Intestinal Colonization by Pathogenic and Commensal Bacteria**. *PLOS Pathog* 2010, **6**:e1000711.

176. Brugiroux S, Beutler M, Pfann C, Garzetti D, Ruscheweyh HJ, Ring D, Diehl M, Herp S, Lötscher Y, Hussain S, et al.: **Genome-guided design of a defined mouse microbiota that confers colonization resistance against Salmonella enterica serovar Typhimurium**. *Nat Microbiol* 2016, **2**:1–12.

177. Li H, Limenitakis JP, Fuhrer T, Geuking MB, Lawson MA, Wyss M, Brugiroux S, Keller I, Macpherson JA, Rupp S, et al.: **The outer mucus layer hosts a distinct intestinal microbial niche**. *Nat Commun* 2015, **6**:1–13.

178. Darnaud M, De Vadder F, Bogeat P, Boucinha L, Bulteau AL, Bunescu A, Couturier C, Delgado A, Dugua H, Elie C, et al.: **A standardized gnotobiotic mouse model harboring a minimal 15-member mouse gut microbiota recapitulates SOPF/SPF phenotypes**. *Nat Commun* 2021, **12**:1–21.

179. Eberl C, Weiss AS, Jochum LM, Durai Raj AC, Ring D, Hussain S, Herp S, Meng C, Kleigrewe K, Gigl M, et al.: **E. coli enhance colonization resistance against Salmonella Typhimurium by competing for galactitol, a context-dependent limiting carbon source**. *Cell Host Microbe* 2021, **29**:1680-1692.e7.

180. Uchimura Y, Wyss M, Brugiroux S, Limenitakis JP, Stecher B, McCoy KD, Macpherson AJ: **Complete Genome Sequences of 12 Species of Stable Defined Moderately Diverse Mouse Microbiota 2**. *Genome Announc* 2016, **4**:951–967.

181. Eberl C, Ring D, Münch PC, Beutler M, Basic M, Slack EC, Schwarzer M, Srutkova D, Lange A, Frick JS, et al.: **Reproducible Colonization of Germ-Free Mice With the Oligo-Mouse-Microbiota in Different Animal Facilities**. *Front Microbiol* 2020, **10**:2999.

182. Hoces D, Lan J, Sun W, Geiser T, Stäubli ML, Cappio Barazzone E, Arnoldini M, Challa TD, Klug M, Kellenberger A, et al.: **Metabolic reconstitution of germ-free mice by a gnotobiotic microbiota varies over the circadian cycle**. *PLoS Biol* 2022, **20**:e3001743.

183. Weiss AS, Burrichter AG, Durai Raj AC, von Strempel A, Meng C, Kleigrewe K, Münch PC, Rössler L, Huber C, Eisenreich W, et al.: **In vitro interaction network of a synthetic gut bacterial community**. *ISME J 2021 164* 2021, **16**:1095–1109.

184. Brugiroux S, Berry D, Ring D, Barnich N, Daims H, Stecher B: **Specific Localization and Quantification of the Oligo-Mouse-Microbiota (OMM12) by Fluorescence In Situ Hybridization (FISH)**. *Curr Protoc* 2022, **2**:e548.

185. Afrizal A, Jennings SAV, Hitch TCA, Riedel T, Basic M, Panyot A, Treichel N, Hager FT, Wong EOY, Wolter B, et al.: **Enhanced cultured diversity of the mouse gut microbiota enables custom-made synthetic communities**. *Cell Host Microbe* 2022, **30**:1630-1645.e25.

186. Cheng AG, Ho PY, Aranda-Díaz A, Jain S, Yu FB, Meng X, Wang M, Iakiviak M, Nagashima K, Zhao A, et al.: **Design, construction, and in vivo augmentation of a complex gut microbiome**. *Cell* 2022, **185**:3617-3636.e19.

187. Nguyen TLA, Vieira-Silva S, Liston A, Raes J: **How informative is the mouse for human gut microbiota research?** *DMM Dis Model Mech* 2015, **8**:1–16.

188. Caruso R, Lo BC, Núñez G: **Host–microbiota interactions in inflammatory bowel disease**. *Nat Rev Immunol 2020 207* 2020, **20**:411–426.

189. Sorbara MT, Pamer EG: **Microbiome-based therapeutics**. *Nat Rev Microbiol 2022 206* 2022, **20**:365–380.

190. Rigottier-Gois L: **Dysbiosis in inflammatory bowel diseases: The oxygen hypothesis**. *ISME J* 2013, **7**:1256–1261.

191. Baldelli V, Scaldaferri F, Putignani L, Del Chierico F: **The Role of Enterobacteriaceae in Gut Microbiota Dysbiosis in Inflammatory Bowel Diseases**. *Microorganisms* 2021, **9**:697.

192. Winter SE, Winter MG, Xavier MN, Thiennimitr P, Poon V, Keestra AM, Laughlin RC, Gomez G, Wu J, Lawhon SD, et al.: **Host-derived nitrate boosts growth of E. coli in the inflamed gut**. *Science (80-)* 2013, **339**:708–711.

193. Cevallos SA, Lee JY, Tiffany CR, Byndloss AJ, Johnston L, Byndloss MX, Bäumler AJ: **Increased epithelial oxygenation links colitis to an expansion of tumorigenic bacteria**. *MBio* 2019, **10**:e02244-19.

194. Byndloss MX, Olsan EE, Rivera-Chávez F, Tiffany CR, Cevallos SA, Lokken KL, Torres TP, Byndloss AJ, Faber F, Gao Y, et al.: **Microbiota-activated PPAR-γ signaling inhibits dysbiotic Enterobacteriaceae expansion**. *Science (80-)* 2017, **357**:570–575.

195. Winter SE, Bäumler AJ: **Dysbiosis in the inflamed intestine: Chance favors the prepared microbe**. *Gut Microbes* 2014, **5**:71–73.

196. Spees AM, Wangdi T, Lopez CA, Kingsbury DD, Xavier MN, Winter SE, Tsolis RM, Bäumler AJ: **Streptomycin-induced inflammation enhances Escherichia coli gut colonization through nitrate respiration**. *MBio* 2013, **4**:e00430-13.

197. Winter SE, Bäumler AJ: **Why related bacterial species bloom simultaneously in the gut: principles underlying the 'Like will to like' concept**. *Cell Microbiol* 2014,

16:179–184.

198. Zhu W, Winter MG, Byndloss MX, Spiga L, Duerkop BA, Hughes ER, Büttner L, de Lima Romão E, Behrendt CL, Lopez CA, et al.: **Precision editing of the gut microbiota ameliorates colitis.** *Nature* 2018, **553**:208–211.
199. Miller BM, Liou MJ, Zhang LF, Nguyen H, Litvak Y, Schorr EM, Jang KK, Tiffany CR, Butler BP, Bäumler AJ: **Anaerobic respiration of NOX1-derived hydrogen peroxide licenses bacterial growth at the colonic surface**. *Cell Host Microbe* 2020, **28**:789.
200. Lopez CA, Miller BM, Rivera-Chávez F, Velazquez EM, Byndloss MX, Chávez-Arroyo A, Lokken KL, Tsolis RM, Winter SE, Bäumler AJ: **Virulence factors enhance Citrobacter rodentium expansion through aerobic respiration**. *Science (80-)* 2016, **353**:1249–1253.
201. Vrancken G, Gregory AC, Huys GRB, Faust K, Raes J: **Synthetic ecology of the human gut microbiota**. *Nat Rev Microbiol* 2019, **17**:754–763.
202. Whary MT, Taylor NS, Feng Y, Ge Z, Muthupalani S, Versalovic J, Fox JG: ***Lactobacillus reuteri*** **promotes** ***Helicobacter hepaticus*****-associated typhlocolitis in gnotobiotic B6.129P2-IL-10^{tm1Cgn} (IL-10$^{-/-}$) mice**. *Immunology* 2011, **133**:165–178.
203. Berkowitz D, Hushon JM, Whitfield HJ, Roth J, Ames BN: **Procedure for identifying nonsense mutations.** *J Bacteriol* 1968, **96**:215–220.
204. Price-Carter M, Tingey J, Bobik TA, Roth JR: **The alternative electron acceptor tetrathionate supports B12-dependent anaerobic growth of Salmonella enterica serovar typhimurium on ethanolamine or 1,2-propanediol**. *J Bacteriol* 2001, **183**:2463–2475.
205. Lamble S, Batty E, Attar M, Buck D, Bowden R, Lunter G, Crook D, El-Fahmawi B, Piazza P: **Improved workflows for high throughput library preparation using the transposome-based Nextera system**. *BMC Biotechnol* 2013, **13**:104.
206. Bray NL, Pimentel H, Melsted P, Pachter L: **Near-optimal probabilistic RNA-seq quantification**. *Nat Biotechnol* 2016, **34**:525–527.

207. Cunningham F, Allen JE, Allen J, Alvarez-Jarreta J, Amode MR, Armean IM, Austine-Orimoloye O, Azov AG, Barnes I, Bennett R, et al.: **Ensembl 2022**. *Nucleic Acids Res* 2022, **50**:D988–D995.

208. Soneson C, Love MI, Robinson MD: **Differential analyses for RNA-seq: Transcript-level estimates improve gene-level inferences**. *F1000Research* 2016, **4**:1521.

209. Ritchie ME, Phipson B, Wu D, Hu Y, Law CW, Shi W, Smyth GK: **limma powers differential expression analyses for RNA-sequencing and microarray studies**. *Nucleic Acids Res* 2015, **43**:e47–e47.

210. Love MI, Huber W, Anders S: **Moderated estimation of fold change and dispersion for RNA-seq data with DESeq2**. *Genome Biol* 2014, **15**:1–21.

211. Durinck S, Moreau Y, Kasprzyk A, Davis S, De Moor B, Brazma A, Huber W: **BioMart and Bioconductor: a powerful link between biological databases and microarray data analysis**. *Bioinformatics* 2005, **21**:3439–3440.

212. Korotkevich G, Sukhov V, Budin N, Shpak B, Artyomov MN, Sergushichev A: **Fast gene set enrichment analysis**. *bioRxiv* 2021, doi:10.1101/060012.

213. Dinno A: **dunn.test: Dunn's Test of Multiple Comparisons Using Rank Sums. R package version 1.3.5**. *https://cran.r-project.org/package=dunn.test* 2017,

214. Gu Z, Eils R, Schlesner M: **Complex heatmaps reveal patterns and correlations in multidimensional genomic data**. *Bioinformatics* 2016, **32**:2847–2849.

215. Langfelder P, Zhang B, Horvath S: **Defining clusters from a hierarchical cluster tree: the Dynamic Tree Cut package for R**. *Bioinformatics* 2008, **24**:719–720.

216. Ge Z, White DA, Whary MT, Fox JG: **Fluorogenic PCR-based quantitative detection of a murine pathogen, Helicobacter hepaticus**. *J Clin Microbiol* 2001, **39**:2598–2602.

217. Yen S, Johnson J, Ilott NE: **Streamlined processing and analysis of 16S rRNA amplicon sequencing data with OCMS_16S and OCMSlooksy**. *Wellcome Open Res* 2022, **7**:68.

218. McMurdie PJ, Holmes S: **phyloseq: An R Package for Reproducible Interactive**

Analysis and Graphics of Microbiome Census Data. *PLoS One* 2013, **8**:e61217.

219. Kuznetsova A, Brockhoff PB, Christensen RHB: **lmerTest Package: Tests in Linear Mixed Effects Models**. *J Stat Softw* 2017, **82**:1–26.

220. Lenth R V.: **emmeans: Estimated Marginal Means, aka Least-Squares Means. R package version 1.7.5.** *https://cran.r-project.org/package=emmeans* 2022,

221. Popov G, Fiebig-Comyn A, Shideler S, Coombes BK, Savchenko A: **Complete Genome Sequence of Citrobacter rodentium Strain DBS100**. *Microbiol Resour Announc* 2019, **8**:e00421-19.

222. Thomassin JL, Leclerc JM, Giannakopoulou N, Zhu L, Salmon K, Portt A, Daigle F, Le Moual H, Gruenheid S: **Systematic analysis of two-component systems in Citrobacter rodentium reveals positive and negative roles in virulence**. *Infect Immun* 2017, **85**:e00654-16.

223. Suerbaum S, Josenhans C, Sterzenbach T, Drescher B, Brandt P, Bell M, Dröge M, Fartmann B, Fischer HP, Ge Z, et al.: **The complete genome sequence of the carcinogenic bacterium Helicobacter hepaticus**. *Proc Natl Acad Sci USA* 2003, **100**:7901–7906.

224. Walsby-Tickle J, Gannon J, Hvinden I, Bardella C, Abboud MI, Nazeer A, Hauton D, Pires E, Cadoux-Hudson T, Schofield CJ, et al.: **Anion-exchange chromatography mass spectrometry provides extensive coverage of primary metabolic pathways revealing altered metabolism in IDH1 mutant cells**. *Commun Biol* 2020, **3**:1–12.

225. Wickham H, Girlich M: **tidyr: Tidy Messy Data. R package version 1.2.0**. *https://cran.r-project.org/package=tidyr* 2022,

226. Wickham H: *Elegant graphics for data analysis*. Springer-Verlag New York; 2016.

227. Kassambara A: **ggpubr: "ggplot2" Based Publication Ready Plots. R package version 0.4.0.** *https://cran.r-project.org/package=ggpubr* 2020,

228. Wickham H, Seidel D: **scales: Scale Functions for Visualization. R package version 1.2.0.** *https://cran.r-project.org/package=scales* 2022,

229. Lee JY, Tsolis RM, Bäumler AJ: **The microbiome and gut homeostasis**. *Science*

(80-) 2022, **377**:eabp9960.

230. Hughes ER, Winter MG, Duerkop BA, Spiga L, Furtado de Carvalho T, Zhu W, Gillis CC, Büttner L, Smoot MP, Behrendt CL, et al.: **Microbial Respiration and Formate Oxidation as Metabolic Signatures of Inflammation-Associated Dysbiosis**. *Cell Host Microbe* 2017, **21**:208–219.

231. Kracke F, Vassilev I, Krömer JO: **Microbial electron transport and energy conservation - The foundation for optimizing bioelectrochemical systems**. *Front Microbiol* 2015, **6**:575.

232. Pool MO, Bouma G, Visser JJ, Kolkman JJ, Tran DD, Meuwissen SGM, Peña AS: **Serum nitrate levels in ulcerative colitis and crohn's disease**. *Scand J Gastroenterol* 1995, **30**:784–788.

233. Levine JJ, Pettei MJ, Valderrama E, Gold DM, Kessler BH, Trachtman H: **Nitric oxide and inflammatory bowel disease: evidence for local intestinal production in children with active colonic disease.** *J Pediatr Gastroenterol Nutr* 1998, **26**:34–8.

234. Chanin RB, Winter MG, Spiga L, Hughes ER, Zhu W, Taylor SJ, Arenales A, Gillis CC, Büttner L, Jimenez AG, et al.: **Epithelial-Derived Reactive Oxygen Species Enable AppBCX-Mediated Aerobic Respiration of Escherichia coli during Intestinal Inflammation**. *Cell Host Microbe* 2020, **28**:780-788.e5.

235. Burke DA, Axon ATR: **Adhesive Escherichia coli in inflammatory bowel disease and infective diarrhoea**. *BMJ* 1988, **297**:102–104.

236. Giaffer MH, Holdsworth CD, Duerden BI: **Virulence properties of Escherichia coli strains isolated from patients with inflammatory bowel disease.** *Gut* 1992, **33**:646–650.

237. Cevallos SA, Lee JY, Velazquez EM, Foegeding NJ, Shelton CD, Tiffany CR, Parry BH, Stull-Lane AR, Olsan EE, Savage HP, et al.: **5-aminosalicylic acid ameliorates colitis and checks dysbiotic escherichia coli expansion by activating PPAR-G signaling in the intestinal epithelium**. *MBio* 2021, **12**:1–10.

238. Williams C, Panaccione R, Ghosh S, Rioux K: **Optimizing clinical use of**

mesalazine (5-aminosalicylic acid) in inflammatory bowel disease. *Therap Adv Gastroenterol* 2011, **4**:237.

239. Cordas CM, Moura JJG: **Molybdenum and tungsten enzymes redox properties – A brief overview**. *Coord Chem Rev* 2019, **394**:53–64.

240. Chassaing B, Aitken JD, Malleshappa M, Vijay-Kumar M: **Dextran Sulfate Sodium (DSS)-Induced Colitis in Mice**. *Curr Protoc Immunol* 2014, **104**:15.25.1-15.25.14.

241. Holgersen K, Kvist PH, Markholst H, Hansen AK, Holm TL: **Characterisation of enterocolitis in the piroxicam-accelerated interleukin-10 knock out mouse--a model mimicking inflammatory bowel disease**. *J Crohns Colitis* 2014, **8**:147–160.

242. Anderson LA, Palmer T, Price NC, Bornemann S, Boxer DH, Pau RN: **Characterisation of the molybdenum-responsive ModE regulatory protein and its binding to the promoter region of the modABCD (molybdenum transport) operon of Escherichia coli**. *Eur J Biochem* 1997, **246**:119–126.

243. Miller JB, Scott DJ, Amy NK: **Molybdenum-sensitive transcriptional regulation of the chlD locus of Escherichia coli**. *J Bacteriol* 1987, **169**:1853–1860.

244. Anderson LA, McNairn E, Leubke T, Pau RN, Boxer DH: **ModE-dependent molybdate regulation of the molybdenum cofactor operon moa in Escherichia coli**. *J Bacteriol* 2000, **182**:7035–7043.

245. Cochran KE, Lamson NG, Whitehead KA: **Expanding the utility of the dextran sulfate sodium (DSS) mouse model to induce a clinically relevant loss of intestinal barrier function**. *PeerJ* 2020, **8**:e8681.

246. Surana NK, Kasper DL: **Moving beyond microbiome-wide associations to causal microbe identification**. *Nature* 2017, **552**:244–247.

247. Hille R: **Molybdenum and tungsten in biology**. *Trends Biochem Sci* 2002, **27**:360–367.

248. Buc J, Santini C-L, Giordani R, Czjzek M, Wu L-F, Giordano G: **Enzymatic and physiological properties of the tungsten-substituted molybdenum TMAO reductase from Escherichia coli**. *Mol Microbiol* 1999, **32**:159–168.

249. Hughes ER, Winter MG, da Silva LA, Muramatsu MK, Jimenez AG, Gillis CC, Spiga L, Chanin RB, Santos RL, Zhu W, et al.: **Reshaping of bacterial molecular hydrogen metabolism contributes to the outgrowth of commensal E. coli during gut inflammation**. *Elife* 2021, **4**:e58609.

250. Misheva M, Ilott NE, McCullagh JSO: **Recent advances and future directions in microbiome metabolomics**. *Curr Opin Endocr Metab Res* 2021, **20**:100283.

251. Lavelle A, Sokol H: **Gut microbiota-derived metabolites as key actors in inflammatory bowel disease**. *Nat Rev Gastroenterol Hepatol* 2020, **17**:223–237.

252. Rivera-Chávez F, Zhang LF, Faber F, Lopez CA, Byndloss MX, Olsan EE, Xu G, Velazquez EM, Lebrilla CB, Winter SE, et al.: **Depletion of Butyrate-Producing Clostridia from the Gut Microbiota Drives an Aerobic Luminal Expansion of Salmonella**. *Cell Host Microbe* 2016, **19**:443–454.

253. Qiu J, Heller JJ, Guo X, Chen ZME, Fish K, Fu YX, Zhou L: **The aryl hydrocarbon receptor regulates gut immunity through modulation of innate lymphoid cells**. *Immunity* 2012, **36**:92–104.

254. Falony G, Joossens M, Vieira-Silva S, Wang J, Darzi Y, Faust K, Kurilshikov A, Bonder MJ, Valles-Colomer M, Vandeputte D, et al.: **Population-level analysis of gut microbiome variation**. *Science (80-)* 2016, **352**:560–564.

255. Ilott NE, Bollrath J, Danne C, Schiering C, Shale M, Adelmann K, Krausgruber T, Heger A, Sims D, Powrie F: **Defining the microbial transcriptional response to colitis through integrated host and microbiome profiling**. *ISME J* 2016, **10**:2389–2404.

256. Abisado RG, Benomar S, Klaus JR, Dandekar AA, Chandler JR: **Bacterial quorum sensing and microbial community interactions**. *MBio* 2018, **9**:e02331-17.

257. Studer N, Desharnais L, Beutler M, Brugiroux S, Terrazos MA, Menin L, Schürch CM, McCoy KD, Kuehne SA, Minton NP, et al.: **Functional Intestinal Bile Acid 7α-Dehydroxylation by Clostridium scindens Associated with Protection from Clostridium difficile Infection in a Gnotobiotic Mouse Model**. *Front Cell Infect*

Microbiol 2016, **6**:191.

258. Bolsega S, Basic M, Smoczek A, Buettner M, Eberl C, Ahrens D, Odum KA, Stecher B, Bleich A: **Composition of the Intestinal Microbiota Determines the Outcome of Virus-Triggered Colitis in Mice**. *Front Immunol* 2019, **10**:1708.

259. Lourenço M, Chaffringeon L, Lamy-Besnier Q, Pédron T, Campagne P, Eberl C, Bérard M, Stecher B, Debarbieux L, De Sordi L: **The Spatial Heterogeneity of the Gut Limits Predation and Fosters Coexistence of Bacteria and Bacteriophages**. *Cell Host Microbe* 2020, **28**:390-401.e5.

260. De Preter V, Machiels K, Joossens M, Arijs I, Matthys C, Vermeire S, Rutgeerts P, Verbeke K: **Faecal metabolite profiling identifies medium-chain fatty acids as discriminating compounds in IBD**. *Gut* 2015, **64**:447–458.

261. Franzosa EA, Sirota-Madi A, Avila-Pacheco J, Fornelos N, Haiser HJ, Reinker S, Vatanen T, Hall AB, Mallick H, McIver LJ, et al.: **Gut microbiome structure and metabolic activity in inflammatory bowel disease**. *Nat Microbiol 2018 42* 2018, **4**:293–305.

262. Litvak Y, Bäumler AJ: **Microbiota-Nourishing Immunity: A Guide to Understanding Our Microbial Self**. *Immunity* 2019, **51**:214–224.

263. Balish E, Warner T: **Enterococcus faecalis Induces Inflammatory Bowel Disease in Interleukin-10 Knockout Mice**. *Am J Pathol* 2002, **160**:2253–2257.

264. Hoffmann M, Kim SC, Sartor RB, Haller D: **Enterococcus faecalis Strains Differentially Regulate Alix/AIP1 Protein Expression and ERK 1/2 Activation in Intestinal Epithelial Cells in the Context of Chronic Experimental Colitis**. *J Proteome Res* 2009, **8**:1183–1192.

265. Hrdý J, Alard J, Couturier-Maillard A, Boulard O, Boutillier D, Delacre M, Lapadatescu C, Cesaro A, Blanc P, Pot B, et al.: **Lactobacillus reuteri 5454 and Bifidobacterium animalis ssp. lactis 5764 improve colitis while differentially impacting dendritic cells maturation and antimicrobial responses**. *Sci Rep* 2020, **10**:1–11.

266. Liu HY, Gu F, Zhu C, Yuan L, Zhu C, Zhu M, Yao J, Hu P, Zhang Y, Dicksved J, et al.:

Epithelial Heat Shock Proteins Mediate the Protective Effects of Limosilactobacillus reuteri in Dextran Sulfate Sodium-Induced Colitis. *Front Immunol* 2022, **13**.

267. Chia J-H, Wu T-S, Wu T-L, Chen C-L, Chuang C-H, Su L-H, Chang H-J, Lu C-C, Kuo A-J, Lai H-C, et al.: **Clostridium innocuum is a vancomycin-resistant pathogen that may cause antibiotic-associated diarrhoea**. *Clin Microbiol Infect* 2018, **24**:1195–1199.
268. Ha CWY, Martin A, Sepich-Poore GD, Shi B, Wang Y, Gouin K, Humphrey G, Sanders K, Ratnayake Y, Chan KSL, et al.: **Translocation of Viable Gut Microbiota to Mesenteric Adipose Drives Formation of Creeping Fat in Humans**. *Cell* 2020, **183**:666-683.e17.
269. Dobranowski PA, Tang C, Sauvé JP, Menzies SC, Sly LM: **Compositional changes to the ileal microbiome precede the onset of spontaneous ileitis in SHIP deficient mice**. *Gut Microbes* 2019, **10**:578–598.
270. Liu Q, Lu W, Tian F, Zhao J, Zhang H, Hong K, Yu L: **Akkermansia muciniphila Exerts Strain-Specific Effects on DSS-Induced Ulcerative Colitis in Mice**. *Front Cell Infect Microbiol* 2021, **11**.
271. Haas KN, Blanchard JL: **Reclassification of the clostridium clostridioforme and clostridium sphenoides clades as enterocloster gen. Nov. and lacrimispora gen. nov., including reclassification of 15 taxa**. *Int J Syst Evol Microbiol* 2020, **70**:23–34.
272. Xu HM, Zhao HL, Guo GJ, Xu J, Zhou YL, Huang HL, Nie YQ: **Characterization of short-chain fatty acids in patients with ulcerative colitis: a meta-analysis**. *BMC Gastroenterol* 2022, **22**:1–9.
273. Morgan XC, Tickle TL, Sokol H, Gevers D, Devaney KL, Ward D V., Reyes JA, Shah SA, LeLeiko N, Snapper SB, et al.: **Dysfunction of the intestinal microbiome in inflammatory bowel disease and treatment.** *Genome Biol* 2012, **13**:1–18.
274. Cervantes-Barragan L, Chai JN, Tianero MD, Di Luccia B, Ahern PP, Merriman J,

Cortez VS, Caparon MG, Donia MS, Gilfillan S, et al.: **Lactobacillus reuteri induces gut intraepithelial CD4+CD8αα+ T cells**. *Science (80-)* 2017, **357**:806–810.

275. Wilck N, Matus MG, Kearney SM, Olesen SW, Forslund K, Bartolomaeus H, Haase S, Mahler A, Balogh A, Marko L, et al.: **Salt-responsive gut commensal modulates TH17 axis and disease**. *Nature* 2017, **551**:585–589.

276. Ehrlich AM, Pacheco AR, Henrick BM, Taft D, Xu G, Huda MN, Mishchuk D, Goodson ML, Slupsky C, Barile D, et al.: **Indole-3-lactic acid associated with Bifidobacterium-dominated microbiota significantly decreases inflammation in intestinal epithelial cells**. *BMC Microbiol* 2020, **20**:1–13.

277. Fernandez-Salguero PM, Ward JM, Sundberg JP, Gonzalez FJ: **Lesions of Aryl-hydrocarbon Receptor-deficient Mice**. *Vet Pathol* 1997, **34**:605–614.

278. Monteleone I, Rizzo A, Sarra M, Sica G, Sileri P, Biancone L, MacDonald TT, Pallone F, Monteleone G: **Aryl Hydrocarbon Receptor-Induced Signals Up-regulate IL-22 Production and Inhibit Inflammation in the Gastrointestinal Tract**. *Gastroenterology* 2011, **141**:237-248.e1.

279. Naganuma M, Sugimoto S, Mitsuyama K, Kobayashi T, Yoshimura N, Ohi H, Tanaka S, Andoh A, Ohmiya N, Saigusa K, et al.: **Efficacy of Indigo Naturalis in a Multicenter Randomized Controlled Trial of Patients With Ulcerative Colitis**. *Gastroenterology* 2018, **154**:935–947.

280. Faber SC, Lahoti TS, Taylor ER, Lewis L, Sapiro JM, Sales VT, Dragan YP, Jeffy BD: **Current Therapeutic Landscape and Safety Roadmap for Targeting the Aryl Hydrocarbon Receptor in Inflammatory Gastrointestinal Indications**. *Cells* 2022, **11**:1708.

281. Fremder M, Kim SW, Hadad U, Cheon JH, Ohana E, Khamaysi A, Shimshilashvili L, Eini-Rider H, Park IS: **A transepithelial pathway delivers succinate to macrophages, thus perpetuating their pro-inflammatory metabolic state**. *CellReports* 2021, **36**:109521.

282. Macias-Ceja DC, Ortiz-Masiá D, Salvador P, Gisbert-Ferrándiz L, Hernández C,

Hausmann M, Rogler G, Esplugues J V., Hinojosa J, Alós R, et al.: **Succinate receptor mediates intestinal inflammation and fibrosis**. *Mucosal Immunol* 2019, **12**:178–187.

283. Connors J, Dawe N, Van Limbergen J: **The Role of Succinate in the Regulation of Intestinal Inflammation**. *Nutrients* 2019, **11**.

284. Chung-Faye G, Hayee B, Maestranzi S, Donaldson N, Forgacs I, Sherwood R: **Fecal M2-pyruvate kinase (M2-PK): a novel marker of intestinal inflammation**. *Inflamm Bowel Dis* 2007, **13**:1374–1378.

285. Tai A, Sawano T, Yazama F, Ito H: **Evaluation of antioxidant activity of vanillin by using multiple antioxidant assays**. *Biochim Biophys Acta* 2011, **1810**:170–177.

286. Kim SJ, Kim MC, Um JY, Hong SH: **The beneficial effect of vanillic acid on ulcerative colitis**. *Molecules* 2010, **15**:7208–7217.

287. Wu SL, Chen JC, Li CC, Lo HY, Ho TY, Hsiang CY: **Vanillin improves and prevents trinitrobenzene sulfonic acid-induced colitis in mice**. *J Pharmacol Exp Ther* 2009, **330**:370–376.

288. Lee G, Na HJ, Namkoong S, Jeong Kwon H, Han S, Ha KS, Kwon YG, Lee H, Kim YM: **4-O-methylgallic acid down-regulates endothelial adhesion molecule expression by inhibiting NF-kappaB-DNA-binding activity**. *Eur J Pharmacol* 2006, **551**:143–151.

289. Da Silva RR, Dorrestein PC, Quinn RA: **Illuminating the dark matter in metabolomics**. *Proc Natl Acad Sci USA* 2015, **112**:12549–12550.

290. Wang X, Howe S, Deng F, Zhao J: **Current Applications of Absolute Bacterial Quantification in Microbiome Studies and Decision-Making Regarding Different Biological Questions**. *Microorganisms* 2021, **9**.

291. Chan V, Crocetti G, Grehan M, Zhang L, Danon S, Lee A, Mitchell H: **Visualization of Helicobacter species within the murine cecal mucosa using specific fluorescence in situ hybridization**. *Helicobacter* 2005, **10**:114–124.

292. Zhao Q, Maynard CL: **Mucus, commensals, and the immune system**. *Gut*

Microbes 2022, **14**.

293. Imdad A, Nicholson MR, Tanner-Smith EE, Zackular JP, Gomez-Duarte OG, Beaulieu DB, Acra S: **Fecal transplantation for treatment of inflammatory bowel disease**. *Cochrane Database Syst Rev* 2018, **2018**.

294. Townsend CM, Parker CE, MacDonald JK, Nguyen TM, Jairath V, Feagan BG, Khanna R: **Antibiotics for induction and maintenance of remission in Crohn's disease**. *Cochrane Database Syst Rev* 2019, **2019**.

295. Kaur L, Gordon M, Baines PA, Iheozor-Ejiofor Z, Sinopoulou V, Akobeng AK: **Probiotics for induction of remission in ulcerative colitis**. *Cochrane Database Syst Rev* 2020, **2020**.

296. Nobrega FL, Vlot M, de Jonge PA, Dreesens LL, Beaumont HJE, Lavigne R, Dutilh BE, Brouns SJJ: **Targeting mechanisms of tailed bacteriophages**. *Nat Rev Microbiol 2018 1612* 2018, **16**:760–773.

297. Federici S, Kredo-Russo S, Valdés-Mas R, Kviatcovsky D, Weinstock E, Matiuhin Y, Silberberg Y, Atarashi K, Furuichi M, Oka A, et al.: **Targeted suppression of human IBD-associated gut microbiota commensals by phage consortia for treatment of intestinal inflammation**. *Cell* 2022, **185**:2879-2898.e24.

298. Atarashi K, Tanoue T, Oshima K, Suda W, Nagano Y, Nishikawa H, Fukuda S, Saito T, Narushima S, Hase K, et al.: **Treg induction by a rationally selected mixture of Clostridia strains from the human microbiota**. *Nature* 2013, **500**:232–236.

299. Bekkers M, Stojkovic B, Kaiko GE: **Mining the Microbiome and Microbiota-Derived Molecules in Inflammatory Bowel Disease**. *Int J Mol Sci* 2021, **22**:11243.

300. Smillie CS, Sauk J, Gevers D, Friedman J, Sung J, Youngster I, Hohmann EL, Staley C, Khoruts A, Sadowsky MJ, et al.: **Strain Tracking Reveals the Determinants of Bacterial Engraftment in the Human Gut Following Fecal Microbiota Transplantation**. *Cell Host Microbe* 2018, **23**:229-240.e5.

301. Rosser EC, Piper CJM, Matei DE, Blair PA, Rendeiro AF, Orford M, Alber DG, Krausgruber T, Catalan D, Klein N, et al.: **Microbiota-Derived Metabolites**

Suppress Arthritis by Amplifying Aryl-Hydrocarbon Receptor Activation in Regulatory B Cells. *Cell Metab* 2020, **31**:837-851.e10.

302. Gasaly N, Hermoso MA, Gotteland M: **Butyrate and the Fine-Tuning of Colonic Homeostasis: Implication for Inflammatory Bowel Diseases**. *Int J Mol Sci* 2021, **22**:1–18.

303. Funabashi M, Grove TL, Wang M, Varma Y, McFadden ME, Brown LC, Guo C, Higginbottom S, Almo SC, Fischbach MA: **A metabolic pathway for bile acid dehydroxylation by the gut microbiome**. *Nature* 2020, **582**:566–570.

304. Singh R, Chandrashekharappa S, Bodduluri SR, Baby B V., Hegde B, Kotla NG, Hiwale AA, Saiyed T, Patel P, Vijay-Kumar M, et al.: **Enhancement of the gut barrier integrity by a microbial metabolite through the Nrf2 pathway**. *Nat Commun* 2019, **10**.

305. Young VB, Knox KA, Pratt JS, Cortez JS, Mansfield LS, Rogers AB, Fox JG, Schauer DB: **In vitro and in vivo characterization of Helicobacter hepaticus cytolethal distending toxin mutants**. *Infect Immun* 2004, **72**:2521–2527.

306. Hei W, Azzi-Martin L, Velasco VR, Lehoursi P, Dubus P, Djavaheri-Mergny M, Ménard A: **The CDT of *Helicobacter hepaticus* induces prosurvival autophagy and nucleoplasmic reticulum formation concentrating the RNA binding proteins UNR/CSDE1 and P62/SQSTM1**. *PLoS Pathog* 2021, **17**:e1009320.

307. Chow J, Mazmanian SK: **A pathobiont of the microbiota balances host colonization and intestinal inflammation**. *Cell Host Microbe* 2010, **7**:265–276.

308. Ge Z, Sterzenbach T, Whary MT, Rickman BH, Rogers AB, Shen Z, Taylor NS, Schauer DB, Josenhans C, Suerbaum S, et al.: ***Helicobacter hepaticus* HHGI1 is a pathogenicity island associated with typhlocolitis in B6.129-IL10^{tm1Cgn} mice**. *Microbes Infect* 2008, **10**:726–733.

309. Rocha DJP, Santos CS, Pacheco LGC: **Bacterial reference genes for gene expression studies by RT-qPCR: survey and analysis**. *Antonie van Leeuwenhoek, Int J Gen Mol Microbiol* 2015, **108**:685–693.

310. Falsafi T, Mahboubi M: **Helicobacter hepaticus, a new pathogenic species of the Helicobacter genus: Similarities and differences with H. Pylori**. *Iran J Microbiol* 2013, **5**:185–194.

311. Hooper L V.: **Bacterial contributions to mammalian gut development**. *Trends Microbiol* 2004, **12**:129–134.

312. Olszak T, An D, Zeissig S, Vera MP, Richter J, Franke A, Glickman JN, Siebert R, Baron RM, Kasper DL, et al.: **Microbial exposure during early life has persistent effects on natural killer T cell function**. *Science (80-)* 2012, **336**:489–493.

313. Ge Z, Feng Y, Ge L, Parry N, Muthupalani S, Fox JG: **Helicobacter hepaticus cytolethal distending toxin promotes intestinal carcinogenesis in 129Rag2-deficient mice**. *Cell Microbiol* 2017, **19**:e12728.

314. Bartonickova L, Sterzenbach T, Nell S, Kops F, Schulze J, Venzke A, Brenneke B, Bader S, Gruber AD, Suerbaum S, et al.: **Hcp and VgrG1 are secreted components of the *Helicobacter hepaticus* type VI secretion system and VgrG1 increases the bacterial colitogenic potential**. *Cell Microbiol* 2013, **15**:992–1011.

315. Yu Y, Yang H, Li J, Zhang P, Wu B, Zhu B, Zhang Y, Fang W: **Putative type VI secretion systems of Vibrio parahaemolyticus contribute to adhesion to cultured cell monolayers**. *Arch Microbiol* 2012, **194**:827–835.

316. Wang S, Yan Q, Zhang M, Huang L, Mao L, Zhang M, Xu X, Chen L, Qin Y: **The role and mechanism of icmF in Aeromonas hydrophila survival in fish macrophages**. *J Fish Dis* 2019, **42**:895–904.

317. Granato ET, Meiller-Legrand TA, Foster KR: **The Evolution and Ecology of Bacterial Warfare**. *Curr Biol* 2019, **29**:R521–R537.

318. Sana TG, Flaugnatti N, Lugo KA, Lam LH, Jacobson A, Baylot V, Durand E, Journet L, Cascales E, Monack DM: **Salmonella Typhimurium utilizes a T6SS-mediated antibacterial weapon to establish in the host gut**. *Proc Natl Acad Sci USA* 2016, **113**:E5044–E5051.

319. Nishida A, Inoue R, Inatomi O, Bamba S, Naito Y, Andoh A: **Gut microbiota in the**

pathogenesis of inflammatory bowel disease. *Clin J Gastroenterol* 2018, **11**.

320. Fan Y, Pedersen O: **Gut microbiota in human metabolic health and disease**. *Nat Rev Microbiol* 2020, **19**:55–71.

321. Durack J, Lynch S V.: **The gut microbiome: Relationships with disease and opportunities for therapy**. *J Exp Med* 2019, **216**:20.

322. Friedrich M, Pohin M, Powrie F: **Cytokine Networks in the Pathophysiology of Inflammatory Bowel Disease**. *Immunity* 2019, **50**:992–1006.

323. Atarashi K, Tanoue T, Shima T, Imaoka A, Kuwahara T, Momose Y, Cheng G, Yamasaki S, Saito T, Ohba Y, et al.: **Induction of colonic regulatory T cells by indigenous Clostridium species**. *Science (80-)* 2011, **331**:337–341.

324. Eisenstein M: **Early investments powering the ascent of microbiome therapeutics**. *Biopharma Deal* 2020, doi:10.1038/D43747-020-01178-X.

325. Peng L, Li ZR, Green RS, Holzman IR, Lin J: **Butyrate Enhances the Intestinal Barrier by Facilitating Tight Junction Assembly via Activation of AMP-Activated Protein Kinase in Caco-2 Cell Monolayers**. *J Nutr* 2009, **139**:1619.

326. ElKorashy RIM, El-Sherif RH: **Gram negative organisms as a cause of acute exacerbation of COPD**. *Egypt J Chest Dis Tuberc* 2014, **63**:345–349.

327. Maloy KJ, Powrie F: **Intestinal homeostasis and its breakdown in inflammatory bowel disease**. *Nature* 2011, **474**:298–306.

328. Zhang L, Day A, McKenzie G, Mitchell H: **Nongastric Helicobacter species detected in the intestinal tract of children**. *J Clin Microbiol* 2006, **44**:2276–2279.

329. Man SM, Zhang L, Day AS, Leach S, Mitchell H: **Detection of enterohepatic and gastric helicobacter species in fecal specimens of children with Crohn's disease**. *Helicobacter* 2008, **13**:234–238.

330. Kaakoush NO, Holmes J, Octavia S, Man SM, Zhang L, Castaño-Rodríguez N, Day AS, Leach ST, Lemberg DA, Dutt S, et al.: **Detection of Helicobacteraceae in intestinal biopsies of children with Crohn's disease**. *Helicobacter* 2010, **15**:549–557.

331. Lundgren A, Suri-Payer E, Enarsson K, Svennerholm AM, Lundin BS: **Helicobacter pylori-specific CD4+ CD25high regulatory T cells suppress memory T-cell responses to H. pylori in infected individuals**. *Infect Immun* 2003, **71**:1755–1762.

332. Bagnoli F, Buti L, Tompkins L, Covacci A, Amieva MR: **Helicobacter pylori CagA induces a transition from polarized to invasive phenotypes in MDCK cells**. *Proc Natl Acad Sci USA* 2005, **102**:16339–16344.

333. Ohnishi N, Yuasa H, Tanaka S, Sawa H, Miura M, Matsui A, Higashi H, Musashi M, Iwabuchi K, Suzuki M, et al.: **Transgenic expression of Helicobacter pylori CagA induces gastrointestinal and hematopoietic neoplasms in mouse**. *Proc Natl Acad Sci USA* 2008, **105**:1003–1008.

334. Doohan D, Rezkitha YAA, Waskito LA, Yamaoka Y, Miftahussurur M: **Helicobacter pylori BabA–SabA Key Roles in the Adherence Phase: The Synergic Mechanism for Successful Colonization and Disease Development**. *Toxins (Basel)* 2021, **13**.

335. Thomas MS, Wigneshweraraj S: **Regulation of virulence gene expression**. *Virulence* 2015, **5**:832–834.

336. Banerji R, Kanojiya P, Saroj SD: **Role of interspecies bacterial communication in the virulence of pathogenic bacteria**. *Crit Rev Microbiol* 2020, **46**:136–146.

337. De Klerk N, Maudsdotter L, Gebreegziabher H, Saroj SD, Eriksson B, Eriksson OS, Roos S, Lindén S, Sjölinder H, Jonsson AB: **Lactobacilli reduce Helicobacter pylori attachment to host gastric epithelial cells by inhibiting adhesion gene expression**. *Infect Immun* 2016, **84**:1526–1535.

338. Khosravi Y, Loke MF, Goh KL, Vadivelu J: **Proteomics Analysis Revealed that Crosstalk between Helicobacter pylori and Streptococcus mitis May Enhance Bacterial Survival and Reduces Carcinogenesis**. *Front Microbiol* 2016, **7**.

339. Rivas MA, Beaudoin M, Gardet A, Stevens C, Sharma Y, Zhang CK, Boucher G, Ripke S, Ellinghaus D, Burtt N, et al.: **Deep resequencing of GWAS loci identifies independent rare variants associated with inflammatory bowel disease**. *Nat Genet* 2011, **43**:1066–1073.

340. Schwechheimer C, Kuehn MJ: **Outer-membrane vesicles from Gram-negative bacteria: biogenesis and functions**. *Nat Rev Microbiol* 2015, **13**:605–619.

341. Hickey CA, Kuhn KA, Martens EC, Stappenbeck TS: **Colitogenic *Bacteroides thetaiotaomicron* antigens access host immune cells in a sulfatase-dependent manner via outer membrane vesicles**. *Cell Host Microbe* 2015, **17**:672–680.

342. Ayers TD, Leonard-Puppa E, Kader HA, Waddell J, Watkins RD, Blanchard SS, Safta AM, Rawal N: **Oral Vancomycin as an Adjuvant Treatment in IBD**. *Crohn's Colitis 360* 2019, **1**.

343. Abarbanel DN, Seki SM, Davies Y, Marlen N, Benavides JA, Cox K, Nadeau KC, Cox KL: **Immunomodulatory effect of vancomycin on Treg in pediatric inflammatory bowel disease and primary sclerosing cholangitis**. *J Clin Immunol* 2013, **33**:397–406.

344. Cox KL, Cox KM: **Oral vancomycin: treatment of primary sclerosing cholangitis in children with inflammatory bowel disease**. *J Pediatr Gastroenterol Nutr* 1998, **27**:580–583.

345. Davies YK, Cox KM, Abdullah BA, Safta A, Terry AB, Cox KL: **Long-term treatment of primary sclerosing cholangitis in children with oral vancomycin: an immunomodulating antibiotic**. *J Pediatr Gastroenterol Nutr* 2008, **47**:61–67.

346. Ge P, Scholl D, Prokhorov NS, Avaylon J, Shneider MM, Browning C, Buth SA, Plattner M, Chakraborty U, Ding K, et al.: **Action of a minimal contractile bactericidal nanomachine**. *Nature* 2020, **580**:658–662.

A. Appendix

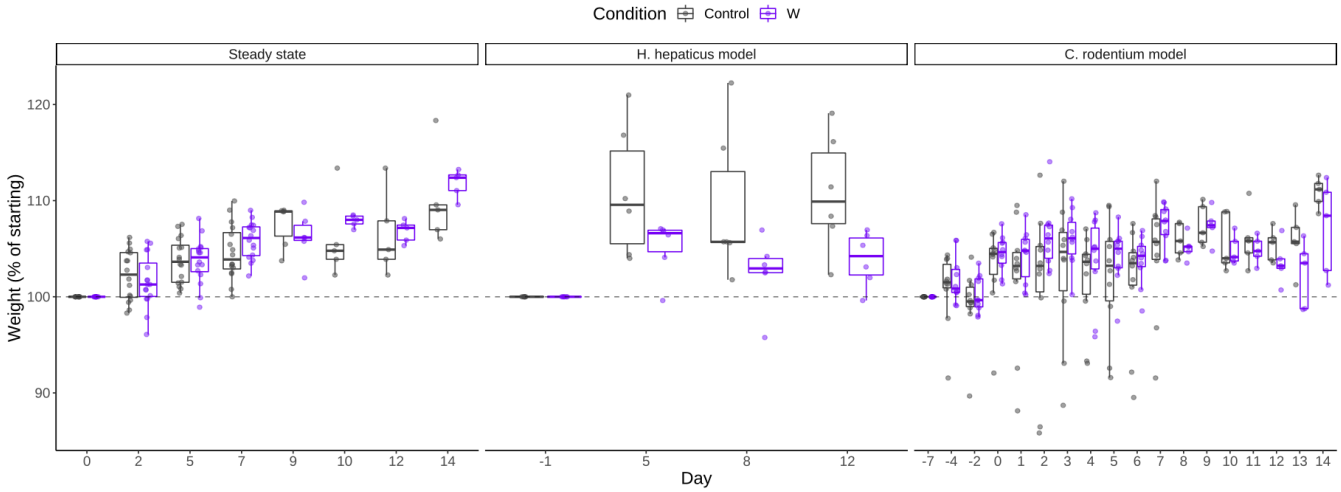


Figure A.1 Tungstate does not influence animal weights in murine colitis models. Weights of *H. hepaticus* + aIL-10R treated and *C. rodentium* infected mice given autoclaved DI (control) or 0.2% tungstate (W) water. Weight is expressed relative to the starting weight. Boxplots denote median and interquartile range and individual data points are shown. All data obtained from 1 experiment.

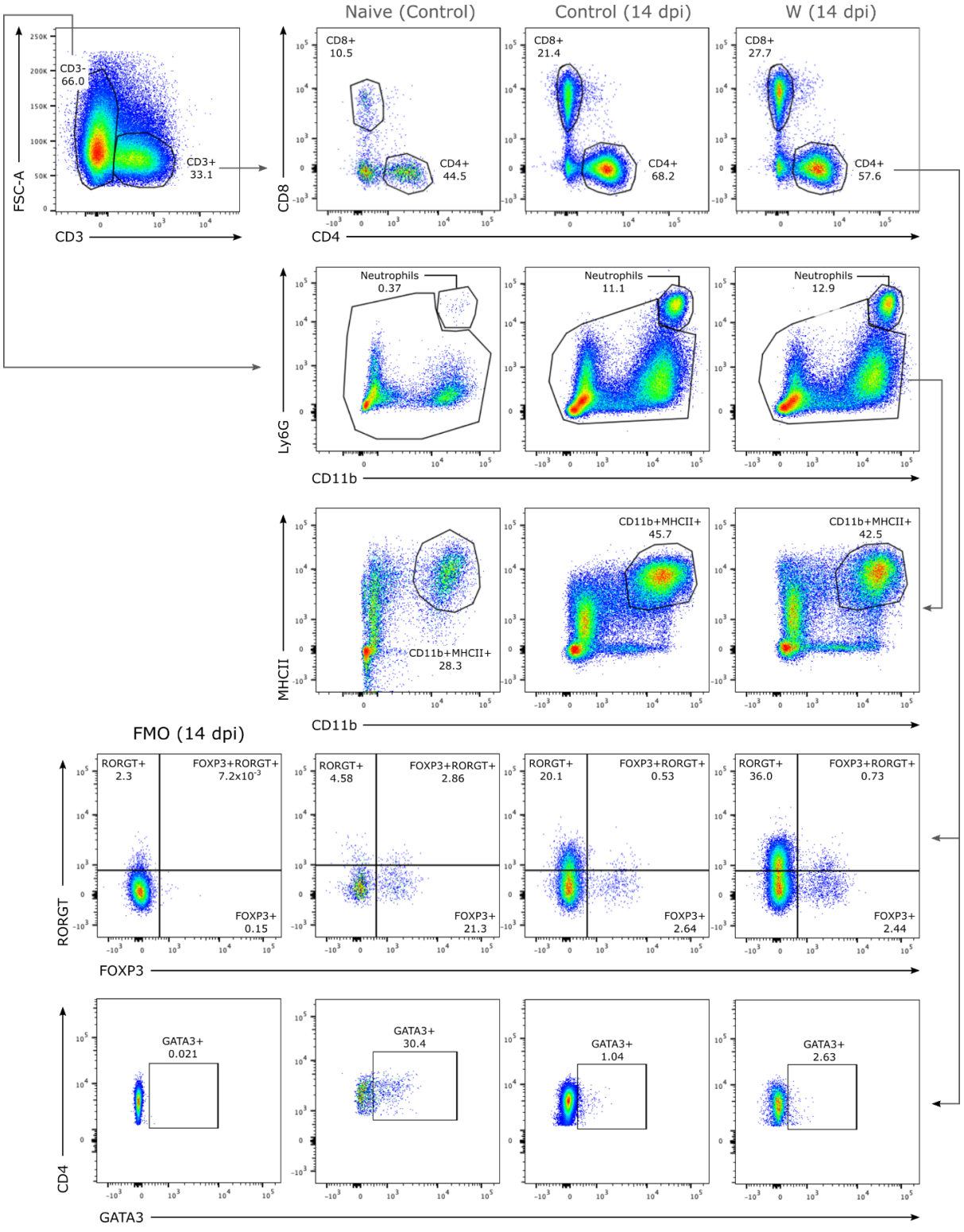


Figure A.2 Gating strategy for flow cytometry. Plots are representative of colonic lamina propria samples obtained from *C. rodentium* infected mice 14 days post infection (dpi). A steady state sample 14 days post control water treatment is used as an exemplar naïve plot.

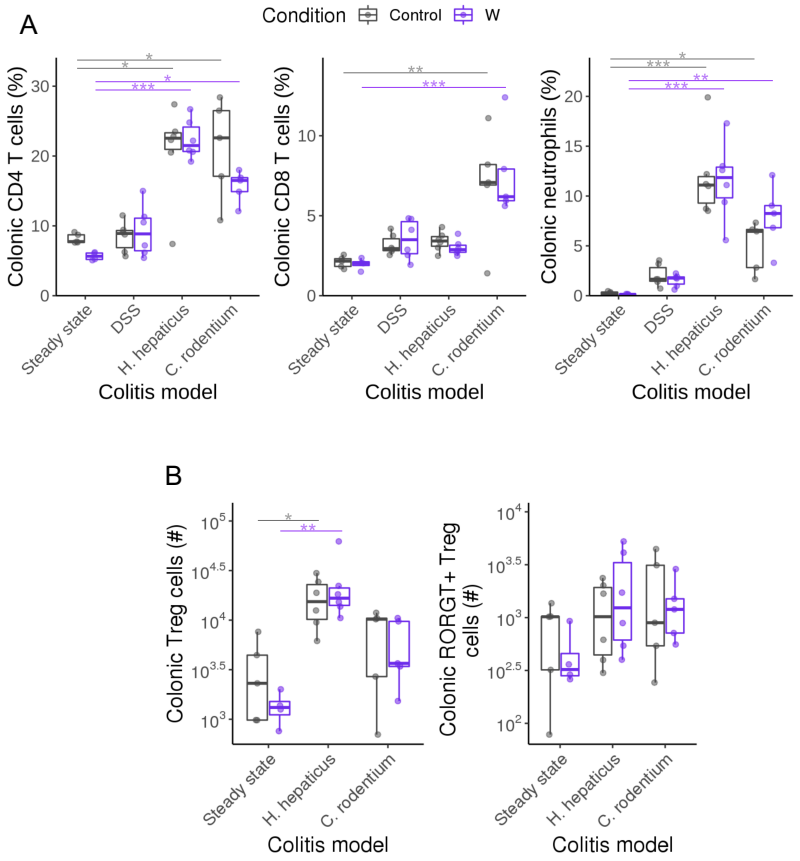


Figure A.3 Tungstate does not influence mucosal inflammation in murine colitis models. A) Left-right CD4 and CD8 T cell and neutrophil frequencies (relative to the total immune cell compartment) in the colonic lamina propria of steady state and DSS, *H. hepaticus* + aIL-10R treated and *C. rodentium* infected mice given autoclaved DI (control) or 0.2% tungstate (W) water. B) Treg and iTreg cell colonic counts obtained from control and W treated steady state and H. hepaticus and C. rodentium colitis model mice. B and C) DSS values were obtained 9 days post model inception. *C. rodentium* and *H. hepaticus* values were obtained 14 days post model inception. Steady state values were obtained 14 days post tungstate treatment. *p<0.05 and **p<0.01 Kruskal Wallis with Dunn's post hoc testing. Boxplots show median and interquartile range and individual data points are shown. All data obtained from1 experiment.

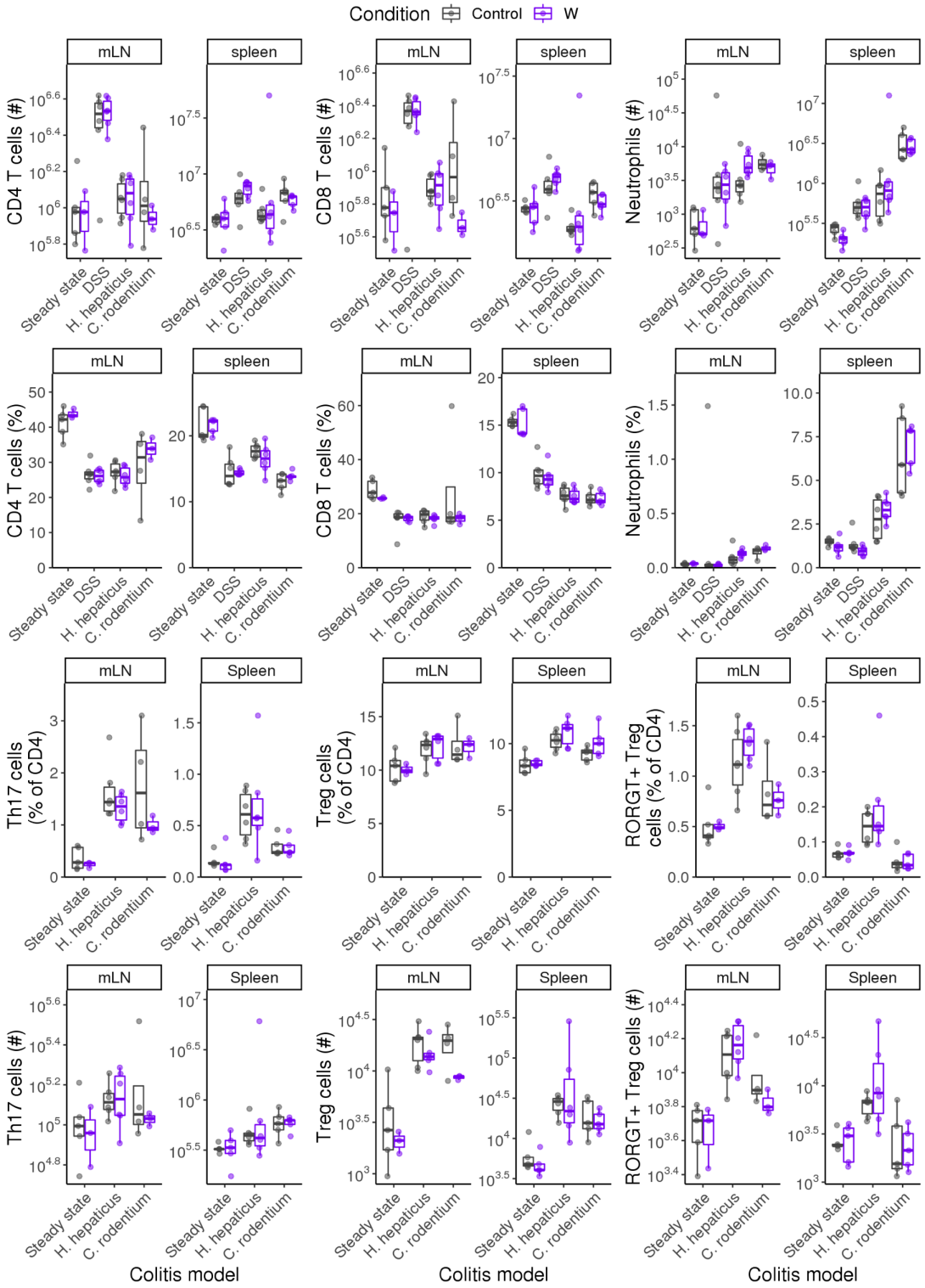


Figure A.4 Tungstate does not influence systemic immune responses across murine colitis models. A and B) Left-right CD4 and CD8 T cell and neutrophil A) counts and B) frequencies (relative to the total immune cell population) in the mesenteric lymph nodes (mLN) and spleens from steady state and DSS, *H. hepaticus* + aIL-10R treated and *C. rodentium* infected mice given autoclaved DI (control) or 0.2% tungstate (W) water. C and D) Left-right Th17, Treg and iTreg cell C) distribution and D) counts in the mLn and spleens obtained from steady state and DSS, *H. hepaticus* + aIL-10R treated and *C. rodentium* infected mice receiving control or W water. DSS values were obtained 12 days post model inception. *C. rodentium* and *H. hepaticus* values were obtained 14 days post model inception. Steady state values were obtained 14 days post tungstate treatment. *p<0.05 and **p<0.01 Kruskal Wallis with Dunn's post hoc testing. Boxplots show median and interquartile range and individual datapoints are shown. All data obtained from1 experiment.

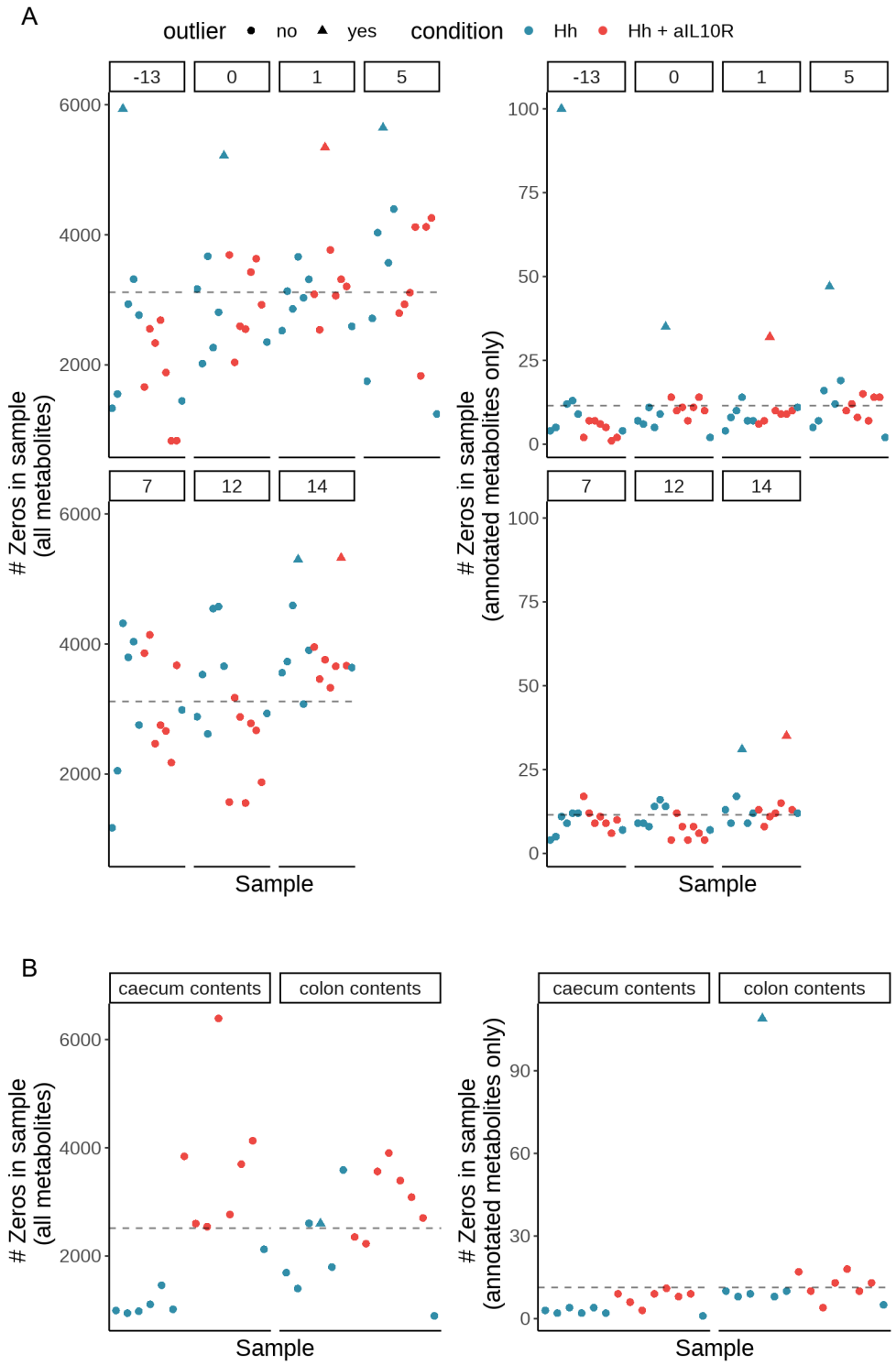


Figure A.5 Outliers in annotated metabolite PCA are driven by elevated zero status. Number of zeros detected in any given A) faecal and B) intestinal content sample and their status as an outlier according to annotated metabolite PCA. All samples obtained from *Helicobacter hepaticus* (Hh) and Hh + anti-interleukin-10 receptor (aIL-10R) treated Oligo-Mouse-Microbiota 12 (OMM^{12}) mice. Data obtained from one experiment.

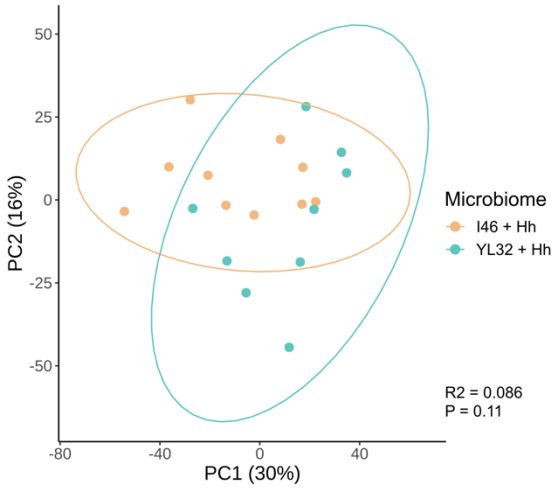


Figure A.6. Inter-bacterial interactions drive subtle changes in homeostatic host gene expression. Principal components analysis of RNA sequencing data of caecum tissues obtained from *Clostridium innocuum* I46 (I46) or *Enterocloster clostridioformis* YL32 (YL32) mice 14 days after *Helicobacter hepaticus* (Hh) colonisation. Data obtained from 2 experiments.